Plant physiological and biophysical regulations of ecohydrological processes in response to strong climate variability

Rong Gan

Thesis submitted in fulfilment of the requirements for the degree of

Doctor of Philosophy

School of Life Sciences, Faculty of Science

University of Technology Sydney

Australia

August 2019

Certificate of Original Authorship

I, Rong Gan declare that this thesis, is submitted in fulfilment of the requirements for the award of Doctor of Philosophy, in the School of Life Sciences/Faculty of Sciences at the University of Technology Sydney.

This thesis is wholly my own work unless otherwise reference or acknowledged. In addition, I certify that all information sources and literature used are indicated in the thesis.

This document has not been submitted for qualifications at any other academic institution.

Signature of student: 

Date: 25 August 2019

Acknowledgement

Reaching the ending point of the PhD journey, I am deeply grateful for this extremely challenging but rewarding experience. This work is unachievable without the support and help from many people and institutions.

I am incredibly thankful to my four supervisors, Professor Qiang Yu, Professor Yongqiang Zhang, Dr. Lu Zhang and Professor Derek Eamus, who provided me guidance and assistance to explore the mystery of ecohydrological science throughout this 4-year period. Professor Qiang Yu has been highly supportive to my application of pursuing PhD at UTS with scholarship and my cooperative research project with the Commonwealth Scientific and Industrial Research Organisation (CSIRO). I have received not only expertise advice but also general support and encouragement to keep going, especially during the most difficult times. I would like to express my sincere gratitude and thanks to my co-supervisor, Professor Yongqiang Zhang, who provided me the great opportunity to collaborate with the prestigious research organisation CSIRO and work with distinguished scientists in Canberra. He leads me into this fantastic world of science and without his invaluable assistance, step-by-step guidance, insightful criticism as well as constructive suggestion, this work could not be imaginable. Professor Yongqiang patiently guided me through each draft of my writing and generously provided me any resources required for my project. I am so much in debt to his genuine advice and unconditional help. My special thanks go to the distinguished scientist Dr. Lu Zhang. Although he joined the panel later in the third year of my PhD, he has been very generous in providing crucial and critical advice especially during the second half of the project. Dr. Lu has always been a fantastic mentor and friend and it was an honour and pleasure to work and talk with him. Without his inspiration, support and encouragement, I could not make it to this point. His scientific achievement and noble personality have profound influence on me which will last long in my life. I am also deeply grateful to Professor Derek Eamus, who has provided insightful suggestions and shared important resources to enhance my research. His immense knowledge and expertise as well as inspirational advice play important role in the project.

This work also involves highly valuable efforts from several scientists working in different fields. I would like to thank Professor Alfredo Huete for reading through the proposal and giving inspiring suggestions during the development of this research. Dr. James Cleverly provided constructive discussions on physiological aspects of ecohydrological modelling. Dr. Francis H.S. Chiew provided advice in hydrological modelling. Professor Yuting Yang has

been generous in sharing inspiring ideas and discussions frequently throughout all the stages of my PhD. Professor Lei Cheng offered theoretical and technological advice countless times. Dr. Hao Shi shared Australian eddy covariance flux data and detailed instructions on programming as well as ecosystem modelling ideas. Dr. Enli Wang shared expertise on crop modelling. Dr. Willianm Woodgate, Dr. Vanessa Harverd and Dr. Ian Harman provided valuable advice on carbon modelling and related manuscript improvement. I would also like to thank Dr. Tim McVicar, Dr. Randall Donohue, Dr. Jorge Luis Peña Arancibia, Dr. Tony Fischer, Dr. Juergen Knauer for their insightful comments and encouragement, also their questions which strengthen this work to a higher level. Dongdong Kong always walks me through coding issues. I could not have imagined having achieved so much without their help.

I thank my fellows from UTS: Jie He, Dr. Jianxiu Shen, Dr. Qinggaozi Zhu, Dr. Xunhe Zhang, Dr. Zunyi Xie, Dr. Xuanlong Ma, Dr. Xueling Li, Dr. Bin Wang, Hong Zhang, Mingxi Zhang, Sicong Gao, and from CSIRO: Dr. Junlong Zhang, Dr. Yuanyuan Wang, Dr. Shulei Zhang, Dr. Chengcheng Zhong, Jean-Michel Perraud, Andrew Freebairn, Chenglu Huang, Yuhan Guo, Dr. Jing Teng, Dr. Dan Zhang, Dr. Haiyang Xi, for the encouragement and support, for the kindness in your hearts, and for all the memorable happy and difficult time we share. I am very grateful to the staff and research fellows from the Australian Energy and Water Exchange Research Initiative (OzEWEX) 2nd Climate and Water Summer Institute, especially Professor Albert van Dijk, Zac Hatfield-Dodds, Dr. Shuci Liu, Dr. Jennifer Wurtzel, for sharing valuable inspirations and joys during the 'low' period of my PhD.

I appreciate my friends, Dr. David Pepper, Dr. Siyuan Tian, Jack Chaney, Lili Zhang, Meghan Castelli, Matthew Young, Yuqi Wang, Dr. Zhigan Zhao, Dr. Di He, Yifei Zhou, Li Zhao, Dr. Bing Xing, Dr. Yufeng Ren, Xuankun Li, Min Zhao, Liwei Zhang and many others for joining my life and being there for me. Last but not the least, I would like to thank my family for their love, encouragement and understanding. My father Xiaojun Gan, mother Cuimei Bu, and my sister Lei Gan, have been supporting me spiritually and financially throughout my PhD far away from China. They have always offered me unconditional help and share my smiles and tears during this journey.

This research was financially supported by International Research Scholarships, University of Technology Sydney, Australia and the China Scholarship Council, Ministry of Education, China. Part of this research was supported by the GBA postgraduate top-up scholarship by CSIRO. UTS and CSIRO provided the facilities, infrastructures and resources for conducting this work, including the library services. I am grateful to consular Jing Zhao from the education

office, the consulate general of P.R. China in Sydney for taking care of the scholarship dispense and providing supportive information and resources. I am thankful to Shannon Hawkins, Maggie Chen, Emaly Black and staff from UTS Science Faculty and Graduate Research School, also Ruth Palmer, Nicole Van Schieveen, Gina Drummond and staff from CSIRO for their administrative assistance and help, which ensured a pleasant environment and convenient workflow during the candidature.

Publications arising from this thesis

Journal papers directly included in this thesis

Gan, R., Zhang, Y., Shi, H., Yang, Y., Eamus, D., Cheng, L., Chiew, F. H. S., & Yu, Q. (2018). Use of satellite leaf area index estimating evapotranspiration and gross assimilation for Australian ecosystems. Ecohydrology, (January), e1974. https://doi.org/10.1002/eco.1974 (Chapter 2)

Gan, R., Zhang, L., Wang, E., Woodgate, W., Zhang, Y., Haverd, V., Kong, D., Fischer, T., Chiew, H. S. F., & Yu, Q. (2019). Estimating ecosystem maximum light use efficiency based on water use efficiency principle. (Under internal review) (Chapter 5)

Parts of the journal papers arising from this thesis

Zhang, Y., Kong, D., Gan, R., Chiew, F. H. S., McVicar, T. R., Zhang, Q., & Yang, Y., (2019). Coupled estimation of 500m and 8-day resolution global evapotranspiration and gross primary production in 2002-2017. Remote Sensing of Environment, 222 (December 2018), 165-182. https://doi.org/S003442571830590X Peer-reviewed conference Proceedings (Chapter 3 and 4)

Peer-reviewed International Conference proceedings

Dec 2019 The 23rd International Congress on Modelling and Simulation (MODSIM), Canberra, Australia, 3-8 December 2019. An ecohydrological model for estimating streamflow, evapotranspiration and gross primary production for Australian catchments (Submitted).

APR 2019 The European Geosciences Union General Assembly (EGU), Vienna, Austria, 7-12 April 2019. Estimating Ecosystem maximum light use efficiency from water use efficiency principle (Poster presentation).

DEC 2018 The American Geophysical Union Fall Meeting (AGU), Washington D.C., USA, 10-14 December 2018. Uncertainty of transpiration estimates from a coupled water and carbon model in grassland ecosystems (Poster presentation)

Dec 2017 The 22nd International Congress on Modelling and Simulation (MODSIM), Hobart, Tasmania, Australia, 3-8 December 2017. Estimating water and carbon fluxes using a simple diagnostic model (Oral presentation).

Contents

List of Figures

List of Tables

Glossary

ET	*evapotranspiration (mm d^{-1})*
E	*evaporation from wet surface (mm d^{-1})*
T	*transpiration from vegetation (mm d^{-1})*
GPP	*gross primary production (µmol m^{-2} s^{-1} or g C m^{-2} d^{-1})*
Q	*Streamflow (mm d^{-1})*
LE	*latent heat (W m^{-2})*
H	*sensible heat (W m^{-2})*
G	*ground heat flux (W m^{-2})*
CO_2	*carbon dioxide*
C_a	*atmospheric* CO_2 concentration (parts per million)
eCO_2	*elevated carbon dioxide concentration in the atmosphere*
G_s	*surface conductance (m s^{-1})*
G_c	*canopy conductance (m s^{-1})*
g_s	*stomatal conductance (m s^{-1})*
k_Q	*light extinction coefficient of shortwave radiation*
k_A	*light extinction coefficient of available energy*
α	*initial slope of the light response curve to assimilation rate (µmol CO_2 (µmol PAR)$^{-1}$)*
η	*initial slope of the CO_2 response curve to assimilation rate (µmol m^{-2} s^{-1} (µmol m^{-2} s^{-1})$^{-1}$)*
$V_{m,25}$	*notional maximum catalytic capacity of Rubisco per unit leaf area at 25 ˚C (µmol m^{-2} s^{-1})*
m	*stomatal conductance coefficient*
MODIS	*Moderate Resolution Imaging Spectroradiometer*
LAI	*leaf area index (m^2 m^{-2})*
SPAC	*soil-plant-atmosphere continuum*
LSMs	*land surface models*
VPD	*water vapour pressure deficit (kPa)*
RR	*rainfall-runoff model*
XAJ	*Xinanjiang model*
ε_{max}	*maximum light use efficiency (g C MJ^{-1} PAR)*
LUE	*light use efficiency (g C MJ^{-1} PAR)*
WUE	*water use efficiency (g C kg^{-1} H_2O)*
uWUE	*underlying water use efficiency (g C kg^{-1} H_2O $kPa^{0.5}$)*
PAR	*photosynthetically active radiation (W m^{-2})*
f_{APAR}	*fraction of vegetation absorbed photosynthetically active radiation (%)*
R_n	*net radiation (W m^{-2})*
f_{Rn}	*fraction of vegetation absorbed net radiation (%)*
f_s	*stress factor (unitless, 0-1)*
PET	*potential evapotranspiration (mm d^{-1})*
PT	*potential transpiration (mm d^{-1})*
A	*assimilation (µmol m^{-2} s^{-1} or g C m^{-2} d^{-1})*
PA	*potential assimilation (µmol m^{-2} s^{-1} or g C m^{-2} d^{-1})*
NSE	*Nash-Sutcliffe efficiency*

R^2	*coefficient of determination*
RMSE	*root mean square error*
PFT	*plant functional type*

Abstract

Understanding of the interaction between hydrological and ecological processes has significant implications in natural resources management especially under climate change. This thesis aims to investigate the coupled water and carbon cycles by developing simple but robust models to quantify and evaluate key ecohydrological variables therefore assist potential decision making requirement.

The literature review stands upon the fundamental coupling relationship between water and carbon exchanges regulated by vegetation within the soil-plant-atmosphere continuum, which highlights the challenge and requirement of water modelling (including evapotranspiration (ET) and streamflow (Q)) considering carbon constraint (photosynthesis, quantified by gross primary production (GPP)), and vice versa. Across ecosystem and catchment scales, simple but robust models are developed and evaluated to understand and quantify the interactions and variations of these key ecohydrological variables, especially under anthropogenic climate change. Consistent findings following the motivation of this thesis demonstrate that:

(1) The coupled relationship between water and carbon fluxes can be incorporated into canopy conductance to simulate ET and GPP simultaneously. A diagnostic model (PML_V2) with simple model structure and limited number of parameter is developed and examined at 9 Australian eddy-covariance flux sites. Result shows that the model is simple and robust in estimating ET and GPP at ecosystem scale, indicated by NSE being about 0.70 and 0.66, and RMSE about 0.96 mm d^{-1} and 1.14 μmol m^{-2} s^{-1} for ET and GPP, respectively. The model can serve as a practical and reliable tool to quantify ET and GPP over larger spatial and longer temporal scales.

(2) To simulate water (ET and Q) and carbon (GPP) processes at catchment scale, the PML-V2 model is further incorporated to a traditional hydrological model (XAJ). The incorporation is done using PML_V2 to replace ET submodule of the original XAJ, and the updated XAJ model has 12 parameters. The updated XAJ model is preliminarily tested across 63 Australian catchments for Q and 13 eddy-covariance flux sites for ET and GPP. Result shows that the model performs reasonably well for estimating catchment Q (NSE about 0.64) and ET (R^2 about 0.5), not so well for GPP (R^2<0.5). The updated XAJ hydrological model has potential to simulate hydrological consequence of atmospheric CO_2 increase. Preliminary model experiment under 45% increase of atmospheric CO_2 suggests a 12% increase in Q, with only 4% decrease in ET as a result of stomata closure in vegetation.

(3) Vegetation control of water exchange via ET is further investigated by evaluating uncertainty in transpiration (T) estimates using PML_V2 model. It is shown that T estimates exhibit high variation across seasons and sites (with GPP taken as carbon constraint), which can be partially explained by vegetation leaf area index and precipitation, respectively. T estimates from PML_V2 model is further compared to that from a water use efficiency based ET partitioning method, with results indicating inconsistent quantity and variation in T/ET, which highlights the uncertainty in T estimates even with carbon constraint taking into consideration.

(4) Based on the coupling relationship of water and carbon exchanges, carbon estimates can be constrained from vegetation water use in mechanism. This leads to the development of an analytical method to estimate maximum light use efficiency (ε_{max}) (that is key for estimating carbon) by implementing the water use efficiency principle. Examination of the method at 52 eddy-covariance flux sites located across the globe suggests the simplicity and capability of the method in providing ε_{max} estimates across ecosystems dominated by different species (with different photosynthetic pathways, e.g., C3, C4) and biomes (with different plant functional types, e.g., forest, grass). The method enables water based interpretation of carbon process and the ε_{max} estimates can be used to simulate GPP with water constraint.

This thesis provides systematic understanding of water and carbon processes over ecosystem and catchment scale using modelling approaches. Particularly, two ecohydrological models have been developed to simulate streamflow, evapotranspiration and gross primary production systematically. Variation and uncertainty of water estimates are investigated based on carbon constraint. An analytical method is developed to evaluate key parameter for GPP estimation based on vegetation water use. To better interpret and quantify key ecohydrological processes under anthropogenic and climate change impacts, the models built in this thesis need to be further developed through better model structure, advanced parameterization schemes or multi-data sources.

Key words: ecohydrology, water and carbon interaction, evapotranspiration, streamflow,

light use efficiency, water use efficiency, model, climate change

Chapter 1. Introduction

1.1 Background to the question

The interaction between terrestrial vegetation and the water cycle is the core ecohydrological process that is investigated in this thesis. The overall objective is to provide a mechanistic understanding of plant regulation of both carbon and water processes via modelling and analytical approaches. As background supporting the research questions addressed within this thesis, this section introduces the relationship between carbon and water, how the two fluxes have been examined using modelling approaches, and the key challenges of ecological and hydrological processes induced by climate change.

1.1.1 Relationship between water and carbon

Terrestrial vegetation is the most important physical medium between the biosphere and the hydrosphere, linking the energy, water, and carbon exchanges of the Earth (Campbell & Norman, 1998; Eagleson, 2005). Driven by energy, the two fundamental ecohydrological processes, namely photosynthesis and evapotranspiration, are both regulated by vegetation to determine the largest carbon and water fluxes between the atmosphere and land the surface (Christian Beer et al., 2010; Good et al., 2015). Plants assimilate carbon dioxide (CO_2) from the atmosphere by photosynthesis to produce carbohydrates for growth. At the same time, water is extracted from the root zone and lost through transpiration to support plant functioning. Thus, mass transfer of carbon and water are biophysically coupled through vegetation.

The coupled relationship between water and carbon processes is inherently complex due to the response and feedback loop as (1) plants respond to water availability (i.e., changes to plant water status in response to soil moisture and precipitation), and (2) plant feedback on water availability (through transpiration to evapotranspiration), all of which are primarily driven by available energy and interrelated to each other within the soil-plant-atmosphere continuum (SPAC).

From a response perspective, plants need water to assimilate carbon. In the short term (hours to days), plant water status, which depends on soil and atmospheric water status, controls the opening and closing of stomatal apertures in plant leaves (Passioura, 1982). Water vapour diffuses through stomatal apertures from the plant to the atmosphere as transpiration, and CO_2 diffuses from the atmosphere into the plant to be utilised for photosynthetic productivity. When

water is ample (wet soil and humid air), stomata tend to open (high stomatal conductance) resulting in higher rates of CO_2 and water vapour transport, which leads to higher rates of photosynthesis and transpiration, respectively (Jarvis, 1976; Ju et al., 2006). However, when water is inadequate (dry soil and arid air), stomata tend to close (low stomatal conductance) and consequently sustain lower rates of photosynthesis and transpiration (Porporato et al., 2001). Hence, plants response to environmental water status (soil and atmospheric) by controlling stomatal behaviour to balance the mass flow of carbon and water (i.e., minimising water use while maximising carbon gain) (Cowan, 1982; Wong et al., 1979). In the long term (seasonal and longer), plant responses to precipitation, which determines environmental water status and thus plant water status, control the number and behaviour of bulk stomata and thereby regulate land surface carbon and water exchange. This biophysical response accumulates at larger levels of plant organisation, where water availability determines plant morphology and phenology by allocating photosynthetic productivity to form roots, leaf area, canopy composition, and vegetation communities. Under certain conditions (e.g., sufficient radiation and nutrient availability), greater precipitation often sustains more plants, greater leaf area index (LAI), denser canopies, and a rich diversity of plant species. Consequently, accumulated number and opening of stomata lead to greater photosynthetic productivity and evapotranspiration across space and time. For instance, precipitation is generally more than 3000 mm y^{-1} over the Amazon rainforests, constituting approximately 400 billion trees that account for up to a quarter of the total carbon uptake over the Earth's land surface and a massive water consumption through evapotranspiration of over 1500 mm y^{-1} (Maeda et al., 2017).

From a feedback viewpoint, plant water use subsequently influences environmental water status, which in turn regulates vegetation behaviour over multiple scales. For example, when vegetation persistently depletes soil moisture through transpiration to a critical level such as the wilting point, water stress is induced causing stomatal closure, which subsequently leads to decreased photosynthesis and transpiration (Zhou et al., 2014). When soil water stress is combined with high atmospheric water demand, biophysical failure, or die-off of plants, often occurs that further reduces photosynthesis and transpiration (Eamus et al., 2013). However, vegetation feedback on the water and carbon cycles is not simply a 'negative' effect. On larger spatiotemporal scales, the more water that is returned to the atmosphere, the more likely precipitation is going to occur. As a result of increased precipitation, water in the soil and the atmosphere is increased to form a more favourable environment for plants to grow, thereby increasing photosynthetic productivity and transpiration (Levis et al., 2000). In another case,

under enhanced CO_2 (eCO_2) conditions due to anthropogenic climate change, soil water can increase in response to reduced plant transpiration (since stomata tend to close under eCO_2, i.e., 'water saving' effect) (Cech et al., 2003). At the same time, soil water can also decrease because more water can be transpired by plants due to increased LAI as a result of enhanced photosynthesis (i.e., 'greening' or 'fertilization' effect) (Zhang et al., 2015). As such, the net effect of vegetation feedback on water and carbon balance depends on both 'negative' and 'positive' impacts (Hovenden et al., 2014; Kergoat et al., 2002), which are often accompanied by great variation across ecosystems and climate conditions (Hovenden et al., 2019; Tietjen et al., 2017; Zeng et al., 2017).

These complex response and feedback mechanisms demonstrate the pivotal role terrestrial vegetation plays in regulating water and carbon budgets, primarily through plant stomata within SPAC (Gentine et al., 2019). Therefore, understanding the biophysical interaction between water and carbon fluxes is significantly important. Better quantification of these two processes will improve essential resource management processes that include water availability and ecosystem productivity within and across the scope of ecohydrology.

1.1.2 Water modelling with carbon constraint

One of the fundamental questions in ecohydrology is how to quantify land surface water after precipitation. This includes water flux from the land surface to the atmosphere, i.e., evapotranspiration (Good et al., 2015; Wang & Dickinson, 2012), and the net difference between precipitation and evapotranspiration, i.e., streamflow (Donohue et al., 2012; Zhang et al., 2018). Although it is apparent and undisputedly acknowledged that evapotranspiration plays an essential role in linking the energy balance, water budget and carbon cycle, it is an important process that is difficult to directly measure or estimate.

A wide variety of observational techniques have been developed to quantify evapotranspiration, including its three main components (transpiration, soil evaporation, and interception). Due to the physical differences among these components, each must be measured directly and separately (Stoy et al., 2019). However, this can be difficult. Chamber, porometer, sap flow and lysimeter techniques have been used to obtain transpiration and/or evaporation from leaves, plants for soil surface (Poyatos et al., 2016; Shuttleworth, 2007). For larger scales measurements (e.g., ecosystem, region, or continent), methods using stable isotopes, eddy covariance, Bowen ratio, and water balance (land surface or atmosphere) have been implemented to infer total evapotranspiration (Shuttleworth, 2007; Verstraeten et al., 2008).

Complimentary observations also involving radiometric spectral images from aerial and satellite sensors are indirect measurements that often need further translation through modelling to derive evapotranspiration over terrestrial surfaces (Kustas and Norman, 1996; Li et al., 2009). While these are considered important observational techniques, they are known to be complex, labour intensive and expensive, and have spatial and temporal limitations (Wang & Dickinson, 2012).

A preferable approach for understanding and quantifying integrated ecohydrological processes across spatiotemporal scales is to use model in conjunction with measurement techniques. A large number of evapotranspiration studies have been conducted and numerous algorithms have been proposed. Because evapotranspiration is an important factor for both energy and water balances, it can be evaluated as either an energy term (from latent heat flux) or water flux, depending on the primary budget of consideration. Comprehensive reviews of typical evapotranspiration algorithms can be found in Li et al., (2009), Shuttleworth, (2007), Verstraeten et al., (2008), Wang and Dickinson, (2012) and Zhang et al., (2016). The current review provided here is distinguished from these previous works by taking the coupled water and carbon perspective, which is based on the fundamental interaction between vegetation and water as demonstrated earlier (Section 1.1.1).

Evapotranspiration has traditionally been estimated based on the mechanistic approach of the Penman-Monteith method. Following the Monin-Obukhov Similarity Theory (MOST) (Monin & Obukhov, 1954), Penman (1948) first proposed the combined formulation of water vapour transport over a saturated surface subjected to both radiative and aerodynamic forcing, known as the Penman equation. Apart from thermodynamic control, Monteith (1965) later emphasised the physiological control of the water transfer process over vegetated surfaces by introducing the surface resistance (resistance is the inverse of conductance) term into the Penman equation. Since then, the Penman-Monteith equation has been extensively investigated and used for evapotranspiration estimation over the past half-century (Dolman et al., 2014). One of the primary challenges has always been parameterising the surface resistance term, as it is a conceptualised biophysical parameter that is difficult to observe or quantify directly (Zhang et al., 2016). Over vegetated surfaces fully coupled with the atmosphere, surface resistance can be viewed as determined only by plant biophysics. Therefore, bulk canopy resistance can be derived by integrating leaf level stomatal resistance (Jarvis & McNaughton, 1986). Considering the intrinsic coupling between water and carbon, this process-based modelling framework can be used to mechanistically incorporate carbon processes into evapotranspiration estimation.

Two stomatal conductance model, namely the Jarvis-Stewart model (Jarvis, 1976; Stewart, 1988) and the Ball-Berry model (Ball et al., 1987), have been widely used for upscaling purposes. Both models are based on the empirical relationships found between stomatal conductance and environmental and/or biophysical variables, such as incident solar radiation, temperature (leaf T_{leaf} or air T_{air}), vapour pressure deficit (VPD), soil moisture (θ), CO_2 concentration (intercellular C_i or atmospheric C_a), and photosynthesis (Damour et al., 2010; Leuning, 1995; Tuzet et al., 2003). These two types of models differ from each other in fundamental ways, by accounting for carbon either implicitly through CO_2 concentration (Jarvis-Stewart) or explicitly through photosynthesis (Ball-Berry). Specifically, while the Jarvis-Stewart model takes CO_2 concentration (together with other environmental variables) as an independent stress factor to reduce maximum stomatal conductance, the Ball-Berry model explicitly expresses stomatal conductance as a function of photosynthesis (Collatz et al., 1991; Farquhar et al., 1980; Medlyn et al., 2011). Therefore, the Ball-Berry model is theoretically advantageous as photosynthesis and transpiration are mechanistically linked through stomatal conductance. Hence, the Ball-Berry model can be used to simulate both fluxes as integrated processes.

Indeed, evapotranspiration (and other water fluxes including streamflow) need to be evaluated with carbon constrain due to physiological control by vegetation, and vice versa. Yet it has only been in the past few decades (with studies initiated around the end of 20th century) that an emerging emphasis and attention has been given to develop coupled frameworks considering energy, water, and carbon budgets in order to address climate change challenges (e.g., eCO_2, land use changes) (Sato et al., 2015). By far, only the third generation of land surface models (LSMs) are such process-based modelling schemes that incorporate and simulate energy, water, and carbon balances simultaneously (Pitman, 2003; Prentice et al., 2015; Sato et al., 2015; Sellers, 1997; Zhao & Li, 2015). With meteorological forcing as inputs (e.g., radiation, temperature, precipitation), LSMs use combined series of sub-models to represent radiation, hydrological, and physiological processes using combined equation series to simulate key ecohydrological variables including evapotranspiration and photosynthesis (Zhao & Li, 2015). The coupled simulation of water and carbon processes using this complicated modelling framework is generally achieved in two steps: (1) simulating photosynthesis through empirical or biochemical photosynthesis sub-models, and (2) combining photosynthesis with transpiration though stomata conductance. For the first step, the most sophisticated biochemical model widely adopted is the well-known Farquhar et al.

(1980) method, with photosynthesis calculated as the minimum rate limited by either Rubisco carboxylation, ribulose-1,5-bisphosphate (RuBP), or triose phosphate utilization (TPU) (Farquhar & von Caemmerer, 1982; Sharkey, 1985). For the second step, the Ball-Berry model is applied, with stomatal conductance calculated as a function of photosynthesis from the previous step. The optimal water use efficiency (WUE, ratio of photosynthesis to transpiration) assumption is used to incorporate these two steps, where vegetation is assumed to regulate carbon gain and water loss to minimise WUE (maximising photosynthesis while minimising transpiration) (Cowan & Farquhar, 1977; Wong et al., 1979). Mathematically, this is achieved by solving the biochemistry model and stomatal conductance model iteratively (the FvCB modelling framework) (Collatz et al., 1991, 1992; Farquhar et al., 1980; Medlyn et al., 2011; Tuzet et al., 2003). When further upscaled to the bulk canopy, these sub-models are incorporated with 'big-leaf' or 'multi-layer' assumptions to formulate canopy to surface resistance, and further combined with a Penman-Monteith type of equation and energy balance (Shuttleworth & Wallace, 1985). As such, LSMs are capable of simulating energy, carbon, and water exchanges simultaneously. Typical LSMs such as SiB2 (Sellers et al., 1996) and CABLE (Wang & Leuning, 1998) all share this similar structure (Rogers et al., 2017). Such combined physical and biophysical modelling schemes are mechanistically profound, and hence have merit for comprehensive interpretation of the ecohydrological responses and feedbacks within the SPAC (Pitman, 2003; Prentice et al., 2015).

However, the inherent complexity (with physical and biosphere processes represented in extensive detail) and focus (on climate and energy) inevitably limit LSMs for practical use. In fact, as a result of combining several of sub-models, LSMs often consist of many numerical equations (e.g., energy partitioning, water and carbon budgets) and a considerable number of parameters (e.g., biochemistry, biophysics, soil properties, land cover) (Prentice et al., 2015). Therefore, solving the equation series and calibrating the model parameters is often highly time-consuming and computationally expensive, and models tend to be subjected to equifinality (Haddeland et al., 2011; Long et al., 2014; Wood et al., 2011). Additionally, while the course spatial resolution (~100 km) of LSMs means that they can be conveniently incorporated with climate models at larger scales (e.g., continental to global), this course spatial resolution is problematic for finer scale investigations (e.g., site to catchment). This is especially the case for heterogeneous terrain features such as when topography, soil, and vegetation become dominant in regulating land surface processes (Zhao & Li, 2015). Additionally, LSMs exhibit noticeably high uncertainty in terms of water modelling, especially

regarding the components of evapotranspiration, despite the fact that total evapotranspiration is usually well constrained (through energy partitioning) (Anav et al., 2013; Miralles et al., 2016; Murray-Tortarolo et al., 2013; Overgaard et al., 2006; Prentice et al., 2015; Wei et al., 2017). Difficulties also remain because of poorly understood or incompletely represented hydrological processes, such as drainage, runoff routing, and groundwater storage., such so that error/uncertainty accumulates when reproducing runoff (Bierkens et al., 2015; Haddeland et al., 2011; Kauffeldt et al., 2016; Pitman, 2003; Prentice et al., 2015; Wood et al., 2011).

In contrast to LSMs, traditional hydrological models tend to focus on water dynamics, with biological processes, especially carbon assimilation, commonly ignored despite their importance. Over the last decade, emerging emphasis have been put to incorporate vegetation dynamics into hydrological modelling (Donohue et al., 2007; Zhang et al., 2001). Studies in this area have shown that when vegetation features (e.g., LAI, rooting depth, fraction of absorbed PAR (fPAR)) were empirically incorporated into hydrological models, simulations of water flow (e.g., evapotranspiration, runoff) were improved in space and time (Zhang et al., 2009), especially under shifting vegetation conditions (Zhou et al., 2013). This indeed emphasises the significant role vegetation plays in regulating the water cycle, although carbon processes are implicitly represented using vegetation indices (Donohue et al., 2012). At the current time, very few statistical (e.g., 'black-box'), conceptual (e.g., rainfall-runoff model), or physical (e.g., distributed model) hydrological models (see hydrological model reviews by Devi et al., 2015; Wood et al., 2011) have explicitly incorporated carbon processes into their modelling schemes. Notwithstanding that some models have incorporated stomatal conductance, where the Jarvis-Stuart formula is used to account for environmental stresses (e.g., soil moisture, solar radiation, temperature, VPD) (Devonec & Barros, 2002; Garcia-Quijano & Barros, 2005; Yildiz & Barros, 2006; Zhang et al., 2009), these models nevertheless lack explicit carbon constraints. However, the challenge of applying the more biophysically based FvCB modelling framework remains because (1) photosynthesis is relatively complicated to simulate using the biochemical model (e.g., Farquhar method), (2) stomatal response and feedback require iterative numerical solutions to solve the biochemical-stomatal equation series, and (3) scaling from leaf to canopy and larger levels is difficult for such complicated mechanisms (Farquhar et al., 2001). This makes the coupling of biophysical processes into hydrological models challenging. Consequently, the comprehensive evaluation of terrestrial carbon and water cycles is difficult.

In summary, advanced ecohydrological models are still in high demand. Compared with the most sophisticated LSMs, less complicated models that are able to present key ecohydrological processes are required. Such models should accurately reproduce not only evapotranspiration (including its components) but also streamflow (Prentice et al., 2015). Also, the inadequate representation of biophysical process in traditional hydrological models should be improved to better simulate vegetation control over water estimates (transpiration and photosynthesis), thereby reducing possible uncertainty. As such, simple but accurate ecohydrological modelling scheme is a promising direction that needs further investigation. Such modelling will not only provide insightful understanding of hydrological and ecological interactions, but also enable sustainable management of resources (water and carbon) based on simple but credible simulations that are mechanistically reliable, especially under anthropogenic climate change (Gentine et al., 2019).

1.1.3 Carbon estimation from a water perspective

Compared with hydrological processes, photosynthesis is a fundamental biological process that is critical to all living organisms, yet even more difficult to measure or estimate due to its intrinsic complexity. Over the past few decades, extensive studies have been conducted to observe and simulate photosynthesis on leaf, plant, ecosystem, and regional scales (Wu et al., 2016; Yin & Struik, 2009). A comprehensive review regarding measuring techniques can be found in Field et al. (2000). Due to the overall water focus of this thesis, only a brief introduction of the photosynthesis modelling approaches is provided here, covering both bottom-up and top-down schemes (for a comprehensive review, refer to Wu et al., 2016; Yin & Struik, 2009). Two of these methods are adopted and will be discussed in greater detail later in connection with the specific purposes of the simulations conducted in this study.

In general, bottom-up algorithms for photosynthesis estimation can be categorised into three groups. The first group is the empirical light use efficiency (LUE) method as originated with Monteith, (1972, 1977). Similar to the Jarvis-Stuart stomatal conductance model, vegetation assimilation rate (A) is expressed simply as a function of maximum LUE multiplied by environmental stress factors scaled between 0-1 to downregulate the maximum. The physiological basis of this framework is that vegetation converts solar energy into biochemical energy (stored in carbohydrates) in a linear manner, and the actual conversion efficiency is often less than the optimal value because of limitations imposed by environmental constraints, such as light quality, temperature threshold, water, and nutrient availability (Medlyn, 1998;

Sinclair & Muchow, 1999). The second group is the semi-empirical model based on a light response curve, such as the representative hyperbola functions of Thornley (1970, 1976). Models in this category have similar photosynthetic response that follow the Michaelis-Menten kinetics, which describes a curvilinear response of enzyme reactions to environmental variables (e.g., light, CO_2) (Maskell, 1928; Thornley, 1998). Either a rectangular or non-rectangular hyperbola function is preferred for simplicity or theoretical considerations, respectively (Johnson & Thornley, 1984; Xu et al., 2014; Ye et al., 2013). Lastly are the process-based biochemical photosynthetic models for C_3 and C_4 species, well-known as the FvCB model (von Caemmerer, 2000, 2013; von Caemmerer & Farquhar, 1981; Farquhar et al., 1980). This is the most sophisticated method, where photosynthetic rate is determined by the minimum of (a) electron transport, which is a function of photosynthetically active radiation (PAR), (b) enzyme kinetics, which represent the activity of the carboxylation enzyme (Rubisco) and (c) transport capacity, which describes the utilisation of photosynthetic products (Farquhar & von Caemmerer, 1982; Sharkey, 1985). A stomatal conductance (g_s) model is required to be incorporated with this photosynthesis model due to its requirement of intercellular CO_2 concentration (Collatz et al., 1991; Ray Leuning, 1995; Tuzet et al., 2003). Numerical iteration can be applied to solved the coupled equation series in order to obtain photosynthesis estimates (Yin & Struik, 2009).

Each of these three algorithms has its own merits and limits. For example, the extreme simplicity of the LUE method makes it practical and efficient for modelling purpose. Hence, it is the mostly widely used framework for estimating photosynthetic gross primary production (GPP), especially on large spatiotemporal scales combined with remote sensing data (Cheng et al., 2014; Gitelson et al., 2015; Prince, 1991; Zhang et al., 2017). Yet it is often criticised because the linear relationship used between absorbed photosynthetically active radiation (APAR) and GPP is contradictory to the nonlinear light response curve widely observed in leaf level experiments (Medlyn, 1998). In this regard, a hyperbolic function provides a more plausible solution for simulating the nonlinear relationship (Johnson & Thornley, 1984; Thornley, 1976). Yet the few model parameters (typically two or three) determined were found to be insufficient to account for other physiological attributes (such as nitrogen content) which significantly influence photosynthesis (Sinclair & Horie, 1989; Sinclair & Muchow, 1999; Xu et al., 2014). In contrast to the relative simplicity of the LUE models, the mechanistic FvCB framework is suitable for detailed representation of the interrelated biochemical and biophysical processes (e.g., electron transport, Rubisco activity, leaf nitrogen, mesophyll

conductance) (Flexas et al., 2008; Yin et al., 2004, 2006). However, such a coupled modelling scheme requires kinetic parameters that are often not available or not yet well quantified (e.g., maximum rate of Rubisco carboxylase activity ($V_{c,max}$), the maximum rate of photosynthetic electron transport (J_{max})) across spatiotemporal scales (Lin et al., 2015; Medlyn et al., 2002; Yin et al., 2006). Because of the great variation that exists in various environmental factors (e.g., T_a, VPD, C_a), additional uncertainty is likely to occur when scaling leaf photosynthesis up to canopy, regional, and global scales (Rogers et al., 2017; Wu et al., 2016; Yin et al., 2004).

Apart from the physically-oriented methods mentioned above, estimates of photosynthesis can be inferred using top-down approaches, such as those based on WUE. In fact, this group of methods directly implements the coupling relationship between photosynthesis and transpiration. The framework follows the fundamental principle that photosynthesis and transpiration are both regulated by plant stomata which follows Fick's law, so that if one of these two variables is known, or can be conveniently estimated, the other can be derived directly based on WUE (Ritchie, 1983; Sinclair et al., 1984; Tanner & Sinclair, 1983). Indeed, WUE is approximately constant when normalised by atmospheric water demand (potential evapotranspiration (PET) or VPD) (Beer et al., 2009; Zhou et al., 2014). Hence, given a certain amount of transpiration, assimilation can be easily estimated by multiplying transpiration with WUE normalised by PET or VPD. This is in fact a widely used framework within the crop modelling community for estimating carbon uptake (e.g., biomass, crop yield) (see the typical crop model APSIM (Holzworth et al., 2014; Keating et al., 2003; Wang et al., 2002)). Earlier studies as reviewed by Sinclair et al. (1984) and Tanner & Sinclair (1983) continue to play a significant role in more recent crop models (Holzworth et al., 2014). Generally, carbon assimilation estimates constrained by vegetation water use can be derived from the relationship between either (1) actual and maximum WUE or (2) actual WUE and environmental conditions (e.g., relative humidity or VPD, CO_2 concentration) (Tanner & Sinclair, 1983). To describe photosynthetic productivity using these relationships, transpiration (either actual and/or potential) can be obtained by employing evapotranspiration models such as the Penman-Monteith equation. When compared with the equation and parameter series required by the bottom-up approaches, the WUE method is theoretically sound and practically simple to use.

Considering the overarching objectives of this thesis, the semi-empirical hyperbola photosynthesis model and Ball-Berry stomata conductance model were adopted to develop a carbon constrained ecohydrological model. The LUE framework was combined with WUE to

derive an analytical solution for a key parameter (constrained by vegetation water use) used to estimate GPP.

1.1.4 Ecohydrological processes under climate change

Evidence of climate change has been observed, and these changes will continue to pose significant challenges upon ecosystems, with subsequent consequences on the vital resources and services they provide to human society, including water and food (IPCC, 2014). One of the fundamental requirements for supporting sustainable development is advanced interpretation of ecohydrological processes within the SPAC (Eagleson, 1978; Hutjes et al., 1998; Montanari et al., 2013). Extensive studies conducted during the past few decades have clearly shown that terrestrial ecosystems and the water cycle have been modified from both ecological and hydrological perspectives.

Within the SPAC, altered energy, carbon, and water exchanges have been observed in response to variations of key climate factors including temperature, water availability, and radiation as well as greenhouse gases (primarily CO_2), along with distinct sensitivity across terrestrial ecosystem types (Seddon et al., 2016). For example, increased latent heat (evapotranspiration in the energy term) was found over grass ecosystems as a result of increased solar radiation and temperature (accelerated soil water depletion in response to increased temperature), while a more conservative response was found for forest ecosystems (less water loss to in response to increased temperature) (Teuling et al., 2010). In Australia, however, forests were shown to increase latent heat (151%) and carbon uptake (112%) during the 2012 heatwave, whereas woodlands experienced the opposite response (Van Gorsel et al., 2016). Other studies have also detected reductions in carbon uptake due to heat and water stress across a variety of ecosystems during the 2003 European drought (Ciais et al., 2005), the 2012 US summer drought (Wolf et al., 2016), and the 2013 southern China drought (Yuan et al., 2015). It is now widely acknowledged that ecosystems are vulnerable to decreases in water availability and increases in temperature (despite different response in direction and magnitude), known as the 'negative effect' of climate change (Allen et al., 2010a; Tietjen et al., 2017). In addition, the 'positive effect' is also evident as a result of elevated carbon dioxide concentration (eCO_2) in the atmosphere. For instance, boosted carbon uptake through photosynthesis (known as 'greening' or 'CO_2 fertilisation') has been observed globally (Donohue et al., 2013; Zhu et al., 2016). This is inevitably accompanied by physiology (stomatal closure) and structural (LAI) responses that subsequently influence ecosystem water use and climate feedback (Ainsworth

& Long, 2005; Ellsworth, 1999; Frank et al., 2015; Lee et al., 2001; Belinda E Medlyn et al., 2001; Tenhunen et al., 1984; Uddling et al., 2009). Highly variable changes in vegetation growth, biochemistry and biophysics have been reported when considering different species (e.g., C_3, C_4 (Lee et al., 2001)) and biome groups (e.g., forests, grasslands (Ainsworth & Long, 2005)) across leaf to ecosystem scales. Therefore, understanding modified ecosystem functioning due to climate change remains a major challenge.

An acceleration of the water cycle has long been recognised as a result of global warming (IPCC, 2014). Key fresh water fluxes over and below land surfaces, including precipitation, evapotranspiration, streamflow, and groundwater, have been modified, echoing the changes of the hydrological cycle (Milly et al., 2005; Stocker & Raible, 2005). These changes can increase precipitation intensity, frequency and uncertainty of distribution of extreme events, which can lead to droughts (Dai, 2011; Trenberth et al., 2014) and floods (Hirabayashi et al., 2013) globally. Evapotranspiration is also altered simultaneously. Increases in evapotranspiration (+7.1 mm yr^{-1}) have been detected during the 1982-1997 period followed by a period of stable evapotranspiration during 1998-2008 (Jung et al., 2010), and another period of increasing evapotranspiration afterwards (+0.88 mm yr^{-1}) (Zhang et al., 2015). In addition to these global trends in evapotranspiration changes, significant variability of evapotranspiration and its components have been reported for different continents (e.g., Africa and America in contrast to Australia and Europe) (Zhang et al., 2016). As a result, water yield (the net difference between precipitation and evapotranspiration) has changed. For the driest continent, Australia, the impact can be extremely significant, where only a 1% decrease in rainfall can be amplified up to a 4.1% decrease in streamflow (Chiew, 2006; Van Dijk et al., 2013). Across the globe, with eCO_2 impact on evapotranspiration through biophysical and physiological processes, streamflow has been found/projected to either decrease (Betts et al., 2007; Ukkola et al., 2015), increase (Gedney et al., 2006), or remain unchanged (Cheng et al., 2017; Piao et al., 2007; Yang et al., 2016). In addition to changes in surface water, groundwater is also facing direct and indirect threats in response to altered land surface processes. Extremely large variations of geophysical recharge and discharge can be induced by snow melting, rainfall patterns, ecosystem functioning, and human activities, with an uncertainty range of up to ±80% across continents (Green et al., 2011; Taylor et al., 2013). Systematically, the altered hydrosphere has significant impacts on and implication for on fresh water availability, which further modifies ecosystem functioning through SPAC.

In the facing of such challenges, mechanistic understanding of the bridging of ecohydrological processes between the biosphere and hydrosphere is central to providing fundamental support for resource management and climate adaptation and mitigation. Coupled relationship between carbon and water should be implemented when simulating the ecohydrological variables. Practical but robust modelling approaches need to be developed and investigated to evaluate variations of key processes under climate change.

1.2 Statement of significance and knowledge gaps

Key ecohydrological processes, including photosynthesis, evapotranspiration, and streamflow, are regulated by vegetation through biophysical and physiological responses and feedback. Significant challenges still remain in understanding and quantifying these processes, requiring further investigation to support natural resources management.

Evapotranspiration and photosynthesis are often estimated separately using different diagnostic models at the ecosystem scale, regardless of the mechanistic link between the two processes (Leuning et al., 2008). Current models may not sufficiently represent the coupled relationship between carbon and water, thereby impeding accurate estimation of both fluxes (Liu et al., 2017). Therefore, it is important to develop new models that simultaneously simulates evapotranspiration and photosynthesis. This will not only enable in-depth interpretation of the fundamental interactions of water and carbon processes, but will also enhance management of water and carbon resources across spatiotemporal scales.

Existing process-based models represent carbon and water processes in extensive detail, yet fail to adequately reproduce hydrological variables (especially water yield) (e.g., LSMs, Sellers et al., 1996; Wang & Leuning, 1998). At the same time, traditional hydrological models almost completely lack representation of vegetation processes, and therefore are inadequate for evaluating the carbon influence on the water cycle (e.g., rainfall-runoff models, Zhao, 1992). At a catchment scale, simple but mechanistic ecohydrological models are required to provide accurate water estimate while considering vegetation regulation. This is especially important in the context of anthropogenic climate change, where the water cycle (evapotranspiration and streamflow) are likely to be altered, and hence water availability can vary greatly due to biophysical and physiological regulation (Lemordant et al., 2018; Ukkola et al., 2015). Accurate quantification of water processes and the variation induced by vegetation processes is crucial for water management and climate change mitigation.

Previous studies have suggested that high uncertainty remains in transpiration estimated by various evapotranspiration partitioning methods (Coenders-Gerrits et al., 2014; Jasechko et al., 2013; Wang et al., 2014), even with carbon processes taking into consideration (Pagán et al., 2019; Wei et al., 2017). As transpiration is inherently related to photosynthesis which also determines the dominant proportion of vegetated land surface water loss, evaluating the uncertainty of spatial and temporal variations in transpiration is of great importance. High uncertainties in transpiration estimates can be misleading and hinder valid interpretation of biophysical processes. Currently it is unclear how estimates of transpiration vary between process-based and empirical models and whether model structure contributes to this uncertainty. This is particularly important for typical terrestrial ecosystems such as forests and grasslands, which together determine the largest proportion of the water and carbon balance on Earth.

Photosynthesis is a vital yet difficult process to estimate. Models based on light use efficiency (LUE) are widely used to estimate photosynthesis across spatiotemporal scales due to their simplicity (Monteith, 1972, 1977). However, all LUE models are subject to parameterisation difficulties, especially regarding the determination of maximum LUE. Recent studies have reported a wide range of this parameter, and controversial views have evolved to interpret its behaviour (Gitelson et al., 2018; Kergoat et al., 2008; Prince, 1991; Zhang et al., 2018). Yet currently there has been little discussion based on coupled carbon and water relationship for estimating maximum LUE. Estimating photosynthesis parameters based on vegetation water use is theoretically advantageous, and the results can be used to estimate ecosystem photosynthesis with higher reliability.

In summary, better understanding of the key ecohydrological variables and the interactions between them requires credible and practical algorithms. For either water or carbon estimates, it is theoretically preferable and practically necessary that the other process is taken into consideration. As such, both water and carbon fluxes should be estimated based on a coupled relationship. Models should incorporate core ecohydrological processes, and at the same time maintain a balance between simplicity and credibility. The models and analysis can serve as fundamental tools to simulate/forecast water and carbon fluxes across different ecosystems and climate. Results of this study can be further implemented to inform water resources and ecosystem functioning management, and to support climate change adaptation and mitigation.

1.3 Research questions and objectives

The overall aim of this thesis are to understand vegetation regulation of key ecohydrological processes (including evapotranspiration and streamflow as well as photosynthesis), and to use analytical and modelling approaches that are simple yet mechanistic to investigate and quantify the variation and uncertainty of these processes across different ecosystems under climate change. These major aims correspond to the significant research gaps outlined above, and can be structured as four specific research questions:

1. How can estimate ecosystem evapotranspiration and gross primary production be estimated with a simple but process-based model that employs the coupled relationship between transpiration and photosynthesis regulated by plant stomata?
2. How can runoff be estiamted considering plant regulation of evapotranspiration and carbon assimilation at a catchment scale with a practical yet mechanistically sound modelling scheme, and how can their variability in response to anthropogenic climate change (eCO_2) be investigated?
3. What is the uncertainty in estimated transpiration (a major component of evapotranspiration) constrained by carbon assimilation?
4. How can the photosynthesis parameter be quantified from a plant water use perspective by employing the coupled water and carbon relationship at an ecosystem scale?

Four specific research objectives were defined to address these questions as elaborated below.

1. Develop a simple but mechanistic model to estimate both evapotranspiration and gross primary production following biophysical and physiological principles.

   The evapotranspiration mechanism was well established by the Penman-Monteith equation, where surface conductance accounts for simultaneous stomatal regulation of both transpiration and photosynthesis. However, the coupled relationship between water loss and carbon gain is either neglected or extensively presented in existing models for evapotranspiration estimation. An intermediate modelling relationship, which would be structurally simple and physiologically sound, is needed to simultaneously quantify evapotranspiration and gross primary production at an ecosystem level. This can be achieved by (1) combining and integrating and intermediate photosynthesis model and a stomatal conductance model to formulate surface conductance, and (2) incorporating the surface conductance into the Penman-Monteith (PM) equation for both evapotranspiration

and gross primary production estimation. Following this rationale, a new model will be developed and evaluated at nine Australian eddy covariance flux sites.

2. Develop a simple ecohydrological model on catchment scale that incorporates water and carbon processes to simulate gross primary production, evapotranspiration and streamflow, and investigate their variations under eCO_2

Catchment ecohydrological processes (including gross primary production, evapotranspiration, and streamflow) are subjected to eCO_2 (anthropogenic climate change) via plant biophysical and physiological response and feedback. While LSMs describe energy and vegetation processes in extensive detail but are less satisfactory in estimating streamflow, traditional hydrological models (e.g., rainfall-runoff model) provide credible water estimates, yet lack biophysical representation of vegetation processes. Hence, a practical and credible modelling framework is required to investigate eCO_2 impact on major ecohydrological processes. This can be achieved by developing a simple ecohydrological model that incorporates primary vegetation processes (i.e., photosynthesis and stomatal conductance) into a rainfall-runoff model. As such, gross primary production, evapotranspiration, and streamflow can be simulated simultaneously without sacrificing model simplicity and accuracy of water simulation, and eCO_2 influence on these key variables can be investigated.

3. Evaluate uncertainty of evapotranspiration partitioning constrained by vegetation carbon uptake comparing process-based and empirical methods.

Vegetation water use (transpiration) is interrelated to photosynthesis and constitutes the largest proportion of evapotranspiration. Hence, transpiration is at the core of understanding vegetation regulation of ecohydrological processes. Partitioning of evapotranspiration into transpiration (the biophysical process) and evaporation (the physical process), however, exhibits high uncertainty using either process-based or empirical approaches, even with carbon constraints taken into consideration. To evaluate the uncertainty of transpiration estimates constrained by photosynthesis, a process-based model and an empirical algorithm is applied to partition evapotranspiration into transpiration and evaporation. The ratio between transpiration and evapotranspiration is then calculated to (1) investigate the variation of vegetation water use over space and time for two distinct ecosystem types and (2) evaluate the results from the two partitioning methods and attribute model uncertainty.

4. Derive key parameter for carbon estimation from a vegetation water use perspective based on the WUE principle.

Maximum light use efficiency (ε_{max}, LUE under optimal conditions) is a critical and challenging parameter for estimating ecosystem gross primary production based on the LUE modelling scheme. A wide range of ε_{max} values have been reported for different species (e.g., C_3, C_4) and biomes (e.g., forests, grasslands) based on observational and modelling approaches. The high uncertainty exhibited by these values needs further investigation. Previous algorithms used for ε_{max} parameterisation are often complex and they neglect the coupled relationship between carbon and water. Therefore, a simple but biophysically robust method for estimating ε_{max} is important and greatly needed. The mechanistic coupling between vegetation water use and carbon gain provides an insightful perspective for estimating ε_{max}. With WUE bridging transpiration and photosynthesis, an analytical method can be derived to estimate ε_{max} from a vegetation water use perspective. The WUE-based ε_{max} has the potential to be incorporated into LUE models for credible carbon estimation and related uncertainty analysis.

1.4 Thesis outline

This thesis covers two primary aspects in ecohydrological knowledge, i.e., vegetation processes and hydrological processes. The research questions were constructed to enhance the understanding of the interactions between the biosphere and hydrosphere from a modelling perspective. Following the consecution of model development and analysis, the thesis is structured in six chapters. The first chapter (Chapter 1) provides research background and the last chapter (Chapter 6) summarizes the overall contribution of knowledge. The other four chapters (Chapter 2-5) are analytical solutions corresponding to the four interrelated research questions contributing to the overall objective of this study. Two chapters (Chapters 2 and 5) from this thesis are based on journal articles which have been submitted or published in leading ecohydrological journals. The outline of this thesis is summarized in Figure 1.1.

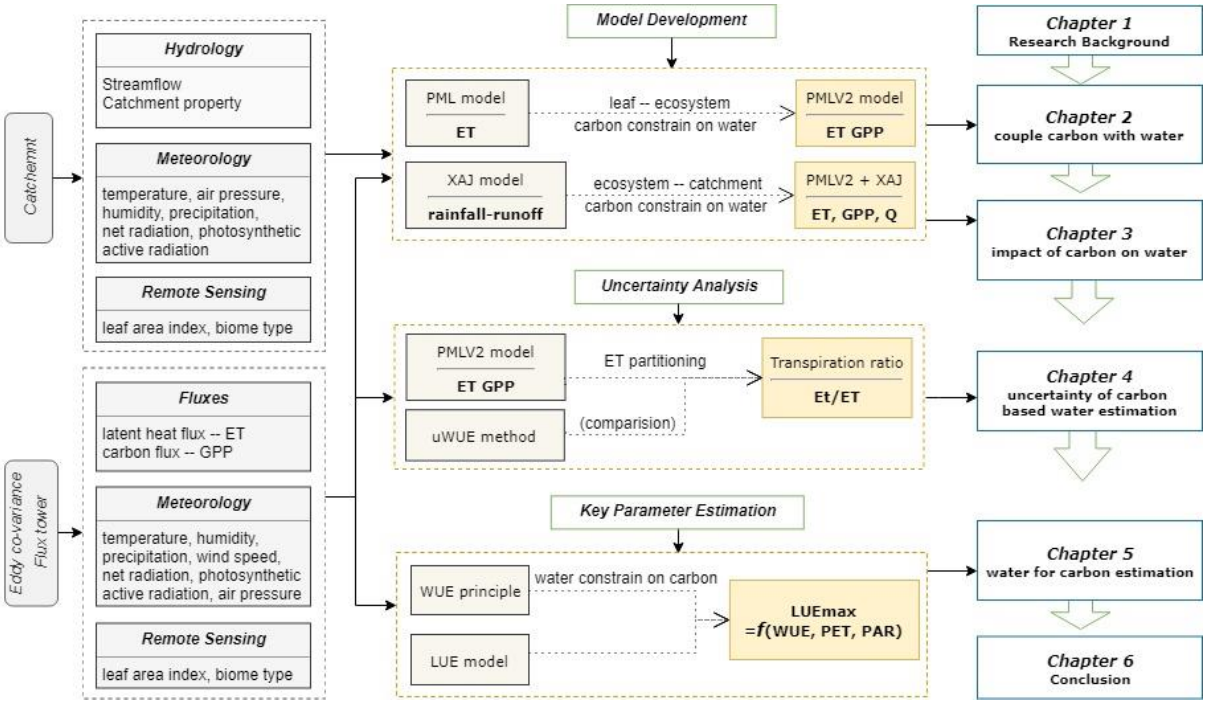

Figure 1-1. Outline of the thesis. Abbreviations see glossary.

Chapter 1 introduces the background of the overall scope of this research. Based on the fundamental vegetation-water processes, this chapter outlines the challenges and knowledge gaps in ecohydrological modelling by reviewing previous studies. Four aspects are identified regarding practical and credible modelling of key ecohydrological variables: (1) estimating evapotranspiration and photosynthesis simultaneously, (2) investigating evapotranspiration and streamflow variation considering photosynthesis under anthropogenic climate change, (3) evaluating uncertainty of transpiration estimates considering photosynthesis constraints, and (4) deriving photosynthesis parameters from transpiration. This chapter provides theoretical and methodological foundations for this thesis.

Chapter 2 corresponds to the first aspect of the study, which aims to quantify photosynthesis and evapotranspiration fluxes simultaneously using a simple yet process-based model. A new ecohydrological model (named as PML_V2) is developed in this chapter by incorporating and integrating a semi-empirical photosynthesis model and stomatal conductance model into the Penman-Monteith equation. The model is tested at an ecosystem scale using water and carbon fluxes observed at nine Australian eddy covariance flux sites. Results show that the model is capable of reproducing both photosynthesis and evapotranspiration across different biome and climate conditions, with explicit merit in simplicity and accuracy.

Chapter 3 corresponds to the second aspect of the study, which is a follow-on study of the first aspect. This chapter aims to investigate streamflow estimates and their variation in response to plant carbon uptake and water use under anthropogenic climate change, using a simple but mechanistic modelling framework. A more comprehensive ecohydrological model is developed by incorporating the PML_V2 model into a conceptual hydrological model. The model is evaluated against streamflow observations at the catchment scale, then used to investigate the eCO_2 impact on streamflow through physiological responses of vegetation via evapotranspiration and photosynthesis. Modelling experiments at 63 Australian catchments show that vegetation regulates photosynthesis and transpiration to increase catchment water yield in response to eCO_2, with significant variance across different catchments.

Chapter 4 addresses the third aspect of the study which considers the significant role that transpiration plays in regulating the water cycle (both mechanistically and under climate change). This chapter focuses on the uncertainty of transpiration estimates based on carbon constraints. Transpiration is partitioned from total evapotranspiration using the PML_V2 model and the result is compared with that from an empirical method, both based on the coupling relationship between transpiration and gross primary production. The ratio between transpiration and total evapotranspiration (T/ET) is used to evaluate the variation and relative uncertainty of the evapotranspiration partitioning methods at the ecosystem level. Results show that the T/ET estimates vary greatly from different models, with high uncertainty in both quantity and temporal variation across globally distributed grasslands. Differences are attributed to model structure and parameterization and variation in T/ET across spatiotemporal scales can be explained by vegetation index and climate conditions.

Chapter 5 is the reversed perspective of the previous three study aspects (water focus considering carbon constraints), which seeks to estimate the carbon uptake parameter from a vegetation water use viewpoint. This is a standalone chapter where an analytical solution is derived to estimate maximum light use efficiency from WUE principles. The method requires only four variables and is capable of distinguishing photosynthetically different species and producing robust estimates of maximum light use efficiency across biomes. When compared with other algorithms, this method is advantageous in terms of vegetation water use constraints, and the estimates can be used for credible quantification of gross primary production.

Chapter 6 is the final chapter and synthesizes all of the knowledge contributions from the previous chapters. The main findings and conclusions of this thesis are summarized here.

Limitations of the study and its findings, as well as future research directions, are briefly discussed.

Regarding the publications related to each of the main chapters:

Chapter 2 is based on the paper entitled “Use of satellite leaf area index estimating evapotranspiration and gross assimilation for Australian ecosystems”, which has been published in Ecohydrology (https://doi.org/10.1002/eco.1974).

Chapters 3 and 4 are extended from international conference abstracts entitled “Estimating water and carbon fluxes using a simple diagnostic model” (MODSIM, Dec 2017, Hobart Australia), and “Uncertainty of transpiration estimates from a coupled water and carbon model in grassland ecosystems” (AGU fall meeting, Dec 2018, Washington, D.C., USA), respectively. Chapter 4 is also partly drawn from the collaborative research article “Coupled estimation of 500 m and 8-day resolution global evapotranspiration and gross primary production in 2002–2017”, which has been published in Remote Sensing of Environment (https://doi.org/10.1016/j.rse.2018.12.031).

Chapter 5 is based on the submitted paper entitled “Estimating ecosystem maximum light use efficiency based on the water use efficiency principle”, which is currently under internal review with expected resubmission to Geophysical Research Letters.

Reference

Ainsworth, E. A., & Long, S. P. (2005). What have we learned from 15 years of free-air CO2 enrichment (FACE)? A meta-analytic review of the responses of photosynthesis, canopy properties and plant production to rising CO2. *New Phytologist*, *165*(2), 351–372. https://doi.org/10.1111/j.1469-8137.2004.01224.x

Allen, C. D., Macalady, A. K., Chenchouni, H., Bachelet, D., McDowell, N., Vennetier, M., et al. (2010). A global overview of drought and heat-induced tree mortality reveals emerging climate change risks for forests. *Forest Ecology and Management*, *259*(4), 660–684. https://doi.org/10.1016/J.FORECO.2009.09.001

Anav, A., Murray-Tortarolo, G., Friedlingstein, P., Sitch, S., Piao, S., & Zhu, Z. (2013). Evaluation of land surface models in reproducing satellite derived leaf area index over the high-latitude northern hemisphere. Part II: Earth system models. *Remote Sensing*, *5*(8), 3637–3661. https://doi.org/10.3390/rs5083637

Ball, J. T., Woodrow, I. E., & Berry, J. A. (1987). A Model Predicting Stomatal Conductance and its Contribution to the Control of Photosynthesis under Different Environmental Conditions. In *Progress in Photosynthesis Research* (pp. 221–224). Springer. https://doi.org/citeulike-article-id:8423355

Beer, C., Ciais, P., Reichstein, M., Baldocchi, D., Law, B. E., Papale, D., et al. (2009). Temporal and among-site variability of inherent water use efficiency at the ecosystem level. *Global Biogeochemical Cycles*, *23*(2), 1–13. https://doi.org/10.1029/2008GB003233

Beer, Christian, Reichstein, M., Tomelleri, E., Ciais, P., Jung, M., Carvalhais, N., et al. (2010). Terrestrial Gross Carbon Dioxide Uptake: Global Distribution and Covariation with Climate. *Science*, *329*(5993), 834 LP – 838. Retrieved from http://science.sciencemag.org/content/329/5993/834.abstract

Betts, R. A., Boucher, O., Collins, M., Cox, P. M., Falloon, P. D., Gedney, N., et al. (2007). Projected increase in continental runoff due to plant responses to increasing carbon dioxide. *Nature*, *448*(August), 1037–1041. https://doi.org/10.1038/nature06045

Bierkens, M. F. P., Bell, V. A., Burek, P., Chaney, N., Condon, L. E., David, C. H., et al. (2015). Hyper-resolution global hydrological modelling: What is next?: “Everywhere and locally relevant” M. F. P. Bierkens et al. Invited Commentary. *Hydrological Processes*, *29*(2), 310–320. https://doi.org/10.1002/hyp.10391

von Caemmerer, S. (2000). *Biochemical models of leaf photosynthesis.* Collingwood: CSIRO Publishing. Retrieved from https://www.cabdirect.org/cabdirect/abstract/20000707636

von Caemmerer, S. (2013). Steady-state models of photosynthesis. *Plant, Cell and Environment*, *36*(9), 1617–1630. https://doi.org/10.1111/pce.12098

von Caemmerer, S., & Farquhar, G. D. (1981). Some relationships between the biochemistry of photosynthesis and the gas exchange of leaves. *Planta*, *153*(4), 376–387. https://doi.org/10.1007/BF00384257

Campbell, G. S., & Norman, J. M. (1998). *An introduction to environmental biophysics* (2nd Editio). New York: Springer-Verlag.

Cech, P. G., Pepin, S., & Körner, C. (2003). Elevated CO2 reduces sap flux in mature

deciduous forest trees. *Oecologia*, *137*(2), 258–268. https://doi.org/10.1007/s00442-003-1348-7

Cheng, L., Zhang, L., Wang, Y.-P., Canadell, J. G., Chiew, F. H. S., Beringer, J., et al. (2017). Recent increases in terrestrial carbon uptake at little cost to the water cycle. *Nature Communications*, *8*(1), 110. https://doi.org/10.1038/s41467-017-00114-5

Cheng, Y., Zhang, Q., Lyapustin, A. I., Wang, Y., & Middleton, E. M. (2014). Impacts of light use efficiency and fPAR parameterization on gross primary production modeling. *Agricultural and Forest Meteorology*, *189–190*, 187–197. https://doi.org/10.1016/J.AGRFORMET.2014.01.006

Chiew, F. H. S. (2006). Estimation of rainfall elasticity of streamflow in Australia. *Hydrological Sciences Journal*, *51*(March), 613–625. https://doi.org/doi: 10.1623/hysj.51.4.613

Ciais, P., Reichstein, M., Viovy, N., Granier, A., Ogée, J., Allard, V., et al. (2005). Europe-wide reduction in primary productivity caused by the heat and drought in 2003. *Nature*, *437*(7058), 529–533. https://doi.org/10.1038/nature03972

Coenders-Gerrits, A. M. J., Van Der Ent, R. J., Bogaard, T. A., Wang-Erlandsson, L., Hrachowitz, M., & Savenije, H. H. G. (2014). Uncertainties in transpiration estimates. *Nature*, *506*(7487), E1–E2. https://doi.org/10.1038/nature12925

Collatz, G. J., Ball, J. T., Grivet, C., & Berry, J. A. (1991). Physiological and environmental regulation of stomatal conductance, photosynthesis and transpiration: a model that includes a laminar boundary layer. *Agricultural and Forest Meteorology*, *54*(2–4), 107–136. https://doi.org/10.1016/0168-1923(91)90002-8

Collatz, G. J., Ribas-Carbo, M., & Berry, J. A. (1992). Coupled Photosynthesis-Stomatal Conductance Model for Leaves of C4 Plants. *Functional Plant Biology*, *19*(5), 519–538. Retrieved from https://doi.org/10.1071/PP9920519

Cowan, I. R. (1982). Regulation of water use in relation to carbon gain in higher plants. In *Physiological Plant Ecology II* (Vol. 12 / B, pp. 589–613). Springer. https://doi.org/10.1007/978-3-642-68150-9_18

Cowan, I. R., & Farquhar, G. D. (1977). Stomatal function in relation to leaf metabolism and environment: Stomatal function in the regulation of gas exchange. *Symposia of the Society for Experimental Biology*, *31*(February), 471:505.

Dai, A. (2011). Drought under global warming: a review. *Wiley Interdisciplinary Reviews: Climate Change*, *2*(1), 45–65. https://doi.org/10.1002/wcc.81

Damour, G., Simonneau, T., Cochard, H., & Urban, L. (2010). An overview of models of stomatal conductance at the leaf level. *Plant, Cell and Environment*, *33*(9), 1419–1438. https://doi.org/10.1111/j.1365-3040.2010.02181.x

Devi, G. K., Ganasri, B. P., & Dwarakish, G. S. (2015). A Review on Hydrological Models. *International Conference On Water Resources, Coastal and Ocean Engineering (ICWRCOE'15)*, *4*, 1001–1007. https://doi.org/10.1016/j.aqpro.2015.02.126

Devonec, E., & Barros, A. P. (2002). Exploring the transferability of a land-surface hydrology model. *Journal of Hydrology*, *265*(1–4), 258–282. https://doi.org/10.1016/S0022-1694(02)00111-7

Van Dijk, A. I. J. M., Beck, H. E., Crosbie, R. S., De Jeu, R. A. M., Liu, Y. Y., Podger, G. M., et al. (2013). The Millennium Drought in southeast Australia (2001-2009): Natural and human causes and implications for water resources, ecosystems, economy, and society. *Water Resources Research*, *49*(2), 1040–1057. https://doi.org/10.1002/wrcr.20123

Dolman, A. J., Miralles, D. G., & de Jeu, R. A. M. (2014). Fifty years since Monteith's 1965 seminal paper: The emergence of global ecohydrology. *Ecohydrology*, *7*(3), 897–902. https://doi.org/10.1002/eco.1505

Donohue, R. J., Roderick, M. L., & McVicar, T. R. (2007). On the importance of including vegetation dynamics in Budyko's hydrological model. *Hydrology and Earth System Sciences*, *11*(2), 983–995. https://doi.org/10.5194/hess-11-983-2007

Donohue, Randall J., Roderick, M. L., McVicar, T. R., & Farquhar, G. D. (2013). Impact of CO2 fertilization on maximum foliage cover across the globe's warm, arid environments. *Geophysical Research Letters*, *40*(12), 3031–3035. https://doi.org/10.1002/grl.50563

Donohue, Randall J, Roderick, M. L., & McVicar, T. R. (2012). Roots, storms and soil pores: Incorporating key ecohydrological processes into Budyko's hydrological model. *Journal of Hydrology*, *436–437*, 35–50. https://doi.org/10.1016/J.JHYDROL.2012.02.033

Eagleson, P. (1978). Climate, Soil and Vegetaion. 1. Introduction to Water Balance Dynamics. *Water Resources Research*, *14*(5), 705–712.

Eagleson, P. S. (2005). *Ecohydrology: Darwinian expression of vegetation form and function*. Cambridge University Press.

Eamus, D., Boulain, N., Cleverly, J., & Breshears, D. D. (2013). Global change-type drought-induced tree mortality: Vapor pressure deficit is more important than temperature per se in causing decline in tree health. *Ecology and Evolution*, *3*(8), 2711–2729. https://doi.org/10.1002/ece3.664

Ellsworth, D. S. (1999). CO2 enrichment in a maturing pine forest: Are CO2 exchange and water status in the canopy affected? *Plant, Cell and Environment*, *22*(5), 461–472. https://doi.org/10.1046/j.1365-3040.1999.00433.x

Farquhar, G. D., & von Caemmerer, S. (1982). Modelling of Photosynthetic Response to Environmental Conditions BT - Physiological Plant Ecology II: Water Relations and Carbon Assimilation. In O. L. Lange, P. S. Nobel, C. B. Osmond, & H. Ziegler (Eds.) (pp. 549–587). Berlin, Heidelberg: Springer Berlin Heidelberg. https://doi.org/10.1007/978-3-642-68150-9_17

Farquhar, G. D., von Caemmener, S., & Berry, J. A. (1980). A Biochemical model of photosynthesis CO2 fixation in leaves of C3 species. *Planta*, *149*, 78–90. Retrieved from http://www.springerlink.com/content/w8264082778042jt/

Farquhar, G. D., Von Caemmerer, S., & Berry, J. A. (1980). A biochemical model of photosynthetic CO2 assimilation in leaves of C3 species. *Planta*, *149*(1), 78–90. https://doi.org/10.1007/BF00386231

Farquhar, G. D., Von Caemmerer, S., & Berry, J. A. (2001). Models of Photosynthesis. *Plant Physiol.*, *125*(February), 42–45. https://doi.org/10.1104/pp.125.1.42

Field, C. B., Ball, J. T., & Berry, J. A. (2000). Photosynthesis: principles and field techniques

- Plant Physiological Ecology: Field methods and instrumentation. In R. W. Pearcy, J. R. Ehleringer, H. A. Mooney, & P. W. Rundel (Eds.) (pp. 209–253). Dordrecht: Springer Netherlands. https://doi.org/10.1007/978-94-010-9013-1_11

Flexas, J., Ribas-Carbo, M., Diaz-Espejo, A., Galmes, J., & Medrano, H. (2008). Mesophyll conductance to CO2: current knowledge and future prospects. *Plant, Cell & Environment*, *31*(5), 602–621. https://doi.org/10.1111/j.1365-3040.2007.01757.x

Frank, D. C., Poulter, B., Saurer, M., Esper, J., Huntingford, C., Helle, G., et al. (2015). Water-use efficiency and transpiration across European forests during the Anthropocene. *Nature Climate Change*, *5*(6), 579–583. https://doi.org/10.1038/nclimate2614

Garcia-Quijano, J. F., & Barros, A. P. (2005). Incorporating canopy physiology into a hydrological model: Photosynthesis, dynamic respiration, and stomatal sensitivity. *Ecological Modelling*, *185*(1), 29–49. https://doi.org/10.1016/j.ecolmodel.2004.08.024

Gedney, N., Cox, P. M., Betts, R. A., Boucher, O., Huntingford, C., & Stott, P. A. (2006). Detection of a direct carbon dioxide effect in continental river runoff records. *Nature*, *439*(7078), 835–838. https://doi.org/10.1038/nature04504

Gentine, P., Green, J., Guerin, M., Humphrey, V., Seneviratne, S. I., Zhang, Y., & Zhou, S. (2019). Coupling between the terrestrial carbon and water cycles - a review. *Environmental Research Letters*. Retrieved from http://iopscience.iop.org/10.1088/1748-9326/ab22d6

Gitelson, A. A., Peng, Y., Arkebauer, T. J., & Suyker, A. E. (2015). Productivity, absorbed photosynthetically active radiation, and light use efficiency in crops: Implications for remote sensing of crop primary production. *Journal of Plant Physiology*, *177*, 100–109. https://doi.org/10.1016/j.jplph.2014.12.015

Gitelson, A. A., Arkebauer, T. J., & Suyker, A. E. (2018). Convergence of daily light use efficiency in irrigated and rainfed C3 and C4 crops. *Remote Sensing of Environment*, *217*, 30–37. https://doi.org/10.1016/J.RSE.2018.08.007

Good, S. P., Noone, D., & Bowen, G. (2015). Hydrologic connectivity constrains partitioning of global terrestrial water fluxes. *Science*, *349*(6244), 175–177. https://doi.org/10.1126/science.aaa5931

Van Gorsel, E., Wolf, S., Cleverly, J., Isaac, P., Haverd, V., Ewenz, C., et al. (2016). Carbon uptake and water use in woodlands and forests in southern Australia during an extreme heat wave event in the "angry Summer" of 2012/2013. *Biogeosciences*, *13*(21), 5947–5964. https://doi.org/10.5194/bg-13-5947-2016

Green, T. R., Taniguchi, M., Kooi, H., Gurdak, J. J., Allen, D. M., Hiscock, K. M., et al. (2011). Beneath the surface of global change: Impacts of climate change on groundwater. *Journal of Hydrology*, *405*(3–4), 532–560. https://doi.org/10.1016/j.jhydrol.2011.05.002

Haddeland, I., Clark, D. B., Franssen, W., Ludwig, F., Voß, F., Arnell, N. W., et al. (2011). Multimodel Estimate of the Global Terrestrial Water Balance: Setup and First Results. *Journal of Hydrometeorology*, *12*(5), 869–884. https://doi.org/10.1175/2011JHM1324.1

Hirabayashi, Y., Mahendran, R., Koirala, S., Konoshima, L., Yamazaki, D., Watanabe, S., et al. (2013). Global flood risk under climate change. *Nature Climate Change*, *3*(9), 816–821. https://doi.org/10.1038/nclimate1911

Holzworth, D. P., Huth, N. I., deVoil, P. G., Zurcher, E. J., Herrmann, N. I., McLean, G., et al. (2014). APSIM – Evolution towards a new generation of agricultural systems simulation. *Environmental Modelling & Software*, *62*, 327–350. https://doi.org/10.1016/J.ENVSOFT.2014.07.009

Hovenden, M. J., Newton, P. C. D., & Wills, K. E. (2014). Seasonal not annual rainfall determines grassland biomass response to carbon dioxide. *Nature*, *511*(7511), 583–586. https://doi.org/10.1038/nature13281

Hovenden, M. J., Leuzinger, S., Newton, P. C. D., Fletcher, A., Fatichi, S., Lüscher, A., et al. (2019). Globally consistent influences of seasonal precipitation limit grassland biomass response to elevated CO 2. *Nature Plants*, *5*(2), 167–173. https://doi.org/10.1038/s41477-018-0356-x

Hutjes, R. W. A., Kabat, P., Running, S. W., Shuttleworth, W. J., Field, C., Bass, B., et al. (1998). Biospheric aspects of the hydrological cycle. *Journal of Hydrology*, *212–213*(1–4), 1–21. https://doi.org/10.1016/S0022-1694(98)00255-8

IPCC. (2014). *Summary for Policymakers*. *Climate Change 2014: Synthesis Report. Contribution of Working Groups I, II and III to the Fifth Assessment Report of the Intergovernmental Panel on Climate Change*. https://doi.org/10.1017/CBO9781107415324

Jarvis, P. G. (1976). The Interpretation of the Variations in Leaf Water Potential and Stomatal Conductance Found in Canopies in the Field. *Philosophical Transactions of the Royal Society B: Biological Sciences*, *273*(927), 593–610. https://doi.org/10.1098/rstb.1976.0035

Jarvis, P. G., & McNaughton, K. G. (1986). Stomatal Control of Transpiration: Scaling Up from Leaf to Region. *Advances in Ecological Research*, *15*, 1–49. https://doi.org/10.1016/S0065-2504(08)60119-1

Jasechko, S., Sharp, Z. D., Gibson, J. J., Birks, S. J., Yi, Y., & Fawcett, P. J. (2013). Terrestrial water fluxes dominated by transpiration. *Nature*, *496*(7445), 347–350. https://doi.org/10.1038/nature11983

Johnson, I. R., & Thornley, J. H. M. (1984). A model of instantaneous and daily canopy photosynthesis. *Journal of Theoretical Biology*, *107*(4), 531–545. https://doi.org/10.1016/S0022-5193(84)80131-9

Ju, W., Chen, J. M., Black, T. A., Barr, A. G., Liu, J., & Chen, B. (2006). Modelling multi-year coupled carbon and water fluxes in a boreal aspen forest. *Agricultural and Forest Meteorology*, *140*(1–4), 136–151. https://doi.org/10.1016/J.AGRFORMET.2006.08.008

Jung, M., Reichstein, M., Ciais, P., Seneviratne, S. I., Sheffield, J., Goulden, M. L., et al. (2010). Recent decline in the global land evapotranspiration trend due to limited moisture supply. *Nature*, *467*(7318), 951–954. Retrieved from http://dx.doi.org/10.1038/nature09396

Kauffeldt, A., Wetterhall, F., Pappenberger, F., Salamon, P., & Thielen, J. (2016). Technical review of large-scale hydrological models for implementation in operational flood forecasting schemes on continental level. *Environmental Modelling and Software*, *75*, 68–76. https://doi.org/10.1016/j.envsoft.2015.09.009

Keating, B. ., Carberry, P. ., Hammer, G. ., Probert, M. ., Robertson, M. ., Holzworth, D., et

al. (2003). An overview of APSIM, a model designed for farming systems simulation. *European Journal of Agronomy*, *18*(3–4), 267–288. https://doi.org/10.1016/S1161-0301(02)00108-9

Kergoat, L., Lafont, S., Douville, H., Bérthelot, B., Dedieu, G., Planton, S., & Royer, J. F. (2002). Impact of doubled CO<inf>2</inf> on global-scale leaf area index and evapotranspiration: Conflicting stomatal conductance and LAI responses. *Journal of Geophysical Research Atmospheres*, *107*(24). https://doi.org/10.1029/2001JD001245

Kergoat, L., Lafont, S., Arneth, A., Le Dantec, V., & Saugier, B. (2008). Nitrogen controls plant canopy light-use efficiency in temperate and boreal ecosystems. *Journal of Geophysical Research: Biogeosciences*, *113*(4). https://doi.org/10.1029/2007JG000676

Kustas, W. P., & Norman, J. M. (1996). Use of remote sensing for evapotranspiration monitoring over land surfaces. *Hydrological Sciences Journal*, *41*(4), 495–516. https://doi.org/10.1080/02626669609491522

Lee, T. D., Tjoelker, M. G., Ellsworth, D. S., & Reich, P. B. (2001). Leaf gas exchange responses of 13 prairie grassland species to elevated CO2 and increased nitrogen supply. *New Phytologist*, *150*(2), 405–418. https://doi.org/10.1046/j.1469-8137.2001.00095.x

Lemordant, L., Gentine, P., Swann, A. S., Cook, B. I., & Scheff, J. (2018). Critical impact of vegetation physiology on the continental hydrologic cycle in response to increasing CO 2 . *Proceedings of the National Academy of Sciences*, *115*(16), 4093–4098. https://doi.org/10.1073/pnas.1720712115

Leuning, R., Zhang, Y. Q., Rajaud, A., Cleugh, H., & Tu, K. (2008). A simple surface conductance model to estimate regional evaporation using MODIS leaf area index and the Penman-Monteith equation. *Water Resources Research*, *44*(10), W10419. https://doi.org/10.1029/2007WR006562

Leuning, Ray. (1995). A critical appraisal of a combined stomatal-photosynthesis model for C3 plants. *Plant, Cell & Environment*, *18*(4), 339–355. https://doi.org/10.1111/j.1365-3040.1995.tb00370.x

Levis, S., Foley, J. A., & Pollard, D. (2000). Large-scale vegetation feedbacks on a doubled CO2 climate. *Journal of Climate*, *13*(7), 1313–1325. https://doi.org/10.1175/1520-0442(2000)013<1313:LSVFOA>2.0.CO;2

Li, Z., Tang, R., Wan, Z., Bi, Y., Zhou, C., Tang, B., et al. (2009). A review of current methodologies for regional Evapotranspiration estimation from remotely sensed data. *Sensors*, *9*(5), 3801–3853. https://doi.org/10.3390/s90503801

Lin, Y.-S., Medlyn, B. E., Duursma, R. A., Prentice, I. C., Wang, H., Baig, S., et al. (2015). Optimal stomatal behaviour around the world. *Nature Clim. Change*, *5*(5), 459–464. Retrieved from http://dx.doi.org/10.1038/nclimate2550

Liu, Z., Wu, C., & Wang, S. (2017). Predicting Forest Evapotranspiration by Coupling Carbon and Water Cycling Based on a Critical Stomatal Conductance Model. *IEEE Journal of Selected Topics in Applied Earth Observations and Remote Sensing*, *PP*(99), 1–9. https://doi.org/10.1109/JSTARS.2017.2715077

Long, D., Longuevergne, L., & Scanlon, B. R. (2014). Uncertainty in evapotranspiration fromland surfacemodeling, remote sensing, and GRACE satellites. *Water Resources Research*, *50*(2), 1131–1151. https://doi.org/10.1002/2013WR014581.Received

Maeda, E. E., Ma, X., Wagner, F., Kim, H., Oki, T., & Eamus, D. (2017). Evapotranspiration seasonality across the Amazon basin Evapotranspiration seasonality across the Amazon basin. *Earth System Dynamics*, (January), 439–454. https://doi.org/10.5194/esd-2016-75

Maskell, J. E. (1928). Experimental researches on vegetable assimilation and respiration. XVIII.—The relation between stomatal opening and assimilation.—A critical study of assimilation rates and porometer rates in leaves of Cherry Laurel. *Proceedings of the Royal Society of London. Series B, Containing Papers of a Biological Character*, *102*(720), 488–533. https://doi.org/10.1098/rspb.1928.0021

Medlyn, B. E., Loustau, D., & Delzon, S. (2002). Temperature response of parameters of a biochemically based model of photosynthesis. I. Seasonal changes in mature maritime pine (Pinus pinaster Ait.). *Plant, Cell and Environment*, *25*(9), 1155–1165. https://doi.org/10.1046/j.1365-3040.2002.00890.x

Medlyn, Belinda E., Duursma, R. A., Eamus, D., Ellsworth, D. S., Prentice, I. C., Barton, C. V. M., et al. (2011). Reconciling the optimal and empirical approaches to modelling stomatal conductance. *Global Change Biology*, *17*(6), 2134–2144. https://doi.org/10.1111/j.1365-2486.2010.02375.x

Medlyn, Belinda E. (1998). Physiological basis of the light use efficiency model. *Tree Physiology*. Retrieved from http://treephys.oxfordjournals.org/content/18/3/167.short

Medlyn, Belinda E, Barton, C. V. M., Droadmeadow, M. S. J., Ceulemans, R., De Angelis, P., Forstreuter, M., et al. (2001). Stomatal conductance of forest species after long-term exposure to elevated CO2 concentration: A synthesis. *New Phytologist*, *149*(2), 247–264. Retrieved from http://onlinelibrary.wiley.com/doi/10.1046/j.1469-8137.2001.00028.x/pdf

Milly, P. C. D., Dunne, K. a, & Vecchia, a V. (2005). Global pattern of trends in streamflow and water availability in a changing climate. *Nature*, *438*(7066), 347–350. https://doi.org/10.1038/nature04312

Miralles, D. G., Jiménez, C., Jung, M., Michel, D., Ershadi, A., Mccabe, M. F., et al. (2016). The WACMOS-ET project - Part 2: Evaluation of global terrestrial evaporation data sets. *Hydrology and Earth System Sciences*, *20*(2), 823–842. https://doi.org/10.5194/hess-20-823-2016

Monin, A. S., & Obukhov, A. M. (1954). Basic laws of turbulent mixing in the atmosphere near the ground. *Tr. Akad. Nauk SSSR Geofiz. Inst*, *24*(151), 163–187.

Montanari, a., Young, G., Savenije, H. H. G., Hughes, D., Wagener, T., Ren, L. L., et al. (2013). "Panta Rhei—Everything Flows": Change in hydrology and society—The IAHS Scientific Decade 2013–2022. *Hydrological Sciences Journal*, *58*(6), 1256–1275. https://doi.org/10.1080/02626667.2013.809088

Monteith, J. L. (1965). Evaporation and environment. *Symposia of the Society for Experimental Biology*, *19*, 205–234. https://doi.org/10.1613/jair.301

Monteith, J. L. (1972). Solar Radiation and Productivity in Tropical Ecosystems. *Journal of Applied Ecology*, *9*(3), 747–766. https://doi.org/10.2307/2401901

Monteith, J. L. (1977). Climate and the Efficiency of Crop Production in Britain [and Discussion]. *Philosophical Transactions of the Royal Society B: Biological Sciences*, *281*(980), 277–294. https://doi.org/10.1098/rstb.1977.0140

Murray-Tortarolo, G., Anav, A., Friedlingstein, P., Sitch, S., Piao, S., Zhu, Z., et al. (2013). Evaluation of land surface models in reproducing satellite-derived LAI over the high-latitude northern hemisphere. Part I: Uncoupled DGVMs. *Remote Sensing*, *5*(10), 4819–4838. https://doi.org/10.3390/rs5104819

Overgaard, J., Rosbjerg, D., & Butts, M. B. (2006). Land-surface modelling in hydrological perspective ? a review. *Biogeosciences*, *3*(2), 229–241. Retrieved from https://hal-sde.archives-ouvertes.fr/hal-00297556/#.WLF5YOl-5No.mendeley

Pagán, B., Maes, W., Gentine, P., Martens, B., & Miralles, D. (2019). Exploring the Potential of Satellite Solar-Induced Fluorescence to Constrain Global Transpiration Estimates. *Remote Sensing*, *11*(4), 413. https://doi.org/10.3390/rs11040413

Passioura, J. B. (1982). Water in the Soil-Plant-Atmosphere Continuum BT - Physiological Plant Ecology II: Water Relations and Carbon Assimilation. In O. L. Lange, P. S. Nobel, C. B. Osmond, & H. Ziegler (Eds.) (pp. 5–33). Berlin, Heidelberg: Springer Berlin Heidelberg. https://doi.org/10.1007/978-3-642-68150-9_2

Penman, L. H. (1948). Natural evaporation from open water, bare soil and grass. *Proceedings of the Royal Society of London. Series A. Mathematical and Physical Sciences*, *193*(1032), 120–145. https://doi.org/10.1098/rspa.1948.0037

Piao, S., Friedlingstein, P., Ciais, P., de Noblet-Ducoudré, N., Labat, D., & Zaehle, S. (2007). Changes in climate and land use have a larger direct impact than rising CO2 on global river runoff trends. *Proceedings of the National Academy of Sciences of the United States of America*, *104*(39), 15242–7. https://doi.org/10.1073/pnas.0707213104

Pitman, A. J. (2003). The evolution of, and revolution in, land surface schemes designed for climate models. *International Journal of Climatology*, *23*(5), 479–510. https://doi.org/10.1002/joc.893

Porporato, A., Laio, F., Ridolfi, L., & Rodriguez-Iturbe, I. (2001). Plants in water-controlled ecosystems: Active role in hydrologic processes and responce to water stress III. Vegetation water stress. *Advances in Water Resources*, *24*(7), 745–762. https://doi.org/10.1016/S0309-1708(01)00007-0

Poyatos, R., Granda, V., Molowny-Horas, R., Mencuccini, M., Steppe, K., & Martínez-Vilalta, J. (2016). SAPFLUXNET: towards a global database of sap flow measurements. *Tree Physiology*, *36*(12), 1449–1455. https://doi.org/10.1093/treephys/tpw110

Prentice, I. C., Liang, X., Medlyn, B. E., & Wang, Y. P. (2015). Reliable, robust and realistic: The three R's of next-generation land-surface modelling. *Atmospheric Chemistry and Physics*, *15*(10), 5987–6005. https://doi.org/10.5194/acp-15-5987-2015

Prince, S. D. (1991). A model of regional primary production for use with coarse resolution satellite data. *International Journal of Remote Sensing*, *12*(6), 1313–1330. https://doi.org/10.1080/01431169108929728

Ritchie, J. T. (1983). Efficient water use in crop production: discussion on the generality of relations between biomass production and evapotranspiration. *Limitations to Efficient Water Use in Crop Production*, 29–44. https://doi.org/10.2134/1983.limitationstoefficientwateruse.c2

Rogers, A., Medlyn, B. E., Dukes, J. S., Bonan, G., von Caemmerer, S., Dietze, M. C., et al. (2017). A roadmap for improving the representation of photosynthesis in Earth system

models. *New Phytologist*, *213*(1), 22–42. https://doi.org/10.1111/nph.14283

Sato, H., Ito, A., Ito, A., Ise, T., & Kato, E. (2015). Current status and future of land surface models. *Soil Science and Plant Nutrition*, *61*(1), 34–47. https://doi.org/10.1080/00380768.2014.917593

Seddon, A. W. R., Macias-Fauria, M., Long, P. R., Benz, D., & Willis, K. J. (2016). Sensitivity of global terrestrial ecosystems to climate variability. *Nature*, *531*(7593), 229–232. https://doi.org/10.1038/nature16986

Sellers, P. J. (1997). Modeling the Exchanges of Energy, Water, and Carbon Between Continents and the Atmosphere. *Science*, *275*(5299), 502–509. https://doi.org/10.1126/science.275.5299.502

Sellers, P. J., Randall, D. A., Collatz, G. J., Berry, J. A., Field, C. B., Dazlich, D. A., et al. (1996). A revised land surface parameterization (SiB2) for atmospheric GCMs. Part I: Model formulation. *Journal of Climate*. https://doi.org/10.1175/1520-0442(1996)009<0676:ARLSPF>2.0.CO;2

Sharkey, T. D. (1985). Photosynthesis in Intact Leaves of C 3 Plants : Physics , Physiology and Rate Limitations Published by : Springer on behalf of New York Botanical Garden Press Stable URL : http://www.jstor.org/stable/4354049 Accessed : 05-03-2016 20 : 39 UTC Your use of t, *51*(1), 53–105.

Shuttleworth, W. J. (2007). Putting the "vap" into evaporation. *Hydrology and Earth System Sciences*, *11*(1), 210–244. https://doi.org/10.5194/hess-11-210-2007

Shuttleworth, W. J., & Wallace, J. S. (1985). Evaporation from sparse crops-an energy combination theory. *The Quarterly Journal of the Royal Meteorological Society*, *111*(465), 839–855. https://doi.org/10.1002/qj.49711146510

Sinclair, T. R., & Horie, T. (1989). Leaf Nitrogen, Photosynthesis, and Crop Radiation Use Efficiency: A Review. *Crop Science*, *29*(1), 90. https://doi.org/10.2135/cropsci1989.0011183X002900010023x

Sinclair, T. R., & Muchow, R. C. (1999). Radiation Use Efficiency. In D. L. B. T.-A. in A. Sparks (Ed.) (Vol. 65, pp. 215–265). Academic Press. https://doi.org/https://doi.org/10.1016/S0065-2113(08)60914-1

Sinclair, T. R., Tanner, C. B., & Bennett, J. M. (1984). Water-Use Efficiency in Crop Production. *Source: BioScience*, *34*(1), 36–40. https://doi.org/10.2307/1309424

Stewart, J. B. (1988). Modelling surface conductance of pine forest. *Agricultural and Forest Meteorology*, *43*(1), 19–35. https://doi.org/10.1016/0168-1923(88)90003-2

Stocker, T. F., & Raible, C. C. (2005). Climate change: Water cycle shifts gear. *Nature*, *434*(7035), 830–833. Retrieved from http://dx.doi.org/10.1038/434830a

Stoy, P. C., El-madany, T., Fisher, J. B., Gentine, P., Gerken, T., & Stephen, P. (2019). Reviews and syntheses : Turning the challenges of partitioning ecosystem evaporation and transpiration into opportunities, (March), 1–47.

Tanner, C. B., & Sinclair, T. R. (1983). Efficient water use in crop production: research or re-search? *Limitations to Efficient Water Use in Crop Production*, 1–27. https://doi.org/10.2134/1983.limitationstoefficientwateruse.c1

Taylor, R. G., Scanlon, B., Döll, P., Rodell, M., Van Beek, R., Wada, Y., et al. (2013). Ground water and climate change. *Nature Climate Change*, *3*(4), 322–329. https://doi.org/10.1038/nclimate1744

Tenhunen, J. D., Lange, O. L., Gebel, J., Beyschlag, W., & Weber, J. A. (1984). Changes in photosynthetic capacity, carboxylation efficiency, and CO2 compensation point associated with midday stomatal closure and midday depression of net CO2 exchange of leaves of Quercus suber. *Planta*, *162*(3), 193–203. https://doi.org/10.1007/BF00397440

Teuling, A. J., Seneviratne, S. I., Stöckli, R., Reichstein, M., Moors, E., Ciais, P., et al. (2010). Contrasting response of European forest and grassland energy exchange to heatwaves. *Nature Geoscience*, *3*(10), 722–727. https://doi.org/10.1038/ngeo950

Thornley, J. H. M. (1970). Respiration, Growth and Maintenance in Plants. *Nature*, *227*(5255), 304–305. https://doi.org/10.1038/227304b0

Thornley, J. H. M. (1976). *Mathematical models in plant physiology: a quantitative approach to problems in plant and crop physiology*. *Experimental botany ; v. 8*. London ; New York: Academic Press.

Thornley, J. H. M. (1998). Temperature and CO2Responses of Leaf and Canopy Photosynthesis : a Clarification using the Non-rectangular Hyperbola Model of Photosynthesis. *Annals of Botany*, *82*(January), 883–892. https://doi.org/10.1006/anbo.1998.0777

Tietjen, B., Schlaepfer, D. R., Bradford, J. B., Lauenroth, W. K., Hall, S. A., Duniway, M. C., et al. (2017). Climate change-induced vegetation shifts lead to more ecological droughts despite projected rainfall increases in many global temperate drylands. *Global Change Biology*, *23*(7), 2743–2754. https://doi.org/10.1111/gcb.13598

Trenberth, K. E., Dai, A., Van Der Schrier, G., Jones, P. D., Barichivich, J., Briffa, K. R., & Sheffield, J. (2014). Global warming and changes in drought. *Nature Climate Change*, *4*(1), 17–22. https://doi.org/10.1038/nclimate2067

Tuzet, A., Perrier, A., & Leuning, R. (2003). A coupled model of stomatal conductance, photosynthesis and transpiration. *Plant, Cell and Environment*, *26*(7), 1097–1116. https://doi.org/10.1046/j.1365-3040.2003.01035.x

Uddling, J., Teclaw, R. M., Pregitzer, K. S., & Ellsworth, D. S. (2009). Leaf and canopy conductance in aspen and aspen-birch forests under free-air enrichment of carbon dioxide and ozone. *Tree Physiology*, *29*(11), 1367–1380. https://doi.org/10.1093/treephys/tpp070

Ukkola, A. M., Prentice, I. C., Keenan, T. F., van Dijk, A. I. J. M., Viney, N. R., Myneni, R. B., & Bi, J. (2015). Reduced streamflow in water-stressed climates consistent with CO2 effects on vegetation. *Nature Climate Change*, *6*(2009), 75–78. https://doi.org/10.1038/nclimate2831

Verstraeten, W. W., Veroustraete, F., & Feyen, J. (2008). Assessment of evapotranspiration and soil moisture content across different scales of observation. *Sensors*, *8*(1), 70–117. https://doi.org/10.3390/s8010070

Wang, E., Robertson, M. J., Hammer, G. L., Carberry, P. S., Holzworth, D., Meinke, H., et al. (2002). Development of a generic crop model template in the cropping system model APSIM. *European Journal of Agronomy*, *18*(1–2), 121–140.

https://doi.org/10.1016/S1161-0301(02)00100-4

Wang, K., & Dickinson, R. E. (2012). A review of global terrestrial evapotranspiration: Observation, modeling, climatology, and climatic variability. *Reviews of Geophysics*, *50*(2). https://doi.org/10.1029/2011RG000373

Wang, L., Stephen, P. G., & Kelly, K. C. (2014). Global synthesis of vegetation control on evapotranspiration partitioning. *Geophysical Research Letters*, *41*(19), 6753–6757. https://doi.org/10.1002/2014GL061439

Wang, Y., & Leuning, R. (1998). A two-leaf model for canopy conductance, photosynthesis and partitioning of available energy I: Model description and comparison with a multi-layered model. *Agricultural and Forest Meteorology*, *91*(1–2), 89–111. https://doi.org/10.1016/S0168-1923(98)00061-6

Wei, Z., Yoshimura, K., Wang, L., Miralles, D. G., Jasechko, S., & Lee, X. (2017). Revisiting the contribution of transpiration to global terrestrial evapotranspiration. *Geophysical Research Letters*, *44*(6), 2792–2801. https://doi.org/10.1002/2016GL072235

Wolf, S., Keenan, T. F., Fisher, J. B., Baldocchi, D. D., Desai, A. R., Richardson, A. D., et al. (2016). Warm spring reduced carbon cycle impact of the 2012 US summer drought. *Proceedings of the National Academy of Sciences*, *113*(21), 5880–5885. https://doi.org/10.1073/pnas.1519620113

Wong, S. C., Cowan, I. R., & Farquhar, G. D. (1979). Stomatal conductance correlates with photosynthetic capacity. *Nature*, *282*, 424–426.

Wood, E. F., Roundy, J. K., Troy, T. J., van Beek, L. P. H., Bierkens, M. F. P., Blyth, E., et al. (2011). Hyperresolution global land surface modeling: Meeting a grand challenge for monitoring Earth's terrestrial water. *Water Resources Research*, *47*(5), W05301. https://doi.org/10.1029/2010WR010090

Wu, A., Song, Y., van Oosterom, E. J., & Hammer, G. L. (2016). Connecting Biochemical Photosynthesis Models with Crop Models to Support Crop Improvement. *Frontiers in Plant Science*, *7*(October), 1–16. https://doi.org/10.3389/fpls.2016.01518

Xu, J. Z., Yu, Y. M., Peng, S. Z., Yang, S. H., & Liao, L. X. (2014). A modified nonrectangular hyperbola equation for photosynthetic light-response curves of leaves with different nitrogen status. *Photosynthetica*, *52*(1), 117–123. https://doi.org/10.1007/s11099-014-0011-3

Yang, Y., Donohue, R. J., McVicar, T. R., Roderick, M. L., & Beck, H. E. (2016). Long-term CO2 fertilization increases vegetation productivity and has little effect on hydrological partitioning in tropical rainforests. *Journal of Geophysical Research G: Biogeosciences*, *121*(8), 2125–2140. https://doi.org/10.1002/2016JG003475

Ye, Z.-P., Suggett, D. J., Robakowski, P., & Kang, H.-J. (2013). A mechanistic model for the photosynthesis–light response based on the photosynthetic electron transport of photosystem II in C3 and C4 species. *New Phytologist*, *199*(1), 110–120. https://doi.org/10.1111/nph.12242

Yildiz, O., & Barros, A. P. (2006). Climate Variability, Water Resources, and Hydrologic Extremes - Modeling the Water and Energy Budgets. *Climate and Hydrology in Mountain Areas*, 291–306. https://doi.org/10.1002/0470858249.ch20

Yin, X., & Struik, P. C. (2009). C3 and C4 photosynthesis models: An overview from the perspective of crop modelling. *NJAS - Wageningen Journal of Life Sciences*, *57*(1), 27–38. https://doi.org/10.1016/j.njas.2009.07.001

Yin, X., Van Oijen, M., & Schapendonk, A. H. C. M. (2004). Extension of a biochemical model for the generalized stoichiometry of electron transport limited C3 photosynthesis. *Plant, Cell & Environment*, *27*(10), 1211–1222. https://doi.org/10.1111/j.1365-3040.2004.01224.x

Yin, X., Harbinson, J., & Struik, P. C. (2006). Mathematical review of literature to assess alternative electron transports and interphotosystem excitation partitioning of steady-state C3 photosynthesis under limiting light. *Plant, Cell & Environment*, *29*(9), 1771–1782. https://doi.org/10.1111/j.1365-3040.2006.01554.x

Yuan, W., Cai, W., Nguy-Robertson, A. L., Fang, H., Suyker, A. E., Chen, Y., et al. (2015). Uncertainty in simulating gross primary production of cropland ecosystem from satellite-based models. *Agricultural and Forest Meteorology*, *207*, 48–57. https://doi.org/10.1016/J.AGRFORMET.2015.03.016

Zeng, Z., Piao, S., Li, L. Z. X., Zhou, L., Ciais, P., Wang, T., et al. (2017). Climate mitigation from vegetation biophysical feedbacks during the past three decades. *Nature Climate Change*, *7*(6), 432–436. https://doi.org/10.1038/nclimate3299

Zhang, K., Kimball, J. S., Nemani, R. R., Running, S. W., Hong, Y., Gourley, J. J., & Yu, Z. (2015). Vegetation Greening and Climate Change Promote Multidecadal Rises of Global Land Evapotranspiration. *Scientific Reports*, *5*, 15956. Retrieved from https://doi.org/10.1038/srep15956

Zhang, K., Kimball, J. S., & Running, S. W. (2016). A review of remote sensing based actual evapotranspiration estimation. *Wiley Interdisciplinary Reviews: Water*, *3*(6), 834–853. https://doi.org/10.1002/wat2.1168

Zhang, L., Dawes, W. R., & Walker, G. R. (2001). Response of mean annual evapotranspiration to vegetation changes at catchment scale. *Water Resources Research*, *37*(3), 701–708. https://doi.org/10.1029/2000WR900325

Zhang, Lu, Cheng, L., & Chiew, F. (2018). Understanding the impacts of climate and landuse change on water yield. *Current Opinion in Environmental Sustainability*, *33*, 167–174. https://doi.org/10.1016/J.COSUST.2018.04.017

Zhang, Yao, Xiao, X., Wu, X., Zhou, S., Zhang, G., Qin, Y., & Dong, J. (2017). A global moderate resolution dataset of gross primary production of vegetation for 2000–2016. *Scientific Data*, *4*, 170165. https://doi.org/10.1038/sdata.2017.165

Zhang, Yao, Xiao, X., Wolf, S., Wu, J., Wu, X., Gioli, B., et al. (2018). Spatio-Temporal Convergence of Maximum Daily Light-Use Efficiency Based on Radiation Absorption by Canopy Chlorophyll. *Geophysical Research Letters*, *45*(8), 3508–3519. https://doi.org/10.1029/2017GL076354

Zhang, Yongqiang, Chiew, F. H. S., Zhang, L., & Li, H. (2009). Use of Remotely Sensed Actual Evapotranspiration to Improve Rainfall–Runoff Modeling in Southeast Australia. *Journal of Hydrometeorology*, *10*(4), 969–980. https://doi.org/10.1175/2009JHM1061.1

Zhang, Yongqiang, Peña-Arancibia, J. L., McVicar, T. R., Chiew, F. H. S., Vaze, J., Liu, C., et al. (2016). Multi-decadal trends in global terrestrial evapotranspiration and its

components. *Scientific Reports*, *6*(August 2015), 19124. https://doi.org/10.1038/srep19124

Zhao, R. (1992). The Xinanjiang model applied in China. *Journal of Hydrology*, *135*(1–4), 371–381. https://doi.org/10.1016/0022-1694(92)90096-E

Zhao, W., & Li, A. (2015). A Review on Land Surface Processes Modelling over Complex Terrain. *Advances in Meteorology*, *2015*, 1–17. https://doi.org/10.1155/2015/607181

Zhou, Sha, Yu, B., Huang, Y., & Wang, G. (2014). The effect of vapor pressure deficit on water use efficiency at the subdaily time scale. *Geophysical Research Letters*, *41*, 5005–5013. https://doi.org/10.1002/2014GL060741.Received

Zhou, Shuangxi, Medlyn, B., Sabaté, S., Sperlich, D., & Colin Prentice, I. (2014). Short-term water stress impacts on stomatal, mesophyll and biochemical limitations to photosynthesis differ consistently among tree species from contrasting climates. *Tree Physiology*, *34*(10), 1035–1046. https://doi.org/10.1093/treephys/tpu072

Zhou, Y., Zhang, Y., Vaze, J., Lane, P., & Xu, S. (2013). Improving runoff estimates using remote sensing vegetation data for bushfire impacted catchments. *Agricultural and Forest Meteorology*, *182–183*, 332–341. https://doi.org/10.1016/j.agrformet.2013.04.018

Zhu, Z., Piao, S., Myneni, R. B., Huang, M., Zeng, Z., Canadell, J. G., et al. (2016). Greening of the Earth and its drivers. *Nature Climate Change*, *6*(August), early online. https://doi.org/10.1038/NCLIMATE3004

Chapter 2. Use of satellite leaf area index estimating evapotranspiration and gross assimilation for Australian ecosystems

This chapter is based on the following manuscript:

Gan, R., Zhang, Y., Shi, H., Yang, Y., Eamus, D., Cheng, L., Chiew, F.H.S., Yu, Q. (2018). Use of satellite leaf area index estimating evapotranspiration and gross assimilation for Australian ecosystems. *Ecohydrology*, DOI: 10.1002/eco.1974

Highlights

- The widely used Penman-Monteith-Leuning (PML) evapotranspiration model was modified to estimate gross primary production
- The PML_V2 model is simple, easily implemented and takes remote sensing vegetation data as model inputs
- It performs well for estimating both evapotranspiration and gross primary production at nine flux sites across Australia

Abstract

Accurate quantification of terrestrial evapotranspiration and ecosystem productivity are of significant merit to better understand and predict the response of ecosystem energy, water and carbon budgets under climate change. Existing diagnostic models have different focus on either water or carbon flux estimates with various model complexity and uncertainties induced by distinct representation of the coupling between water and carbon processes. Here we propose a diagnostic model to estimate evapotranspiration and gross primary production that is based on biophysical mechanism yet simple for practical use. This is done by coupling the carbon and water fluxes via canopy conductance used in the Penman-Monteith-Leuning equation (named as PML_V2 model). The PML_V2 model takes Moderate Resolution Imaging Spectrometer (MODIS) leaf area index and meteorological variables as inputs. The model was tested against evapotranspiration and gross primary production observations at nine eddy-covariance sites in Australia, which are widely spread across climate conditions and ecosystems. Results indicate that the simulated evapotranspiration and gross primary production by the PML_V2 model are in good agreement with the measurements at 8-day timescale, indicated by the cross-site Nash-Sutcliffe Efficiency being 0.70 and 0.66, R^2 being 0.80 and 0.75 and root mean square error being 0.96 mm d^{-1} and 1.14 μmol m^{-2} s^{-1} for

evapotranspiration and gross primary production, respectively. As the PML_V2 model only requires readily available climate and MODIS vegetation dynamics data and has few parameters, it can potentially be applied to estimate evapotranspiration and carbon assimilation simultaneously at long-term and large spatial scales.

Key words: evapotranspiration, gross primary production, canopy conductance, eddy covariance, modelling

2.1 Introduction

The critical biophysical link between terrestrial water and carbon cycle is stomatal aperture. At leaf level, it not only regulates water vapour diffusion from leaves to the atmosphere (transpiration), but also controls plant fixation of carbon dioxide (CO_2) from the atmosphere through photosynthesis (carbon assimilation) simultaneously (Baldocchi et al., 1991). At ecosystems level, evapotranspiration (ET) and gross primary production (GPP) play vital roles in determining the global water and carbon balance (Beer et al., 2010; Jasechko et al., 2013). The degree of stomatal control on these water and carbon fluxes is quantified by bulk stomatal conductance (i.e., canopy conductance), estimate of which yet remains a major challenge for accurate estimate of ET and GPP (Kelliher et al., 1995).

Over decades, coupled carbon-water models based on diverse structure and parameterisation schemes have been developed to estimate canopy conductance (G_c) for such purpose. They can roughly be classified into two groups. One is the 'top-down' method, which utilises observed water and carbon exchanges to deduce G_c directly (Baldocchi et al., 1991; Granier et al., 2000; Stewart, 1988; Yebra et al., 2015, 2013). Due to the lack of consideration regarding the interrelated water and carbon processes, these models have difficulties in interpreting the underlying mechanism and uncertainties in predictions. The other one is 'bottom-up' upscaling approach, which usually integrates individual leaf stomatal response to environmental and physiological controlling factors up to canopy scale (Bonan et al., 2014, 2012; Cox et al., 1998; Dai et al., 2004; Running & Coughlan, 1988; Sellers, 1997; Tuzet et al., 2003; Wang et al., 2011). Models developed in this way tend to imply mechanistic equations to represent water loss and carbon fixation interactively from leaves to canopy, from stand to regional scales. Although these process-based models are widely used, the relatively high complexity turns out to impede general application and the performance can vary greatly across spatiotemporal scales (Bonan et al., 2014; De Kauwe et al., 2015; Morales et al., 2005; Wang et al., 2011).

Therefore, credible and feasible modelling scheme of water and carbon fluxes is still highly required and representation of a practical yet biophysically based G_c model remains elusive.

Numerous models have been developed to estimate ET (Norman et al., 1995; Bastiaanssen et al., 1998a, 1998b; McVicar & Jupp, 2002; Cleugh et al., 2007; Mu et al., 2007; Leuning et al., 2008; Zhang et al., 2009; Guerschman et al., 2009; Sun et al., 2011; Long and Singh, 2012; Yang et al., 2013; Fang et al., 2015) and GP*P* (Running et al., 2004; Ma et al., 2014; Yang et al., 2015; Yebra et al., 2015; Hu et al., 2017), from stand to regional and global scale during the past few decades. On the one hand, the Penman-Monteith (PM) equation (Monteith, 1965) based ET models have been proven as biophysically solid, which is often applied in combination with land surface information (e.g., radiation and vegetation) derived from remotely sensed imageries (Cleugh et al., 2007; Leuning et al., 2008; Mu et al., 2011; Morillas et al., 2013; Mallick et al., 2015; Zhang et al., 2016, 2017). However, carbon flux and the corresponding stomatal response are usually neglected in these models, which could induce uncertainties regardless of structure and conductance formulation (Liu et al., 2017). On the other hand, to couple carbon and water fluxes, biochemical photosynthesis models (Farquhar & von Caemmerer, 1892; Collatz et al., 1991) are commonly incorporated into stomatal conductance (g_s) models (e.g., Ball-Berry model) (Jarvis, 1976; Ball et al., 1987; Stewart, 1988; Collatz et al., 1991; Leuning, 1995; Tuzet et al., 2003; Medlyn et al., 2011) to obtain G_c and thereby simulate ET and GPP in earth system schemes (Sellers et al., 1996; Kowalczyk et al., 2006; Bonan et al., 2012). Additionally, there are also models that implies empirical carbon uptake function together with conductance models, where GPP is calculated by simply multiplying light use efficiency with environmental constrains (Hu et al., 2017; Liu et al., 2017). These coupled model structure can vary greatly according to the principles applied to conceptualise the canopy structural (e.g., big-leaf or multilayer) and physiology (e.g., sunlit and shaded) properties, as well as the photosynthesis model used to estimate assimilation rate (Wang & Dickinson, 2012; Zhu et al., 2016). As a result, evaluation of the model uncertainty in ET and GPP estimates remains difficult and application problematic.

Recognizing the relative advantages of satellite-based PM model in estimating ET, and the common employment of photosynthesis model in combination with g_s model, this study therefore explores the possibility of developing a relatively simple yet physiologically based model that couples water and carbon flux into G_c to calculate ET and GPP simultaneously. The couped model should be easily applicable using readily available environmental variables as model inputs only and have few parameters that are easy to be parameterised, yet maintain

basic physiological fundamentals. To achieve this, a Ball-Berry g_s model developed by Yu et al. (2004, 2001) and a hyperbola assimilation formula by Thornley (1976) is incorporated and integrated to derive a novel G_c model, which is then introduced into a remotely sensed data based PM model (Leuning et al., 2008; Zhang et al., 2016, 2017). In this way, GPP can be calculated as canopy assimilation and ET can be calculated from PM equation, respectively. The objectives of this study are as follows:

(1) Upscaling the assimilation and g_s model to obtain the coupled G_c model that is then introduced to the PM equation;

(2) Applying this simple coupled model together with remotely sensed leaf area index (LAI) to simulate ET and GPP; and

(3) Using carbon and water flux observations at flux towers to test the model performance.

2.2 Model Development

2.2.1 PML Model and Canopy Conductance

The two main components of terrestrial ET are transpiration from vegetation canopy (E_t) and evaporation from soil surface (E_s). Among the satellite based ET models (Cleugh et al., 2007; Mu et al., 2007, 2011; Leuning et al., 2008), the Penman-Monteith-Leuning (PML) model (Leuning et al., 2008) has routinely been used to estimate terrestrial ET and its components as a process-based approach (Zhang et al., 2017, 2016; Zhou et al., 2013). Hence, the PML model is used in this study as the prototype to develop a coupled water and carbon model. In the PML model, E_c and E_s are explicitly accounted for in the form of latent heat flux (λE) following:

$$\lambda E = \lambda E_c + \lambda E_s \quad \text{(Eq.2-1)}$$

$$\lambda E_c = \frac{\varepsilon Q_{A,c} + (\rho c_p/\gamma) D_a G_a}{\varepsilon + 1 + G_a/G_c} \quad \text{(Eq.2-2)}$$

$$\lambda E_s = \frac{f \varepsilon Q_{A,s}}{\varepsilon + 1} \quad \text{(Eq.2-3)}$$

where λ is the latent heat of evaporation (MJ kg^{-1}), Q_A is the total available energy (W m^{-2}), which is partitioned into canopy ($Q_{A,c}$) and soil ($Q_{A,s}$) available energy according to $\tau = exp(-k_A \cdot LAI)$, where $\tau = Q_{A,s}/Q_A$, k_A is extinction coefficient of Q_A and LAI is leaf area index derived from satellite imageries (Fisher et al., 2008; Leuning et al., 2008). In this model, transpiration is calculated by applying the PM equation exclusively to the canopy (Eq.2-2), where ε is the ratio of slope of the curve relating saturation water vapour pressure to temperature (Δ, kP_a $^oC^-$

^{1}) over the psychrometric constant (γ, $kPa\ ^{\circ}C^{-1}$), ρ is the air density ($kg\ m^{-3}$), D_a is the water vapour pressure deficit (VPD) of the air (kPa), G_a is the aerodynamic conductance ($m\ s^{-1}$), which is estimated following Leuning et al. (2008). G_c is the canopy conductance to water vapour ($m \cdot s^{-1}$).

Yet no carbon flux is explicitly taken into account in the PML model, the parameter G_c in Eq.2-2 provides the vital connection between plant biophysical process (i.e., stomatal control) and the environmental variables (e.g. solar radiation, humidity) (Hirose, 2005; Kelliher et al., 1995; Leuning et al., 2008), which can be calculated as:

$$G_c = \frac{g_{s,max}}{k_Q} ln\left\{\frac{Q_h+Q_{50}}{Q_{50}\exp(-k_Q LAI)+Q_{50}}\right\}\frac{1}{1+D_a/D_{50}} \quad \text{(Eq.2-4)}$$

where $g_{s,max}$ is the maximum stomatal conductance of the leaves at the top of the canopy ($m\ s^{-1}$), Q_h is the photosynthetically active radiation (PAR) ($W\ m^{-2}$), k_Q is the extinction coefficient of PAR, Q_{50} and D_{50} are the canopy absorbed PAR ($W\ m^{-2}$) and VPD (kPa) when $g_s = g_{s,max}/2$, respectively. This formulation of G_c is integrated from leaf level stomatal response to PAR only, with the carbon flux neglected and other environmental conditions assumed optimal. Detailed deduction of Eq.2-4 can be found in Kelliher et al. (1995) and Leuning et al. (2008).

Soil evaporation (E_s) in Eq.2-3 is calculated by reducing the Priestley-Taylor equilibrium evaporation (Priestley and Taylor, 1972) with a soil evaporation coefficient *f* that reflects the influence of water limitation on evaporation. A relatively robust formula developed by Zhang et al. (2010) is adopted in this study to estimate *f* as a variable controlled by precipitation and equilibrium evaporation (Fisher et al., 2008; Morillas et al., 2013; Zhang et al., 2010), which is expressed as:

$$f_{Zhang} = \min\left\{\frac{\sum_{i-n}^{i} P_i}{\sum_{i-n}^{i} E_{eq,s,i}}, 1\right\} \quad \text{(Eq.2-5)}$$

where *n* is the length of the 'time lag' used to balance soil water content after precipitation, P_i is precipitation in the *i*th day ($mm\ d^{-1}$), $E_{eq.s.i}$ is the equilibrium E_s ($mm\ d^{-1}$). For each of the *i*th day in the time series, *f* is calculated as the accumulative proportion of precipitation to soil evaporative demand of the previous *n* days (Zhang et al., 2010). Because *f* is insensitive to variations in *n*, after a sensitivity analysis, *n* = 32 days is given in Eq.2-5 in this study.

2.2.2 Coupled Canopy Conductance Model

As mentioned above, carbon assimilation is not considered in Eq.2-4 for calculating the key parameter G_c. To estimate the closely coupled water and carbon fluxes, this study tries to

formulate a novel G_c model that maintains biophysical meanings yet based on simple modelling framework for practical benefit. Following the upscaling principles, our canopy level G_c model is elaborated from leaf level g_s model and is given as follows:

$$G_c = \int_0^{LAI} g_s dl = m\frac{P_1}{k(P_2+P_4)}\left\{kLAI + ln\frac{P_2+P_3+P_4}{P_2+P_3\exp(kLAI)+P_4}\right\}\frac{1}{1+D/D_0} \quad \text{(Eq.2-6)}$$

where GPP is calculated as:

$$GPP = A_{c,g} = \frac{P_1 C_a}{k(P_2+P_4)}\left\{kLAI + ln\frac{P_2+P_3+P_4}{P_2+P_3\exp(kLAI)+P_4}\right\} \quad \text{(Eq.2-7)}$$

Detailed deduction of the G_c model and definition of each variable are illustrated in appendix.

Hence, a coupled G_c formula is obtained. This model can therefore be used to replace the original G_c equation (Eq.2-4) in the PML model to simulate ET, and GPP can be calculated by implementing Eq.2-6. The advantage of this coupled water and carbon PM model is that it requires routine environmental variables only for ET and GPP simulation, and has few parameters which maintain the physiological significances of stomatal response and assimilation process. Owing to the capacity of estimating ecosystem carbon fixation and water loss at the same time, this model is herein named as PML_V2 model. A summary of the seven parameters in this model is given in Table 2-1.

Table 2-1**.** Details of Seven Parameters in the PML_V2 Model

Parameter symbol	Definition	Unit	Allowed range
α	Initial slope of the light response curve to assimilation rate (i.e. quantum efficiency)	μmol CO_2 (μmol *PAR*)$^{-1}$	0.01-0.07
η	Initial slope of the CO_2 response curve to assimilation rate (i.e. carboxylation efficiency)	μmol m^{-2} s^{-1} (μmol m^{-2} s^{-1})$^{-1}$	0.01-0.07
m	Stomatal conductance coefficient	-	2-20
$V_{m,25}$	Notional maximum catalytic capacity of Rubisco per unit leaf area at 25 ˚C	μmol m^{-2} s^{-1}	10-120
D_0	Water vapour pressure deficit of the air	kPa	0.5-1.5
k_Q	Extinction coefficient of *PAR*	-	0.1-1
k_A	Extinction coefficient of available energy	-	0.5-0.8

2.3 Data and Methods

2.3.1 Eddy Covariance observations

The eddy covariance observations of energy, carbon and water exchange have been widely used to interpret terrestrial ecosystem processes. The OzFlux (http://www.ozflux.org.au/) is part of the Australian Terrestrial Ecosystem Research Network (TERN) and the global flux network (https://fluxnet.ornl.gov/). Within Australian continent, OzFlux provides continuous micrometeorological measurements of over 30 flux sites that covers most Australian climate range and ecosystem types (Isaac et al., 2016). This provides us the excellent dataset for model development and testing for the distinct Australian ecosystems.

Observations of water and carbon flux at nine flux sites in OzFlux network were used to evaluate the proposed PML_V2 model (Figure 2-1). The following criteria were used to filter available flux sites and measurements: (1) the flux site should have more than two years of continuous observations (since 2000), (2) observations of low confidence were excluded and the reliable data should be more than 80% within each year at each site, and (3) half-hourly observations of each variable were filtered to obtain daytime measurements only and further processed to obtain daily observations. Night time observations were eliminated using the incoming shortwave radiation (R_s) greater than 20 W m^{-2} to avoid micrometeorological and instrument uncertainties (Ershadi et al., 2014; Isaac et al., 2016). Daytime GPP was calculated as the difference of observed net ecosystem exchange (NEE) and daytime ecosystem respiration (R_d), where R_d is estimated from observed night time ecosystem respiration (Bruhn et al., 2011; Papale et al., 2006; Reichstein et al., 2005; Shi et al., 2014). The GPP calculated from this algorithm was used as the observed GPP_{obs} for model use. The daily dataset is further aggregated to obtain 8-day average values in accordance with the temporal resolution of remote sensed LAI (Hu et al., 2017; Papale & Valentini, 2003; Shi et al., 2014).

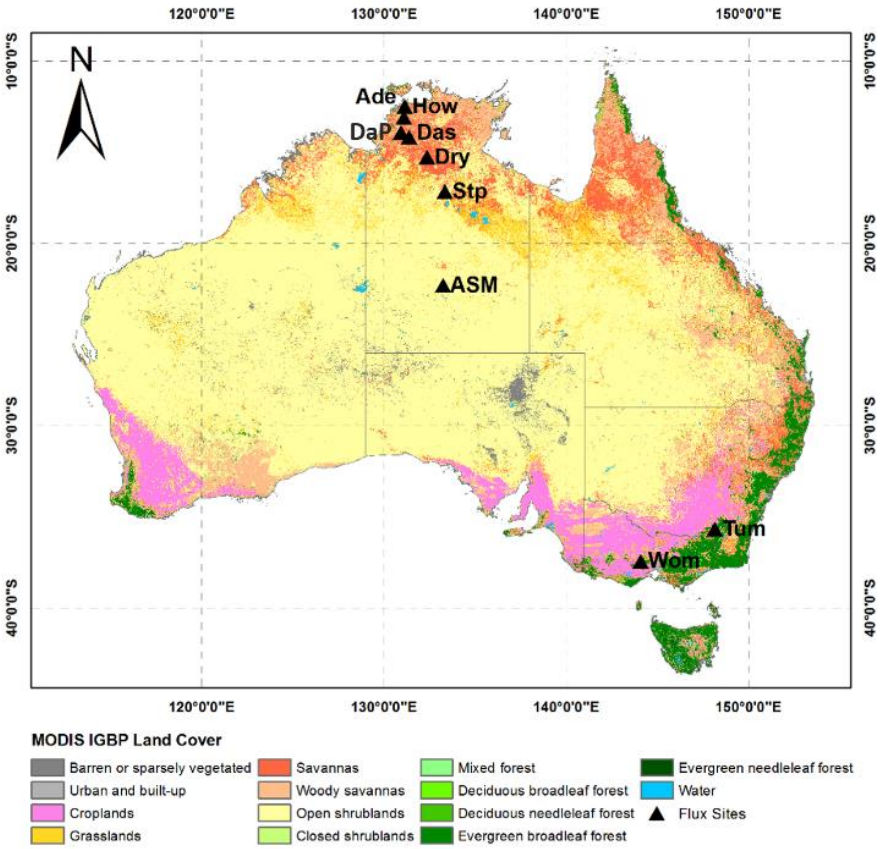

Figure 2-1**.** IGBP Land Cover Type Classification across Australia and locations of the flux sites used in this study. Remote sensing land cover data was downloaded from Moderate Resolution Imaging Spectrometer MCD12Q1 product.

In total, nine Australian flux sites with 45 site-years (482 site-months) of *in situ* eddy covariance measurements were selected at last for further analysis. These sites represent a wide range of Australian climate regions from tropical to temperate and across five different plant functional types (PFTs), including 3 savannas (SA), 1 woody savanna (WSA), 2 grasslands (GRA), 1 open shrub land (OSH) and 2 evergreen broadleaf forests (EBF). Site details are presented in Table 2-1.

Table 2-1. Details of The Nine Australian Flux Sites Used in This Study to Evaluate The PML_V2 model.

Site Code	Site Name	Climate*	PFTs	S Latitude	E Longitude	Canopy Height (m)	Annual Precipitation (mm/year)	T_{air}(˚C) Range	LAI (m^2 m^{-2}) Range	Period Start-End (year)	Reference
AU-ASM	Alice Springs Mulga	TR	OSH	-22.28	133.25	6.5	306	-4~46	0.18~0.61	2011~2012	(*Cleverly et al.*, 2013)
AU-Ade	Adelaide River	TR	SA	-13.08	131.12	16.4	1730	16~36	0.60~1.74	2007~2008	(*Beringer et al.*, 2016)
AU-DaP	Daly River Pasture	TR	GRA	-14.06	131.32	1.8	1250	15~31	0.53~3.68	2007~2012	(*Beringer et al.*, 2016)

AU-Das	Daly River Uncleared	TR	SA	-14.16	131.39	16.4	1170	12~37	0.72~2.00	2007~2012	(*Beringer et al.*, 2016)
AU-Dry	Dry River	TR	SA	-15.26	132.37	0.15	895	14~37	0.82~1.65	2010~2012	(*Beringer et al.*, 2016)
AU-How	Howard Springs	TR	WSA	-12.50	131.15	16	1700	20~33	0.76~2.36	2004~2012	(*Beringer et al.*, 2016)
AU-Stp	Sturt Plains	TR	GRA	-17.15	133.35	0.5	640	11~39	0.23~1.02	2010~2012	(*Beringer et al.*, 2016)
AU-Tum	Tumbarumba	T	EBF	-35.66	148.15	40	1000	-10~30	2.72~5.52	2001~2012	(*Leuning et al.*, 2005)
AU-Wom	Wombat State Forest	T	EBF	-37.42	144.09	25	650	1~30	3.24~5.32	2011~2012	(*Van Gorsel et al.*, 2016)

* Climate is categorised into tropical (TR) and temporal (T).

In situ eddy covariance energy flux data werse eliminated when λE observations were negative and $||R_n - G| - |H + \lambda E|| > 250$ W m^{-2} to ensure the surface energy balance closure, where R_n, G and H are the measured net radiation, ground heat flux and sensible heat flux, respectively (Cleugh et al., 2007; Leuning et al., 2008; Wilson et al., 2002). Consequently, the observed λE is used in the parameterisation and evaluation of the PML_V2 model.

2.3.2 Remotely Sensed Data

Remotely sensed LAI with the temporal resolution of 8-day and the spatial resolution of 1km was acquired from MODIS products (MOD15A2) (http://daac.ornl.gov). At each flux site, LAI data lie in the 3 × 3 km centred grid matrix according to the flux coordinates was selected to obtain LAI time series. The 3 × 3 km centred grid data is used to reduce the mismatch between the course MODIS pixels and the footprint size of the flux sites (Shi et al., 2014). The 8-day data was processed through quality control, interpolation and filtering using the TIMESAT tool (Jönsson & Eklundh, 2004) to obtain high quality LAI for model use (Zhang & Wegehenkel, 2006).

Additionally, remote sensed ET from MOD16A2 and GPP from MOD17A2, with 8-day temporal resolution were downloaded from the Numerical Terradynamic Simulation Group (NTSG) (http://www.ntsg.umt.edu), which were then extracted at each flux site for comparison with the PML_V2 modelled results.

2.3.3 Evaluation of Model Performance

The global optimisation method –genetic algorithm– in MATLAB® (The MathWorks, Inc.) was used to calibrate the PML_V2 model parameters at each flux site. A multi-objective cost function (F_{cost}) was setup to maximise the sum of the Nash-Sutcliffe efficiency (NSE) between simulated and observed ET and GPP as:

$$F_{cost} = NSE_{ET} + NSE_{GPP} \quad (2\text{-}8)$$

$$NSE_{ET} = 1 - \frac{\sum_{i=1}^{N} |ET_{sim,i} - ET_{obs,i}|^2}{\sum_{i=1}^{N} |ET_{obs,i} - \overline{ET}_{obs}|^2} \quad (2\text{-}9)$$

$$NSE_{GPP} = 1 - \frac{\sum_{i=1}^{N} |GPP_{sim,i} - GPP_{obs,i}|^2}{\sum_{i=1}^{N} |GPP_{obs,i} - \overline{GPP}_{obs}|^2} \quad (2\text{-}10)$$

Where subscripts *obs* and *sim* represent observation and simulation, respectively. *N* is the length of the 8-day time series at each site. Thus, estimates of ET and GPP using the PML_V2 model was evaluated using the NSE of 8-day ET and GPP, respectively. At each flux site, the four parameters are optimised to maximise NSE_{ET} + NSE_{GPP} as given in Equation 8-10 using available data. Optimised parameters that gives the best estimation of both ET and GPP with maximum F_{cost} are selected as the site-specific parameter set.

In addition to NSE, we also used the standard metrics for evaluating model performance, namely the linear regression slope, the coefficient of determination (R^2) and the Root Mean Square Error (RMSE), as given below:

$$R^2 = \left(\frac{\sum_{i=1}^{N} (X_{sim,i} - \overline{X}_{sim})(X_{obs,i} - \overline{X}_{obs})}{\sqrt{\sum_{i=1}^{N} (X_{sim,i} - \overline{X}_{sim})^2 \sum_{i=1}^{N} (X_{obs,i} - \overline{X}_{obs})^2}} \right)^2 \quad (2\text{-}11)$$

$$RMSE = \sqrt{\frac{1}{\mathrm{N}} \sum_{i=1}^{N} (X_{sim,i} - X_{obs,i})} \quad (2\text{-}12)$$

where *X* represents the evaluated variable, either ET or GPP in this study. Higher slope, NSE and R^2 and lower RMSE indicates good model performance.

Two experiments were set to evaluate the ability of the model in estimating ET and GPP. Firstly, the PML_V2 model was calibrated at each flux site using all available data individually. In this way, model performance and parameter variability are examined across sites. Secondly, the available data at each flux site was split into half and each of the half data set was used to calibrate the model in turn. The predicted ET and GPP from the validation period was then accumulated to obtain continuous time series at each site as predictions. This experiment tests the robustness of the model in predicting ET and GPP.

2.4 Results

2.4.1 Sensitivity Analysis

Among the seven parameters (Table 2-1), previous studies have shown that D_0, k_Q and k_A are insensitive parameters to estimate ET in the PML model (Leuning et al., 2008; Zhang et al., 2008). Similarly, we conducted a sensitivity analysis for all the parameters in the PML_V2

model. With all of the seven parameters optimized, the values ranged between 0.50–1.5 for D_0, 0.10–0.82 for k_Q and 0.50–0.80 for k_A across the nine sites. However, when given D_0=0.7, k_Q= 0.6 and k_A=0.7 as constants, we yield identical estimates for the rest four parameters (α, η, m, and $V_{m,25}$) and the statistics of simulated ET and GPP (data not shown). Thus, a similar conclusion was drawn that performance of the PML_V2 model is relatively insensitive to variations in D_0, k_Q and k_A. Therefore, all the following results are presented with only the free parameters: α, η, m, and $V_{m,25}$ optimised in this study. Additionally, as the model is relatively insensitive to variations in the atmospheric CO_2 concentration and the observation is not readily available, C_a is given as 380 μmol mol^{-1} despite the value can vary in reality. Since water and carbon fluxes are coupled via G_c (Section 2.2), the sensitivity of G_c to variations in α, η, m, and $V_{m,25}$ is herein examined as shown in Figure 2-1.

As can be seen from Figure 2-2, lower α results in a lower G_c and so does η. With α or η increasing to its upper limit (i.e., 0.07), the sensitivity of G_c to these two parameters reduces to a smaller degree than that of their lower limits. However, it is not the case for m, where G_c shows an equal variation degree within the allowed limits. As for $V_{m,25}$, variation in G_c within lower $V_{m,25}$ values (below 70 μmol m^{-2} s^{-1}) is much higher than that of larger $V_{m,25}$ range (70~120 μmol m^{-2} s^{-1}). Hence the model performance is likely to be relatively sensitive in variations of the parameter η and m but less so in α and $V_{m,25}$. Further model experiment indicates that the parameterised values of η and m show a larger variation across biomes, which means they are key parameters that control ET and GPP estimates in this model.

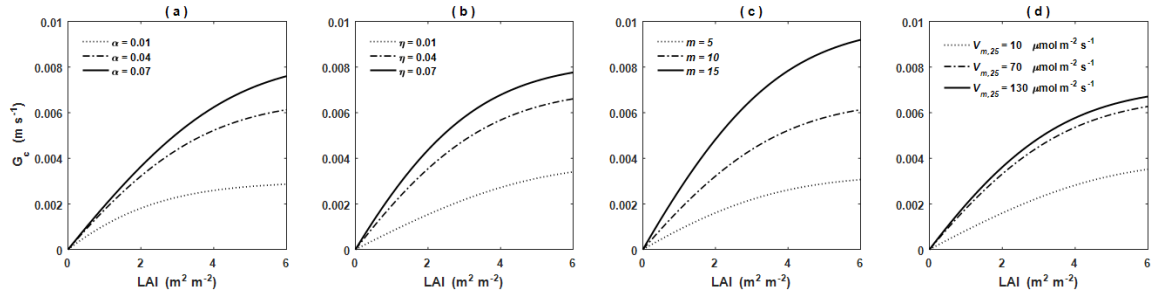

Figure 2-2. Response of G_c to (a) α , (b) η , (c) m , (d) $V_{m,25}$. Except when varied, parameter values are α = 0.04, η = 0.03, m = 10, $V_{m,25}$ = 50 μmol m^{-2} s^{-1}. R_s = 500 W m^{-2}, PAR is assumed to be 0.45R_s, D = 1 kPa, D_0 = 0.7 kPa, Pa = 100 kPa, T_{air} = 25 ˚C, C_a = 380 μmol mol^{-1}, k_A = k_Q = 0.6.

2.4.2 Parameterization

For individual parameterisation at each flux site, the optimised values of the four parameters are presented in Table 2-3. All of the parameters vary within a wide range across sites in general. The initial slopes of the assimilation response curves to light (α) and CO_2 (η) ranged between 0.05–0.07 (μmol CO_2 (μmol PAR)$^{-1}$) and 0.013–0.063 (μmol m^{-2} s^{-1} (μmol m^{-2} s^{-1})$^{-1}$), respectively. While α shows a relatively small variation amongst nine sites (average 0.067 μmol CO_2 (μmol PAR)$^{-1}$), smaller η values were detected at two forest sites (about 0.015 μmol m^{-2} s^{-1} (μmol m^{-2} s^{-1})$^{-1}$) when compared to that of the non-forest sites in general (between 0.013-0.063 μmol m^{-2} s^{-1} (μmol m^{-2} s^{-1})$^{-1}$). Besides, stomatal conductance coefficient (m) ranged from 5.75 to 20 across all biomes. In addition, $V_{m,25}$ also varied considerably from 34 μmol m^{-2} s^{-1} at DaP to 120 μmol m^{-2} s^{-1} at five different sites (Das, Dry, ASM, Tum and Wom). However, no clear pattern was observed for the difference in m and $V_{m,25}$ values across biomes.

Table 2-2. Optimised Parameter Values of the PML_V2 Model at Nine Australian Flux Sites

Site Name	PFT	Optimized Parameter Values			
		α	η	m	$V_{m,25}$
ASM	OSH	0.07	0.026	5.7	120
Ade	SA	0.07	0.063	13.4	36
DaP	GRA	0.07	0.013	9.75	34
Das	SA	0.07	0.024	12.2	120
Dry	SA	0.07	0.020	8.6	120
How	WSA	0.07	0.028	16.5	108
Stp	GRA	0.07	0.022	20	82
Tum	EBF	0.06	0.014	14.7	120
Wom	EBF	0.05	0.015	12.6	120
Parameter Range		0.01-0.07	0.01-0.07	2-20	10-100

* The model is calibrated by maximizing $NSE_{ET} + NSE_{GPP}$ using all available data at each site independently.

2.4.3 Model Calibration

Site-specific parametrisation results are used to evaluate the model performance with the parameters α, η, m, and $V_{m,25}$ optimised. Figure 2-3 presents the statistics of simulated ET and GPP at 8-day temporal resolution when compared to observations. It can be seen that the model performs well in simulating both ET and GPP. Collectively, the model explains 80% and 71% of variations in ET and GPP, respectively, with the average NSE values at 0.71 for ET and 0.63

for GPP across biomes. This indicates a reasonably high degree of estimating water and carbon fluxes using the PML_V2 model. This is further evident from a large linear regression slope and lower RMSE values (Figure 2-3). Additionally, the PML_V2 model performed slightly better in 8-day ET estimates than GPP. On average, the model explains 9% higher of ET variation than that of GPP, yet with a much smaller difference in NSE (about 0.07). The lower slopes of GPP indicate that the algorithm tends to underestimate GPP by 20-40% across sites.

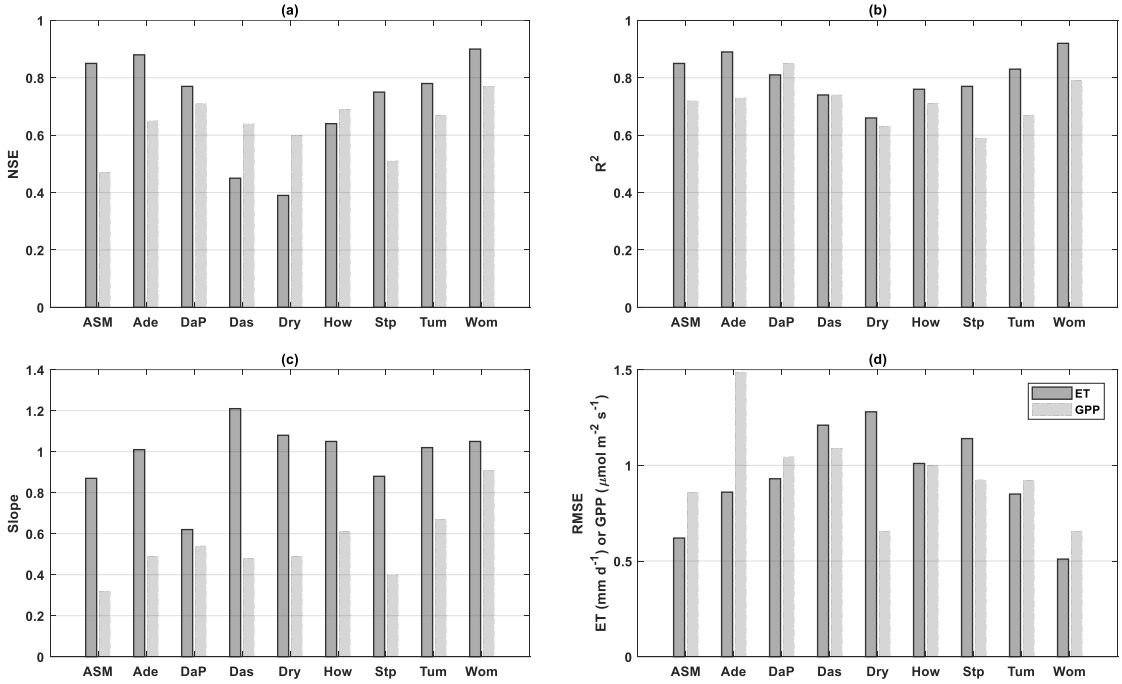

Figure 2-3. Statistics of model performance at 8-day time scale for ET and GPP estimates. The parameters are derived from independent optimisation using all available data at each site. Nash-Sutcliffe efficiency (NSE), coefficient of determination (R^2), linear regression slope and RMSE, root mean square error of simulation against observation for both ET and GPP are presented.

Except general good performance, the model can successfully capture seasonal variation in ET and GPP as well. The observed and simulated 8-day time series ET and GPP are presented in Figure 2-4 and Figure 2-5 for each of the nine study sites, respectively. Result in Figure 2-4 indicates that the model is capable of reproducing seasonal pattern in actual ET, yet a slightly better performance can be found during higher precipitation periods when compared to that of lower precipitation periods for most sites. The higher consistency between simulated and observed ET is detected for forest sites (Tum and Wom) than non-forest sites throughout the year, especially during lower precipitation periods. Additionally, the PML_V2 model could also reproduce reasonably good temporal dynamics for GPP (Figure 2-5). Using observed GPP as benchmark, the best model performance was found at the grassland site DaP (NSE=0.85),

followed by the forest site Wom (0.79) and two savanna sites Das (R^2=0.74) and Ade (R^2=0.73). However, the model performs worst at the grassland site Stp (R^2=0.59). The seasonal variation in GPP tends to be overestimated during lower GPP periods where water availability (precipitation) is limited, especially for non-forest biomes (SA, OSH and GRA).

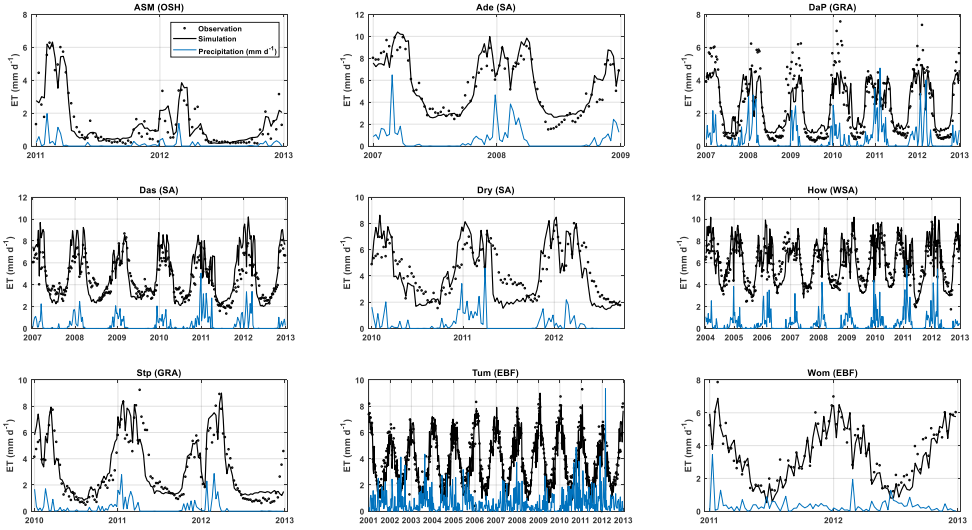

Figure 2-4. Time series of 8-day average ET and precipitation in mm d^{-1} at nine flux sites. Observed ET is derived from latent heat flux measurements. Simulated ET is result yielded from PML_V2 model with four parameters optimised at each site independently (i.e., Table 2-3).

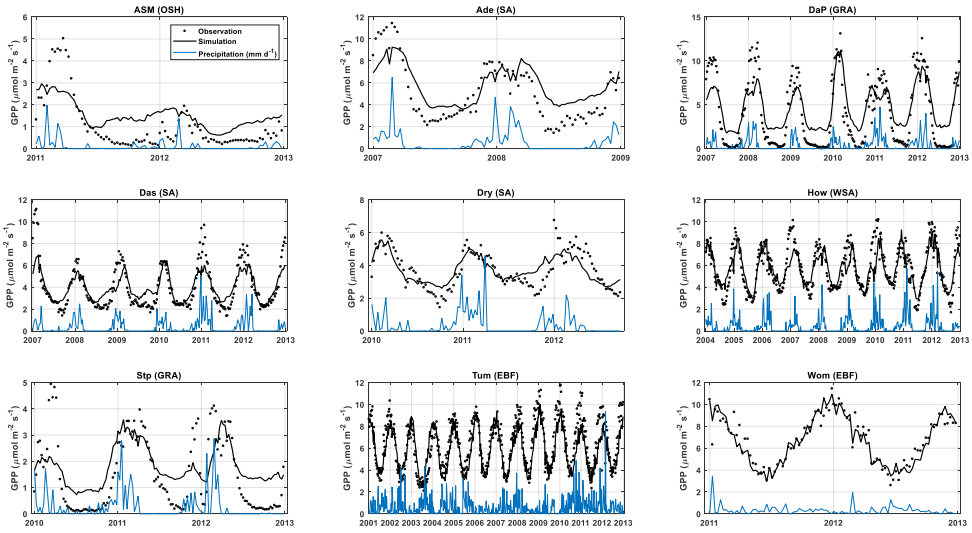

Figure 2-5. Time series of 8-day average GPP in μmol m^{-2} s^{-1} at nine flux sites. Observed GPP is derived from carbon flux measurements. Simulated GPP is result yielded from PML_V2 model with four parameters optimised at each site independently (i.e., Table 2-3).

2.4.4 Model Validation

Time series derived from the half-split validation experiment (section 3.3) were used to evaluate the model robustness of predicting ET and GPP. For each of the nine sites, we split the data into half and used each half data for calibration and the remaining half for validation in turn. Thereby the ET and GPP predictions during each of the half validation period is yield by applying the model with optimised parameters obtained from calibration period. Since the two parameter sets yield for each site are very close to those optimised with all data at the same site in general, the two half predictions are merged into a full time series at each site to evaluate model performance.

Collectively, the cross site average NSE, R^2 and slope are 0.70, 0.80 and 0.97 for 8-day ET and 0.61, 0.71 and 0.54 for 8-day GPP, respectively. RMSE is 0.95 mm d^{-1} for ET and 1.02 μmol m^{-2} s^{-1} for GPP across sites (data not shown). This result is very close to that of calibration (Figure 2). Figure 2-6 presents the model performance degradation from calibration to validation, as indicated by the statistical difference between the two at each site. As can be seen that there is only slight degradation found in both ET and GPP. NSE and R^2 of 8-day ET was nearly identical with that of model calibration, with the maximum difference of NSE found at Ade and Das, yet the overall RMSE increased less than 0.1 mm d^{-1}. Additionally, despite the minor degradation in R^2 value for 8-day GPP at most sites, maximum decrease in NSE is found at ASM and Tum (0.05), followed by Ade (0.03) and Stp (0.02), and RMSE increased less than 0.12 μmol m^{-2} s^{-1} for all sites, which indicate a marginal degradation in general. Note that a better validation is detected for GPP at Stp in terms of R^2 and for ET at Tum in terms of RMSE, yet the difference is minor. This is caused by optimising the Eq. 2-11, where the optimal solution is achieved by compromising NSE between GPP and ET. When the ET validation increases, the GPP validation depredates to obtain better overall results. The overall results imply that the PML_V2 model is of high robustness in predicting both ET and GPP.

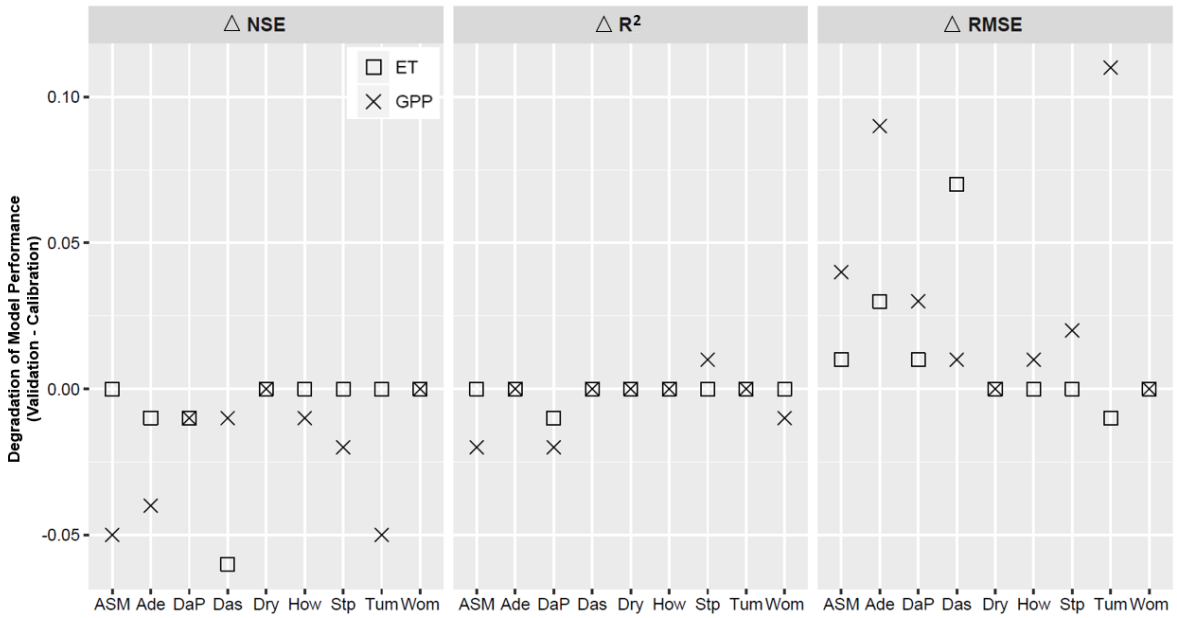

Figure 2-6. Degradation of model performance from calibration to validation at each of the nine sites. Statistics shown are the difference of R^2, NSE and RMSE as validation minus calibration, with the black and shaded symbols representing the values of ET and GPP, respectively.

2.5 Discussion

2.5.1 Model Parameters

The values of the optimised parameters were comparable to previous studies. The average quantum efficiency α yield from PML_V2 (0.067 μmol CO_2 (μmol PAR)$^{-1}$) is consistent with the values in Yu et al. (2004). Results with the four parameters calibrated show that α is clearly different between forest and non-forest sites. Lower α values (about 0.58 μmol CO_2 (μmol PAR)$^{-1}$) in site Tum and Wom indicate the heterogeneity in the radiation response in these energy-limited ecosystems, whereas higher α (0.070 μmol CO_2 (μmol PAR)$^{-1}$) at other sites represents a roughly similar pattern of light response among savanna, shrubs and grassland for their patchy vegetation cover. The estimated carboxylation efficiency η is generally lower in forest sites (about 0.015 μmol m^{-2} s^{-1} (μmol m^{-2} s^{-1})$^{-1}$) and higher at non-forest sites (vary from 0.013 to 0.63 μmol m^{-2} s^{-1} (μmol m^{-2} s^{-1})$^{-1}$). This implies that the woody ecosystem is relatively insensitive response to changes in CO_2 concentration than herbaceous ones. Meanwhile, the stomatal conductance coefficient m shows a wide variation across biomes, which all fall into the optimal range. In addition, smaller $V_{m,25}$ values were found in Ade, DaP and Stp with all

the rest sites having larger $V_{m,25}$ values. As canopy conductance became insensitive at high $V_{m,25}$ values (Figure 2-2), this could be a result of the fixed *a* and *b* given as a constant under 25 ˚C and 41 ˚C in the model as mentioned above.

In the PML_V2 model, α was calibrated as a constant whereas in reality, it could change with water availability, being higher in the wet season but lower in the dry season as higher water availability usually induces higher quantum efficiency (Eamus et al., 2013). Further study is required to obtain α that varies against water factors such as precipitation or soil water content, to improve model performance in the dry season. Besides, we introduced a notional catalytic capacity $V_{m,25}$ into the model, which is different from the commonly used maximum carboxylation rate $V_{c,max}$, yet a similar optimal range was given for optimisation (Kattge & Knorr, 2007; Bonan et al., 2012). Although $V_{m,25}$ has been adjusted to temperature accordingly, it should be noted that the obtained values is different from those of $V_{c,max}$. However, the model performance is relatively insensitive to variations of this parameter at 8-day temporal scale despite the leaf level internal control of conductance to photosynthesis (Chen et al., 1999).

2.5.2 Comparison with MODIS products and other studies

The MODIS products are widely used to map global ET and GPP and compare with modelled results. We hereby conducted a brief comparison of the predicted results using PML_V2 model with that derived from MODIS product. MODIS ET (MOD15A2) (ET_{MODIS}) and GPP (MOD17A2) (GPP_{MODIS}) time series was extracted and processed at the nine study sites. The predicted ET and GPP from PML_V2 model were compared with ET_{MODIS} and GPP_{MODIS} at 8-day scale against observations as shown in Figure 2-7. As expected, MODIS products perform worse than PML_V2 model in general. Despite negative NSE values of MODIS (set to zero in Figure 2-7(a) and (d)), the average R^2 yield from MODIS products across sites is 0.68 for ET and 0.51 for GPP, which explains 12% and 22% less variations in ET and GPP when compared to PML_V2 model, respectively. Moreover, the RMSE values of PML_V2 are clearly lower than that of MODIS. Specifically, ET_{MODIS} tends to underestimate actual ET at non-forest sites (i.e., Ade, Das, Dry, How, ASM and Stp), especially during low precipitation periods, but overestimates at forests (i.e., Tum and Wom) throughout the study period (data not shown). This suggests that it is hard to satisfactorily use the globally parameterised two MODIS products for Australian biomes, where the proposed PML_V2 model is of high reliability and robustness in ET and GPP estimate.

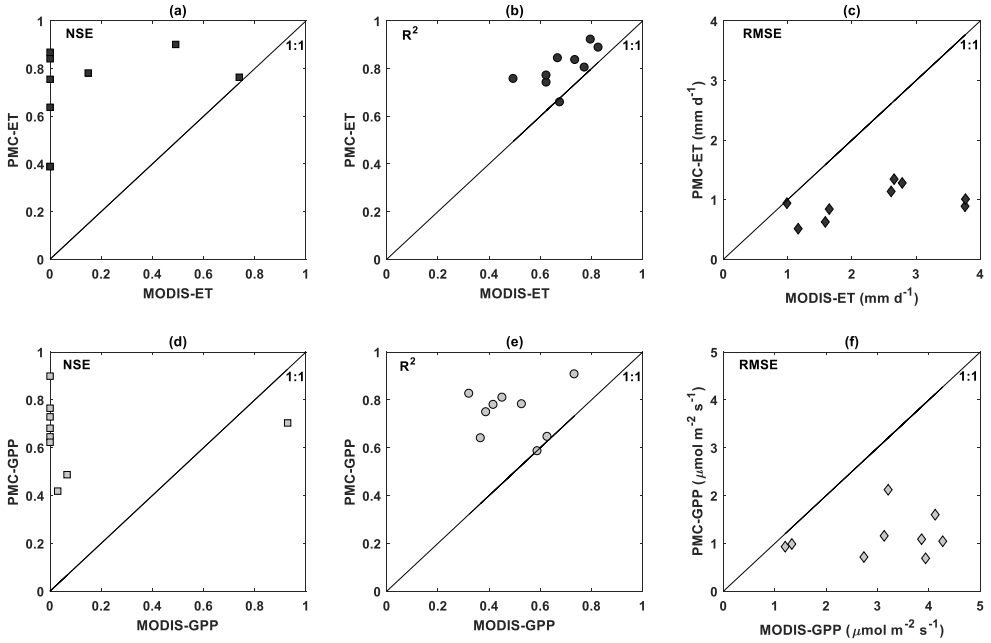

Figure 2-7**.** Statistic comparison of PML_V2 model (in validation mode) and MODIS products at nine Australian flux sites. NSE, R^2 and RMSE are given for ET (a-c) as black and GPP (d-f) as shaded symbols, respectively. The negative NSE values of MODIS products in (a) and (d) are set to zero to indicate low performance.

In addition, we also compared our modelled results with other two coupled models at sites where available, namely How and Tum which are commonly used in the literature. Only the site-specific parameterisation performance is used for fair comparison as given in Table 2-4. On average, the R^2 and RMSE of ET is better or about the same with that obtained by Hu et al. 2017 and Yebra et al. (2013), and GPP is closely comparable, or better than the simulation yield by Hu et al. (2017) and Yebra et al. (2015) using their coupled model. This gives us confidence that the PML_V2 model proposed here is relatively simple yet reliable to estimate ET and GPP.

Table 2-3. Model comparison with MODIS and reference at two Flux Sites (How and Tum). Shown are the Coefficient of Determination (R^2) and Root mean square error (RMSE) derived from the PML_V2 model predictions and results from literature.

Reference	Temporal Period	Temporal Resolution	How				Tum			
			ET	ET	GPP	GPP	ET	ET	GPP	GPP
			R^2	RMSE mm d^{-1}	R^2	RMSE μmol m^{-2} s^{-1}	R^2	RMSE mm d^{-1}	R^2	RMSE μmol m^{-2} s^{-1}
This study	2001-2012	8-day	0.76	1.01	0.75	1.04	0.84	0.84	0.81	1.09

Yebra et al. (2015, 2013)	2001-2006	16-day(ET) 8-day(GPP)	0.79	0.14	0.76	1.17	0.68	0.52	0.53	1.85
Hu et al. (2017)	2001-2006	8-day	0.67	0.90	0.57	1.79	0.85	0.84	0.78	2.43

2.5.3 Model uncertainty

The advantage of the PML_V2 model is, as described in the Eq. 2-6, inclusion of both energy and carbon responses in a simple coupled formulation, which keeps the biological energy-driven mechanism, and includes CO_2 as an independent environmental constraint (Thornley, 1976, 1998a; Kelliher et al., 1995). Compared with the eddy covariance observations, the PML_V2 model yield satisfactory estimates of ET and GPP in general (Figure 2-3, 2-4), with slightly better performance for ET than GPP detected (Figure 2-3, 2-5). This could be a result of the following factors. First, available energy is the foremost environmental driving variable triggering stomatal activities, rather than CO_2 concentration. The PML_V2 model kept the energy-driven response of stomata to multiple environmental variables, yet the photosynthesis model was introduced. This induces a lower model sensitivity of simulating ET with the energy driven G_c formula, in which GPP was calculated as a relatively weak carbon constrain. Second, regarding the two components of ET, transpiration through stomata in the PML_V2 model depends on canopy interaction with the atmosphere, whereas soil evaporation is not related to stomatal behaviour. The uncertainty of estimated transpiration from the carbon constraint is mitigated by evaluating total ET as the sum of transpiration and soil evaporation. Third, GPP is controlled not only by PAR and temperature but also other environmental factors such as soil moisture (Eamus et al., 2013; Cleverly et al., 2016a) and atmospheric CO_2 concentration (Donohue et al., 2013), which is not explicitly considered in the present PML_V2 model due to model simplicity and data availability concern. However, among the nine flux sites used in our study, seven of which are located in warm and arid environments where the ecosystems are water limited (Figure 2-4, 2-5). Vegetation in these ecosystems relies on water availability and may have developed deep root system to support growth during relatively short dry period. This can be an explanation for less satisfactory model performance at the non-forest sites, where high GPP periods are underestimated by our model. However, when precipitation remains extremely low, GPP is again water limited during long dry periods, yet the model lacks the water constrain in calculating GPP during these periods. Additionally, these warm and dry ecosystems are sensitive to variations in CO_2 concentration, yet which value is given as 380 μmol mol^{-1} across sites. As the study period is relatively short, this is a fair assumption but not

for long term pattern. The model performance is likely to be improved by introducing other environmental constrains such as precipitation and soil moisture into the model. At specific sites, the model well captured the GPP variation throughout the study period at EBF sites (i.e., Tum and Wom), but less so at OSH (ASM) and GRA (Stp and DaP) sites during both peak and low GPP periods. Considering the fact that the peaks at ASM and Stp were real (Cleverly et al., 2013; Eamus et al., 2013) and contributes greatly to the global carbon sink anomaly (Poulter et al., 2014; Cleverly et al., 2016b), the relatively less satisfactory model performance on high and low GPP values can be explained as a result of using NSE as the objective function to parameterise the PML_V2 model (Eq. 2-11, 2-12). NSE could induce sub-optimal solutions when the dataset contains extremely large values. For ASM, with only two years data available, extreme high GPP observations at the beginning of 2011 can cause large uncertainties in model performance, thus bring large bias for GPP peaks in wet season and minima in dry season (Figure 4). For Stp and DaP, extreme low GPP observations occur repeatedly each year and hence jeopardise the overall model performance. Additionally, the photosynthesis principles adopted in PML_V2 model is relatively simple and empirical (rectangular hyperbola), which generally accounts for C_3 rather than C_4 species. Despite there is a fair difference between C_3 and C_4 assimilation process, and some of the non-forest sites are partly C_4 grass dominated, the model fails to distinguish this difference thus lead to poor results at these sites. Further investigation is required to test how and to what level would the biological process influence modelled ET and GPP.

It is also noteworthy that we adopted the big-leaf scaling-up method to obtain canopy level carbon uptake and conductance, which could induce uncertainties in ET and GPP estimates due to scaling effect. In fact, there is a diffuse difference of radiation between sunlit and shaded leaves, which means the water vapour flux and assimilation rate can vary greatly between the these two type of leaves and the effect is detectable at canopy level (Irmak et al., 2008; Zhang et al., 2011). However, this difference is neglected in the big-leaf approach thus bring uncertainties for simulating ET and GPP. The canopy heterogeneity at both horizontal and vertical direction also means the bulk canopy conductance and assimilation is not simply the sum of the leaf level water loss and carbon gain. Hence, higher accuracy of ET and GPP estimates are expected by taking such scaling issues into consideration in future study.

2.6 Conclusions

This study developed a coupled PML_V2 model to estimate evapotranspiration and carbon assimilation using a relatively simple structure while retaining reasonable biophysical significance. The model was examined against observations from eight flux sites that cover a wide range of climate and biome types in Australia. The model performed well in both ET and GPP simulation at 8-day temporal scale. Sensitivity analysis and validation experiment as well as comparison with other modelled results further demonstrate that the proposed PML_V2 model is good for estimating ecosystem water and carbon fluxes. This is an ongoing study. We are testing its performance in other parts of world, and integrating the PML_V2 model into catchment hydrological modelling for broader ecological and hydrological applications from catchment to region.

Appendix

The canopy conductance G_c in the PML_V2 model is deducted from stomata conductance as follows:

The widely used Ball-Berry g_s model (Ball et al., 1987) was developed from leaf gas exchange experiments as:

$$g_s = g_0 + m\frac{A_n h_s}{C_s} \quad \text{(2-A1)}$$

where g_0 is the value of g_s at the light compensation point (mol m^{-2} s^{-1}), m is stomatal conductance coefficient, C_s is leaf surface CO_2 concentration (μmol mol^{-1}), h_s is relative humidity and A_n is net assimilation rate (μmol m^{-2} s^{-1}). As stomata response to leaf surface VPD (D_s) rather than h_s, Leuning (1995) replaced h_s in Eq.2-A1 with a hyperbolic constrain of D_s to g_s and gave:

$$g_s = g_0 + m\frac{A_n}{(C_s - \Gamma)(1 + D_s/D_0)} \quad \text{(2-A2)}$$

in which Γ is CO_2 compensation concentration (μmol mol^{-1}) and D_0 is a parameter that represents the sensitivity of g_s to D_s. Note that above mentioned g_s models (Eq. 2-A1 and Eq. 2-A2) simulates stomatal conductance to carbon flux, and the stomatal conductance to water vapour can be approximated as 1.6 times of that to carbon flux (Medlyn et al., 2011; Yebra et al., 2015).

To obtain g_s according to Eq. 2-A1 or Eq. 2-A2, the biochemical photosynthesis model developed by Farquhar et al. (1980) is commonly implemented to calculate A_n, in which the rate of CO_2 uptake is limited either by Rubisco activity (J_c), electron transport (J_e) or exportation or utilisation capacity of photosynthetic products (J_s) (Collatz et al., 1991). Although this method is widely used, parameters of this model are difficult to obtain, and the description of the underlying processes remains elusive (Thornley, 1998b).

On the aware of practicability of the model, we therefore intend to develop a simple and coupled G_c model based on gross photosynthesis and stomatal response. According to Yu et al. (2001), considering the fact that g_s increases immediately with light incidence, A_n should be replaced by gross assimilation rate (A_g, μmol m^{-2} s^{-1}) and use C_s instead of $C_s - \Gamma$ in Eq.2-A2. Additionally, A_g and g_o goes to zero in dark, D_s and C_s can be approximated using D_a and C_a, respectively, Yu et al. (2004) suggests that g_s can be written as a function of A_g, C_a and D_a at leaf level as:

$$g_s = m\frac{A_g}{C_a(1+D_a/D_0)} \tag{2-A3}$$

in which C_a is the atmospheric CO_2 concentration, the gross assimilation A_g is calculated following Thornley (1976) as a rectangular hyperbola function to both PAR and C_a as:

$$A_g = \frac{A_m\alpha I\eta C_a}{A_m\alpha I + A_m\eta C_a + \alpha I\eta C_a} \tag{2-A4}$$

where α is the initial slope of the light response curve to assimilation rate (i.e. quantum efficiency) (μmol CO_2 (μmol PAR) $^{-1}$), η is the initial slope of the CO_2 response curve to assimilation rate (i.e. carboxylation efficiency) (μmol m^{-2} s^{-1} (μmol m^{-2} s^{-1})$^{-1}$), I is the incident flux of PAR (μmol m^{-2} s^{-1}), which is converted from PAR to photon flux assuming 4.6 μmol photons per Joule (Oleson et al., 2010), and A_m is the maximum photosynthetic rate obtained when both I and C_a are saturating (μmol m^{-2} s^{-1}).

Values of the light and carbon saturated rate of photosynthesis (A_m) is sensitive to species and can be reached either by Rubisco-limited J_c, electron-limited J_e or transport-capacity-limited J_s in the Farquhar model (Farquhar & Sharkey, 1982), with the other environmental factors (e.g., water status) are assumed optimal (Thornley, 1998b). Given that the three limitation rates of assimilation (J_c, J_e and J_s) are all directly or indirectly related to the maximum catalytic capacity of Rubisco ($V_{c,max}$), we simplify the photosynthesis model by using a notional capacity V_m, to represent A_m in Eq.2-A4. As V_m is a kinetic parameter needs to be adjusted to temperature, it can be described by the equation (Campbell & Norman, 1998; Katul et al., 2010, 2000):

$$V_m = \frac{V_{m,25}\exp[a(T-25)]}{1+\exp[b(T-41)]} \quad \text{(2-A5)}$$

where $V_{m,25}$ is the value of V_m when $T = 25$ ˚C, T (˚C) is temperature, a and b are temperature coefficients given as 0.031 and 0.115, respectively (Campbell & Norman, 1998). Note that the V_m introduced here is different from those used as $V_{c,max}$. At this point, Eq.2-A3 can be rewritten into:

$$g_s = m\frac{V_m\alpha I\eta}{V_m\alpha I+V_m\eta C_a+\alpha I\eta C_a}\frac{1}{1+D/D_0} \quad \text{(2-A6)}$$

On the canopy scale, we can hence calculate gross assimilation rate ($A_{c,g}$) from Eq.2-A4 and canopy conductance (G_c) from Eq.2-A6 following the integration principle. The light extinction law $I = I_0\exp(-kl)$ is adopted here to obtain:

$$A_{c,g} = \int_0^{LAI} A_g dl = \frac{V_m\alpha\eta C_a}{k(V_m\alpha+\alpha\eta C_a)}\left\{kLAI + ln\frac{(\alpha V_m+\alpha\eta C_a)I_0+\eta V_m C_a}{(\alpha V_m+\alpha\eta C_a)I_0\exp(-kLAI)+V_m\eta C_a}\right\} \quad \text{(2-A7)}$$

where I_0 is the flux density of PAR at the top of the canopy (μmol m^{-2} s^{-1}), l is the unit leaf area (m^2 m^{-2}), $k = k_Q$ is the extinction coefficient. To simplify, we have:

$$P_1 = V_m\alpha I_0\eta, \quad P_2 = V_m\alpha I_0, \quad P_3 = V_m\eta C_a, \quad P_4 = \alpha I_0\eta C_a \quad \text{(2-A8)}$$

As a result, canopy gross assimilation rate, or ecosystem GPP is simplified as:

$$GPP = A_{c,g} = \frac{P_1 C_a}{k(P_2+P_4)}\left\{kLAI + ln\frac{P_2+P_3+P_4}{P_2+P_3\exp(kLAI)+P_4}\right\} \quad \text{(2-A9)}$$

Furthermore, by integrating Eq.2-A6 up to canopy level, one can obtain the following new G_c model:

$$G_c = \int_0^{LAI} g_s dl = m\frac{P_1}{k(P_2+P_4)}\left\{kLAI + ln\frac{P_2+P_3+P_4}{P_2+P_3\exp(kLAI)+P_4}\right\}\frac{1}{1+D/D_0} \quad \text{(2-A10)}$$

References

Baldocchi, D. D., Luxmoore, R. J., & Hatfield, J. L. (1991). Discerning the forest from the trees: an essay on scaling canopy stomatal conductance. *Agricultural and Forest Meteorology*, *54*(2–4), 197–226. https://doi.org/10.1016/0168-1923(91)90006-C

Ball, J. T., Woodrow, I. E., & Berry, J. A. (1987). A Model Predicting Stomatal Conductance and its Contribution to the Control of Photosynthesis under Different Environmental Conditions. In *Progress in Photosynthesis Research* (pp. 221–224). Springer. https://doi.org/citeulike-article-id:8423355

Bastiaanssen, W. G. M., Menenti, M., Feddes, R. A., & Holtslag, A. A. M. (1998). A remote sensing surface energy balance algorithm for land (SEBAL): 1. Formulation. *Journal of Hydrology*, *212–213*(1–4), 198–212. https://doi.org/10.1016/S0022-1694(98)00253-4

Bastiaanssen, W. G. M., Pelgrum, H., Wang, J., Ma, Y., Moreno, J. F., Roerink, G. J., & Van Der Wal, T. (1998). A remote sensing surface energy balance algorithm for land (SEBAL): 2. Validation. *Journal of Hydrology*, *212–213*(1–4), 213–229. https://doi.org/10.1016/S0022-1694(98)00254-6

Beer, C., Reichstein, M., Tomelleri, E., Ciais, P., Jung, M., Carvalhais, N., et al. (2010). Terrestrial Gross Carbon Dioxide Uptake: Global Distribution and Covariation with Climate. *Science*, *329*(5993), 834 LP – 838. Retrieved from http://science.sciencemag.org/content/329/5993/834.abstract

Bonan, G. B., Williams, M., Fisher, R. A., & Oleson, K. W. (2014). Modeling stomatal conductance in the earth system: Linking leaf water-use efficiency and water transport along the soil-plant-atmosphere continuum. *Geoscientific Model Development*, *7*(5), 2193–2222. https://doi.org/10.5194/gmd-7-2193-2014

Bonan, Gordon B., Oleson, K. W., Fisher, R. A., Lasslop, G., & Reichstein, M. (2012). Reconciling leaf physiological traits and canopy flux data: Use of the TRY and FLUXNET databases in the Community Land Model version 4. *Journal of Geophysical Research: Biogeosciences*, *117*(2), 1–19. https://doi.org/10.1029/2011JG001913

Bruhn, D., Mikkelsen, T. N., Herbst, M., Kutsch, W. L., Ball, M. C., & Pilegaard, K. (2011). Estimating daytime ecosystem respiration from eddy-flux data. *BioSystems*, *103*(2), 309–313. https://doi.org/10.1016/j.biosystems.2010.10.007

Campbell, G. S., & Norman, J. M. (1998). *An introduction to environmental biophysics* (2nd Editio). New York: Springer-Verlag.

Chen, J. ., Liu, J., Cihlar, J., & Goulden, M. . (1999). Daily canopy photosynthesis model through temporal and spatial scaling for remote sensing applications. *Ecological Modelling*, *124*(2–3), 99–119. https://doi.org/10.1016/S0304-3800(99)00156-8

Cleugh, H. A., Leuning, R., Mu, Q., & Running, S. W. (2007). Regional evaporation estimates from flux tower and MODIS satellite data. *Remote Sensing of Environment*, *106*(3), 285–304. https://doi.org/10.1016/j.rse.2006.07.007

Cleverly, J., Boulain, N., Villalobos-Vega, R., Grant, N., Faux, R., Wood, C., et al. (2013). Dynamics of component carbon fluxes in a semi-arid Acacia woodland, central Australia. *Journal of Geophysical Research: Biogeosciences*, *118*(3), 1168–1185. https://doi.org/10.1002/jgrg.20101

Cleverly, J., Eamus, D., Restrepo Coupe, N., Chen, C., Maes, W., Li, L., et al. (2016). Soil

moisture controls on phenology and productivity in a semi-arid critical zone. *Science of the Total Environment*, *568*, 1227–1237. https://doi.org/10.1016/j.scitotenv.2016.05.142

Cleverly, J., Eamus, D., Luo, Q., Restrepo Coupe, N., Kljun, N., Ma, X., et al. (2016). The importance of interacting climate modes on Australia's contribution to global carbon cycle extremes. *Scientific Reports*, *6*(November 2015), 23113. https://doi.org/10.1038/srep23113

Collatz, G. J., Ball, J. T., Grivet, C., & Berry, J. A. (1991). Physiological and environmental regulation of stomatal conductance, photosynthesis and transpiration: a model that includes a laminar boundary layer. *Agricultural and Forest Meteorology*, *54*(2–4), 107–136. https://doi.org/10.1016/0168-1923(91)90002-8

Cox, P. ., Huntingford, C., & Harding, R. . (1998). A canopy conductance and photosynthesis model for use in a GCM land surface scheme. *Journal of Hydrology*, *212–213*, 79–94. https://doi.org/10.1016/S0022-1694(98)00203-0

Dai, Y., Dickinson, R. E., Wang, Y.-P. P., Al, D. A. I. E. T., Dai, Y., Dickinson, R. E., & Wang, Y.-P. P. (2004). A Two-Big-Leaf Model for Canopy Temperature, Photosynthesis, and Stomatal Conductance. *Journal of Climate*, *17*(12), 2281–2299. https://doi.org/10.1175/1520-0442(2004)017<2281:ATMFCT>2.0.CO;2

Donohue, R. J., Roderick, M. L., McVicar, T. R., & Farquhar, G. D. (2013). Impact of CO2 fertilization on maximum foliage cover across the globe's warm, arid environments. *Geophysical Research Letters*, *40*(12), 3031–3035. https://doi.org/10.1002/grl.50563

Eamus, D., Cleverly, J., Boulain, N., Grant, N., Faux, R., & Villalobos-Vega, R. (2013). Carbon and water fluxes in an arid-zone Acacia savanna woodland: An analyses of seasonal patterns and responses to rainfall events. *Agricultural and Forest Meteorology*, *182–183*, 225–238. https://doi.org/10.1016/j.agrformet.2013.04.020

Ershadi, A., McCabe, M. F., Evans, J. P., Chaney, N. W., & Wood, E. F. (2014). Multi-site evaluation of terrestrial evaporation models using FLUXNET data. *Agricultural and Forest Meteorology*, *187*, 46–61. https://doi.org/10.1016/j.agrformet.2013.11.008

Farquhar, G D, von Caemmener, S., & Berry, J. A. (1980). A Biochemical model of photosynthesis CO2 fixation in leaves of C3 species. *Planta*, *149*(1), 78–90. Retrieved from http://www.springerlink.com/content/w8264082778042jt/

Farquhar, Graham D., & von Caemmerer, S. (1892). Modelling of Photosynthetic Response to Environmental Conditions. *Physiological Plant Ecology II*, 550–583.

Farquhar, Graham D, & Sharkey, T. D. (1982). Stomatal Conductance and Photosynthesis. *Annual Review of Plant Physiology*, *33*(1), 317–345. https://doi.org/10.1146/annurev.pp.33.060182.001533

Fisher, J. B., Tu, K. P., & Baldocchi, D. D. (2008). Global estimates of the land-atmosphere water flux based on monthly AVHRR and ISLSCP-II data, validated at 16 FLUXNET sites. *Remote Sensing of Environment*, *112*(3), 901–919. https://doi.org/10.1016/j.rse.2007.06.025

Granier, A., Biron, P., & Lemoine, D. (2000). Water balance, transpiration and canopy conductance in two beech stands. *Agricultural and Forest Meteorology*, *100*(4), 291–308. https://doi.org/10.1016/S0168-1923(99)00151-3

Guerschman, J. P., Van Dijk, A. I. J. M., Mattersdorf, G., Beringer, J., Hutley, L. B., Leuning, R., et al. (2009). Scaling of potential evapotranspiration with MODIS data

reproduces flux observations and catchment water balance observations across Australia. *Journal of Hydrology*, *369*(1–2), 107–119. https://doi.org/10.1016/j.jhydrol.2009.02.013

Hirose, T. (2005). Development of the Monsi-Saeki theory on canopy structure and function. *Annals of Botany*, *95*(3), 483–494. https://doi.org/10.1093/aob/mci047

Hu, Z., Wu, G., Zhang, L. L., Li, S., Zhu, X., Zheng, H., et al. (2017). Modeling and partitioning of regional evapotranspiration using a satellite-driven water-carbon coupling model. *Remote Sensing*, *9*(1), 1–5. https://doi.org/10.3390/rs9010054

Isaac, P., Cleverly, J., McHugh, I., van Gorsel, E., Ewenz, C., & Beringer, J. (2016). OzFlux Data: Network integration from collection to curation. *Biogeosciences Discussions*, (May), 1–41. https://doi.org/10.5194/bg-2016-189

Jarvis, P. G. (1976). The Interpretation of the Variations in Leaf Water Potential and Stomatal Conductance Found in Canopies in the Field. *Philosophical Transactions of the Royal Society B: Biological Sciences*, *273*(927), 593–610. https://doi.org/10.1098/rstb.1976.0035

Jasechko, S., Sharp, Z. D., Gibson, J. J., Birks, S. J., Yi, Y., & Fawcett, P. J. (2013). Terrestrial water fluxes dominated by transpiration. *Nature*, *496*(7445), 347–350. https://doi.org/10.1038/nature11983

Jönsson, P., & Eklundh, L. (2004). TIMESAT - A program for analyzing time-series of satellite sensor data. *Computers and Geosciences*, *30*(8), 833–845. https://doi.org/10.1016/j.cageo.2004.05.006

Kattge, J., & Knorr, W. (2007). Temperature acclimation in a biochemical model of photosynthesis: A reanalysis of data from 36 species. *Plant, Cell and Environment*, *30*(9), 1176–1190. https://doi.org/10.1111/j.1365-3040.2007.01690.x

Katul, G., Manzoni, S., Palmroth, S., & Oren, R. (2010). A stomatal optimization theory to describe the effects of atmospheric CO2 on leaf photosynthesis and transpiration. *Annals of Botany*, *105*(3), 431–442. https://doi.org/10.1093/aob/mcp292

Katul, G. G., Ellsworth, D. S., & Lai, C. T. (2000). Modelling assimilation and intercellular CO2 from measured conductance: A synthesis of approaches. *Plant, Cell and Environment*, *23*(12), 1313–1328. https://doi.org/10.1046/j.1365-3040.2000.00641.x

De Kauwe, M. G., Kala, J., Lin, Y. S., Pitman, A. J., Medlyn, B. E., Duursma, R. A., et al. (2015). A test of an optimal stomatal conductance scheme within the CABLE land surface model. *Geoscientific Model Development*, *8*(2), 431–452. https://doi.org/10.5194/gmd-8-431-2015

Kelliher, F. M., Leuning, R., Raupach, M. R., & Schulze, E. D. (1995). Maximum conductences for evaporation from global vegetation types. *Agricultural and Forest Meteorology*, *1923*(94), 1–14.

Kowalczyk, E. A., Wang, Y. P., & Law, R. M. (2006). The CSIRO Atmosphere Biosphere Land Exchange (CABLE) model for use in climate models and as an offline model. *CSIRO Marine and Atmospheric Research Paper*, *13*(November 2015), 42. https://doi.org/1921232390

Leuning, R. (1995). A critical appraisal of a combined stomatal-photosynthesis model for C3 plants. *Plant, Cell & Environment*, *18*(4), 339–355. https://doi.org/10.1111/j.1365-3040.1995.tb00370.x

Leuning, R., Zhang, Y. Q., Rajaud, A., Cleugh, H., & Tu, K. (2008). A simple surface

conductance model to estimate regional evaporation using MODIS leaf area index and the Penman-Monteith equation. *Water Resources Research*, *44*(10), W10419. https://doi.org/10.1029/2007WR006562

Liu, Z., Wu, C., & Wang, S. (2017). Predicting Forest Evapotranspiration by Coupling Carbon and Water Cycling Based on a Critical Stomatal Conductance Model. *IEEE Journal of Selected Topics in Applied Earth Observations and Remote Sensing*, *PP*(99), 1–9. https://doi.org/10.1109/JSTARS.2017.2715077

Long, D., & Singh, V. P. (2012). A Two-source Trapezoid Model for Evapotranspiration (TTME) from satellite imagery. *Remote Sensing of Environment*, *121*, 370–388. https://doi.org/10.1016/j.rse.2012.02.015

Ma, X., Huete, A., Yu, Q., Restrepo-Coupe, N., Beringer, J., Hutley, L. B., et al. (2014). Parameterization of an ecosystem light-use-efficiency model for predicting savanna GPP using MODIS EVI. *Remote Sensing of Environment*, *154*(1), 253–271. https://doi.org/10.1016/j.rse.2014.08.025

Mallick, K., Boegh, E., Trebs, I., Alfieri, J. G., Kustas, W. P., Prueger, J. H., et al. (2015). Reintroducing radiometric surface temperature into the Penman-Monteith formulation. *Water Resources Research*, *51*(8), 6214–6243. https://doi.org/10.1002/2014WR016106

McVicar, T. R., & Jupp, D. L. B. (2002). Using covariates to spatially interpolate mositure availability in the Murray-Darling Basin: a novel use of remotel sensed data. *Remote Sensing of Environment*, *79*(2), 199–212.

Medlyn, B. E., Duursma, R. A., Eamus, D., Ellsworth, D. S., Prentice, I. C., Barton, C. V. M., et al. (2011). Reconciling the optimal and empirical approaches to modelling stomatal conductance. *Global Change Biology*, *17*(6), 2134–2144. https://doi.org/10.1111/j.1365-2486.2010.02375.x

Monteith, J. L. (1965). Evaporation and environment. *Symposia of the Society for Experimental Biology*, *19*, 205–234. https://doi.org/10.1613/jair.301

Morales, P., Sykes, M. T., Prentice, I. C., Smith, P., Smith, B., Bugmann, H., et al. (2005). Comparing and evaluating process-based ecosystem model predictions of carbon and water fluxes in major European forest biomes. *Global Change Biology*, *11*(12), 2211–2233. https://doi.org/10.1111/j.1365-2486.2005.01036.x

Morillas, L., Leuning, R., Villagarcía, L., García, M., Serrano-Ortiz, P., & Domingo, F. (2013). Improving evapotranspiration estimates in Mediterranean drylands: The role of soil evaporation. *Water Resources Research*, *49*(10), 6572–6586. https://doi.org/10.1002/wrcr.20468

Mu, Q., Heinsch, F. A., Zhao, M., & Running, S. W. (2007). Development of a global evapotranspiration algorithm based on MODIS and global meteorology data. *Remote Sensing of Environment*, *111*(4), 519–536. https://doi.org/10.1016/j.rse.2007.04.015

Mu, Q., Zhao, M., & Running, S. W. (2011). Improvements to a MODIS global terrestrial evapotranspiration algorithm. *Remote Sensing of Environment*, *115*(8), 1781–1800. https://doi.org/10.1016/j.rse.2011.02.019

Norman, J. M., Kustas, W. P., & Humes, K. S. (1995). A two-source approach for estimating soil and vegetation energy fluxes from observations of directional radiometric surface temperature. *Agricultural and Forest Meteorology*, *77*(3–4), 263–293. https://doi.org/Doi 10.1016/0168-1923(95)02265-Y

Oleson, K. W., Lawrence, D. M., Gordon, B., Flanner, M. G., Kluzek, E., Peter, J., et al. (2010). Technical Description of version 4 . 0 of the Community Land Model (CLM). *NCAR Technical Note*, (April).

Papale, D., Reichstein, M., Aubinet, M., Canfora, E., Bernhofer, C., Kutsch, W., et al. (2006). Towards a standardized processing of Net Ecosystem Exchange measured with eddy covariance technique: algorithms and uncertainty estimation. *Biogeosciences*, *3*(4), 571–583. https://doi.org/10.5194/bg-3-571-2006

Papale, Dario, & Valentini, R. (2003). A new assessment of European forests carbon exchanges by eddy fluxes and artificial neural network spatialization. *Global Change Biology*, *9*(4), 525–535. https://doi.org/10.1046/j.1365-2486.2003.00609.x

Poulter, B., Frank, D., Ciais, P., Myneni, R. B., Andela, N., Bi, J., et al. (2014). Contribution of semi-arid ecosystems to interannual variability of the global carbon cycle. *Nature*, *509*(7502), 600–603. https://doi.org/10.1038/nature13376

Priestley, C. H. B., & Taylor, R. J. (1972). On the Assessment of Surface Heat Flux and Evaporation Using Large-Scale Parameters. In *Monthly Weather Review* (Vol. 100, pp. 81–92). https://doi.org/10.1175/1520-0493(1972)100<0081:OTAOSH>2.3.CO;2

Reichstein, M., Falge, E., Baldocchi, D., Papale, D., Aubinet, M., Berbigier, P., et al. (2005). On the separation of net ecosystem exchange into assimilation and ecosystem respiration: review and improved algorithm. *Global Change Biology*, *11*(9), 1424–1439. https://doi.org/10.1111/j.1365-2486.2005.001002.x

Running, S. W., & Coughlan, J. C. (1988). A general model of forest ecosystem processes for regional applications I. Hydrologic balance, canopy gas exchange and primary production processes. *Ecological Modelling*, *42*(2), 125–154. https://doi.org/10.1016/0304-3800(88)90112-3

Running, S. W., Nemani, R. R., Heinsch, F. A., Zhao, M., Reeves, M., & Hashimoto, H. (2004). A Continuous Satellite-Derived Measure of Global Terrestrial Primary Production. *BioScience*, *54*(6), 547–560. Retrieved from http://dx.doi.org/10.1641/0006-3568(2004)054[0547:ACSMOG]2.0.CO

Sellers, P. J. (1997). Modeling the Exchanges of Energy, Water, and Carbon Between Continents and the Atmosphere. *Science*, *275*(5299), 502–509. https://doi.org/10.1126/science.275.5299.502

Sellers, P. J., Randall, D. A., Collatz, G. J., Berry, J. A., Field, C. B., Dazlich, D. A., et al. (1996). A revised land surface parameterization (SiB2) for atmospheric GCMs. Part I: Model formulation. *Journal of Climate*. https://doi.org/10.1175/1520-0442(1996)009<0676:ARLSPF>2.0.CO;2

Shi, H., Li, L., Eamus, D., Cleverly, J., Huete, A., Beringer, J., et al. (2014). Intrinsic climate dependency of ecosystem light and water-use-efficiencies across Australian biomes. *Environmental Research Letters*, *9*(10), 104002. https://doi.org/10.1088/1748-9326/9/10/104002

Stewart, J. B. (1988). Modelling surface conductance of pine forest. *Agricultural and Forest Meteorology*, *43*(1), 19–35. https://doi.org/10.1016/0168-1923(88)90003-2

Thornley, J. H. M. (1976). *Mathematical models in plant physiology: a quantitative approach to problems in plant and crop physiology*. *Experimental botany ; v. 8*. London ; New York: Academic Press.

Thornley, J. H. M. (1998a). Dynamic Model of Leaf Photosynthesis with Acclimation to Light and Nitrogen. *Annals of Botany*, *81*(3), 421–430. https://doi.org/10.1006/anbo.1997.0575

Thornley, J. H. M. (1998b). Temperature and CO2Responses of Leaf and Canopy Photosynthesis : a Clarification using the Non-rectangular Hyperbola Model of Photosynthesis. *Annals of Botany*, *82*(January), 883–892. https://doi.org/10.1006/anbo.1998.0777

Tuzet, A., Perrier, A., & Leuning, R. (2003). A coupled model of stomatal conductance, photosynthesis and transpiration. *Plant, Cell and Environment*, *26*(7), 1097–1116. https://doi.org/10.1046/j.1365-3040.2003.01035.x

Wang, K., & Dickinson, R. E. (2012). A review of global terrestrial evapotranspiration: Observation, modeling, climatology, and climatic variability. *Reviews of Geophysics*, *50*(2). https://doi.org/10.1029/2011RG000373

Wang, Y. P., Kowalczyk, E., Leuning, R., Abramowitz, G., Raupach, M. R., Pak, B., et al. (2011). Diagnosing errors in a land surface model (CABLE) in the time and frequency domains. *Journal of Geophysical Research: Biogeosciences*, *116*(1). https://doi.org/10.1029/2010JG001385

Wilson, K., Goldstein, A., Falge, E., Aubinet, M., Baldocchi, D., Berbigier, P., et al. (2002). Energy balance closure at FLUXNET sites. *Agricultural and Forest Meteorology*, *113*(1–4), 223–243. https://doi.org/10.1016/S0168-1923(02)00109-0

Yang, Y., Long, D., & Shang, S. (2013). Remote estimation of terrestrial evapotranspiration without using meteorological data. *Geophysical Research Letters*, *40*(12), 3026–3030. https://doi.org/10.1002/grl.50450

Yang, Y., Donohue, R. J., McVicar, T. R., & Roderick, M. L. (2015). An analytical model for relating global terrestrial carbon assimilation with climate and surface conditions using a rate limitation framework. *Geophysical Research Letters*, *42*(22), 9825–9835. https://doi.org/10.1002/2015GL066835

Yebra, M., Van Dijk, A., Leuning, R., Huete, A., & Guerschman, J. P. (2013). Evaluation of optical remote sensing to estimate actual evapotranspiration and canopy conductance. *Remote Sensing of Environment*, *129*, 250–261. https://doi.org/10.1016/j.rse.2012.11.004

Yebra, M., Van Dijk, A. I. J. M. J. M., Leuning, R., & Guerschman, J. P. (2015). Global vegetation gross primary production estimation using satellite-derived light-use efficiency and canopy conductance. *Remote Sensing of Environment*, *163*, 206–216. https://doi.org/10.1016/j.rse.2015.03.016

Yu, Q., Goudriaan, J., & Wang, T. D. (2001). Modelling diurnal courses of photosynthesis and transpiration of leaves on the basis of stomatal and non-stomatal responses, including photoinhibition. *Photosynthetica*. https://doi.org/10.1023/A:1012435717205

Yu, Q., Zhang, Y., Liu, Y., & Shi, P. (2004). Simulation of the stomatal conductance of winter wheat in response to light, temperature and CO2 changes. *Annals of Botany*, *93*(4), 435–441. https://doi.org/10.1093/aob/mch023

Zhang, Y. Q., Chiew, F. H. S., Zhang, L., Leuning, R., & Cleugh, H. A. (2008). Estimating catchment evaporation and runoff using MODIS leaf area index and the Penman-Monteith equation. *Water Resources Research*, *44*(10), 1–15. https://doi.org/10.1029/2007WR006563

Zhang, Y, & Wegehenkel, M. (2006). Integration of MODIS data into a simple model for the spatial distributed simulation of soil water content and. *Remote Sensing of Environment*, *104*(4), 393–408. https://doi.org/10.1016/j.rse.2006.05.011

Zhang, Yongqiang, Chiew, F. H. S., Zhang, L., & Li, H. (2009). Use of Remotely Sensed Actual Evapotranspiration to Improve Rainfall–Runoff Modeling in Southeast Australia. *Journal of Hydrometeorology*, *10*(4), 969–980. https://doi.org/10.1175/2009JHM1061.1

Zhang, Yongqiang, Leuning, R., Hutley, L. B., Beringer, J., McHugh, I., & Walker, J. P. (2010). Using long-term water balances to parameterize surface conductances and calculate evaporation at 0.05 spatial resolution. *Water Resources Research*, *46*(5), W05512. https://doi.org/10.1029/2009WR008716

Zhang, Yongqiang, Peña-Arancibia, J. L., McVicar, T. R., Chiew, F. H. S., Vaze, J., Liu, C., et al. (2016). Multi-decadal trends in global terrestrial evapotranspiration and its components. *Scientific Reports*, *6*(August 2015), 19124. https://doi.org/10.1038/srep19124

Zhang, Yongqiang, Chiew, F., Peña-Arancibia, J., Sun, F., Li, H., & Leuning, R. (2017). Global variation of transpiration and soil evaporation and the role of their major climate drivers. *Journal of Geophysical Research: Atmospheres*. https://doi.org/10.1002/2017JD027025

Zhou, Y., Zhang, Y., Vaze, J., Lane, P., & Xu, S. (2015). Impact of bushfire and climate variability on streamflow from forested catchments in southeast Australia. *Hydrology and Earth System Sciences Discussions*, *10*(4), 4397–4437. https://doi.org/10.5194/hessd-10-4397-2013

Zhu, Z., Piao, S., Myneni, R. B., Huang, M., Zeng, Z., Canadell, J. G., et al. (2016). Greening of the Earth and its drivers. *Nature Climate Change*, *6*(August), early online. https://doi.org/10.1038/NCLIMATE3004

Chapter 3. A simple ecohydrological model for estimating streamflow, evapotranspiration, and gross primary production for Australian catchments

This chapter is based on the following international conference abstract:

Gan, R., Zhang, Y., Yu, Q. (2019). A simple ecohydrological model for estimating streamflow, evapotranspiration and gross primary production for Australian catchments. The 23rd International Congress on Modelling and Simulation (MODSIM), Canberra, 1-6 December 2019 (submitted)

Highlights

- A simple ecohydrological model was developed by incorporating a conceptualised hydrological model with a process-based evapotranspiration and gross primary production model.
- The ecohydrological model was tested at 63 Australian catchments against streamflow, evapotranspiration, and gross primary production observations.
- Results showed that the biophysical response of stomatal conductance to increased CO_2 led to increased streamflow, decreased evapotranspiration, and increased gross primary production across the study catchments.

Abstract

Streamflow (Q), evapotranspiration (ET), and gross primary production (GPP) are interrelated ecohydrological processes which are driven by energy to determine the water and carbon budgets of the land surface. Plants regulate these processes. However, existing models either extensively or inadequately represent the coupled relationship between water and carbon as regulated by plant stomata, which limits their capability to evaluate climate change-induced impacts on Q, ET, and GPP. Here we propose an intermediate solution for simultaneously estimating Q, ET, and GPP using a simple ecohydrological model. The model was developed from a conceptual hydrological model and a process-based ET and GPP model having only 12 free parameters. The model was tested against observed daily Q from 63 catchments and ET and GPP from 13 adjacent eddy covariance flux sites across Australia. Results showed that the simulated Q was in good agreement with the observed Q, with Nash-Sutcliffe Efficiency of

about 0.64 averaged across the 63 catchments. Simulations of ET and GPP at the catchment scale were comparable to the observations from their adjacent flux sites. Model experiment showed that with a 45% increase in CO_2, Q is increased by 12%, which was three times the decrease in ET (-4%). The model had a simple structure and required few parameters, thus having the potential to be used for estimating Q, ET, and GPP for other catchments located inside and outside of Australia, and for investigating CO_2-induced variations in these key ecohydrological processes via plant biophysical responses. Further study will be required to better constrain ET and GPP simulations and incorporate physiological feedback under elevated CO_2.

Key words: streamflow, evapotranspiration, gross primary production, anthropogenic climate change, eCO_2

3.1 Introduction

Steadily increasing atmospheric CO_2 concentrations have profound implications for determining the terrestrial water and carbon budgets via interrelated climatological and ecohydrological processes (Allen and Ingram, 2002; Eagleson, 2005; Huntington, 2008; Morton, 1983). In response to elevated CO_2 (eCO_2), plant regulated biophysical and physiological responses and feedback can induce significant variations in water and carbon exchanges, including streamflow (Q), evapotranspiration (ET), and gross primary production (GPP) (Huntington, 2008; Piao et al., 2007; P. J. Sellers et al., 1996; Ukkola et al., 2015). In general, plants tend to close their stomata under eCO_2, and transpiration is thus suppressed ('water-saving' effect) (Ainsworth and Long, 2005; Eamus, 1991; Ellsworth, 1999; Medlyn et al., 2001; Uddling et al., 2009). This leaf-level biophysical response can decrease ET via supressed transpiration (a dominant component of ET (Coenders-Gerrits et al., 2014; Jasechko et al., 2013; Wang et al., 2014)), leading to increased soil water availability that may generate more Q on the catchment scale (Cao et al., 2010; Gedney et al., 2006). At the same time, eCO_2 boosts photosynthesis, leading to greater GPP and stimulated plant growth, i.e., vegetation 'greening' or 'fertilization' effect (Donohue et al., 2013; Zhu et al., 2016). Such structural feedback following 'greening' (with increased leaf area, bulk stomatal conductance, and transpiration) offsets the 'water-saving' effect, thus leading to increased ET and decreased Q (Betts et al., 1997; Piao et al., 2007; Ukkola et al., 2015). Heterogenic environmental conditions (e.g., climate and land surfaces) further complicate the net effect (amplitude and magnitude) of eCO_2, thereby inducing highly uncertain variations in Q, ET, and GPP across spatiotemporal

scales (Ainsworth and Long, 2005; Eamus, 1991; Gedney et al., 2006; Piao et al., 2007; Ukkola et al., 2015; Yang et al., 2016), and reinforcing the need for reliable and systematic investigations.

Numerous models have been developed to evaluate water and carbon budgets, traditionally via different trajectories with focus on either of these two processes separately. On the one hand, hydrological models (metric (e.g., unit graph), conceptual/lumped (e.g., rainfall-runoff, RR) and physically-based) provide reliable water estimates (i.e., Q, ET) within a practical and robust framework (e.g., simple model structure and few parameters) (Rodda and Robinson, 2015). However, the vegetation processes are often neglected or over-simplified. For example, most recent models have attempted to incorporate vegetation indexes and/or stomatal functions that consider eCO_2 effects in the physically-based hydrological models, yet stomatal conductance and leaf area index (LAI) are represented as semi-empirical functions only responding to CO_2 concentration without photosynthesis being considered (Niu et al., 2013; Wu et al., 2012). The lack of a process-based representation of carbon uptake is inadequate to mechanistically evaluate the eCO_2-induced variations in water flux. On the other hand, the state-of-the-art Land Surface Models (LSMs) or the Dynamic Global Vegetation Models (DGVMs) describe multi-disciplinary processes (i.e., energy, water, carbon, nutrient) between the land surface and the atmosphere in exhaustive detail (Prentice et al., 2007; Sato et al., 2015; Zhao & Li, 2015). As a result, they generally have a sophisticated series of equations and a considerable number of parameters (Pitman, 2003). Operating at a fine temporal resolution (seconds/hours) but a course spatial resolution (several degrees), these models can be conveniently coupled with General Circulation Models (GCMs), and are thus advantageous for systematically investigating integrated interactions across atmosphere, biosphere and hydrosphere, including eCO_2-induced challenges (Cao et al., 2010; Piao et al., 2007; Sellers et al., 1996, 1997). However, except for ET and GPP, such frameworks often fail to represent water flow (within land surface, subsurface, and interactions), and as a result they produce less reliable water estimates, especially of Q at a catchment scale (Overgaard et al., 2006; Wang and Dickinson, 2012). Therefore, hydrological models or the LSMs and DGVMs are still limited regarding the balance between practicability and accuracy. As water availability is a primary resource that is determined by Q, which depends on both ET (via water balance) and GPP (via physiological regulation), a simple but reliable modelling framework which maintains fundamental mechanisms will be beneficial.

Conceptual hydrological models such as the rainfall-runoff (RR) models are widely used for Q estimation (Zhang & Chiew, 2009; Zhao, 1992). With a water focus, RR models have a simple model structure and few parameters, and thus are practical and accurate water modelling schemes, yet they seldomly consider vegetation processes (Zhang et al., 2009). Because vegetation is important in regulating water dynamics, there have been attempts to incorporate vegetation information into hydrological models (Donohue et al., 2007; Donohue et al., 2012). Such studies have proven that the accuracy of RR models can be improved by incorporating vegetation indexes (e.g., leaf area index (LAI)) (Li et al., 2009; Zhang et al., 2009; Zhou et al., 2013). However, vegetation indexes such as LAI are only a semi-empirical representation of how vegetation regulates water exchanges through ET. Taking the PML model proposed by Leuning et al., (2008) (which has been incorporated with RR models) as a representative example, the underlying assumption is that canopy conductance only responds to energy availability and its attribution to the canopy and soil surface (via LAI using Beer's law) and atmospheric water demand (via VPD). This approach is inadequate in terms of (1) a mechanistic principle, as canopy conductance not only responds to energy and VPD, but also to CO_2 concentration due to the coupled stomatal regulation of both water loss (transpiration) and carbon uptake (photosynthesis), and (2) practical use, either used by itself or combined with and RR model (Li et al., 2009; Morillas et al., 2013; Zhang et al., 2009; Zhou et al., 2013). Such models are incapable of evaluating carbon constraints on water dynamics (ET and/or streamflow) explicitly. Therefore, not considering CO_2 response mechanics could hamper RR modelling in simulating hydrological processes and in predicting Q under climate change. To further reduce uncertainty in water estimates, it is necessary for hydrological models to include eCO_2-induced variations in key ecohydrological processes.

Based on the above concerns, the overall objective of this study was to find an intermediate solution for ecohydrological modelling that would produce acceptable estimates of the quantity and variation of Q, ET, and GPP. The specific objectives were to: (1) develop a simple ecohydrological model for simultaneously estimating Q, ET, and GPP; (2) examine the model simulations at the catchment scale using available data; and (3) investigate the variations of Q, ET, and GPP induced by vegetation responses to eCO_2.

3.2 Model development

3.2.1 Xinanjiang model

The Xinanjiang (XAJ) model is a representative conceptual RR model proposed by Zhao, (1992) that has been which widely used for streamflow estimates for catchments located across continents including Australia (Li et al., 2009; Zhang et al., 2009; Zhou et al., 2013). XAJ consists of four semi-empirical sub-models that are linked through 'water buckets' representing ET, runoff generation, separation, and routing processes, respectively. The ET sub-model in XAJ is based on potential ET (PET) driven by radiative forcing and its balance with water availability through layers of soil water 'buckets'. The model has 14 free parameters that require calibration. Detailed XAJ model structure, linkages between water storages ('buckets'), and parameters are summarised in Figure 3-1.

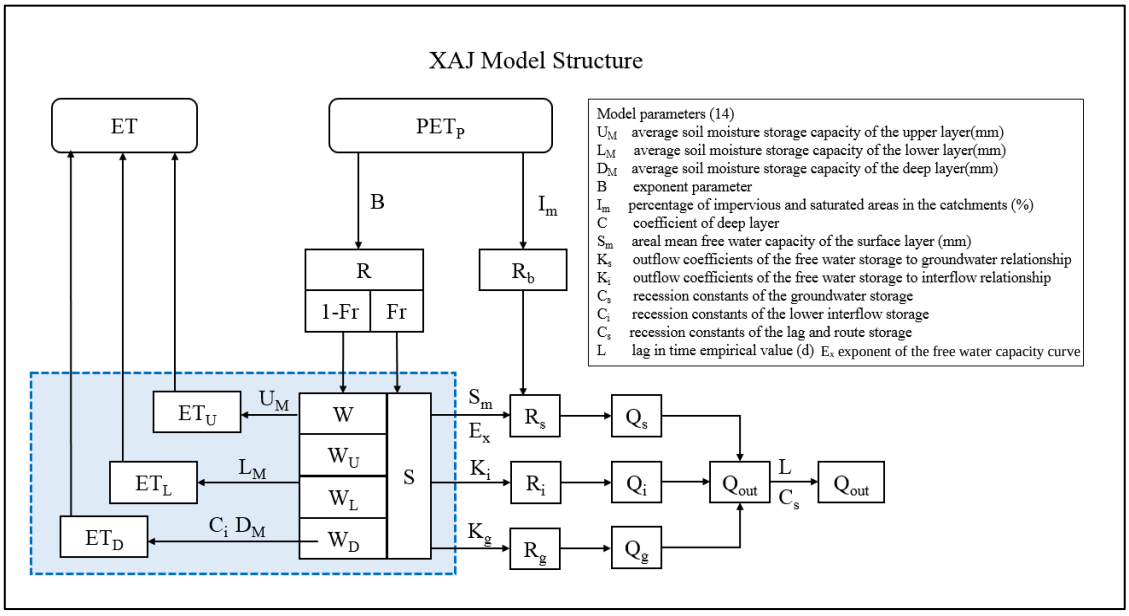

Figure 3-1. The Xinanjiang (XAJ) model structure, water storages (in boxes), and parameters (on arrow lines). The evapotranspiration sub-model is highlighted in the blue box, which will be revised later to alignment with the objectives of this study.

3.2.2 PML_V2 model

The PML_V2 model is a process-based model that simultaneously simulates both ET and GPP (Gan et al., 2018). The model is based on the Penman-Monteith (PM) equation (Monteith, 1965) and its further-developed version that uses remote-sensing data for ET estimation (PML) (Cleugh et al., 2007; Leuning et al., 2008). PML_V2 is a simple and robust modelling framework which has been validated and implemented for global ET and GPP simulation

(Zhang et al., 2019). The PML_V2 model uses remotely-sensed LAI to simulate ET and GPP as:

$$\lambda ET = \frac{\varepsilon A_c + (\rho c_p/\gamma) D_a G_a}{\varepsilon + 1 + G_a/G_c} + \frac{f \varepsilon A_s}{\varepsilon + 1} \qquad (Eq. 3-1)$$

$$G_c = m \frac{GPP}{C_a} \frac{1}{1 + D_a/D_0} \qquad (Eq. 3-1.1)$$

$$GPP = \frac{P_1 C_a}{k(P_2 + P_4)} \left\{ k_{PAR} LAI + ln \frac{P_2 + P_3 + P_4}{P_2 + P_3 \exp(kLAI) + P_4} \right\} \qquad (Eq. 3-2)$$

$$P_1 = V_m \alpha I_0 \eta, \quad P_2 = V_m \alpha I_0, \quad P_3 = V_m \eta C_a, \quad P_4 = \alpha I_0 \eta C_a \qquad (Eq. 3-2.1)$$

$$V_m = \frac{V_{m,25} \exp[a(T_a - 25)]}{1 + \exp[b(T_a - 41)]} \qquad (Eq. 3-2.2)$$

In Eq.3-1 (ET), λ is the latent heat of evaporation (MJ kg^{-1}), A is available energy, A_c and A_s are A attributed to the canopy and the soil surface, respectively. According to Beer's law: $A_s/A = \exp(-k_A LAI)$, in which k_A is the extinction coefficient of A, LAI is the leaf area index, which can be derived from satellite images (Fisher et al., 2008; Leuning et al., 2008). $\varepsilon = s/\gamma$, where $s = de^*/dt$ is the slope of the curve relating saturation water vapour pressure (e^*) to temperature ($kPa\ ^\circ C^{-1}$), γ is the psychrometric constant ($kPa\ ^\circ C^{-1}$), and ρ is the air density ($kg\ m^{-3}$). D_a is the atmospheric water vapour pressure deficit (VPD, kPa), G_a is the aerodynamic conductance ($m\ s^{-1}$), which is a function of wind speed and will be estimated following Leuning et al. (2008). G_c is the canopy conductance to water vapour ($m\ s^{-1}$), which is a function of GPP, VPD, and atmospheric CO_2 concentration (C_a, parts-per-million (ppm)) (Eq.3-1.1) (Gan et al., 2018). m is the stomatal conductance coefficient. f is a parameter that varies between 0 and 1, and is estimated as a function of precipitation and equilibrium soil evaporation according to Morillas et al., (2013) and Zhang et al., (2010).

In Eq. 3-2 (GPP), I_0 is the incident photon flux of photosynthetically active radiation (PAR) ($\mu mol\ m^{-2}\ s^{-1}$), which can be converted from PAR in the energy term ($MJ\ m^{-2}\ s^{-1}$) to photon flux assuming 4.6 µmol photons per Joule (Oleson et al., 2010). k_{PAR} is the extinction coefficient of PAR. α is the initial slope of the light response curve to assimilation rate (i.e. quantum efficiency, µmol CO_2 (µmol PAR)$^{-1}$). η is the initial slope of the CO_2 response curve to assimilation rate (i.e. carboxylation efficiency, µmol $m^{-2}\ s^{-1}$ (µmol $m^{-2}\ s^{-1}$)$^{-1}$). $V_{m,25}$ is the notional maximum catalytic capacity of Rubisco per unit leaf area at 25 ˚C, a and b are

empirical temperature coefficients set to 0.031 and 0.115, respectively (Campbell and Norman, 1998).

The PML_V2 model contains seven parameters, of which five are relatively insensitive (Gan et al., 2018; Leuning et al., 2008). Therefore, only two parameters, namely m and η, require optimisation in order to implement the model for estimating ET and GPP.

3.2.3 Incorporating PML_V2 into the Xinanjiang model

The ET sub-model in the XAJ model has previously been replaced by the more process-based ET model (i.e., the PML model (Leuning et al., 2008)) to simulate ET and Q simultaneously using remotely-sensed vegetation indexes (Li et al., 2009; Zhou et al., 2013). Here we incorporate the carbon process into the RR model by replacing the ET sub-model in the original XAJ model (Figure 3-1) with the PML_V2 model (named hereafter as XAJ-PML_V2 model herein). Since PML_V2 model explicitly represents canopy conductance in response to carbon uptake (GPP) and CO_2 (Eq.3-1, 2), the revised XAJ-PML_V2 model is mechanistically more integrated and capable of evaluating CO_2 impacts on water dynamics. Therefore, the XAJ-PML_V2 model is expected to (a) provide water and carbon estimates including Q, ET, and GPP, and (b) be capable of investigating variations in these ecohydrological variables in response to increased CO_2 through vegetation.

We further modified the GPP function (Eq. 3-2) in the XAJ-PML_V2 model to account for the environmental (soil and/or atmospheric) water stress on carbon uptake and canopy conductance. The modified GPP function is:

$$GPP = \frac{P_1 C_a}{k(P_2 + P_4)}\left\{k_{PAR} LAI + ln\frac{P_2 + P_3 + P_4}{P_2 + P_3 \exp(kLAI) + P_4}\right\} \cdot \min(f_{VPD}, f_{SWC}) \quad (Eq. 3-3)$$

$$f_{VPD} = \frac{1}{1 + D_a/D_0} \quad and \quad f_{SWC} = W/W_m \quad (Eq. 3-3.1)$$

where W is the soil water content calculated as a water balance state variable over each time step, W_m is the maximum value of W, which is a free parameter in the original XAJ model. In this way, carbon uptake is dynamically constrained by the water balance using Eq. 3-3. The environmental constraints induced by atmospheric (f_{VPD}) and soil water status (f_{SWC}) are well-known to covary with each other, thus only the minimum of the two is used in this study to avoid duplication of the limiting influence of both VPD and SWC.

To this end, the ecohydrological model XAJ-PML_V2 was developed, and contains 17 free parameters. four parameters of the original XAJ ET sub-model (U_M, L_M, D_M, and C) were replaced by seven parameters in PML_V2 model (α, η, m, $V_{m,25}$, D_0, k_Q, k_A). Among the seven new parameters introduced, α, $V_{m,25}$, D_0, k_Q, and k_A are relatively insensitive (Gan et al., 2018; Leuning et al., 2008), thus constant values are used in this study. Therefore, only 12 parameters require optimisation to simultaneously simulate Q, ET, and GPP, including the two sensitive parameters, i.e., η and m in PML_V2 and the other 10 parameters in XAJ.

3.3 Data and Methods

3.3.1 Catchments and eddy covariance flux sites

Catchment meteorological data, remotely-sensed LAI, and Q time series were obtained from the collation of 780 Australian unregulated catchments from Zhang et al., (2011), which spanned a temporal period from 1975 to 2012. In this collation, the 0.05°×0.05° grid daily time series of meteorological data was from the SILO Data Drill of the Queensland Department of Natural Resources and Water (https://www.dnrme.qld.gov.au/), which is interpolated from point measurements by the Australian Bureau of Meteorology (http://www.bom.gov.au/). Daily LAI data were obtained from the Moderate Resolution Imaging Spectroradiometer (MODIS, product MOD15A2) with 8-day temporal resolution and 1-km spatial resolution (https://modis.gsfc.nasa.gov/data/). These data were processed after quality control and interpolation over each catchment. Only data from 63 catchments in this collation were selected and used to test the proposed XAJ-PML_V2 model. This is because the model simultaneously simulates Q, ET, and GPP, yet only Q observations were available at the catchment scale. ET and GPP were measured at a few adjacent eddy covariance flux sites close to the catchments in this catchment collation (distance between catchment and flux sites <50 km). Locations of the selected 63 catchments and the flux sites are shown in Figure 3-2.

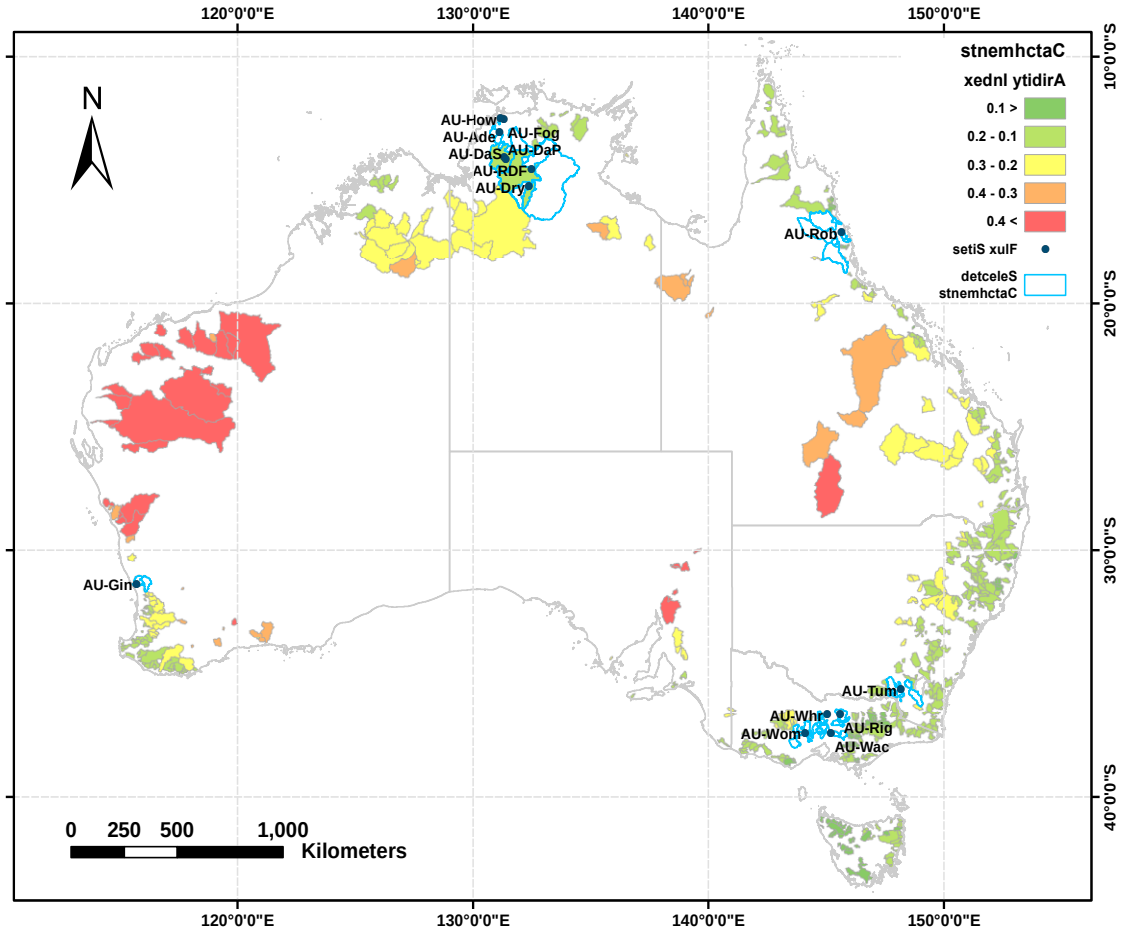

Figure 3-2. Location of 63 Australian catchments (cyan polygons) and 13 eddy covariance flux sites (black labels) used in this study. Distance between the flux sites and the geological centre of each catchment were calculated according to their coordinates. Only the catchments within 50 km distance from the flux sites were selected. Aridity index was calculated as the ratio of long-term annual potential evapotranspiration to precipitation for each catchment.

ET and GPP data from 13 eddy covariance flux sites were obtained from the OzFlux website (http://www.ozflux.org.au/) as part of the Australian Terrestrial Ecosystem Research Network (TERN). These flux sites have continuous observations over a minimum of 3-year period until the end of 2012 (aligned with the catchment data coverage) (Isaac et al., 2016). The selected flux sites cover the major climate and ecosystem types on the Australian continent, including five plant functional types (PFTs): savanna (SAV), woody savanna (WSA), grassland (GRA), wetland (WET), and evergreen broadleaf forest (EBF). The half-hourly data were processed and gap filled into daily time steps following the methods described by Shi et al., (2014) and Gan et al., (2018). Then the daily ET and GPP time series were used as observations to compare with the XAJ-PML_V2 model simulations. Selected information about the 13 flux sites and the adjacent 63 catchments areas is summarised in Table 3-1 (see Figure 3-2 for locations).

Table 3-1. Summary information for the 13 flux sites and their adjacent 63 catchments used in this study.

Flux Site Code	PFT Type	Number of Catchments with Distance <50km	Average Distance (km)	Average Forest Ratio of Catchments (%)	Long-term Precipitation (mm yr^{-1})
Ade	SAV	7	34	9.0	1532
DaP	GRA	1	44	15.2	1319
DaS	SAV	1	44	15.2	1319
Dry	SAV	1	47	17.0	896
Fog	WET	1	25	6.4	1631
Gin	WSA	4	31	30.5	606
How	WSA	2	34	9.6	1630
RDF	WSA	1	35	14.6	1060
Rig	GRA	8	30	42.8	799
Tum	EBF	9	33	59.2	974
Wac	EBF	12	34	45.5	870
Whr	EBF	7	33	30.7	594
Wom	EBF	11	28	49.5	751

*For a given flux site, average distance is the mean distance of a number of catchments selected (Number of Catchments) that are within 50km. Also shown is the long-term average forest ratio and precipitation of the catchments adjacent to each flux site. PFT as plant functional type. Full names of the flux sites can be found at http://www.ozflux.org.au/monitoringsites/.

3.3.2 Model evaluation

The XAJ-PML_V2 model was calibrated against Q observations at each of the selected 63 Australian catchments. Nash-Sufficient-Efficiency (NSE) was used to evaluate the accuracy of the simulated daily Q against observed daily Q. The 12 model parameters were optimised using a Genetic Algorithm (GA) to maximise the NSE as:

$$NSE_Q = 1 - \frac{\sum_{i=1}^{N} |Q_{sim,i} - Q_{obs,i}|^2}{\sum_{i=1}^{N} |Q_{obs,i} - \overline{Q}_{obs}|^2} \qquad Eq.3-4$$

where Q is daily streamflow, subscripts *obs* and *sim* represent observation and simulation, respectively. N is the length of the daily time series at each catchment. Parameters that gives the best estimation of Q with maximum NSE_Q were selected as the catchment-specific parameter set.

In addition to NSE, we also used the coefficient of determination (R^2) and linear regression slope (referred to hereafter as slope) to evaluate the model performance. R^2 was calculated as:

$$R^2 = \left(\frac{\sum_{i=1}^{N} (Q_{sim,i} - \overline{Q}_{sim})(Q_{obs,i} - \overline{Q}_{obs})}{\sqrt{\sum_{i=1}^{N} (Q_{sim,i} - \overline{Q}_{sim})^2 \sum_{i=1}^{N} (Q_{obs,i} - \overline{Q}_{obs})^2}} \right)^2 \qquad Eq.3-5$$

High values of NSE, R^2, and slope (approaching 1) indicated that the simulated Q values from the XAJ-PML_V2 model were close to observed Q values.

These statistical metrics were also used for evaluating the model performance of ET and GPP estimates at each catchment, with simulations from XAJ-PML_V2 compared with the observations from adjacent flux sites (distance <50 km from the centre of the catchment). ET and GPP from nearby flux sites were used in this study because they were the most reliable observations at the ecosystem scale based on our current knowledge. However, the NSE values of ET and GPP were not incorporated directly to optimise the model parameter set. This was because (1) the observations from a given flux site covered a much smaller spatial footprint (ecosystem scale, usually <5 km) than the streamflow spatial footprint (catchment scale, >10 km), and (2) the flux sites available were often located outside the selected catchments. Thus, flux site observations were not equivalent to catchment observations and thus are only used as a supplementary reference. Nonetheless, it was assumed that ET and GPP at the flux sites should be comparable to ET and GPP of their adjacent catchments, at least in terms of temporal characteristics due to climate and/or geographical similarity.

A modelling experiment was conducted to investigate the variation of Q, ET, and GPP under an increased CO_2 scenario. The model was first calibrated using an atmospheric CO_2 concentration of 380 ppm to simulate benchmark values of Q, ET, and GPP. Then the CO_2 concentration was increased by about 45% to 550 ppm and the calibrated model parameters were used to simulate ET, GPP, and Q. 550 ppm was set as the elevated CO_2 scenario according to the Free-air CO_2 Enrichment (FACE) experiments (Ainsworth and Long, 2005). For each of the 63 catchments, the simulated time series of Q, ET and GPP based on 380 ppm and 550 ppm were then compared to calculate the relative variation as:

$$X_{variation} = (X_{550} - X_{380})/X_{380} * 100 \qquad Eq. 3-6$$

where X represents the simulated Q, ET, and GPP values at the designated CO_2 concentrations. The X values were then used to evaluate the CO_2 impact on water and carbon processes.

3.4 Results

3.4.1 Model performance

The XAJ-PML_V2 model performance for Q, ET, and GPP are summarised in the statistics shown in Figure 3-3. When compared with Q observations at the catchment scale, the model

was capable of reproducing streamflow across the 63 catchments, with median NSE, R^2, and slope of 0.64, 0.68, and 0.9, respectively. When compared with ET observations at adjacent flux sites, the model gave ET estimates that had performance statistics that were generally comparable to those obtained for Q, with median NSE and R^2 values of about 0.44 and slope of about 0.82. In contrast, there was a much greater difference between simulated (catchment) and observed (flux site) GPP, where all three of the performance statistics were below 0.25. This was expected since GPP was not a part of the water balance components and model calibration always mimics the best possible streamflow time series. Despite the scale discrepancy between catchment and flux sites, the model was still capable of simulating daily ET for catchment areas that compared well with flux site observations.

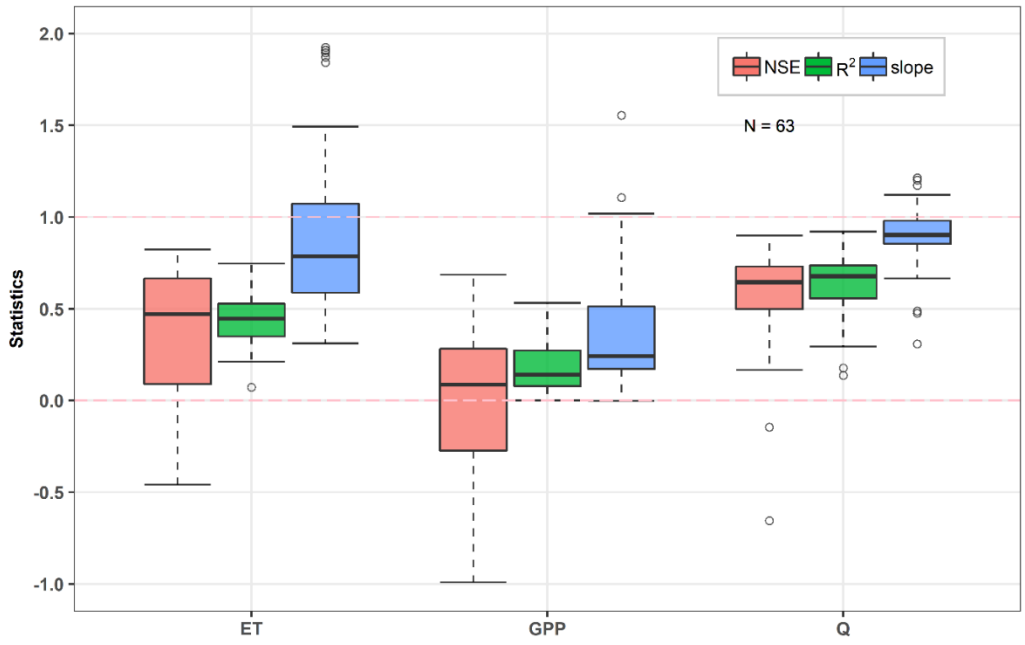

Figure 3-3. Summary of XAJ-PML_V2 model performance for streamflow (Q), evapotranspiration (ET), and gross primary production (GPP) across 63 (N) Australian catchments. The model was calibrated against observed daily Q at the catchment scale only. Simulated ET and GPP were compared with observed ET and GPP from adjacent eddy covariance flux sites near these catchments. Nash-Sutcliffe Efficiency (NSE), coefficient of determination (R^2), and linear regression slope (slope) are shown across 63 catchments. The solid line in each box represents the median value, whiskers are the 5th and 95th percentiles, open circles represents outliers. The 25th and 75th percentiles are shown as the lower and upper boundaries of each box.

The model performance statistics described above were for daily. The model was further evaluated for monthly values grouped by the 13 flux sites. Simulated and observed Q, ET, and GPP from corresponding catchments (Table 3-1) are compared in Figure 3-4.1, 2, and 3,

respectively. For monthly Q, the model performed well for most catchments (R^2>0.7), except those close to Dry and Gin (R^2≤0.6) (Figure 3-4.1). For ET, the simulated ET at the catchment level explained 15~70% of the variation in observed ET for 11 out of the 13 flux sites, all except Fog and Whr (<1%) (Figure 3-4.2). The simulated monthly catchment GPP values were different from GPP values observed at the flux sites (Figure 3-4.3). Simulated GPP values explained the highest amount of observed variation at at Das (61%) and Fog (51%), but less than 40% at all the other flux sites.

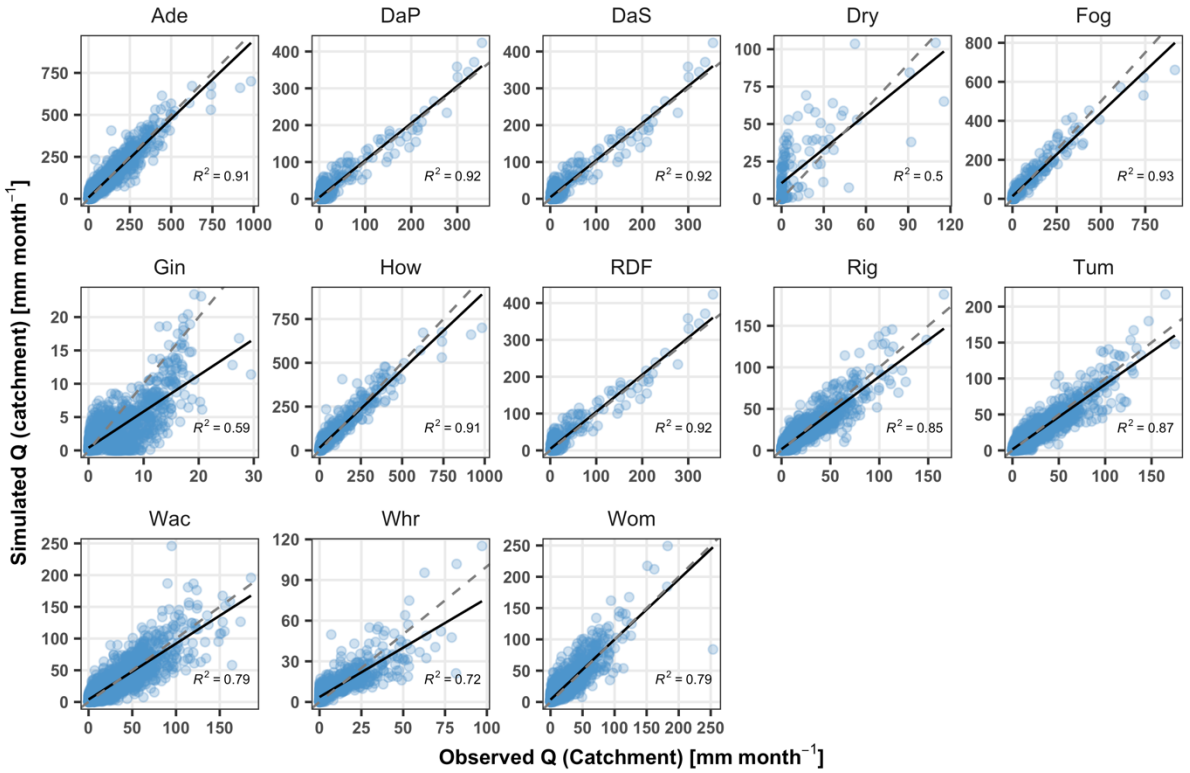

Figure 3-4.1. Simulated monthly catchment streamflow (Q, mm month^{-1}) vs observed streamflow grouped by adjacent flux sites for 63 Australian catchments. The reference 1:1 line (dashed grey) and the linear regression line (y = ax+b, solid black) are shown for comparison.

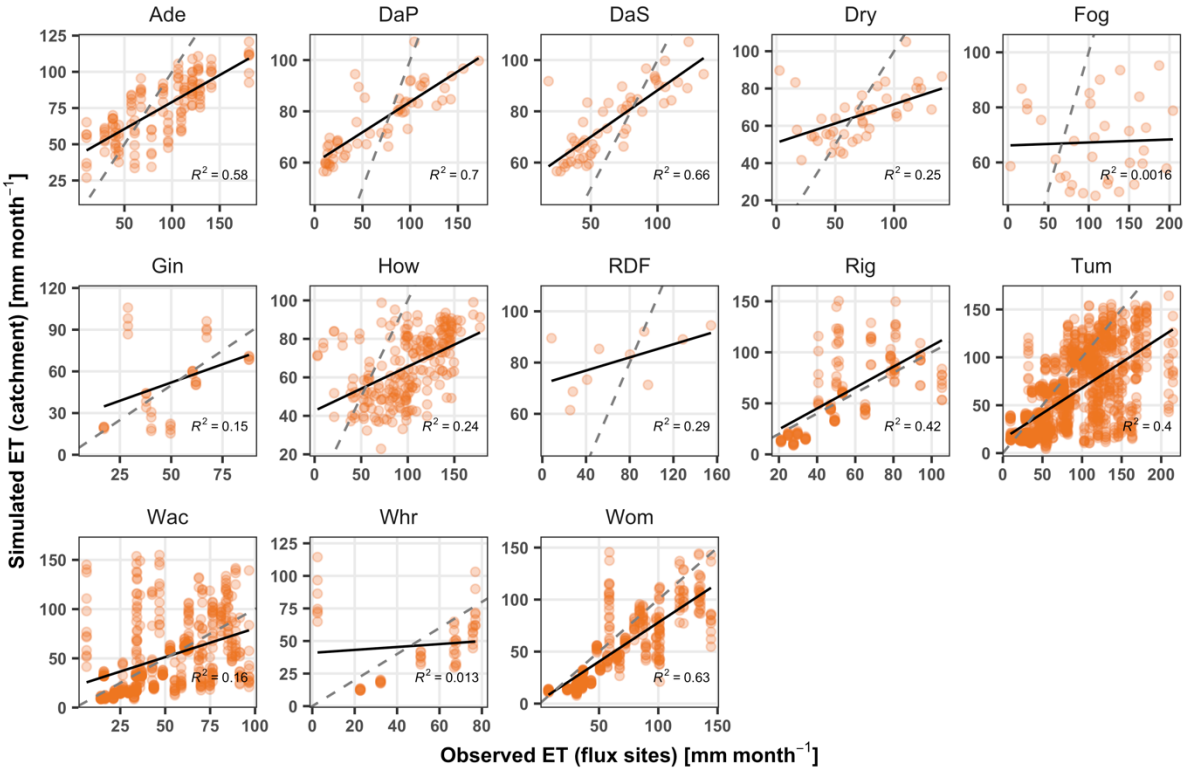

Figure 3-4.2. Simulated monthly evapotranspiration (ET mm month^{-1}) vs observed ET from grouped by adjacent flux sites for 63 Australian catchments. The reference 1:1 line (dashed grey) and the linear regression line (y = ax+b, solid black) are shown for comparison.

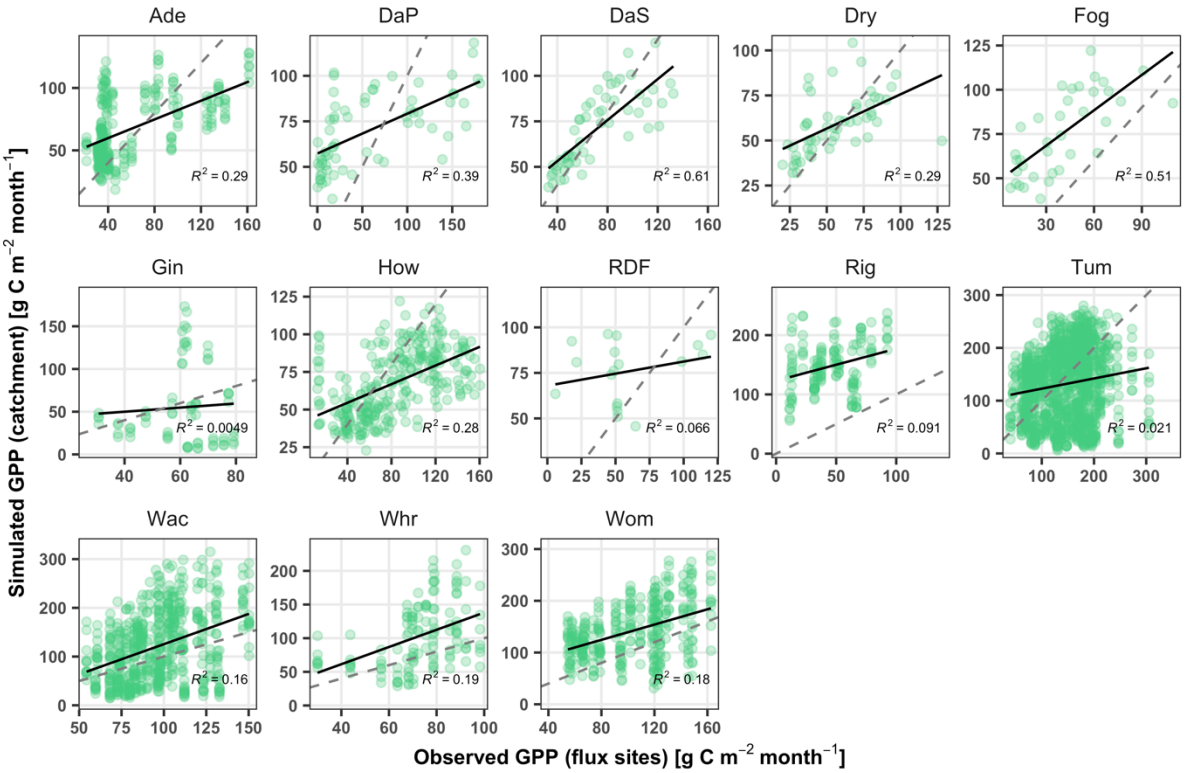

Figure 3-4.3. Simulated monthly gross primary production (GPP g C m^{-2} $month^{-1}$) grouped by adjacent flux sites for 63 Australian catchments. The reference 1:1 line (dashed grey) and the linear regression line (y = ax+b, solid black) are shown for comparison.

3.4.2 Model experiment

eCO_2 influences streamflow through water balance via ET. Over vegetated surfaces, ET is predominantly determined by plant water use (transpiration), which is controlled by canopy conductance. Plant biophysical regulation of canopy conductance in response to increased CO_2 is thus important for understanding variations in the water balance. Here we conducted (1) a sensitivity analysis to show how canopy conductance changes in response to eCO_2, and (2) a model experiment to investigate the variations in Q, ET, and GPP under eCO_2. Sensitivity analysis (Figure 3-5) showed that when atmospheric CO_2 increased by 45% and all other variables were kept constant, average assimilation rate increased by about 24%. At the same time, average canopy conductance was reduced by about 14%. The magnitude of increase in assimilation and decrease in conductance increase along with increase in LAI. This indicates that the higher the vegetation density, the more significant the biophysical response is to eCO_2. It is expected that under variable environmental conditions (reality), the magnitude of assimilation rate and canopy conductance can vary greatly across spatiotemporal scales. Hence, the variations in Q, ET, and GPP due to such biophysical responses can vary greatly across different ecosystems and catchments.

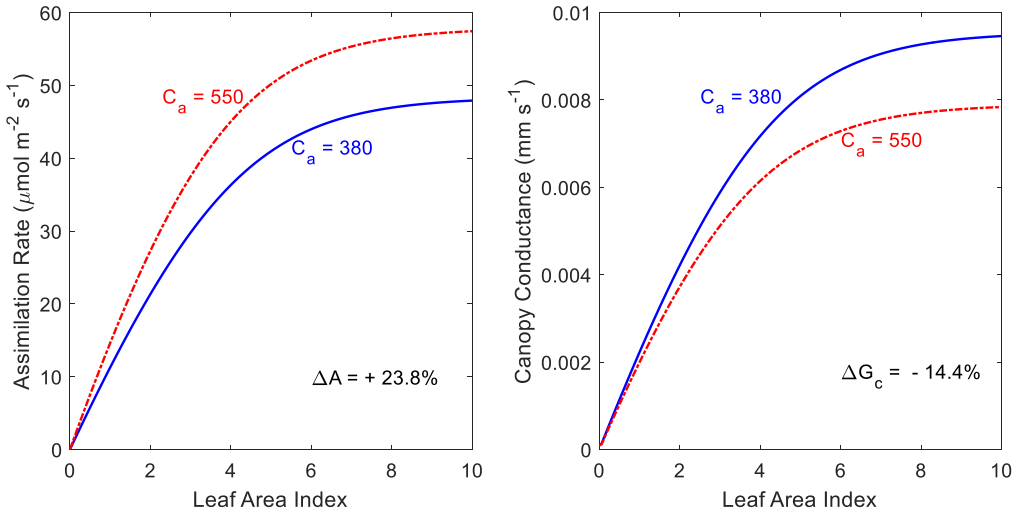

Figure 3-5. Sensitivity of carbon assimilation rate and canopy conductance to increased in atmospheric CO_2 concentration. C_a = 380 (ppm, or μmol mol^{-1}) was set as the benchmark, C_a = 550 μmol mol^{-1} was the eCO_2 scenario. Environmental variables were given as Pa = 90 kPa, R_s = 500 W m^{-2}, PAR was set as 0.45 of Rs, T_{air} = 25 ˚C, VPD = 3 kPa. Parameters were D_0 = 0.7 kPa, α = 0.103, η = 0.04, k_Q = 0.6, m = 9, $A_{m,25}$ = 100 μmol m^{-2} s^{-1}. CO_2 was prescribed to increase by 45% (380 ppm set as benchmark elevated to 550 ppm). Variation in assimilation rate and canopy conductance was calculated according to Eq. 3-6.

Based on the model calibration and experiment (Section 3.3.2), results shown in Figure 3-6 indicate that the model predicts great variation in monthly Q, ET and GPP in response to a 45% increase in CO_2 concentration across the 63 study catchments. Although there was great variation in magnitude across each catchment, the overall trend was that multi-year average monthly ET decreased by less than 10% and GPP increased by less than 40%. As a result, Q increased by less than 25% in general. When the catchments are grouped by their adjacent flux sites (Table 3-2), it can be seen that the variations in Q, ET, and GPP ranged between 8 and 18% (average 12%), 2 and -7% (average -4%), 19 and 33% (average 23%), respectively. This demonstrates that under eCO_2, less water will be returned from land surfaces to the atmosphere via ET, and more carbon will be fixed by plants (increased water use efficiency). In terms of water availability, the relatively small decrease in ET of about -4% was amplified three times to increase streamflow of about 12%. Catchments grouped in EBF showed lower decreases in ET (less than about 2%) than those grouped in the non-forests (SAV, GRA, WSA) (over 5%) in general. Yet no significant difference was found for Q and GPP variations across different PFTs.

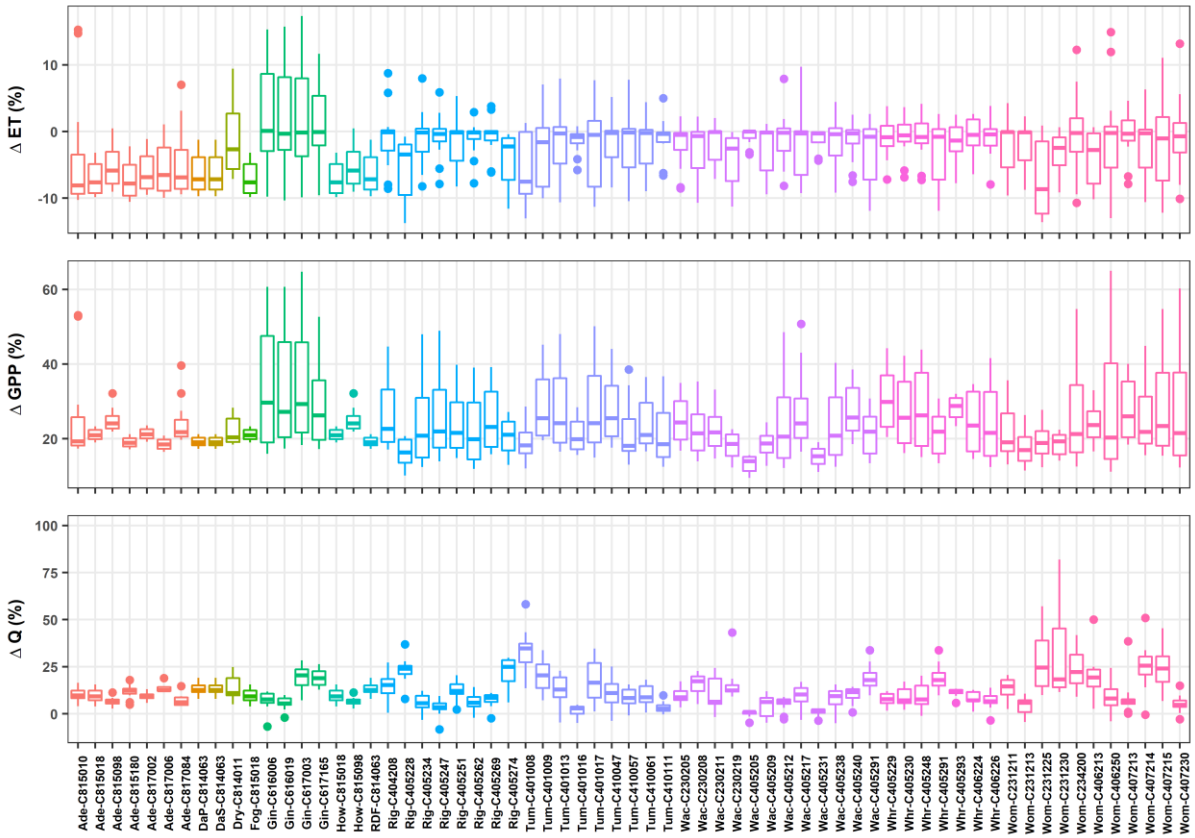

Figure 3-6. Variation in multi-year average monthly Q, ET, and GPP in response to increased atmospheric CO_2 concentration. CO_2 increase by 45% (from 380 ppm to 550 ppm). For all three variables, simulated values with the 380 ppm CO_2 concentration were used as benchmark. Variation was calculated as the difference between simulated values under 380 ppm and those under 550 ppm (Eq. 3-6). The solid line in each box represents the median value, whiskers are the 5th and 95th percentiles, solid circles represents outliers. The 25th and 75th percentiles are shown as the lower and upper boundaries of each box.

Table 3-2. Summary of variation in Q, ET, and GPP grouped according to flux site.

site	Ade	DaP	DaS	Dry	Fog	Gin	How	RDF	Rig	Tum	Wac	Whr	Wom
PFT	SAV	GRA	SAV	SAV	WET	WSA	WSA	WSA	GRA	EBF	EBF	EBF	EBF
ΔGPP (%)	22.16	19.24	19.24	22.03	21.06	**33.16**	22.97	19.24	23.28	24.43	21.63	26.49	24.33
ΔET (%)	-5.58	-6.22	-6.22	-0.93	**-7.09**	1.74	-6.16	-6.22	-1.90	-2.03	-2.04	-1.35	-2.21
ΔQ (%)	9.65	13.05	13.05	14.15	9.63	12.92	7.91	13.05	11.77	13.18	9.05	10.29	**17.49**

*positive value denotes increase and negative value denotes decrease. 63 catchments grouped by their adjacent flux site.

3.5 Discussion

3.5.1 Advantages of the simple ecohydrological model

As discussed in Section 3.1, while the RR models are accurate and simple for water estimates and lack physiological constraints, LSMs and DGVMs represent energy, water, and carbon exchange in extensive detail and thus are complicated and exhibit high uncertainties (Overgaard et al., 2006; Pitman, 2003; Rodda and Robinson, 2015; Zhao and Li, 2015). Simple ecohydrological models such as XAJ-PML_V2 as developed in this study provide an intermediate solution by incorporating key ecohydrological processes. These types of models are advantageous because (1) the major water and carbon fluxes are simultaneously quantified by Q, ET, and GPP. This allows systematic interpretation of the behaviour of key water and carbon exchanges as a whole at the catchment scale. The model (only calibrated for Q) achieved satisfactory simulations of ET, but not GPP since GPP is not part of the water balance components. The simulations can be used to understand the interactions between water flow and ecosystem functioning from a holistic viewpoint rather than investigating each of them separately; (2) the model maintains high performance of Q simulation with Q and ET explicitly constrained by carbon estimates (GPP). This indicates that introducing carbon processes into hydrological modelling does not necessarily sacrifice model accuracy on water estimates or simplicity on model structure and parameter. Specifically, with only 12 model parameters in the XAJ-PML_V2 model, it is relatively simple and effective when compared with other models as discussed above; and (3) uncertainty in water estimates with carbon constraint can be reduced if XAJ-PML_V2 model can also be also calibrated against observed or remotely-sensed GPP estimates (see discussion in Section 3.5.3). ET components include biophysical transpiration from vegetation and physical evaporation from wet surfaces. Because transpiration contributes a significant proportion of ET and mechanistically links water and carbon processes. If transpiration is estimated without considering carbon constraint, the mechanism will be incorrectly represented in the model. As a result, the estimated ET partitioning process will be biased, regardless of the overall quantity, i.e., ET can be accurate. This impedes in-depth interpretation of the model behaviour and the substantial physical/biophysical process. However, to validate this assumption, further data and investigation are required to evaluate the accuracy and reliability of the ET estimates including the components of ET and its impact on Q regime in greater detail.

3.5.2 Ecohydrological response to eCO2

We showed that although Q, ET, and GPP varied greatly in response to eCO_2 across the 63 catchments (Figure 3-6), the overall trends were for GPP to increase, ET to decrease and Q to increase (Table 3-2). This is to be expected because currently the XAJ-PML_V2 model only simulates enhanced photosynthesis and stomatal closure in response to eCO_2, which in fact means the 'water-saving' effect only (Figure 3-5). 'Water-saving' under eCO_2, however, can further boost photosynthesis and increase LAI, which consequently leads to an increase in bulk stomatal conductance and transpiration. Such structural feedback over the long-term and over large spatial scale is not yet incorporated into the model. Therefore, variations in Q, ET, and GPP as shown in this study only evaluated the 'response' rather than the 'net' effect considering 'feedback' under eCO_2. However, our quantified increase in GPP, i.e., 23% on average, is comparable with the range of that reported by the FACE experiments conducted at the ecosystem level, where CO_2 concentration was increased from ambient to 475-600 ppm (mostly 550 ppm, the same as used in our model experiment), carbon assimilation increased about 20-45% on average (ranging between about 5-60%) across grasses, shrubs, legumes, and trees (Ainsworth and Long, 2005). This indicates that our model provides reliable quantification of enhanced carbon uptake under eCO_2. For ET, our simulations showed a variation of about -4%, which is comparable to that reported by Cheng et al. (2014) for an energy-limited forest catchment in Australia, where a simple ecohydrological model (WAVES) was used to show that the changes in ET were less than -2.5% (for simulations with CO_2 concentration of 550 ppm compared with 370 ppm). Furthermore, our estimated increase in Q (about 12%) is in agreement with that of Gedney et al., (2006), who suggested that the observed increasing trend in Q across global catchments could be explained by stomatal closure using an LSM. These comparisons suggest that our model is capable of evaluating variations in Q, ET, and GPP induced by vegetation biophysical responses under eCO_2.

However, as noted above, further development will be required for the XAJ-PML_V2 model to enable investigation of the 'net' effect to accounting for 'feedback' processes. Currently the model does not allocate carbon uptake to generate LAI as an interactive process but rather uses remotely-sensed LAI as model inputs. Further research following this study should be conducted to employ either an empirical relationship between LAI and GPP, or a process-based algorithm to attribute GPP to dynamically simulate LAI. This is necessary because both the magnitude and direction of variations in ecohydrological processes especially Q and ET, can

be altered through such 'feedback' processes, as suggested by many other authors (Betts et al., 1997; Cheng et al., 2014; Piao et al., 2007; Ukkola et al., 2016, 2015; Yang et al., 2016). The current debate over the eCO_2 effect on ecohydrological processes is partially due to the variety of different models used in different studies and their underlying assumptions which can give contradictory results. The XAJ-PML_V2 model with further development could serve as a practical tool to contribute integrative quantification and evaluation of ecohydrological processes regarding this cutting-edge topic.

3.5.3 Potential limitations and implications

Due to current data availability limits, the proposed model was only calibrated against catchment Q observations, whereas the other key ecohydrological variables, i.e., ET and GPP, were only compared to observations at adjacent flux sites close to catchments. Despite the fact that the eddy covariance observations used in this study were already the most advanced and reliable data available at the ecosystem level, measurements made at flux sites have only limited spatial coverage that is considerably smaller than that of observed catchment streamflow (Section 3.3). It is widely acknowledged that ET and GPP are difficult to directly observe over large scales, but our simulations could possibly be calibrated/validated against ET and GPP simulations from other models, such as the MODIS product (MOD16A2 for ET and MOD17A2 for GPP) (Mu et al., 2011, 2007; Running and Zhao, 2015), the MTE product (Jung et al., 2017, 2011, 2009; Tramontana et al., 2016), or the LSM simulations (Beer et al., 2010; Dai et al., 2003; Le Quéré et al., 2014; Miralles et al., 2011). The gridded time series of ET and GPP from these simulations could be extracted according to catchment boundaries and then averaged to compare with those simulated from the XAJ-PML_V2 model. Further studies could also be conducted to include more PFTs under different climate conditions to investigate the difference in variation across catchments dominated by various ecosystems (Cheng et al., 2014; Yang et al., 2016). Such comparisons would provide deeper understanding of the model performance and the physical processes.

This study only focused on historical climate conditions by using the available meteorological observations. Climate change scenarios could be incorporated to predict variations in Q, ET, and GPP in the near future when the CO_2 concentration is predicted to reach 550 ppm. As the interactions between climate and ecohydrological processes could be significantly different from those under current conditions, it can be assumed that greater variations will be found in Q, ET, and GPP. This should be considered during further model development to account for

'feedback' as a primary condition that will result in more robust predictions of variations in water and carbon budgets.

3.6 Conclusion

In this study, a new ecohydrological model was developed to simultaneously simulate Q, ET, and GPP. The model is simple in structure and contains only 12 free parameters. The model was calibrated against daily Q observations from 63 Australian catchments and was then used to estimate ET and GPP, which were then evaluated against observations from 13 adjacent eddy covariance flux sites. Results showed that the model was good at simulating Q, and simulated ET reasonably well, but not GPP. This indicates that it is possible to develop a practical ecohydrological model that simulates key ecohydrological processes without sacrificing model simplicity and accuracy, but that improvement in GPP estimation is still required. An additional model experiment showed that when CO_2 concentration increased by 45% (from 380 ppm to 550 ppm), the model predicted a 12% increase in Q as a result of a 4% decrease in ET across 63 catchments. This result demonstrated the importance of vegetation biophysical regulation in response to eCO_2 and highlighted the requirement of incorporating not only response but also feedback processes when considering an integrated water and carbon system. The model has the potential to be further implemented, validated, and developed for a more comprehensive understanding of the ecohydrological processes and their variations under climate change that includes eCO_2.

Reference

Ainsworth, E.A., Long, S.P., 2005. What have we learned from 15 years of free-air CO2 enrichment (FACE)? A meta-analytic review of the responses of photosynthesis, canopy properties and plant production to rising CO2. New Phytol. 165, 351–372. https://doi.org/10.1111/j.1469-8137.2004.01224.x

Allen, M.R., Ingram, W.J., 2002. Constraints on future changes in climate and the hydrologic cycle. Nature 419, 224–232.

Beer, C., Reichstein, M., Tomelleri, E., Ciais, P., Jung, M., Carvalhais, N., Rödenbeck, C., Arain, M.A., Baldocchi, D., Bonan, G.B., Bondeau, A., Cescatti, A., Lasslop, G., Lindroth, A., Lomas, M., Luyssaert, S., Margolis, H., Oleson, K.W., Roupsard, O., Veenendaal, E., Viovy, N., Williams, C., Woodward, F.I., Papale, D., 2010. Terrestrial Gross Carbon Dioxide Uptake: Global Distribution and Covariation with Climate. Science (80-.). 329, 834 LP – 838.

Betts, A.R., Cox, M.P., Lee, E.S., Woodward, I.F., 1997. Contrasting Physiological and Structural Vegetation Feedbacks in Climate Change Simulations. Nature 387, 796–799. https://doi.org/10.1038/42924

Campbell, G.S., Norman, J.M., 1998. An introduction to environmental biophysics, 2nd Editio. ed. Springer-Verlag, New York.

Cao, L., Bala, G., Caldeira, K., Nemani, R., Ban-Weiss, G., 2010. Importance of carbon dioxide physiological forcing to future climate change. Proc. Natl. Acad. Sci. 107, 9513–9518. https://doi.org/10.1073/pnas.0913000107

Cheng, L., Zhang, L., Wang, Y.P., Yu, Q., Eamus, D., O'Grady, A., 2014. Impacts of elevated CO2, climate change and their interactions on water budgets in four different catchments in Australia. J. Hydrol. 519, 1350–1361. https://doi.org/10.1016/j.jhydrol.2014.09.020

Cleugh, H.A., Leuning, R., Mu, Q., Running, S.W., 2007. Regional evaporation estimates from flux tower and MODIS satellite data. Remote Sens. Environ. 106, 285–304. https://doi.org/10.1016/j.rse.2006.07.007

Coenders-Gerrits, A.M.J., Van Der Ent, R.J., Bogaard, T.A., Wang-Erlandsson, L., Hrachowitz, M., Savenije, H.H.G., 2014. Uncertainties in transpiration estimates. Nature 506, E1–E2. https://doi.org/10.1038/nature12925

Dai, Y., Zeng, X., Dickinson, R.E., Baker, I., Bonan, G.B., Bosilovich, M.G., Denning, A.S., Dirmeyer, P.A., Houser, P.R., Niu, G., Oleson, K.W., Schlosser, C.A., Yang, Z.-L., 2003. The Common Land Model. Bull. Am. Meteorol. Soc. 84, 1013–1023. https://doi.org/10.1175/BAMS-84-8-1013

Donohue, R.J., Roderick, M.L., McVicar, T.R., 2012. Roots, storms and soil pores: Incorporating key ecohydrological processes into Budyko's hydrological model. J. Hydrol. 436–437, 35–50. https://doi.org/10.1016/J.JHYDROL.2012.02.033

Donohue, R.J., Roderick, M.L., McVicar, T.R., 2007. On the importance of including vegetation dynamics in Budyko's hydrological model. Hydrol. Earth Syst. Sci. 11, 983–995. https://doi.org/10.5194/hess-11-983-2007

Donohue, R.J., Roderick, M.L., McVicar, T.R., Farquhar, G.D., 2013. Impact of CO2

fertilization on maximum foliage cover across the globe's warm, arid environments. Geophys. Res. Lett. 40, 3031–3035. https://doi.org/10.1002/grl.50563

Eagleson, P.S., 2005. Ecohydrology: Darwinian expression of vegetation form and function. Cambridge University Press.

Eamus, D., 1991. The interaction of rising CO2 and temperatures with water use efficiency. Plant. Cell Environ. 14, 843–852. https://doi.org/10.1111/j.1365-3040.1991.tb01447.x

Ellsworth, D.S., 1999. CO2 enrichment in a maturing pine forest: Are CO2 exchange and water status in the canopy affected? Plant, Cell Environ. 22, 461–472. https://doi.org/10.1046/j.1365-3040.1999.00433.x

Fisher, J.B., Tu, K.P., Baldocchi, D.D., 2008. Global estimates of the land-atmosphere water flux based on monthly AVHRR and ISLSCP-II data, validated at 16 FLUXNET sites. Remote Sens. Environ. 112, 901–919. https://doi.org/10.1016/j.rse.2007.06.025

Gan, R., Zhang, Y., Shi, H., Yang, Y., Eamus, D., Cheng, L., Chiew, F.H.S., Yu, Q., 2018. Use of satellite leaf area index estimating evapotranspiration and gross assimilation for Australian ecosystems. Ecohydrology e1974. https://doi.org/10.1002/eco.1974

Gedney, N., Cox, P.M., Betts, R.A., Boucher, O., Huntingford, C., Stott, P.A., 2006. Detection of a direct carbon dioxide effect in continental river runoff records. Nature 439, 835–838. https://doi.org/10.1038/nature04504

Huntington, T.G., 2008. CO2-induced suppression of transpiration cannot explain increasing runoff. Hydrol. Process. 22, 311–314. https://doi.org/10.1002/hyp.6925

Isaac, P., Cleverly, J., McHugh, I., van Gorsel, E., Ewenz, C., Beringer, J., 2016. OzFlux Data: Network integration from collection to curation. Biogeosciences Discuss. 1–41. https://doi.org/10.5194/bg-2016-189

Jasechko, S., Sharp, Z.D., Gibson, J.J., Birks, S.J., Yi, Y., Fawcett, P.J., 2013. Terrestrial water fluxes dominated by transpiration. Nature 496, 347–350. https://doi.org/10.1038/nature11983

Jung, M., Reichstein, M., Bondeau, A., 2009. Towards global empirical upscaling of FLUXNET eddy covariance observations: validation of a model tree ensemble approach using a biosphere model. Biogeosciences Discuss. 6, 5271–5304. https://doi.org/10.5194/bgd-6-5271-2009

Jung, M., Reichstein, M., Margolis, H.A., Cescatti, A., Richardson, A.D., Arain, M.A., Arneth, A., Bernhofer, C., Bonal, D., Chen, J., Gianelle, D., Gobron, N., Kiely, G., Kutsch, W., Lasslop, G., Law, B.E., Lindroth, A., Merbold, L., Montagnani, L., Moors, E.J., Papale, D., Sottocornola, M., Vaccari, F., Williams, C., 2011. Global patterns of land-atmosphere fluxes of carbon dioxide, latent heat, and sensible heat derived from eddy covariance, satellite, and meteorological observations. J. Geophys. Res. Biogeosciences 116, 1–16. https://doi.org/10.1029/2010JG001566

Jung, M., Reichstein, M., Schwalm, C.R., Huntingford, C., Sitch, S., 2017. Compensatory water effects link yearly global land CO2 sink changes to temperature. Nature (In Press), 516–520. https://doi.org/10.1038/nature20780

Le Quéré, C., Peters, G.P., Andres, R.J., Andrew, R.M., Boden, T.A., Ciais, P., Friedlingstein, P., Houghton, R.A., Marland, G., Moriarty, R., Sitch, S., Tans, P., Arneth, A., Arvanitis, A., Bakker, D.C.E., Bopp, L., Canadell, J.G., Chini, L.P., Doney,

S.C., Harper, A., Harris, I., House, J.I., Jain, A.K., Jones, S.D., Kato, E., Keeling, R.F., Klein Goldewijk, K., Körtzinger, A., Koven, C., Lefèvre, N., Maignan, F., Omar, A., Ono, T., Park, G.-H., Pfeil, B., Poulter, B., Raupach, M.R., Regnier, P., Rödenbeck, C., Saito, S., Schwinger, J., Segschneider, J., Stocker, B.D., Takahashi, T., Tilbrook, B., van Heuven, S., Viovy, N., Wanninkhof, R., Wiltshire, A., Zaehle, S., 2014. Global carbon budget 2013. Earth Syst. Sci. Data 6, 235–263. https://doi.org/10.5194/essd-6-235-2014

Leuning, R., Zhang, Y.Q., Rajaud, A., Cleugh, H., Tu, K., 2008. A simple surface conductance model to estimate regional evaporation using MODIS leaf area index and the Penman-Monteith equation. Water Resour. Res. 44, W10419. https://doi.org/10.1029/2007WR006562

Li, H., Zhang, Y., Chiew, F.H.S., Xu, S., 2009. Predicting runoff in ungauged catchments by using Xinanjiang model with MODIS leaf area index. J. Hydrol. 370, 155–162. https://doi.org/10.1016/j.jhydrol.2009.03.003

Medlyn, B.E., Barton, C.V.M., Droadmeadow, M.S.J., Ceulemans, R., De Angelis, P., Forstreuter, M., Freeman, M., Jackson, S.B., Kellomaki, S., Laitat, E., Rey, A., Roberntz, P., Sigurdsson, B.D., Strassemeyer, J., Wang, K., Curtis, P.S., Jarvis, P.G., 2001. Stomatal conductance of forest species after long-term exposure to elevated CO2 concentration: A synthesis. New Phytol. 149, 247–264.

Miralles, D.G., Holmes, T.R.H., De Jeu, R.A.M., Gash, J.H., Meesters, A.G.C.A., Dolman, A.J., 2011. Global land-surface evaporation estimated from satellite-based observations. Hydrol. Earth Syst. Sci. 15, 453–469. https://doi.org/10.5194/hess-15-453-2011

Monteith, J.L., 1965. Evaporation and environment. Symp. Soc. Exp. Biol. 19, 205–234. https://doi.org/10.1613/jair.301

Morillas, L., Leuning, R., Villagarcía, L., García, M., Serrano-Ortiz, P., Domingo, F., 2013. Improving evapotranspiration estimates in Mediterranean drylands: The role of soil evaporation. Water Resour. Res. 49, 6572–6586. https://doi.org/10.1002/wrcr.20468

Morton, F.I., 1983. Operational estimates of areal evapotranspiration and their significance to the science and practice of hydrology. J. Hydrol. 66, 1–76. https://doi.org/10.1016/0022-1694(83)90177-4

Mu, Q., Heinsch, F.A., Zhao, M., Running, S.W., 2007. Development of a global evapotranspiration algorithm based on MODIS and global meteorology data. Remote Sens. Environ. 111, 519–536. https://doi.org/10.1016/j.rse.2007.04.015

Mu, Q., Zhao, M., Running, S.W., 2011. Improvements to a MODIS global terrestrial evapotranspiration algorithm. Remote Sens. Environ. 115, 1781–1800. https://doi.org/10.1016/j.rse.2011.02.019

Niu, J., Sivakumar, B., Chen, J., 2013. Impacts of increased CO2 on the hydrologic response over the Xijiang (West River) basin, South China. J. Hydrol. 505, 218–227. https://doi.org/10.1016/J.JHYDROL.2013.09.051

Oleson, K.W., Lawrence, D.M., Gordon, B., Flanner, M.G., Kluzek, E., Peter, J., Levis, S., Swenson, S.C., Thornton, E., Dai, A., Decker, M., Dickinson, R., Feddema, J., Heald, C.L., Lamarque, J., Niu, G., Qian, T., Running, S., Sakaguchi, K., Slater, A., Stöckli, R., Wang, A., Yang, L., Zeng, Xiaodong, Zeng, Xubin, 2010. Technical Description of version 4 . 0 of the Community Land Model (CLM). NCAR Tech. Note.

Overgaard, J., Rosbjerg, D., Butts, M.B., 2006. Land-surface modelling in hydrological perspective ? a review. Biogeosciences 3, 229–241.

Piao, S., Friedlingstein, P., Ciais, P., de Noblet-Ducoudré, N., Labat, D., Zaehle, S., 2007. Changes in climate and land use have a larger direct impact than rising CO2 on global river runoff trends. Proc. Natl. Acad. Sci. U. S. A. 104, 15242–7. https://doi.org/10.1073/pnas.0707213104

Pitman, A.J., 2003. The evolution of, and revolution in, land surface schemes designed for climate models. Int. J. Climatol. 23, 479–510. https://doi.org/10.1002/joc.893

Prentice, I.C., Bondeau, A., Cramer, W., Harrison, S.P., Hickler, T., Lucht, W., Sitch, S., Smith, B., Sykes, M.T., 2007. Dynamic Global Vegetation Modeling: Quantifying Terrestrial Ecosystem Responses to Large-Scale Environmental Change BT - Terrestrial Ecosystems in a Changing World, in: Canadell, J.G., Pataki, D.E., Pitelka, L.F. (Eds.), . Springer Berlin Heidelberg, Berlin, Heidelberg, pp. 175–192. https://doi.org/10.1007/978-3-540-32730-1_15

Rodda, J.C., Robinson, M., 2015. Progress in Modern Hydrology: Past, Present and Future. Book 408.

Running, S.W., Zhao, M., 2015. Daily GPP and Annual NPP (MOD17A2/A3) products NASA Earth Observing System MODIS Land Algorithm - User's guide V3 28. https://doi.org/http://doi.org/10.5067/MODIS/MOD17A3H.006

Sato, H., Ito, Akihiko, Ito, Akinori, Ise, T., Kato, E., 2015. Current status and future of land surface models. Soil Sci. Plant Nutr. 61, 34–47. https://doi.org/10.1080/00380768.2014.917593

Sellers, J.P., Los, O.S., Tucker, J.C., Justice, O.C., Dazlich, A.D., Collatz, G.J., Randall, A.D., 1996. A revised land surface parameterization (SiB2) for atmospheric GCMs. Part II: The generation of global fields of terrestrial biophysical parameters from satellite data. J. Clim. https://doi.org/10.1175/1520-0442(1996)009<0706:ARLSPF>2.0.CO;2

Sellers, P.J., Bounoua, L., Collatz, G.J., Randall, D.A., Dazlich, D.A., Los, S.O., Berry, J.A., Fung, I., Tucker, C.J., Field, C.B., Jensen, T.G., 1996. Comparison of Radiative and Physiological Effects of Doubled Atmospheric CO_2 on Climate. Science (80-.). 271, 1402–1406.

Sellers, P.J., Dickinson, R.E., Randall, D.A., Betts, A.K., Hall, F.G., Berry, J.A., Collatz, G.J., Denning, A.S., Mooney, H.A., Nobre, C.A., Sato, N., Field, C.B., Henderson-Sellers, A., 1997. Modeling the Exchanges of Energy, Water, and Carbon Between Continents and the Atmosphere. Science (80-.). 275, 502–509. https://doi.org/10.1126/science.275.5299.502

Shi, H., Li, L., Eamus, D., Cleverly, J., Huete, A., Beringer, J., Yu, Q., van Gorsel, E., Hutley, L., 2014. Intrinsic climate dependency of ecosystem light and water-use-efficiencies across Australian biomes. Environ. Res. Lett. 9, 104002. https://doi.org/10.1088/1748-9326/9/10/104002

Tramontana, G., Jung, M., Schwalm, C.R., Ichii, K., Camps-Valls, G., Ráduly, B., Reichstein, M., Arain, M.A., Cescatti, A., Kiely, G., Merbold, L., Serrano-Ortiz, P., Sickert, S., Wolf, S., Papale, D., 2016. Predicting carbon dioxide and energy fluxes across global FLUXNET sites with regression algorithms. Biogeosciences 13, 4291–4313. https://doi.org/10.5194/bg-13-4291-2016

Uddling, J., Teclaw, R.M., Pregitzer, K.S., Ellsworth, D.S., 2009. Leaf and canopy conductance in aspen and aspen-birch forests under free-air enrichment of carbon dioxide and ozone. Tree Physiol. 29, 1367–1380. https://doi.org/10.1093/treephys/tpp070

Ukkola, A.M., Keenan, T.F., Kelley, D.I., Prentice, I.C., 2016. Vegetation plays an important role in mediating future water resources. Environ. Res. Lett. 11, 094022. https://doi.org/10.1088/1748-9326/11/9/094022

Ukkola, A.M., Prentice, I.C., Keenan, T.F., van Dijk, A.I.J.M., Viney, N.R., Myneni, R.B., Bi, J., 2015. Reduced streamflow in water-stressed climates consistent with CO2 effects on vegetation. Nat. Clim. Chang. 6, 75–78. https://doi.org/10.1038/nclimate2831

Wang, K., Dickinson, R.E., 2012. A review of global terrestrial evapotranspiration: Observation, modeling, climatology, and climatic variability. Rev. Geophys. 50. https://doi.org/10.1029/2011RG000373

Wang, L., Stephen, P.G., Kelly, K.C., 2014. Global synthesis of vegetation control on evapotranspiration partitioning. Geophys. Res. Lett. 41, 6753–6757. https://doi.org/10.1002/2014GL061439

Wu, Y.P., Liu, S.G., Abdul-Aziz, O.I., 2012. Hydrological effects of the increased CO2 and climate change in the Upper Mississippi River Basin using a modified SWAT. Clim. Change 110, 977–1003. https://doi.org/DOI 10.1007/s10584-011-0087-8

Yang, Y., Donohue, R.J., McVicar, T.R., Roderick, M.L., Beck, H.E., 2016. Long-term CO2 fertilization increases vegetation productivity and has little effect on hydrological partitioning in tropical rainforests. J. Geophys. Res. G Biogeosciences 121, 2125–2140. https://doi.org/10.1002/2016JG003475

Zhang, Y., Chiew, F.H.S., 2009. Relative merits of different methods for runoff predictions in ungauged catchments. Water Resour. Res. 45. https://doi.org/10.1029/2008WR007504

Zhang, Y., Chiew, F.H.S., Zhang, L., Li, H., 2009. Use of Remotely Sensed Actual Evapotranspiration to Improve Rainfall–Runoff Modeling in Southeast Australia. J. Hydrometeorol. 10, 969–980. https://doi.org/10.1175/2009JHM1061.1

Zhang, Y., Kong, D., Gan, R., Chiew, F.H.S., McVicar, T.R., Zhang, Q., Yang, Y., 2019. Coupled estimation of 500 m and 8-day resolution global evapotranspiration and gross primary production in 2002–2017. Remote Sens. Environ. 222, 165–182. https://doi.org/https://doi.org/10.1016/j.rse.2018.12.031

Zhang, Y., Leuning, R., Hutley, L.B., Beringer, J., McHugh, I., Walker, J.P., 2010. Using long-term water balances to parameterize surface conductances and calculate evaporation at 0.05 spatial resolution. Water Resour. Res. 46, W05512. https://doi.org/10.1029/2009WR008716

Zhang, Y.Q., Viney, N.R., Chen, Y., Li, H.Y., 2011. Collation of stream-flow datasets for 719 unregulated Australian catchments. CSIRO Water a Heal. Ctry. Natl. Res. Flagsh. https://doi.org/https://doi.org/10.4225/08/58b5baad4fcc2

Zhao, R., 1992. The Xinanjiang model applied in China. J. Hydrol. 135, 371–381. https://doi.org/10.1016/0022-1694(92)90096-E

Zhao, W., Li, A., 2015. A Review on Land Surface Processes Modelling over Complex Terrain. Adv. Meteorol. 2015, 1–17. https://doi.org/10.1155/2015/607181

Zhou, Y., Zhang, Y., Vaze, J., Lane, P., Xu, S., 2013. Improving runoff estimates using remote sensing vegetation data for bushfire impacted catchments. Agric. For. Meteorol. 182–183, 332–341. https://doi.org/10.1016/j.agrformet.2013.04.018

Zhu, Z., Piao, S., Myneni, R.B., Huang, M., Zeng, Z., Canadell, J.G., Ciais, P., Sitch, S., Friedlingstein, P., Arneth, A., Liu, R., Mao, J., Pan, Y., Peng, S., Peñuelas, J., Poulter, B., 2016. Greening of the Earth and its drivers. Nat. Clim. Chang. 6, early online. https://doi.org/10.1038/NCLIMATE3004

Chapter 4. Uncertainty of grassland ecosystem transpiration estimates from a coupled water and carbon model

This chapter is based on the following international conference abstract:

Gan, R., Zhang, Y., Yu, Q. (2018). Uncertainty of transpiration estimates from a coupled water and carbon model in grassland ecosystems. The American Geophysical Union Fall Meeting (AGU), Washington D.C., USA, 10-14 December 2018 (poster presentation)

Highlights

- Ecosystem evapotranspiration is partitioned based on the coupled relationship between transpiration and carbon uptake for 15 grasslands sites widely distributed across the globe.
- Contributions of transpiration to total evapotranspiration exhibit strong variation and uncertainty across seasons and sites despite the shared ecosystem type.
- Variations in partitioning of evapotranspiration can be partially explained by temporal variations of leaf area index and spatial variations of precipitation.

Abstract

Evapotranspiration (ET) partitioning plays a significant role in interpreting ecosystem regulation of energy, water, and carbon budgets. Estimating transpiration (T) is a difficult but important task as it not only dominants ET, but also links water and carbon exchanges through biophysical processes. This study employed a process-based model (PML_V2) to partition ET into T and evaporation (E) constrained by carbon uptake at fifteen grassland ecosystems widely distributed across the globe. The model was optimised to obtain best ET and gross primary production (GPP) estimates (Nash-Sutcliffe Efficiency and coefficient of determination (R^2) over 0.8 for ET and about 0.7 for GPP). The T estimate was then used to calculate the ratio of T/ET to evaluate ET partitioning. Results showed that T/ET exhibits strong seasonal variations, with ET generally dominated by T during the peak growing season. Distinct T/ET values were found for different grasslands, which varied between 0.1 and 0.87 and averaged about 0.53 across sites. Regression analysis demonstrates that seasonal variation of T/ET could be partially explained by leaf area index (LAI) (exponential relationship, R^2>0.8 for seven out of 15 sites), whereas the spatial variation in T/ET was related to precipitation gradient (natural logarithm relationship, R^2=0.5 across 89 site-years). When T/ET from the PML_V2 model was compared

with that of an empirical ET partitioning method based on underlying water use efficiency (uWUE), the PML_V2 model tended to give higher T/ET estimates under high precipitation and LAI (~0.7) but lower estimates under low precipitation (~0.3). The uWUE algorithm produced relatively constant values of T/ET (~0.45) despite different climate and vegetation conditions. This implies that high uncertainty still remains in ET partitioning using either process-based or empirical methods even with carbon constrain taken into consideration. This study demonstrated the climate and vegetation control of ET partitioning across spatiotemporal scales and supported the necessity for further evaluation of model uncertainty with regards to estimates of ET components.

Key words: evapotranspiration partitioning, transpiration, model, uncertainty, grassland, eddy covariance

4.1 Introduction

Transpiration (T) is the critical link of the energy and mass exchanges within the soil-plant-atmosphere continuum as it is a dominant component of evapotranspiration (ET) and a biophysical process closely coupled with carbon uptake (Coenders-Gerrits et al., 2014; Fatichi and Pappas, 2017; Good et al., 2015; Hatfield and Dold, 2019; Katul et al., 2012; Lian et al., 2018; Miralles et al., 2016; Schlesinger and Jasechko, 2014; Wong et al., 1979). Better understanding and quantification of T, including its spatiotemporal variation and controlling factors, is thus of great significance for evaluating energy, water, and carbon budgets over terrestrial ecosystems (Katul et al., 2012). Measurements of T can be obtained by using chambers, lysimeters, sap flow gauges and isotope techniques (Kool et al., 2014). However, despite the importance of filed observations of T, such methods are often costly and labour intensive and subject to space and time limitations (Wang & Dickinson, 2012). A practical and popular alternative is to derive T by partitioning ET using modelling approaches (Hu et al., 2017; Lian et al., 2018; Prentice et al., 2014; Wang et al., 2014; Wei et al., 2017; Zhang et al., 2016).

Numerous models have been implemented to partition ET into its biotic component (T) and its purely physical component, evaporation (E) at site, ecosystem, and global scales. Significant uncertainty remains across studies as indicated by the various range of T/ET values (20-90%) reported in the literature (Anderson et al., 2017; Stoy et al., 2019; Wei et al., 2017). While the most sophisticated climate and land surface schemes (e.g., GSWP, CLMs, STEAM) tend to give lower T/ET estimates ranging from 20 to 60%, the relatively simple models (e.g., PML,

PT-JPL) estimate T/ET close to isotopic and measurement-based values of about 65% (Gu et al., 2018; Guan and Wilson, 2009; Schlesinger and Jasechko, 2014; Wei et al., 2017). However, it is not yet clear how T/ET varies from season-to-season and site-to-site (such as with T/ET estimates from PML (Leuning et al., 2008; Zhang et al., 2016)). Also known is the uncertainty of ET partitioning in the absence of validation with observations and/or mechanistic constraints of the closely coupled carbon process (Fatichi and Pappas, 2017; Hu et al., 2009; Kool et al., 2014; Sutanto et al., 2012; Talsma et al., 2018). In addition to T/ET research with models varying in degrees of complexity, other research has been conducted to quantify the partitioning of ET based on the coupled relationship between transpiration and photosynthesis. Representative studies, such as Scanlon & Sahu (2008), Scott & Biederman (2017), Zhou et al. (2016) and Li et al, (2019), have all followed the fundamental principle that water loss and carbon gain are simultaneously regulated by plant stomata, and thus water flux can be inferred from carbon flux by differentiating stomatal fluxes (T and carbon uptake) and non-stomatal fluxes (E and respiration). These methods are usually empirical but mechanistically advantageous (de Wit, 1958; Hanks, 1983), and often uses the most reliable data from eddy covariance flux sites (Li et al., 2019; Zhou et al., 2018). However, due to the inherent complexity of T and the various assumptions employed by different methods, there is no single method capable of reproducing T/ET accurately across a wide range of climate and ecosystems (Wang et al., 2014; Zhou et al., 2018). Therefore, evaluating ET partitioning across models, e.g., process-based to empirical models, could be helpful in providing systematic interpretation (Gu et al., 2018; Wei et al., 2017).

In quantifying T/ET, it is not yet clear what factors and to what extent T/ET is controlled across space and time. Both climatic (e.g., precipitation, potential ET) and vegetation (e.g., LAI, EVI, NDVI) information have been used to explain the variability of T/ET. Controversial conclusions have been made that T/ET can be either dependent (in terms of timing, Knauer et al., 2018) or independent (in terms of amount, Schlesinger & Jasechko, 2014) of precipitation. While some studies have shown that EVI and LAI can explain up to 75% of the variation in T/ET (Zhou et al., 2018, 2016), others have found that only ~43% of the T/ET variation was explained by EVI or LAI (Gu et al., 2018; Wang et al., 2014). Fatichi and Pappas (2017) found no significant relationship between T/ET and LAI. Such inconsistences suggest that there is still a lack of in-depth understanding regarding the ecohydrological processes involved with T/ET, as well as evaluation and prediction of climate and vegetation responses and feedback,

thus requiring further investigation to better guide agricultural, hydrological, and ecological management of natural resources (Katul et al., 2012; Kool et al., 2014).

Grasslands cover 20 to 40 % of total land surface of the Earth (Goldewijk et al., 2007), and thus play a significant role in determining terrestrial energy, water, and carbon balances (Hovenden et al., 2019, 2014; Teuling et al., 2010). However, the spatial coverage of grasslands (in terms of leaf area index) varies from site to site and normally exhibits strong seasonal variability, which suggests that T/ET should also vary largely across sites. Therefore, grassland is an ideal ecosystem type to examine the uncertainties of ET partitioning using a coupled water and carbon model, i.e., the PML_V2 model (Gan et al., 2018). Furthermore, grasslands are an important ecosystem type to study because they are highly sensitive to climate change. Besides, grasslands have relatively simple species composition which minimises the possible uncertainty of ET partitioning and its attribution to controlling factors when compared to more complex ecosystems (e.g., rain forest). The PML_V2 model is a practical process-based algorithm that is consistent with the PML model (Leuning et al., 2008; Zhang et al., 2016), which has been shown to reasonably estimate T/ET on a global scale (Gu et al., 2018; Wei et al., 2017), but is further constrained by carbon processes (Gan et al., 2018). As stated above, multi-model comparisons could be beneficial (especially when T observations are not available), and the results from PML_V2 can be compared to those of a typical empirical method based on carbon uptake, as proposed by Zhou et al. (2016). As such, the specific objectives of this study were to (1) partition ET using the PML_V2 model for a variety of grassland ecosystems, (2) evaluate the spatial and temporal variation of T/ET and its controlling factors, and (3) investigate the uncertainty of ET partitioning based on two different methods (PML_V2 and uWUE).

4.2 Methods and materials

4.2.1 Methodology

The PML_V2 model is based on the satellite-based ET model developed by Cleugh et al. (2007) and Leuning et al. (2008), and estimates ET and its components, namely T and E, in the form of latent heat as:

$$\lambda ET = \lambda T + \lambda E \tag{4-1}$$

$$\lambda T = \frac{\varepsilon A_c + (\rho c_p/\gamma) D G_a}{\varepsilon + 1 + G_a/G_c} \tag{4-2}$$

$$\lambda E = \frac{f \varepsilon A_s}{\varepsilon + 1} \quad (4\text{-}3)$$

where λ (MJ kg^{-1}) is the latent heat of vaporisation of water, A_c and A_s are the available energy (A, W m^{-2}) over vegetated and soil surfaces, respectively; $\varepsilon = \Delta/\gamma$, where Δ (kP_a $^{\circ}C^{-1}$) is the slope of the curve between saturation water vapour pressure and temperature; γ (kP_a $^{\circ}C^{-1}$) is the psychrometric constant; ρ (kg m^{-3}) is the density of the air; c_p (kJ kg^{-1}) is the specific heat capacity of the air; D (kP_a) is the atmospheric water vapour pressure deficit (VPD); G_a (m s^{-1}) is the aerodynamic conductance, which is a function of wind speed and can be estimated following Leuning et al. (2008); and f is related to the moisture near the soil surface, which can be estimated following Zhang et al., (2010). According to the mechanistically coupled regulation of plant stomata to both water and carbon exchanges, canopy conductance (G_c, m s^{-1}) to water vapour should be constrained by carbon uptake, which can be written as (Gan et al., 2018):

$$G_c = m \frac{GPP}{C_a} \frac{1}{1 + D/D_0} \quad (4\text{-}4)$$

where GPP (μmol m^{-2} s^{-1}) is the gross primary production of the canopy, C_a (parts per million, ppm) is the concentration of carbon dioxide in the atmosphere, and m is the stomatal conductance coefficient.

It can be seen from Eq. 4-2 and 4-4 that T in the PML_V2 model is calculated from GPP, which means that T is constrained by the carbon uptake of the canopy. Previous studies on water use efficiency (WUE, GPP/T) have shown that WUE is relatively constant when normalised by atmospheric water demand (potential ET (PET) or VPD) (de Wit, 1958; Hanks, 1974; Ritchie, 1983; Sinclair et al., 1984). This implies that under a certain environmental condition, GPP can be used to inform/derive T. Therefore, this study assumed that when simulated GPP is close to observed GPP, simulated T will be close to actual T (as observed T was not available). Thus, the PML_V2 model is optimised to minimise the difference between simulated and observed values of both ET and GPP. As such, ET partitioning based on the PML_V2 model was achieved by simulating ET and GPP simultaneously. All of the seven model parameters were optimised to obtain the best simulation and ET partitioning.

Zhou et al., (2016) proposed an analytical method based on underlying WUE (uWUE) to directly estimate T from GPP observations. The method employs the above-mentioned relationship between T and GPP when normalised by VPD (Zhou et al., 2014). By assuming a maximum uWUE ($uWUE_p$) when T approaches ET under full vegetation coverage during

growing season, T/ET can be estimated as the ratio between apparent uWUE ($uWUE_a$) and $uWUE_p$, that is:

$$uWUE = \frac{GPP\sqrt{VPD}}{T} \quad (4\text{-}5)$$

$$\frac{T}{ET} = \frac{uWUE_a}{uWUE_p} \quad (4\text{-}6)$$

The method uses eddy covariance flux site observations and has been tested against observed T (Zhou et al., 2018). For a specific flux site, the uWUE method requires ET, GPP and VPD measurements at half-hourly intervals. The site specific $uWUE_p$ is estimated as the 95-quantile regression slope of $GPP \cdot VPD^{0.5}$ over ET (forced through the origin), and the $uWUE_a$ is estimated as the linear regression slope using data from each period of interest (daily or longer temporal scale). Then ET is partitioned by the ratio of $uWUE_a/uWUE_p$.

As both the PML_V2 model and the uWUE method partitions ET based on carbon uptake as quantified by GPP, it was expected that the T/ET estimates from these two methods were likely to be comparable. The T/ET values were also compared to investigate temporal and spatial variations as well as the controlling factors.

4.2.2 FLUXNET data and remote sensing data processing

The meteorological and flux observations were derived from the global FLUXNET2015 Tier2 data set (https://fluxnet.fluxdata.org/), for eddy covariance flux sites identified as being grassland. To meet model requirements (both PML_V2 and uWUE methods), the data for 37 flux sites were processed using standard protocols (Reichstein et al., 2005) after screening, quality control, energy balance, and gap filling following similar principles as used by Gan et al. (2018) and Zhang et al. (2019). This resulted in 89 site-years of data at 15 flux sites (Table 4-1). The selected flux sites spanned a wide range of climate (annual precipitation ranging between 200 and 1700 mm y^{-1}) and vegetation (LAI ranging between 0.2 and 4.1 m^2 m^{-2}) conditions. ET derived from latent heat (LE) measurements (converted by latent heat of vaporisation of water, λ=2.45 MJ kg^{-1}) and GPP (generated from night time partitioning algorithm based on net ecosystem carbon exchange) were consistently used as observations in this study. Half-hourly meteorological and flux observations were aggregated to daily averages and used for modelling purpose.

At each of the 15 flux sites, remotely-sensed LAI time series from the Moderate Resolution Imaging Spectroradiometer (MODIS, product MOD15A2) were obtained and processed to represent the site level vegetation index following the same procedure as Gan et al. (2018).

Only the pixels within the 1×1 km centred grid specified by the flux site coordinates were selected and composed to match the footprint of the measurements. The LAI data covered a maximum temporal period of 14 years (from 2001 to 2014). The 8-day time series were interpolated into daily data to conform with *in-situ* observations, which were then used together to optimise the PML_V2 model parameters and obtain ET, GPP, and T simulations.

Table 4-1. Summary information for the grassland eddy covariance flux sites used in this study.

Site Code	Country	Site name	Latitude	Longitude	Period	Precipitation mm y^{-1}	LAI $m^2 m^{-2}$
AT-Neu	Austria	Neustift	47.12	11.32	2003-2012	852	1.39
AU-DaP	Australia	Daly River Savanna	-14.06	131.32	2008-2013	1111	1.42
AU-Stp	Australia	Sturt Plains	-17.15	133.35	2009-2014	708	0.49
CH-Cha	Switzerland	Chamau	47.21	8.41	2006-2014	1136	4.13
CH-Fru	Switzerland	Früebüel	47.12	8.54	2007-2014	1651	1.56
CH-Oe1	Switzerland	Oensingen grassland	47.29	7.73	2003-2008	1100	1.08
CN-Cng	China	Changlin	44.59	123.51	2008-2010	300	0.46
CN-Du2	China	Dangxiong	42.05	116.28	2007-2008	283	0.42
DE-RuR	Germany	Rollesbroich	50.62	6.3	2012-2014	1033	1.68
IT-MBo	Italy	Monte Bondone	46.01	11.05	2003-2013	1214	0.95
IT-Tor	Italy	Torgnon	45.84	7.58	2009-2014	920	0.74
US-ARb	USA	ARM Southern Great Plains burn site-Lamont	35.55	-98.04	2005-2006	591	1.13
US-ARc	USA	ARM Southern Great Plains control site-Lamont	35.55	-98.04	2005-2006	614	1.13
US-SRG	USA	Santa Rita Grassland	31.79	-110.83	2008-2014	420	0.4
US-Wkg	USA	Walnut Gulch Kendall Grasslands	31.73	-109.94	2004-2014	407	0.27

* Precipitation and LAI are presented as multiyear average during the study period. LAI is based on the remotely-sensed product MOD15A2 from MODIS. Further details of the flux sites can be found at https://fluxnet.fluxdata.org/.

4.3 Results

4.3.1 PML_V2 model parameterization and performance

At each of the 15 flux sites, the seven model parameters of the PML_V2 model were optimised to obtain the best estimates of both ET and GPP when compared with observations at the 8-day time step (Table 4-2). All of the optimised parameters fell into their theoretical ranges, yet they varied greatly despite the shared grassland ecosystem type. The quantum and carboxylation efficiencies (α and η) ranged between 0.03 and 0.10 (μmol CO_2 (μmol PAR)$^{-1}$) and between 0.011 and 0.060 (μmol m^{-2} s^{-1} (μmol m^{-2} s^{-1})$^{-1}$), respectively. Both the stomatal conductance coefficient (m) and $V_{m,25}$ varied considerably between 2 and 38 and 5 and 120 (μmol m^{-2} s^{-1}), respectively. In addition, 11 of the 15 sites had a value of 0.5 kPa for the

insensitive parameter D_0 (all sites except AT-Neu, CH-Cha, IT-MBo and IT-Tor). For the radiative extinction coefficients, while the optimised k_Q ranged between 0.1 and 1.0, k_A showed a relatively narrower (0.5 to 0.9). The various parameter sets indicated distinct ecosystem functioning across sites under different environments (Table 4-1).

Table 4-2. Optimised PML_V2 model parameters at 15 eddy covariance flux sites.

site unit	α μmol CO_2 (μmol PAR)$^{-1}$	η μmol m^{-2} s^{-1} (μmol m^{-2} s^{-1})$^{-1}$	m -	$V_{m,25}$ μmol m^{-2} s^{-1}	D_0 kPa	k_Q -	k_A -
AT-Neu	0.100	0.044	6.80	120.0	2.00	1.00	0.90
AU-DaP	0.030	0.017	8.14	12.9	0.50	0.10	0.50
AU-Stp	0.100	0.023	12.10	5.9	0.50	0.10	0.90
CH-Cha	0.100	0.033	10.00	5.0	1.89	0.58	0.50
CH-Fru	0.098	0.038	38.26	45.9	0.50	1.00	0.78
CH-Oe1	0.100	0.047	14.50	35.6	0.50	1.00	0.50
CN-Cng	0.058	0.026	9.20	15.3	0.50	0.10	0.90
CN-Du2	0.048	0.011	5.86	11.9	0.50	0.10	0.50
DE-RuR	0.074	0.050	14.97	24.7	0.50	1.00	0.76
IT-MBo	0.099	0.040	9.06	26.3	2.00	0.80	0.90
IT-Tor	0.087	0.037	10.25	22.7	1.00	0.81	0.90
US-ARb	0.017	0.045	9.75	25.2	0.50	0.10	0.54
US-ARc	0.019	0.059	10.92	14.9	0.50	0.23	0.50
US-SRG	0.073	0.019	5.56	10.7	0.50	0.10	0.90
US-Wkg	0.069	0.018	2.00	9.4	0.50	0.10	0.90

* The parameters were optimised to maximise $NSE_{ET} + NSE_{GPP}$ independently at each of the study sites using all available data. '-' denotes unitless.

When simulated ET and GPP were compared to observations, statistics showed that the overall model performance was satisfactory (Figure 4-1), as evidenced by high values of NSE, R^2, and slope (close to 1) and low values of RMSE (close to 0). NSE, R^2, and slope values averaged across the 15 study sites were 0.81, 0.83, 0.91, respectively, and RMSE was 0.53 (mm d^{-1}) for ET. For GPP, the average NSE, R^2, and slope is 0.71, 0.74, and 0.67, respectively, and RMSE was 1.74 (μmol m^{-2} s^{-1}). The model performed the best for both ET and GPP at IT-Tor, US-ARb and US-ARc (NSE >0.85), whereas less satisfactory results were found at US-Wkg for ET (NSE<0.7) and CH-Cha for GPP (NSE=0.5). The model tended to simulate comparable quantities of ET (slope>0.75) for all sites, but underestimated GPP at five of the flux sites (slope<0.6). Relatively high RMSE was found for ET at AU-DaP (about 0.75 mm d^{-1}) and for GPP at CH-Cha (about 3.5 μmol m^{-2} s^{-1}). However, the overall statistics indicated reliable ET and GPP simulations across the 15 flux sites. Therefore, the simulated times series were used to further analyse uncertainties of ET partitioning.

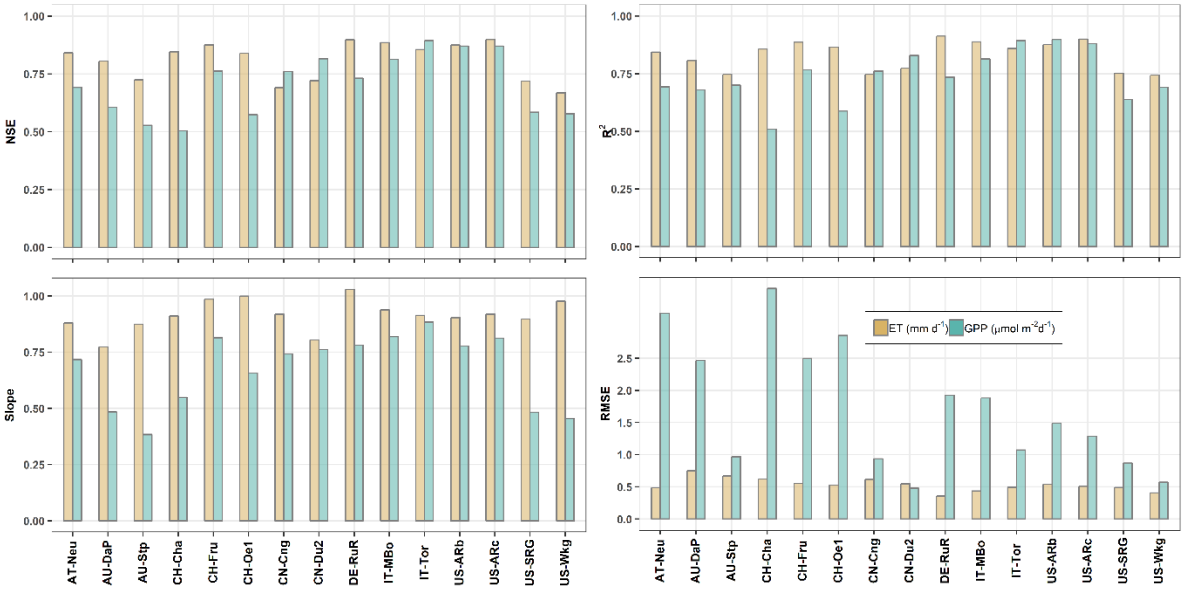

Figure 4-1. Statistics of model performance for 8-day time scale simulated ET and GPP. The model was optimised independently at each site based on available data. Nash-Sutcliffe efficiency (NSE), coefficient of determination (R^2), linear regression slope (Slope) and RMSE (Root Mean Square Error) values were based on simulated versus observed data for both ET (yellow) and GPP (green).

4.3.2 Estimates of ET components

Simulated ET and T by PML_V2 were used to calculate the transpiration ratio (T/ET) (Figure 4-2). At each of the 15 study sites, T and ET estimates are averaged for each site-year and then the mean values were used to calculate the ratio of T/ET. It can be seen that, despite the shared ecosystem type, T/ET varied greatly from 0.09 (US-Wkg) to 0.87 (CH-CHa) across the 89 site-years (average of 0.55). For flux sites with a minimum of five years of data, the interannual variation of T/ET was the largest at AU-Stp (range of about 0.3 to 0.5, average of 0.42 across 6 years) and the smallest variation was observed at US-Wkg (average value close to 0.1 across 11 years). However, the variation of annual T/ET wass less than 0.1 at several individual sites, which indicates consistent performance of ET partitioning at the annual scale using the PML_V2 model.

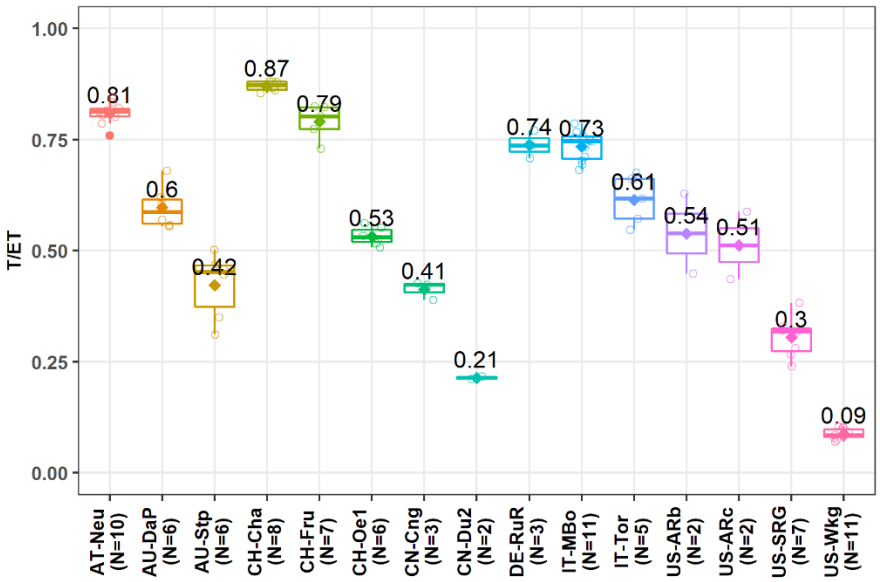

Figure 4-2. Multiyear average T/ET estimates by the PML_V2 model. N represents the number of years used at each study site. The mean (solid diamond (number in black) and median (horizontal line) values are shown in each box. Values for individual site-years are shown as circles, and the 25th and 75th percentiles are shown as the lower and upper boundaries of each box. Whiskers represent the 5th and 95th percentiles.

4.3.3 Spatiotemporal dynamics and controlling factors of T/ET

The estimates of T/ET by the PML_V2 model and the uWUE method were compared to examine the spatiotemporal dynamics of ET partitioning and its controlling factors. Significant differences were found between the two methods. The mean T/ET from both methods (when T estimates were divided by observed ET) were relatively close (0.53 from PML_V2 and 0.45 from uWUE) across sites. However, a much wider range of T/ET was found for PML_V2 (about 0.1 to 0.9) when compared with that of uWUE (0.2 to 0.6). The maximum and minimum T/ET values estimated by the PML_V2 model were found at CH-Cha and US-Wkg, while those values by the uWUE method were found at CN-Du2 and AU-DaP, respectively. When the seasonal (monthly) time series of T/ET were compared, the two models presented larger discrepancies in terms of temporal variations (Figure 4-3). In general, T/ET based on the PML_V2 model exhibited stronger seasonal variation than T/ET based on the uWUE method, with higher values observed during the growing season (LAI/LAI_{max}>0.2) and lower values during the other months across multiple years (except US-ARb and US-ARc (northern hemisphere), AU-DaP, AU-Stp (southern hemisphere)). At sites where the PML_V2 model gave significantly higher T/ET estimates (AT-Neu, CH-Cha and CH-Fru), growing season

T/ET was estimated to be about double the value of T/ET from the uWUE method. However, similar T/ET estimates by both algorithms were obtained for the other sites. Considering both seasonality and quantity, T/ET estimates from PML_V2 corresponded the well T/ET from uWUE at only three sites, namely CH-Oe1 (0.46 vs 0.52), CN-Cng (0.39 vs 0.35) and CN-Du2 (0.25 vs 0.18). Seasonal variation in T/ET from both methods was generally in good agreement with variations in precipitation and LAI, especially at sites where precipitation and LAI showed strong seasonality, such as at CH-Cha and CH-Fru.

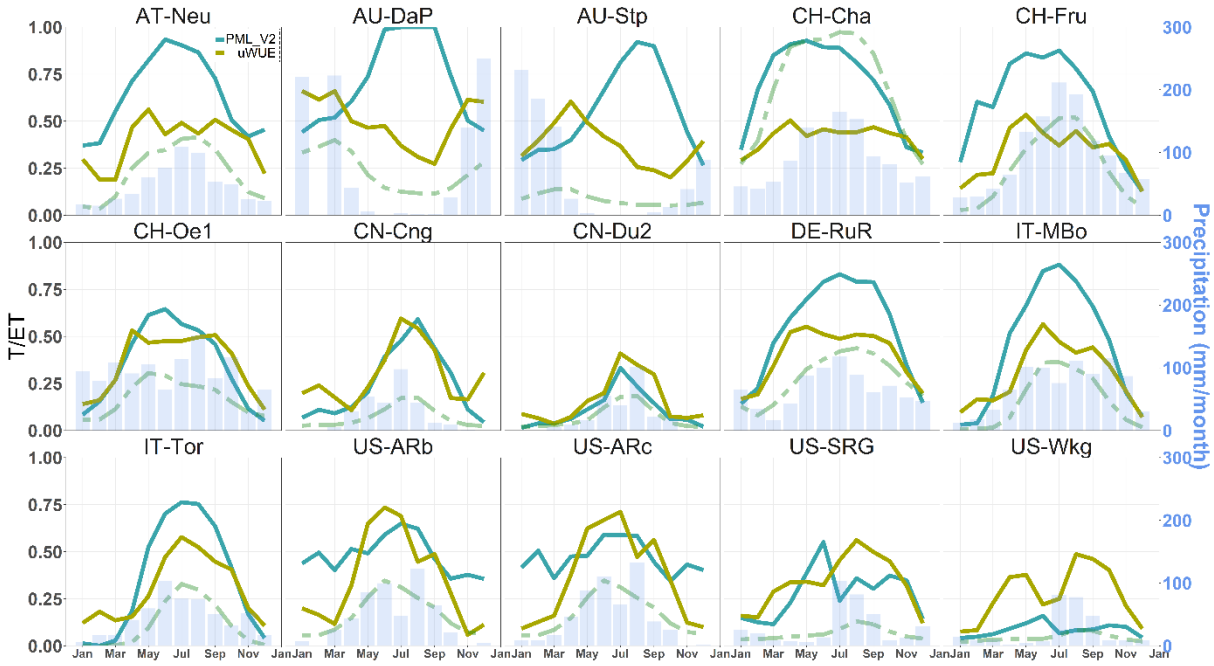

Figure 4-3. Multiyear average of monthly T/ET from the PML_V2 model (turquoise) and the uWUE method (yellow green) at each flux site. T estimates from both PML_V2 and uWUE were divided by observed ET to obtain the T/ET ratios (values of T/ET larger than 1 are not shown). LAI values normalized by their maximum value are shown as dashed green lines (LAI/LAI_{max}, where LAI_{max} was set to 6). Monthly precipitation averaged across site-years is shown in light blue bars.

In addition to magnitude and temporal variations, seasonal T/ET estimates from the PML_V2 model and the uWUE method presented different relationships with LAI and precipitation (Figures 4-4, 4-5). Seasonal variations in T/ET from the PML_V2 model were well explained by monthly LAI, with R^2>0.8 (natural exponential regression, $T/ET = a+b\cdot\exp(-LAI)$) for seven out of the 15 flux sites (namely AT-Neu, CH-Cha, CH-Fru, CH-Oe1, DE-RuR, IT-MBo and IT-Tor). Yet comparable statistics were found only at four sites for T/ET based on the uWUE method (IT-MBo, IT-Tor, US-ARb and US-ARc). The largest discrepancy between the two

algorithms with regard to LAI explaining variations in T/ET was found at AT-Neu, CH-Cha, and CH-Fru, with the PML_V2 model outperforming the uWUE method ($R^2 \geq 0.8$ from PML_V2 compared to $R^2 \leq 0.5$ from uWUE). However, the reverse was observed at two other sites, namely US-SRG and US-Wkg ($R^2 < 0.02$ from PML_V2 and $R^2 > 0.6$ from uWUE). The relationships between monthly T/ET and LAI were mostly positive (T/ET increasing with increasing of LAI) for both methods, yet negative relationships were found for the PML_V2 model at sites where maximum LAI<1.5 (AU-DaP, AU-Stp, CN-Cng, CN-Du2, US-SRG, and US-Wkg).

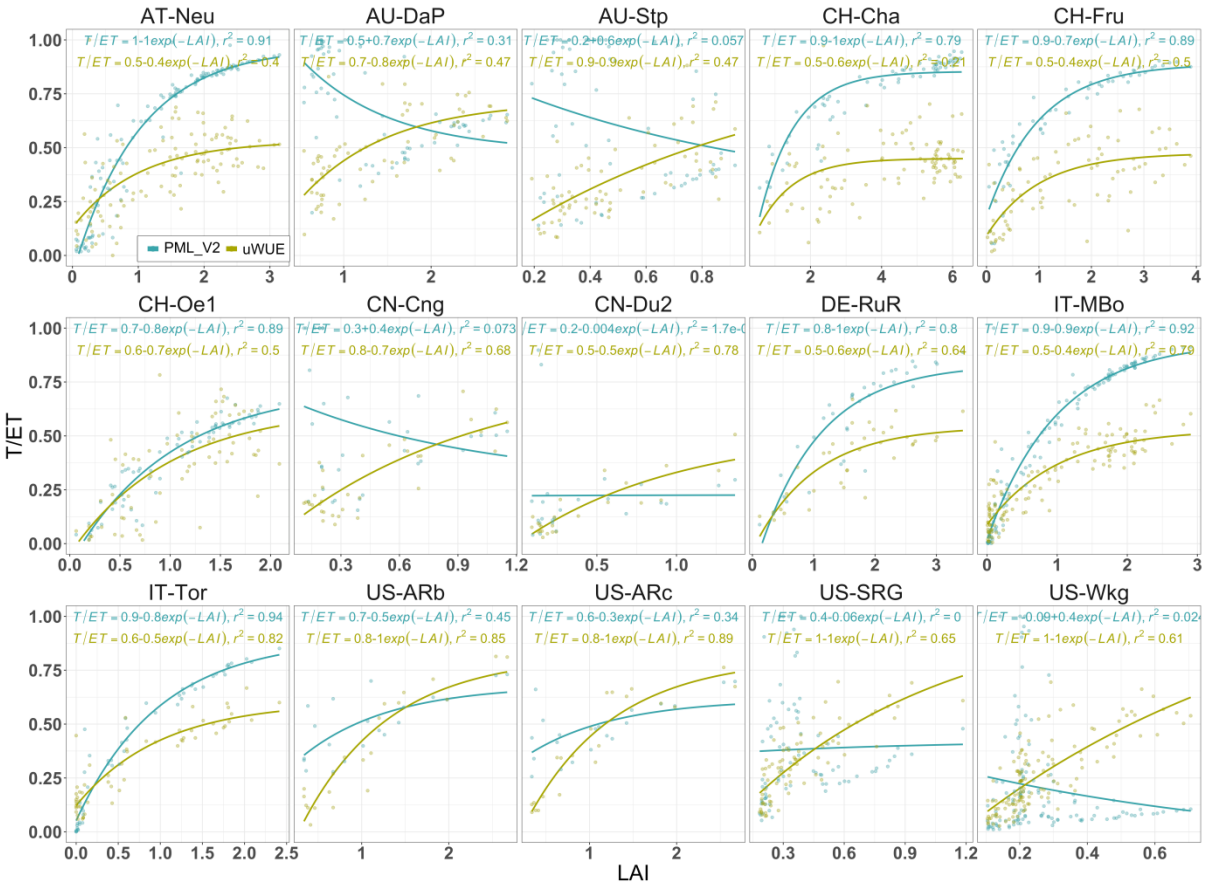

Figure 4-4. Relationship between monthly LAI and T/ET from the PML_V2 model (turquoise) and the uWUE (yellow green) method for each of the 15 flux sites. The natural exponential regression was performed between LAI and T/ET based on the two ET partitioning algorithms, with the fitted equation and R^2 shown accordingly.

Across sites and years, spatial variations of T/ET was well explained by precipitation (Figure 4-5). Annual precipitation explained 50% of the variation in T/ET across the 89 site-years based on PML_V2 partitioning, with higher precipitation corresponding to higher T/ET. This was not

the case for T/ET based on uWUE partitioning, where precipitation only explained 17% of the variation in T/ET. In fact, when the study sites were grouped by climate (precipitation) and vegetation index (LAI) gradients, it was found that the PML_V2 model gave T/ET estimates that varied along with the precipitation and LAI gradients, while uWUE gave relatively constant T/ET estimates across the gradients (Table 4-3). Across wet, medium and dry sites with average precipitation ranging from 700 to 1100 mm y^{-1} and average LAI ranging from 0.6 to 2 m^2 m^{-2}, PML_V2 estimated T/ET to vary between 0.3 and 0.7, while uWUE estimated T/ET close to 0.45, regardless of the different water availability (precipitation) and vegetation (LAI) conditions across sites.

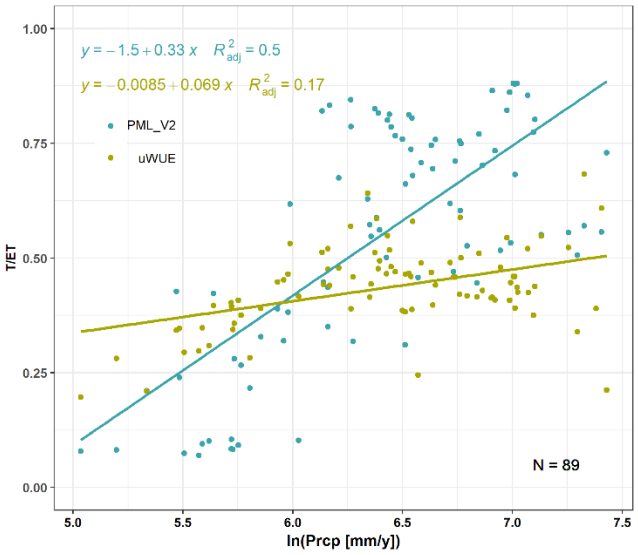

Figure 4-5. Relationship between annual precipitation (converted to natural logarithm) and T/ET from the PML_V2 model (turquoise) and the uWUE method (yellow green). N represents the total number of years across 15 flux sites.

Table 4-3. T/ET from the PML_V2 model and the uWUE method grouped by precipitation and LAI gradients. Values of precipitation, LAI, and T/ET are shown as averages across sites.

Group	Precipitation mm y^{-1}	Number of Sites	LAI m^2 m^{-2}	T/ET PML_V2	T/ET uWUE
Wet	>1100	4	1.828	0.69	0.47
Medium	700~1100	4	1.075	0.64	0.46
Dry	<700	7	0.635	0.33	0.42

4.4 Discussion

4.4.1 Variation and uncertainty of T/ET estimates

Constrained by GPP, the PML_V2 model was capable of partitioning ET into its components, with comparable T/ET values as reported in previous by experimental studies (Table 4-4). Across a variety of grasslands, PML_V2 estimated T/ET to range between 0.21 and 0.87 (Figure 4-2) (except at US-Wkg), which is in good agreement with the range of values shown in Table 4-4 (0.32-0.77) reported in previous research. Based on isotope observations, Hsieh et al. (1998) demonstrated that T/ET increased with increasing precipitation, with T/ET values of about 0.3 at relatively dry sites (precipitation about 300 mm y^{-1}), 0.6 at intermediate sites (precipitation about 500-1300 mm y^{-1}), and 0.7 at a wet site (precipitation over 2000 mm y^{-1}). This increasing trend aligns well with our ET partitioning result using the PML_V2 model as summarized in Table 4-3, where similar T/ET values were found across the precipitation gradient, i.e., about 0.3, 0.6, and 0.7 at the dry, intermediate, and wet sites, respectively. Our modeled T/ET was also close to that from other studies based on isotopes, lysimeters, and sap flow gauges (Bachand et al., 2014; Ferretti et al., 2003; Flumignan et al., 2011; Roupsard et al., 2006; Wang et al., 2013), especially during the growing season. Although observational T/ET was not available at our study sites, it can be seen that reasonable ET partitioning can be obtained through with the PML_V2 model, with avalues that are comparable to values reported by these experiment-based studies.

Table 4-4. Summary of previously published T/ET observed at grassland and cropland sites.

Type	Ecoregion	Country	Lat	Long	Location	Period	Method of measurement	T/ET %	LAI	Prcp mm y^{-1}	Reference
GRA	Trop-Grassland	USA	40.70	-106.80	Colorado: Central Plains Experimental Range	Dec 1993 - Nov 1994	isotope	0.56	-	320	(Ferretti et al., 2003)
GRA	Grassland	New Mexico	32.30	106.80	Jornada Experimental Range	1991 - 1992	micro-lysimeters, Bowen ratio energy balance	0.45	-	241	(Dugas et al., 1995)
CRO	Crop-wetland	USA	38.60	-121.60	Yolo Bypass, Sacramento River Watershed	2000/2001 - 2009/2010 (July -June)	Hydrologic and tracer mass budgets	0.55~ 0.74	-	420	(Bachand et al., 2014)
CRO	Crop (young coffee tree)	Brazil	23.30	-51.20	Londrina, Parana State	Sep 2004 - Aug 2006	weighting Lysimeters, micro-lysimeters	0.65	2.7-9.6	1211.4	(Flumignan et al., 2011)
CRO	Trop-Crop(coconut)	Vanuatu	-15.40	167.20	Espiritu Santo	Oct 2001 - Sep 2004	EC, sapflow	0.68	2.95	2763	(Roupsard et al., 2006)
GRA	grassland	USA	34.98	-97.52	Kessler Farm field Laboratory, Oklahoma	May-Jun 2011	isotope, chamber	0.65~ 0.77	-	911.4	(Wang et al., 2013)
CRO	crop	Argentina	-28.50	-66.82	Aimogasta, La Rioja	2006-2007, May, Aug, Nov, Jan, Mar	sapflow, lysimeter	0.75	-	455	(Rousseaux et al., 2009)

GRA	pasture grass	USA	19.6	-155.5	Kohala Peninsula, Hawaii	Dec 1993-Nov 1994, Mar 1995-Sep1995	isotope	0.32	-	316	(Hsieh et al., 1998)
GRA	pasture grass	USA	19.6	-155.5	Kohala Peninsula, Hawaii	Dec 1993-Nov 1994, Mar 1995-Sep1995	isotope	0.59	-	500	(Hsieh et al., 1998)
GRA	pasture grass	USA	19.6	-155.5	Kohala Peninsula, Hawaii	Dec 1993-Nov 1994, Mar 1995-Sep1995	isotope	0.61	-	1287	(Hsieh et al., 1998)
GRA	pasture grass	USA	19.6	-155.5	Kohala Peninsula, Hawaii	Dec 1993-Nov 1994, Mar 1995-Sep1995	isotope	0.72	-	2240	(Hsieh et al., 1998)

* T/ET studies conducted over croplands are also included here for comparison. Lat, latitude; Long, longitude; Prcp, precipitation; Trop-, tropical; GRA, grassland; CRO, cropland.

The PML_V2 model gave extremely high estimates of T/ET (close to 1) during the non-growing season months (May to September) at AU-DaP and AU-Stp, which is not likely to be true in reality (under very low precipitation and LAI). This finding could be a result of (1) precipitation interception not being considered in this study, which ccould contribute a significant proportion of ET during non-growing season months; and (2) the energy partitioning principle used in this model. With LAI approaching its minimum value (about 0.6), the big-leaf assumption used in the PML_V2 model still allocated a considerable proportion of incident radiation to the canopy (based on Beer's law, k_A>0.5, Table 4-2) regardless of the land cover profile. This in turn could induce an overestimation of canopy conductance and thus transpiration. Furthermore, it is known that the extinction coefficient varies along with vegetation growing stages (Zheng et al., 2018), yet the constant k_A was optimised as an site-specific parameter. This is inappropriate in principle considering that the value of k_A could be different across seasons, which may lead to distinct ET partitioning results. Additionally, the low T/ET estimates found at US-Wkg are a result of the overall low vegetation coverage, where LAI is generally below 0.5 throughout the annual cycle (Figure 4-3). As GPP is underestimated at similar sites with dry climate (GPP slope<0.5, AU-Dap, AU-Stp, US-SRG, precipitation <100 mm during most months), high uncertainty of T estimates is expected even though the total amount of estimated ET seems reasonably accurate (ET slope>0.75). Additionally, LAI as used by the PML_V2 model was derived from remotely-sensed images rather than from *in-situ* observations. Therefore, the T/ET uncertainty could also be induced by remotely-sensed LAI time series. Observed values of T, E, or LAI and further investigation of the model assumptions will be required to quantitively evaluate the uncertainty in ET partitioning based on the PML_V2 model. Advanced measurements, such as those available from SAPFLUXNET when it is publicly released, will provide a powerful dataset to evaluate the uncertainty of ET partitioning (Poyatos et al., 2016). Similar datasets can be incorporated with the methods used

in this study as well as other models outside this study to evaluate T/ET at larger spatial and longer temporal scales.

4.4.2 Controlling factors of T/ET

This study attempted to explain the temporal and spatial variations in T/ET using two widely used explanatory factors: a physiological factor (i.e., LAI) and a climatic factor (i.e., precipitation). At stand level, ET partitioning is expected to vary along with seasonal LAI during a year. Because LAI controls energy partitioning, it thus determines T/ET. This is explicitly expressed in the PML_V2 model because (1) the total available energy is allocated to vegetated and soil surfaces based on Beer's law as a function of LAI, and (2) the canopy conductance is calculated from GPP, which is also directly a function of LAI (Gan et al., 2018). As a result, LAI can explain up to 94% of the variation in T/ET using this model (R^2>0.8 for seven out of 15 sites, Figure 4-3). However, the same regression analysis based on the PML_V2 model performed worse at other sites, where T/ET was better explained by LAI based on uWUE partitioning. This illustrates that although both partitioning methods are constrained by GPP, the T estimates can be distinct from each other, thus leading to different relationships between T/ET and LAI. At this point, it is difficult to conclude which method performs the best with the respect to ET partitioning (in the absence of observed T and/or E). Yet the results of this study clearly demonstrated that LAI controls the seasonality of T/ET. In terms of spatial variations, precipitation (precipitation converted by natural logarithm) explained about 50% of the variation in T/ET across the 89 site-years when the PML_V2 model was used, but only 17% of the variation in T/ET when the uWUE method was used. This indicated that the PML_V2 model tended to produce variable T/ET along the precipitation gradient, but with the uWUE method T/ET was not so strongly influenced by precipitation. In principle, vegetation coverage (LAI) and plant growth (GPP) should be greater under ample water availability when compared with water-limited environment. Under high precipitation conditions, T values are more likely to reach the total value of ET. Simulations with the PML_V2 model agree well with this conclusion and with previous studies (Hsieh et al., 1998; Li et al., 2019). The relatively conservative T/ET estimates from the uWUE method, however, did not show this trend. This is likely explained by the underlying assumptions used in this method. Specifically, a constant $uWUE_p$ was estimated as the linear slope of 95^{th} quantile regression to assume that T approaches ET. This statistical treatment can be problematic under relatively invariant high or low vegetation coverage conditions, where $uWUE_a$ is close to $uWUE_p$ over most periods (such

as at CH-Cha), and where T could hardly reach ET due to low LAI (such as at US-Wkg). The constant $uWUE_p$ is also inappropriate when inferring T from GPP because uWUE can vary in response to different environmental parameters (e.g., water, CO_2). Others researchers have also highlighted the importance of radiation in determining uWUE (Boese et al., 2017) and the difference between leaf and canopy scale uWUE (Medlyn et al., 2017). Therefore, the uWUE method will require further investigation and validation to be used for ET partitioning. A more recent ET partitioning method based on stomatal conductance proposed by Li et al. (2019) and a machine learning method (TEA) proposed by Nelson et al. (2018) could be compared with the PML_V2 model to investigate the uncertainty of T/ET estimates constrained by carbon processes.

4.5 Conclusions

This study used a simple process-based carbon and water model to partition ET into T and E across 15 grassland flux sites widely distributed across the globe. Results showed that the model was capable of simulating reliable ET and GPP estimates, with mean NSE of 0.8 and 0.7, respectively. The T/ET estimates from the PML_V2 model ranged between about 0.1 and 0.9, and averaged about 0.5, a value that was close to observation-based values reported in the literature. The seasonal variations of ET partitioning as indicated by monthly T/ET values can likely be explained by variations in LAI, and the spatial pattern of T/ET across site-years was positively related to precipitation. Comparisons between T/ET from the process-based PML_V2 model and the empirical uWUE method showed that high uncertainty existed in T estimates, where the seasonality and explanatory factors exhibited significant differences between the two at most of the study sites. Greater attention should be given evaluating ET components, especially T, even with carbon constraint taken into consideration. Underlying model assumptions and principles are likely to explain controversial estimates of T/ET from different models. Further datasets and investigations will be required to validate the models and to evaluate uncertainties in order to enhance process-based understandings and to guide natural resources management policies under climate change.

Reference

Anderson, R.G., Zhang, X., Skaggs, T.H., 2017. Measurement and Partitioning of Evapotranspiration for Application to Vadose Zone Studies. Vadose Zo. J. 16, 0. doi:10.2136/vzj2017.08.0155

Bachand, P.A.M., Bachand, S., Fleck, J., Anderson, F., Windham-Myers, L., 2014. Differentiating transpiration from evaporation in seasonal agricultural wetlands and the link to advective fluxes in the root zone. Sci. Total Environ. 484, 232–248. doi:10.1016/j.scitotenv.2013.11.026

Boese, S., Jung, M., Carvalhais, N., Reichstein, M., 2017. The importance of radiation for semiempirical water-use efficiency models. Biogeosciences 14, 3015–3026. doi:10.5194/bg-14-3015-2017

Cleugh, H.A., Leuning, R., Mu, Q., Running, S.W., 2007. Regional evaporation estimates from flux tower and MODIS satellite data. Remote Sens. Environ. 106, 285–304. doi:10.1016/j.rse.2006.07.007

Coenders-Gerrits, A.M.J., Van Der Ent, R.J., Bogaard, T.A., Wang-Erlandsson, L., Hrachowitz, M., Savenije, H.H.G., 2014. Uncertainties in transpiration estimates. Nature 506, E1–E2. doi:10.1038/nature12925

de Wit, C.T., 1958. Transpiration and crop yields. Versl. Landbouwk. Onderz. 64. 6. 88. doi:.

Dugas, W.A., Hicks, R.A., Gibbens, R.P., 1995. Structure and function of C3 and C4 Chihuanhuan desert plant communities. Energy balancs components. J. Arid Environ.

Fatichi, S., Pappas, C., 2017. Constrained variability of modeled T:ET ratio across biomes. Geophys. Res. Lett. 44, 6795–6803. doi:10.1002/2017GL074041

Ferretti, D.F., Pendall, E., Morgan, J.A., Nelson, J.A., LeCain, D., Mosier, A.R., 2003. Partitioning evapotranspiration fluxes from a Colorado grassland using stable isotopes: Seasonal variations and ecosystem implications of elevated atmospheric CO2. Plant Soil 254, 291–303. doi:10.1023/A:1025511618571

Flumignan, D.L., de Faria, R.T., Prete, C.E.C., 2011. Evapotranspiration components and dual crop coefficients of coffee trees during crop production. Agric. Water Manag. 98, 791–800. doi:10.1016/j.agwat.2010.12.002

Gan, R., Zhang, Y., Shi, H., Yang, Y., Eamus, D., Cheng, L., Chiew, F.H.S., Yu, Q., 2018. Use of satellite leaf area index estimating evapotranspiration and gross assimilation for Australian ecosystems. Ecohydrology e1974. doi:10.1002/eco.1974

Good, S.P., Noone, D., Bowen, G., 2015. Hydrologic connectivity constrains partitioning of global terrestrial water fluxes. Science (80-.). 349, 175–177. doi:10.1126/science.aaa5931

Gu, Chunjie, Ma, J., Zhu, G., Yang, H., Zhang, K., Wang, Y., Gu, Chunli, 2018. Partitioning evapotranspiration using an optimized satellite-based ET model across biomes. Agric. For. Meteorol. 259, 355–363. doi:10.1016/j.agrformet.2018.05.023

Guan, H., Wilson, J.L., 2009. A hybrid dual-source model for potential evaporation and transpiration partitioning. J. Hydrol. 377, 405–416. doi:10.1016/J.JHYDROL.2009.08.037

Hanks, R.J., 1983. Yield and water-use relationships: An overview. Limitations to Effic.

water use Crop Prod. 393–411.

Hanks, R.J., 1974. Model for Predicting Plant Yield as Influenced by Water Use.

Hatfield, J.L., Dold, C., 2019. Water-Use Efficiency: Advances and Challenges in a Changing Climate. Front. Plant Sci. 10, 1–14. doi:10.3389/fpls.2019.00103

Hovenden, M.J., Leuzinger, S., Newton, P.C.D., Fletcher, A., Fatichi, S., Lüscher, A., Reich, P.B., Andresen, L.C., Beier, C., Blumenthal, D.M., Chiariello, N.R., Dukes, J.S., Kellner, J., Hofmockel, K., Niklaus, P.A., Song, J., Wan, S., Classen, A.T., Langley, J.A., 2019. Globally consistent influences of seasonal precipitation limit grassland biomass response to elevated CO 2. Nat. Plants 5, 167–173. doi:10.1038/s41477-018-0356-x

Hovenden, M.J., Newton, P.C.D., Wills, K.E., 2014. Seasonal not annual rainfall determines grassland biomass response to carbon dioxide. Nature 511, 583–586. doi:10.1038/nature13281

Hsieh, J.C.C., Chadwick, O.A., Kelly, E.F., Savin, S.M., 1998. Oxygen isotopic composition of soil water: Quantifying evaporation and transpiration. Geoderma 82, 269–293. doi:10.1016/S0016-7061(97)00105-5

Hu, Z., Wu, G., Zhang, L.L., Li, S., Zhu, X., Zheng, H., Zhang, L.L., Sun, X., Yu, G., 2017. Modeling and partitioning of regional evapotranspiration using a satellite-driven water-carbon coupling model. Remote Sens. 9, 1–5. doi:10.3390/rs9010054

Hu, Z., Yu, G., Zhou, Y., Sun, X., Li, Y., Shi, P., Wang, Y., Song, X., Zheng, Z., Zhang, L., Li, S., 2009. Partitioning of evapotranspiration and its controls in four grassland ecosystems: Application of a two-source model. Agric. For. Meteorol. 149, 1410–1420. doi:10.1016/j.agrformet.2009.03.014

Katul, G.G., Oren, R., Manzoni, S., Higgins, C., Parlange, M.B., 2012. Evapotranspiration: A process driving mass transport and energy exchange in the soil-plant-atmosphere-climate system. Rev. Geophys. 50. doi:10.1029/2011rg000366

Klein Goldewijk, K., Van Drecht, G., Bouwman, A.F., 2007. Mapping contemporary global cropland and grassland distributions on a 5 × 5 minute resolution. J. Land Use Sci. 2, 167–190. doi:10.1080/17474230701622940

Knauer, J., Zaehle, S., Medlyn, B.E., Reichstein, M., Williams, C.A., Migliavacca, M., De Kauwe, M.G., Werner, C., Keitel, C., Kolari, P., Limousin, J.-M.M., Linderson, M.-L.L., 2018. Towards physiologically meaningful water-use efficiency estimates from eddy covariance data. Glob. Chang. Biol. 24, 694–710. doi:10.1111/gcb.13893

Kool, D., Agam, N., Lazarovitch, N., Heitman, J.L., Sauer, T.J., Ben-Gal, A., 2014. A review of approaches for evapotranspiration partitioning. Agric. For. Meteorol. 184, 56–70. doi:10.1016/j.agrformet.2013.09.003

Leuning, R., Zhang, Y.Q., Rajaud, A., Cleugh, H., Tu, K., 2008. A simple surface conductance model to estimate regional evaporation using MODIS leaf area index and the Penman-Monteith equation. Water Resour. Res. 44, W10419. doi:10.1029/2007WR006562

Li, X., Gentine, P., Lin, C., Zhou, S., Sun, Z., Zheng, Y., Liu, J., Zheng, C., 2019. A simple and objective method to partition evapotranspiration into transpiration and evaporation at eddy-covariance sites. Agric. For. Meteorol. 265, 171–182. doi:https://doi.org/10.1016/j.agrformet.2018.11.017

Lian, X., Piao, S., Huntingford, C., Li, Y., Zeng, Z., Wang, X., Ciais, P., McVicar, T.R., Peng, S., Ottlé, C., Yang, H., Yang, Y., Zhang, Y., Wang, T., 2018. Partitioning global land evapotranspiration using CMIP5 models constrained by observations. Nat. Clim. Chang. 8, 640–646. doi:10.1038/s41558-018-0207-9

Medlyn, B.E., De Kauwe, M.G., Lin, Y.S., Knauer, J., Duursma, R.A., Williams, C.A., Arneth, A., Clement, R., Isaac, P., Limousin, J.M., Linderson, M.L., Meir, P., Martin-Stpaul, N., Wingate, L., 2017. How do leaf and ecosystem measures of water-use efficiency compare? New Phytol. doi:10.1111/nph.14626

Miralles, D.G., Jiménez, C., Jung, M., Michel, D., Ershadi, A., Mccabe, M.F., Hirschi, M., Martens, B., Dolman, A.J., Fisher, J.B., Mu, Q., Seneviratne, S.I., Wood, E.F., Fernández-Prieto, D., 2016. The WACMOS-ET project - Part 2: Evaluation of global terrestrial evaporation data sets. Hydrol. Earth Syst. Sci. 20, 823–842. doi:10.5194/hess-20-823-2016

Nelson, J.A., Carvalhais, N., Cuntz, M., Delpierre, N., Knauer, J., Ogée, J., Migliavacca, M., Reichstein, M., Jung, M., 2018. Coupling Water and Carbon Fluxes to Constrain Estimates of Transpiration: The TEA Algorithm. J. Geophys. Res. Biogeosciences 123, 3617–3632. doi:10.1029/2018JG004727

Poyatos, R., Granda, V., Molowny-Horas, R., Mencuccini, M., Steppe, K., Martínez-Vilalta, J., 2016. SAPFLUXNET: towards a global database of sap flow measurements. Tree Physiol. 36, 1449–1455. doi:10.1093/treephys/tpw110

Prentice, I.C., Dong, N., Gleason, S.M., Maire, V., Wright, I.J., 2014. Balancing the costs of carbon gain and water transport: Testing a new theoretical framework for plant functional ecology. Ecol. Lett. 17, 82–91. doi:10.1111/ele.12211

Reichstein, M., Falge, E., Baldocchi, D., Papale, D., Aubinet, M., Berbigier, P., Bernhofer, C., Buchmann, N., Gilmanov, T., Granier, A., Grunwald, T., Havrankova, K., Ilvesniemi, H., Janous, D., Knohl, A., Laurila, T., Lohila, A., Loustau, D., Matteucci, G., Meyers, T., Miglietta, F., Ourcival, J.-M., Pumpanen, J., Rambal, S., Rotenberg, E., Sanz, M., Tenhunen, J., Seufert, G., Vaccari, F., Vesala, T., Yakir, D., Valentini, R., 2005. On the separation of net ecosystem exchange into assimilation and ecosystem respiration: review and improved algorithm. Glob. Chang. Biol. 11, 1424–1439. doi:10.1111/j.1365-2486.2005.001002.x

Ritchie, J.T., 1983. Efficient water use in crop production: discussion on the generality of relations between biomass production and evapotranspiration. Limitations to Effic. Water Use Crop Prod. 29–44. doi:10.2134/1983.limitationstoefficientwateruse.c2

Roupsard, O., Bonnefond, J.M., Irvine, M., Berbigier, P., Nouvellon, Y., Dauzat, J., Taga, S., Hamel, O., Jourdan, C., Saint-André, L., Mialet-Serra, I., Labouisse, J.P., Epron, D., Joffre, R., Braconnier, S., Rouzière, A., Navarro, M., Bouillet, J.P., 2006. Partitioning energy and evapo-transpiration above and below a tropical palm canopy. Agric. For. Meteorol. 139, 252–268. doi:10.1016/j.agrformet.2006.07.006

Rousseaux, M.C., Figuerola, P.I., Correa-Tedesco, G., Searles, P.S., 2009. Seasonal variations in sap flow and soil evaporation in an olive (Olea europaea L.) grove under two irrigation regimes in an arid region of Argentina. Agric. Water Manag. 96, 1037–1044. doi:10.1016/j.agwat.2009.02.003

Scanlon, T.M., Sahu, P., 2008. On the correlation structure of water vapor and carbon dioxide in the atmospheric surface layer: A basis for flux partitioning. Water Resour. Res. 44, 1–15. doi:10.1029/2008WR006932

Schlesinger, W.H., Jasechko, S., 2014. Transpiration in the global water cycle. Agric. For. Meteorol. 189–190, 115–117. doi:10.1016/j.agrformet.2014.01.011

Scott, R.L., Biederman, J.A., 2017. Partitioning evapotranspiration using long-term carbon dioxide and water vapor fluxes. Geophys. Res. Lett. 44, 6833–6840. doi:10.1002/2017GL074324

Sinclair, T.R., Tanner, C.B., Bennett, J.M., 1984. Water-Use Efficiency in Crop Production. Source Biosci. 34, 36–40. doi:10.2307/1309424

Stoy, P.C., El-madany, T., Fisher, J.B., Gentine, P., Gerken, T., Stephen, P., 2019. Reviews and syntheses : Turning the challenges of partitioning ecosystem evaporation and transpiration into opportunities. Biogeosciences Discuss. 1–47.

Sutanto, S.J., Wenninger, J., Coenders-Gerrits, A.M.J., Uhlenbrook, S., 2012. Partitioning of evaporation into transpiration, soil evaporation and interception: A comparison between isotope measurements and a HYDRUS-1D model. Hydrol. Earth Syst. Sci. 16, 2605–2616. doi:10.5194/hess-16-2605-2012

Talsma, C.J., Good, S.P., Jimenez, C., Martens, B., Fisher, J.B., Miralles, D.G., McCabe, M.F., Purdy, A.J., 2018. Partitioning of evapotranspiration in remote sensing-based models. Agric. For. Meteorol. 260–261, 131–143. doi:10.1016/j.agrformet.2018.05.010

Teuling, A.J., Seneviratne, S.I., Stöckli, R., Reichstein, M., Moors, E., Ciais, P., Luyssaert, S., Van Den Hurk, B., Ammann, C., Bernhofer, C., Dellwik, E., Gianelle, D., Gielen, B., Grünwald, T., Klumpp, K., Montagnani, L., Moureaux, C., Sottocornola, M., Wohlfahrt, G., 2010. Contrasting response of European forest and grassland energy exchange to heatwaves. Nat. Geosci. 3, 722–727. doi:10.1038/ngeo950

Wang, K., Dickinson, R.E., 2012. A review of global terrestrial evapotranspiration: Observation, modeling, climatology, and climatic variability. Rev. Geophys. 50. doi:10.1029/2011RG000373

Wang, L., Niu, S., Good, S.P., Soderberg, K., McCabe, M.F., Sherry, R.A., Luo, Y., Zhou, X., Xia, J., Caylor, K.K., 2013. The effect of warming on grassland evapotranspiration partitioning using laser-based isotope monitoring techniques. Geochim. Cosmochim. Acta 111, 28–38. doi:10.1016/j.gca.2012.12.047

Wang, L., Stephen, P.G., Kelly, K.C., 2014. Global synthesis of vegetation control on evapotranspiration partitioning. Geophys. Res. Lett. 41, 6753–6757. doi:10.1002/2014GL061439

Wei, Z., Yoshimura, K., Wang, L., Miralles, D.G., Jasechko, S., Lee, X., 2017. Revisiting the contribution of transpiration to global terrestrial evapotranspiration. Geophys. Res. Lett. 44, 2792–2801. doi:10.1002/2016GL072235

Wong, S.C., Cowan, I.R., Farquhar, G.D., 1979. Stomatal conductance correlates with photosynthetic capacity. Nature 282, 424–426.

Zhang, Y., Kong, D., Gan, R., Chiew, F.H.S., McVicar, T.R., Zhang, Q., Yang, Y., 2019. Coupled estimation of 500 m and 8-day resolution global evapotranspiration and gross primary production in 2002–2017. Remote Sens. Environ. 222, 165–182. doi:https://doi.org/10.1016/j.rse.2018.12.031

Zhang, Y., Leuning, R., Hutley, L.B., Beringer, J., McHugh, I., Walker, J.P., 2010. Using long-term water balances to parameterize surface conductances and calculate evaporation at 0.05 spatial resolution. Water Resour. Res. 46, W05512.

doi:10.1029/2009WR008716

Zhang, Y., Peña-Arancibia, J.L., McVicar, T.R., Chiew, F.H.S., Vaze, J., Liu, C., Lu, X., Zheng, H., Wang, Y., Liu, Y.Y., Miralles, D.G., Pan, M., 2016. Multi-decadal trends in global terrestrial evapotranspiration and its components. Sci. Rep. 6, 19124. doi:10.1038/srep19124

Zheng, Y., Zhang, L., Xiao, J., Yuan, W., Yan, M., Li, T., Zhang, Z., 2018. Sources of uncertainty in gross primary productivity simulated by light use efficiency models: Model structure, parameters, input data, and spatial resolution. Agric. For. Meteorol. 263, 242–257. doi:10.1016/J.AGRFORMET.2018.08.003

Zhou, S., Yu, B., Huang, Y., Wang, G., 2014. The effect of vapor pressure deficit on water use efficiency at the subdaily time scale. Geophys. Res. Lett. 41, 5005–5013. doi:10.1002/2014GL060741.Received

Zhou, S., Yu, B., Zhang, Y., Huang, Y., Wang, G., 2018. Water use efficiency and evapotranspiration partitioning for three typical ecosystems in the Heihe River Basin, northwestern China. Agric. For. Meteorol. 253–254, 261–273. doi:10.1016/J.AGRFORMET.2018.02.002

Zhou, S., Yu, B., Zhang, Y., Huang, Y., Wang, G., 2016. Partitioning evapotranspiration based on the concept of underlying water use efficiency. Water Resour. Res. 52, 1160–1175. doi:10.1002/2015WR017766

Chapter 5. Estimating ecosystem maximum light use efficiency based on the water use efficiency principle

This chapter is based on the following manuscript:

Gan, R., Zhang, L., Wang, E., Woodgate, W., Zhang, Y., Haverd, V., Kong, D., Fischer, T., Chiew, F.H.S., Yu, Q. (2019). Estimating ecosystem maximum light use efficiency based on the water use efficiency principle. (Under internal review)

Highlights

- An analytical method of estimating maximum light use efficiency was developed based on the intrinsic coupling between water and carbon fluxes
- The method is simple and requires only four variables that are routinely measured at eddy covariance flux sites
- The method provides robust estimates of maximum light use efficiency for C_3 and C_4 species, with small variation between years and between sites for the same plant functional type
- The maximum LUE estimate can be used with LUE models to robustly estimate gross primary production

Abstract

Light use efficiency (LUE) defines the vegetation efficiency of converting radiative energy into biochemical energy through photosynthesis. Estimating the maximum LUE (ε_{max}) is critical yet problematic for quantifying gross primary production (GPP) using LUE-based models. This paper describes an analytical method for estimating ε_{max} based on the coupled relationship between plant water use and carbon gain. Unlike other complex parameterisation schemes, this water use efficiency (WUE) method is simple and requires only four variables readily available at eddy covariance flux sites. The WUE-based estimates of ε_{max} compared favourably with values reported in the literature, and clearly distinguished ε_{max} between C_3 (1.48 ± 0.33 g C MJ^{-1} PAR) and C_4 (2.63 ± 0.21 g C MJ^{-1} PAR) dominated ecosystems. The range in ε_{max} for different years and sites within a plant functional type was relatively narrow. The WUE-based ε_{max} estimate is theoretically constrained by vegetation water use and can be directly incorporated into LUE models to estimate GPP across different ecosystems.

Key words: maximum light use efficiency, water use efficiency, carbon, water, ecosystem

5.1 Introduction

Vegetation converts solar energy into biochemical energy stored in carbohydrates through photosynthesis. At the ecosystem level, the efficiency of this process can be quantified as the ratio of gross primary production (GPP) to photosynthetically active radiation (PAR), commonly known as light use efficiency (LUE) (Monteith, 1977, 1972). The theoretical maximum value of LUE (ε_{max}) under optimal conditions (Bolton and Hall, 1991) is usually downregulated due to biophysical and environmental constraints to obtain the actual amount of carbon assimilation, i.e., $\varepsilon_{max} = GPP/(PAR \cdot f_{APAR} \cdot f_s)$, where f_{APAR} is the fraction of absorbed PAR determined by light conditions and canopy properties, and f_s is the environmental stress factor representing limits induced by temperature, and availability of water and nutrients (Monteith, 1972). This is a practical and widely adopted conceptual framework for GPP simulation across spatiotemporal scales (Landsberg and Waring, 1997; Potter et al., 1993; Running et al., 2004; Veroustraete et al., 2002; Xiao et al., 2004; Yuan et al., 2007). The accuracy of such GPP models, however, relies heavily on the parameterisation of ε_{max} (Cramer et al., 1999; Ruimy et al., 1999; Wei et al., 2017).

Previously published experiments have shown that ε_{max} values for different species and biomes can vary by a factor of five for different species and biomes based on experimental evidence (Choudhury, 2000; Gitelson and Gamon, 2015; Medlyn, 1998). Early studies conducted by Monteith, (1977, 1986) suggested an average ε_{max} of about 1.5 g $C \cdot MJ^{-1}$ for C_3 plants and 2.4 g $C \cdot MJ^{-1}$ for C_4 plants. However, other studies found ε_{max} values varied greatly from 0.24 to 4.82 g $C \cdot MJ^{-1}$ for various plant types (see Prince, 1991). Consequently, discussions have centred on whether ε_{max} is a consistent or variable parameter across species and biomes with different physical environments (Field, 1991; Gitelson et al., 2018; Kergoat et al., 2008; Medlyn, 1998; Prince, 1991; Ruimy et al., 1994; Zhang et al., 2018). While a consistent ε_{max} is often interpreted as a result of an evolutionary plant response to resource availability (Field, 1991; Gitelson et al., 2018; Monteith, 1977), evidence to the contrary can be explained by biotic and abiotic factors attributed to plant or ecosystem types (Albrizio and Steduto, 2005; Gallagher and Biscoe, 1978; Landsberg and Waring, 1997; Prince, 1991; Sinclair and Muchow, 1999), light quality (Choudhury, 2000; Wang et al., 2018), water availability (Passioura, 1982; Shi et al., 2014), nitrogen (Kergoat et al., 2008; Sinclair and Horie, 1989) and atmospheric CO_2 concentration (Dewar et al., 1998; Norby et al., 2003) from

both observational and theoretical perspectives (Medlyn, 1998; Ruimy et al., 1994). It is important to understand how ε_{max} varies across different species (i.e., C_3 and C_4) and biomes (e.g., forests to grasslands) to allow more robust estimation of GPP (Gitelson and Gamon, 2015; Prince, 1991; Wohlfahrt and Gu, 2015).

Various methods have been used to estimate ε_{max} and they fall into two broad categories: (1) fitting light response curves, and (2) inverting the LUE model (i.e., $\varepsilon_{max} = GPP/(PAR \cdot f_{APAR} \cdot f_s)$). In the first category, ε_{max} is a fitted parameter based on the Michaelis-Menten light response curve fitted to observed GPP and absorbed PAR data (He et al., 2014; Wang et al., 2010; Wei et al., 2017). The estimation is largely determined by the choice of either a linear or nonlinear model, with results varying by a factor of two (Ruimy et al., 1995). The second is the most commonly used approach (Chen et al., 2011; Gitelson et al., 2018; Sánchez et al., 2015), where ε_{max} estimation relies on the parameterisation of f_{APAR} and f_s for a given GPP and PAR using the LUE framework. Specifically, f_{APAR} partitions available energy to vegetated and soil surfaces, and is usually derived from a vegetation index (VI) (Mu et al., 2007) and/or Beer's law using VI and a light extinction coefficient (k_{APAR}) (Yuan et al., 2010). f_s is a multiplicative limiting factor varying from 0 to 1 to account for temperature, water (soil/atmospheric), and nutrient conditions. On an ecosystem scale, ε_{max} can be calibrated against GPP using various f_{APAR} and f_s schemes, often with (a) remotely-sensed VI images (e.g., leaf area index (LAI), normalised difference vegetation index (NDVI) and enhanced vegetation index (EVI)) scaled to match the flux site foot-print (Li et al., 2012; Yuan et al., 2014) independently or in combination with constant k_{APAR}, and with (b) f_s as a multiplied limiting factor, based on water, nutrients, temperature, and other limiting variables obtained in-situ or from remotely-sensed data (Yuan et al., 2007). Although this approach of employing VI and f_s to estimate ε_{max} is practical, there are challenges that need to be overcome. First, there is a spatiotemporal discrepancy between the footprint of flux measurements (typically half-hourly, less than 1-3 km^2) (Chen et al., 2012) and that of remotely-sensed VIs (typically 8+ days, 10^1-10^2 km^2) (Chen et al., 2008; Fu et al., 2014). Second, k_{APAR} is not invariant, as it varies with canopy properties, seasonality, and vegetation type (Woodgate et al., 2015; Zhang et al., 2014). Therefore, f_{APAR} can be biased when it is calculated from the remotely-sensed VIs and/or constant k_{PAR}, and may not accurately represent the local vegetation profile. Third, the use of the multiplied limiting factor f_s can be ambiguous. For example, soil moisture, vapour pressure deficit, and temperature are widely acknowledged as covariant variables, yet they are often multiplied as independent factors to formulate f_s. Additionally, the scale

discrepancy similar to VIs also applies for f_s when the limiting factors are obtained from remote sensing images. Thus, difficulties and uncertainties still remain in quantifying f as a combination of VIs (with/without k_{PAR}) and f_s. Not surprisingly, a large range of ε_{max} values have been reported across species (e.g., C_3 to C_4) and biomes (e.g., forests to grasslands). This variability further introduces high uncertainties into model-derived GPP estimates, especially for multi-model and multi-scale assessments (even within the LUE framework) (Chen et al., 2011; Ruimy et al., 1999; Yuan et al., 2014; Zheng et al., 2018). These challenges highlight the need for a better understanding of this parameter and developing a reliable method for ε_{max} estimation that is robust and independent of f.

The objectives of this study were to develop a new method for estimating ε_{max} that does not depend on the stress factor f, and to characterise the variability of ε_{max} across different species and biomes. For the first objective, we derived and tested a simple method for estimating ε_{max} from a coupled water and carbon perspective based on the water use efficiency (WUE) principle. For the second objective, we evaluated and characterised the variation of ε_{max} at globally distributed eddy covariance flux sites for C_3 and C_4 species as well as major biome types. Our results can be implemented into GPP models that are based on the LUE framework and will be useful for informing uncertainty analysis regarding carbon cycle simulations.

5.2 Materials and Methods

5.2.1 Derivation of light use efficiency from the water use efficiency principle

The intrinsic coupling of carbon uptake and water loss through vegetation stomata is commonly quantified by WUE, which is the ratio of actual CO_2 assimilation (A, $\mathrm{g\,C\,m^{-2}d^{-1}}$) to transpiration (T, $\mathrm{mm\ d^{-1}}$). For modelling purpose, A and T are usually assumed to reach their theoretical maximum, as potential assimilation (PA) and potential transpiration (PT), respectively when they are not subject to resource constraints (e.g., soil water availability) (Hanks, 1974). The relationship between actual and potential assimilation and transpiration has been extensively used in biomass prediction (Monteith, 1986; Ritchie, 1983; Sinclair and Horie, 1989), and is often given in the following form (de Wit, 1958; Hanks, 1983, 1974; Monteith, 1986; Stewart et al., 1977)

$$\frac{A}{PA} = \frac{T}{PT} \qquad Eq.5-1$$

This empirical relationship implies the assumption that a fractional change in assimilation is associated with a corresponding fractional change in transpiration, due to the simultaneous stomatal control of both carbon and water fluxes (Monteith, 1988). By rearranging Eq. 5-1, we can obtain an explicit expression of WUE as follows

$$WUE = \frac{A}{T} = \frac{PA}{PT} \qquad Eq.5-2$$

In order to derive ε_{max} from this equation, a straightforward method is to express PA by applying the LUE framework using ε_{max}. Specifically, the potential assimilation rate under non-stressed conditions for a certain canopy can be calculated as

$$PA = \varepsilon_{max}\, PAR\, f_{APAR} \qquad Eq.5-3$$

where PAR is photosynthetically active radiation (MJ m^{-2} d^{-1}), ε_{max} is maximum light use efficiency (g C MJ^{-1}PAR), f_{APAR} is the fraction of PAR that is absorbed by the canopy. For simplicity and consistency, PAR here is defined as the proportion of incident shortwave radiation (R_s) that falls into the 400-700 nm waveband, which is calculated as 0.45×Rs throughout this study (Britton and Dodd, 1976; Monteith, 1972).

Additionally, for the PA/PT term in Eq. 5-2, we assumed that the denominator (PT) for a given canopy could be approximated from potential evapotranspiration (PET) by attributing total PET to the vegetated area (Brisson et al., 1993; Childs et al., 1977; Guan & Wilson, 2009; Impens & Lemeur, 1969). Therefore

$$PT = PET\, f_{R_n} \qquad Eq.5-4$$

where f_{R_n} is the fraction of net radiation (R_n) that is absorbed by the canopy. Detailed elaboration of this equation is referred to in Text S1 (supporting information). We further assumed that the fraction of absorbed PAR approximated the fraction of absorbed R_n over the same canopy, i.e., $f_{APAR} \approx f_{R_n}$. Therefore

$$PT = PET f_{APAR} \qquad Eq.5-4a$$

By substituting Eq. 5-3 and Eq. 5-4a to Eq. 5-2, f_{APAR} is eliminated to give:

$$\frac{A}{T} = \frac{\varepsilon_{max}\, PAR}{PET} \qquad Eq.5-5$$

To obtain ε_{max}, we simply rearranged this equation:

$$\varepsilon_{max} = \frac{A \cdot PET}{T \cdot PAR} \qquad Eq.5-6$$

$$or \qquad \varepsilon_{max} = WUE\ \frac{PET}{PAR} = \frac{A}{PAR} \cdot \frac{1}{T/PET} \qquad Eq.5-6a$$

Eq. 5-6 shows that ε_{max} is linearly related to actual assimilation and transpiration (or WUE, Eq. 5-6a) and is dependent on radiation (PAR) and atmospheric water demand (PET) conditions. This equation does not require additional information such as canopy profile (VIs, k_{PAR}), a and stress factor (f_s), or other variables needed by the LUE framework to parameterise f at flux sites. Alternatively, T/PET can be interpreted as f (Eq. 5-6a), which corresponds to the effective fraction of PAR that is ultimately converted to biochemical energy stored in A. At an ecosystem scale, the use of T/PET is advantageous as it avoids the difficulty and uncertainty of calculating f_{PAR} based on k_{PAR} (fitted parameter with ambiguous mechanism) and VIs (e.g., NDVI, EVI, LAI) as well as f_s (e.g., temperature, water, nutrients) derived from observational and/or remote sensing techniques as discussed in the Introduction.

Among the four variables required in Eq. 5-6, PET and PAR are relatively easy to obtain from readily available meteorological measurements at flux sites. PAR can be calculated from R_s observations (calculated as $0.45 \times R_s$ throughout this study). As for PET, we simply adopted the radiation-based Priestley-Taylor equation (Priestley and Taylor, 1972), which is one of the most widely used methods to account for atmospheric water demand in hydrological and land surface modelling (Maes et al., 2018; Milly and Dunne, 2016; Pagán et al., 2019). Additionally, since A can be reasonably approximated by GPP at an ecosystem level, the only variable required to apply Eq. 5-6 is transpiration (T). It is widely acknowledged that T is difficult to measure directly and its simulation exhibits high uncertainty and large discrepancies based on the choice of methods (Medlyn et al., 2017; Wang et al., 2014; Wei et al., 2017; Zhou et al., 2018). However, ET can be easily derived from latent heat flux observations and can be used as a reasonable approximation of T under certain conditions (Knauer et al., 2018; Zhou et al., 2018). In this study we adopted the common assumption that ET is a reasonable approximation of T under conditions of high vegetation cover and negligible soil evaporation during rain-free periods. Consequently, Eq. 5-6 becomes

$$\varepsilon_{max} = \frac{GPP \cdot PET}{ET \cdot PAR} \qquad Eq.5-7$$

As a result, ε_{max} can be estimated from GPP, ET, PAR, and PET. For practical purposes, ε_{max} can be estimated as the slope of the linear regression between GPP·PET and ET·PAR. This method for estimating ε_{max} is herein referred to as the WUE-based method in the following discussions and throughout this paper. The analysis was performed under R studio with the linear regression method (https://cran.r-project.org/).

5.2.2 FLUXNET data and vegetation index

To test the WUE-based method of determining ε_{max}, meteorological and eddy covariance measurements at 52 flux sites (318 site-years of observation) were obtained from the FLUXNET database (http://fluxnet.fluxdata.org/). A brief description of the selected sites is presented in Table S5-1 and Figure S5-1. Half-hourly observations of latent heat flux ($LE, W\ m^{-2}$), R_n ($W\ m^{-2}$), R_s ($W\ m^{-2}$), and air temperature (T_a, °C) were used. Estimates of GPP derived from the night time partitioning algorithm provided by FLUXNET were adopted as GPP observations in this study. PET was calculated from the Priestley-Taylor equation with the multiplication factor α_{PT} set to 1.26. As stated earlier, PAR was taken as 45% of the total R_s. The selected global flux sites included seven plant functional types (PFTs) where high vegetation coverage was observed during the growing season, including evergreen broadleaf forests (EBF), deciduous broadleaf forests (DBF), evergreen needle leaf forests (ENF), grasslands (GRA), woody savannas (WSA), wetlands (WET) and croplands (CRO). Three crop sites with an annual soybean (*Glycine max* L.) (C_3) and maize (*Zea mays* L.) (C_4) rotation were selected to represent C_3 and C_4 species in order to determine the effect of different photosynthetic pathways on ε_{max}.

The original half-hourly data were filtered to retrieve reliable observations according to standardised quality control protocols (Reichstein et al., 2005). The following criteria were used for further screening of available data for ε_{max} estimation: (1) only daytime observations with R_s greater than 20 $W\ m^{-2}$ were used; (2) negative values of LE and GPP were eliminated; (3) data on rainy days (rainfall > 0.5 mm) and the subsequent two days were excluded to focus only on transpiration (Beer et al., 2009; Knauer et al., 2018); (4) only growing season dates with high vegetation coverage present were used; and (5) a minimum of 10 days of valid observations during each growing season were required for robust regression analysis. The growing season was defined according to Zhou et al., (2014, 2016) as the days when daytime average GPP exceeded 10% of 95th percentile of daily GPP at a given site. High vegetation coverage was further ensured by high daily values of LAI in addition to the GPP selection criterion. Observations during days when LAI exceeded a certain threshold (LAI≥2) were used to assure conditions where ET was a reasonable representation of T (Ritchie, 1983).

At each of the study sites, LAI was estimated using remotely-sensed LAI (8-day, 500m resolution) from MODIS (MOD15A2 product) using observations within a 1 km × 1 km cell centred on the site coordinates (Gan et al., 2018). Original 8-day LAI time series were (a)

filtered according to quality flags to select reliable entries, (b) smoothed using Savitzky-Golay filter, and (c) linearly interpolated to determine daily values (Zhang et al., 2019). These daily LAI time series were then used to assist data screening during the growing season at each site.

5.3 Results

5.3.1 Comparison of ε_{max} estimates for C_3 and C_4 species

Long-term site-level estimates of ε_{max} are illustrated in Figure 5-1 (a) and (b) for typical C_3 and C_4 species, respectively, at US-Ne2 (maize-soybean rotation, irrigated) (Eq. 5-7). Taking Figure 5-1 (a) as an example, long-term ε_{max} of soybean was estimated as the linear regression slope between GPP·PET and ET·PAR (Section 2.1), using data from the soybean growing seasons over multiple years (Section 2.2). The regression was forced to pass through the origin to be consistent with the fact that both photosynthesis and transpiration reach zero when stomata are closed. A strong linear correlation was found between GPP·PET and ET·PAR, with the coefficient of determination (R^2) equal 0.96 (p < 0.001). The long-term ε_{max} was then estimated as 1.47 g C MJ^{-1} PAR for soybean (C_3) at this site. To examine the applicability of the method for C_4 species, we performed the same regression during the maize years as shown in Figure 5-1 (b). As expected, a clear difference was detected for the regression slope between soybean and maize. While exhibiting the same high coefficient of determination as soybean years, maize years presented a much higher ε_{max} value of 2.53 g C MJ^{-1} PAR.

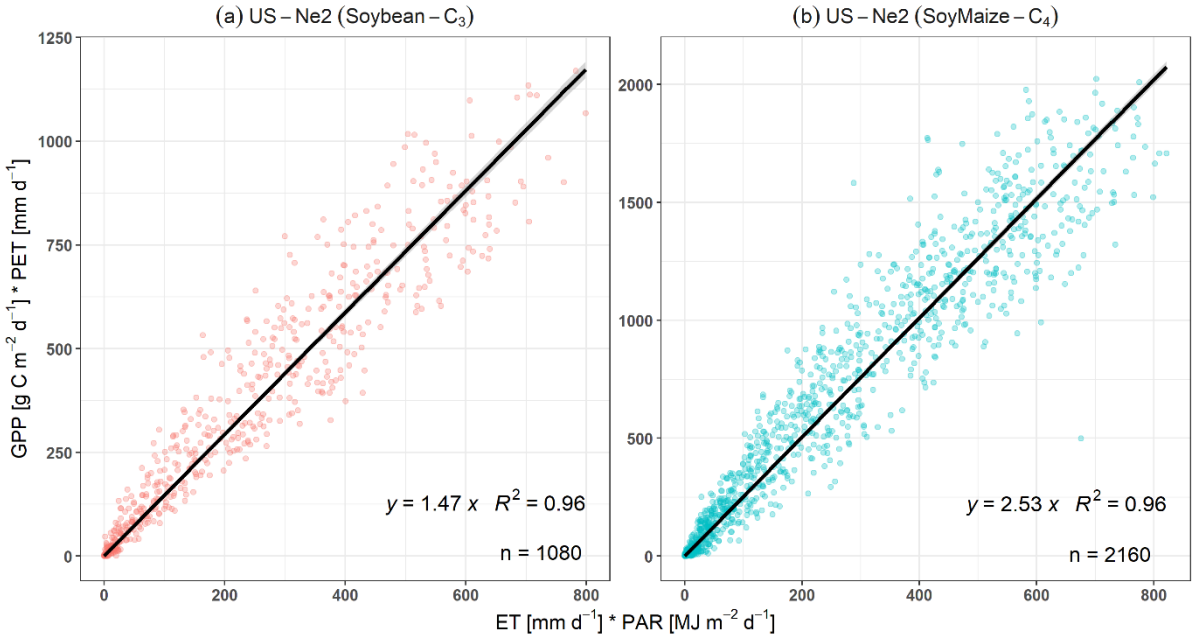

Figure 5-1. Comparison of ε_{max} estimates for C_3 and C_4 species at US-Ne2 (soybean grown in Nebraska, USA in 2002, 2004, 2006, and 2008 and maize grown in all other years) based on hourly observations during 2001-2012. The ε_{max} was estimated to be 1.47 g C MJ^{-1} PAR for C_3 (soybean) and 2.53 g C MJ^{-1} PAR for C_4 (maize) based on linear regression forced through the origin. 'n' represents the number of available hourly observations at this site.

The WUE-based method also provided comparable estimates of ε_{max} for C_3 and C_4 crops at two adjacent sites, namely US-Ne1 (continuous maize, irrigated) and US-Ne3 (maize-soybean rotation, rain fed), with strong linear correlation ($R^2 \geq 0.95$) and ε_{max} estimated at 2.62 g C MJ^{-1} PAR for maize at US-Ne1 (irrigated), and 1.84 and 2.87 g C MJ^{-1} PAR for soybean and maize at US-Ne3 (rain-fed), respectively (Table S5-1). These estimates were close to those obtained at US-Ne2 shown in Figure 5-1.

The robustness of the method was further examined on an annual scale, with ε_{max} from each site-year calculated and summarised in Table 5-1. For soybean, the average annual ε_{max} across US-Ne1, US-Ne2, and US-Ne3 was about 1.6 g C MJ^{-1} PAR, with a standard deviation (SD) of 0.21 g C MJ^{-1} PAR and a coefficient of variation (CV) of about 13% across 6 site-years. For maize, the annual mean ε_{max} was about 2.63 g C MJ^{-1} PAR, with an SD of 0.21 g C MJ^{-1} PAR and a CV of about 8% across 15 site-years. It can be seen that the annual average value of ε_{max} for maize was significantly higher than that of soybean, which agrees well with the long-term value estimated at US-Ne2. The greater ε_{max} estimates for C_4 species obtained here corresponds well with its genetically determined higher photosynthetic capacity compared with the C_3 species, which demonstrates the applicability of the WUE-based method for distinguishing C_3 and C_4 dominated ecosystems.

Table 5-1. Summary of mean annual ε_{max} estimates across species and biomes. Cross site averages of annual ε_{max} (± one standard deviation (SD)), coefficients of determination (R^2), and coefficient of variation (CV) are presented. CRO-C_3 and CRO-C_4 groups were generated from US-Ne1, US-Ne2, and US-Ne3 data sets in years when soybean (C_3) and maize (C_4) were grown. N represents available number of years for each species or biome group.

PFT	ε_{max}	R^2	CV (%)	Number of Site-year (N)
CRO-C_4	2.63 ± 0.21	0.97	7.96	15
CRO-C_3	1.60 ± 0.21	0.97	12.94	6
CRO	1.71 ± 0.38	0.94	22.09	13
DBF	1.57 ± 0.23	0.89	14.96	46
EBF	1.65 ± 0.38	0.84	22.73	39
ENF	1.80 ± 0.52	0.88	28.93	112

GRA	1.34 ± 0.34	0.92	25.39	57
WET	1.00 ± 0.36	0.94	35.56	14
WSA	1.14 ± 0.22	0.93	19.43	3
Average (except C_4)	1.48 ± 0.33	0.91	22.30	305

*ε_{max} estimates are shown in the table. An ε_{max} value is estimated for each year of data at each site (see Column 5). Column 2 shows the mean of these ε_{max} estimates and the standard deviation, with the CV (percentage of the ratio between standard deviation and mean) shown in Colum 4. R^2 is calculated between GPP·PET and ET·PAR at each site-year. Plant functional types (PFTs) are defined as: CRO-C_3: soybean cropland; CRO-C_4: maize cropland; CRO: other cropland (species unspecified); DBF: deciduous broadleaf forests; EBF: evergreen broadleaf forests; ENF: evergreen needle leaf forests; GRA: grasslands; WET: wetlands and WSA: woody savannas.

5.3.2 Variations of ε_{max} across different biomes

Site-specific ε_{max} was also calculated using all available data during the growing season at each of the 52 flux sites (Table S5-1). A summary of cross-biome ε_{max} estimates is presented in Figure 5-2. ε_{max} exhibited considerable variation within and across biome types. Among all natural ecosystems, forests (DBF, EBF, and ENF) presented slightly higher photosynthetic capacity (greater ε_{max}) when compared with non-forests (GRA, WET, and WSA). Broadleaf forests (DBF and EBF, 11 sites) with high vegetation coverage during the growing season had similar average ε_{max} estimates that fell in a narrow range between 1.50-1.58 g C MJ^{-1} PAR. These values were in good agreement with the C_3 crop (1.66 g C MJ^{-1} PAR). ENF presented the largest variation, with ε_{max} ranging from about 0.9 to 2.4 g C MJ^{-1} PAR, and the average of 1.58 g C MJ^{-1} PAR was comparable to that of the C_3 crop. Non-forest GRA and WSA had much lower ε_{max} (less than 1.2 g C MJ^{-1} PAR on average). In addition, wetlands were the least efficient in terms of light use for photosynthesis with the lowest ε_{max} of only about 0.83 g C MJ^{-1} PAR. For the four cropland sites under agricultural management (with C_3 or C_4 species unspecified), ε_{max} varied from about 1.3 to 2.0 g C MJ^{-1} PAR with an average of about 1.62 g C MJ^{-1} PAR. All natural systems dominated by C_3 vegetation had much lower ε_{max} values than the C_4 crop. Although ENF and CRO had a few large values that exceeded 2 g C MJ^{-1} PAR, most C_3 dominanted ecosystems had mean ε_{max} values generally below 2 g C MJ^{-1} PAR. In contrary, ε_{max} for the C_4 crop was obviously larger than 2.4 g C MJ^{-1} PAR.

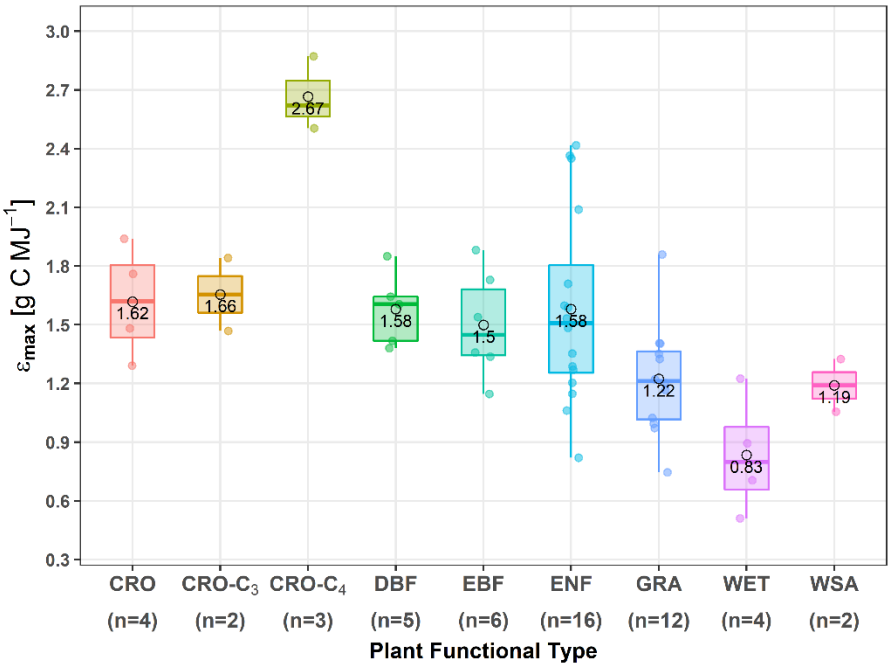

Figure 5-2. Estimated long-term ε_{max} for different biomes using the WUE-based method at 52 eddy covariance flux sites. For each biome group, the mean value of ε_{max} across sites is shown as a black outline circle and the median value is shown as coloured horizontal line (both within the box). The 25th and 75th quantiles are shown as the lower and the upper boundaries of each box, respectively. CRO-C_3 and CRO-C_4 are the ε_{max} estimates at US-Ne1, US-Ne2, and US-Ne3 from available years when soybean and maize was grown. 'n' represents the number of flux sites within each biome group. Abbreviations for plant functional types are given in Table 5-1.

For each site-year, annual ε_{max} was calculated to examine the interannual consistency of the WUE-based method and the results are summarized in Table 5-1. There results showed that the interannual variation was small for most biome types as indicated by low SD and CV. The largest CV was found for ENF and WET (about 29 and 35%, respectively), and the minimum CV was found for CRO-C_4 (about 8%). Overall CV was about 20% across all C_3 dominated ecosystems. High coefficient of determination values (R^2=0.91, mean annual) also provided evidence of the robustness of this method across the annual scale for different biome groups.

5.4 Discussion

5.4.1 Comparison of ε_{max} from different methods

The ε_{max} values estimated here for different species and biomes using the WUE-based method were generally similar to the values reported from experimental and modelling studies in the literature. The ε_{max} values estimated for the C_3 and C_4 crops at US-Ne1, US-Ne2, and US-Ne3

are summarised and compared with values reported in the literature in Figure S5-2. Based on measured green LAI and intercepted PAR at the same sites, Gitelson et al. (2018) reported relatively similar ε_{max} values to those determined in our study for soybean and maize of about 1.45 and 2.23 g C MJ^{-1} PAR, respectively. Our estimates were slightly higher (1.66 and 2.67 g C MJ^{-1} PAR), but were close to these observation-based results. Our ε_{max} estimates were almost identical to those obtained by Nguy-Robertson et al. (2015) for both soybean (1.72 g C MJ^{-1} PAR) and maize (2.42 g C MJ^{-1} PAR), and comparable to those of Chen et al. (2011) for maize (1.95 g C MJ^{-1} PAR) using optimised LUE models. Additionally, our estimates were in good agreement with the chlorophyll-based ε_{max} values suggested by Zhang et al. (2017, 2016), where C_3 ε_{max} was less than 2 g C MJ^{-1} PAR and C_4 had ε_{max} close to 3 g C MJ^{-1} PAR. These comparisons showed that the WUE-based method can provide reasonable estimates of ε_{max} for species with distinct photosynthetic capacity differences.

For the other biome types, the WUE-based method also produced ε_{max} estimates that were similar to those reported in the literature (summarised in Figure S5-3). Our WUE-based ε_{max} estimates were close to those from the EC-LUE model across most biomes (DBF, EBF, ENF, GRA, and WSA). The estimates were also similar to the results obtained with two other models, namely MODIS and CFix reported by Yuan et al. (2014). However, small differences were found between the WUE-based ε_{max} estimates here and the results of Yuan et al. (2014) for broad leaf forests (DBF and EBF) when compared with other biome types on average, except for one model (VPRM). Major differences for forest and crops were found when compared with other biomes from Wang et al. (2010) and the MODIS look-up-table (Running and Zhao, 2015). The differences between our WUE-based method and these modelling results can be partly attributed to the difficulty in parameterising the f factor (i.e., VIs, k_{PAR}, f_s) in the LUE model (as explained in the Introduction), which contains scale discrepancy and covariant issues. The uncertainty in parameterising the f factor is a major limitation of the LUE model, and can result in errors and inconsistent estimates of ε_{max} (Yuan et al., 2014; Zheng et al., 2018).

We also compared our WUE-based ε_{max} values to the values determined from experimental studies. In the original LUE study, Monteith (1972, 1977) suggested a relatively consistent ε_{max} of about 1.4 g C MJ^{-1} PAR for C_3 crops. However, lower ε_{max} values that varied between 0.2-1.5 g C MJ^{-1} PAR were found for woody vegetation (Raymond Hunt, E., 1994). Other experimental results presented a wider range of 0.2-4.8 g C MJ^{-1} PAR as summarised by Prince (1991). In comparison, our ε_{max} estimates showed a narrower range of variation between 0.83-1.66 g C MJ^{-1} PAR for C_3 dominated ecosystems, which agreed well with these previous

studies. The biomass measurements conducted by Cannell et al. (1988) estimated ε_{max} of 1.5 to 1.6 g C MJ^{-1} PAR for the broad-leaf forests (DBF and EBF), which is practically the same as the WUE-based ε_{max} estimates in this study (1.50 to 1.58 g C MJ^{-1} PAR). Since it is difficult to obtain ground-truth measurements for such a wide range of biome types globally distributed, we can infer from the above modelling and experimental comparisons that the WUE method is reliable for ε_{max} estimation in accordance with current knowledge.

5.4.2 Advantages of the WUE-based method for estimating ε_{max}

The WUE-based method proposed in this study provides a new perspective and a coupled approach for estimating ecosystem scale ε_{max}. Unlike traditional methods that require parameterisation (e.g., GPP at light saturation point) by fitting the Michaelis-Menten function, the WUE-based method does not require any a-priori parameterisation. The WUE-based method is relatively simple to use, requiring only four variables that are routinely measured at flux sites to estimate ε_{max}. A limitation of obtaining ε_{max} by reversing the LUE models is the consideration of water (e.g., soil moisture) as an abiotic limit for carbon assimilation (He et al., 2014; Hu et al., 2018; Wagle et al., 2016; Yuan et al., 2014), implying that limited water availability constrains carbon assimilation. The intrinsic biophysical coupling between water loss and carbon gain, however, demonstrates that the two depend on each other and constrain each other interactively (Katul et al., 2010; Medlyn et al., 2011). Accordingly, the energy-converting efficiency of carbon processes should be related to the water use efficiency. The WUE-based method presents this coupling relationship explicitly, where ε_{max} is a function of WUE (biophysical processes), environmental conditions (atmospheric water demand (PET), and energy availability (PAR)). The WUE-based method directly conceptualises and presents the joint regulation of vegetation on both water and carbon processes.

Our results also demonstrate that the WUE-based method is simple and robust for ε_{max} estimation. The much higher ε_{max} for C_4 crops which have a different photosynthetic pathway than for C_3 plants is clearly distinguishable. The method produced reliable ε_{max} estimates for C_3 and C_4 that were comparable with values reported in the literature (Section 4.1, Figure S5-2). The method was also capable of producing consistent ε_{max} for different ecosystems under a wide range of climate, in agreement with previous studies (Figure S5-3). For the cropland flux sites used in this study (Table 5-1), the slightly wider variation of ε_{max} estimates (CV=22%) is likely due to possible changes in species grown within and across the crop sites and years (possible C_3 and C_4 rotation), and this may require further information and

investigation. For other ecosystems, the variation in the ε_{max} values, across the different years, and across the different sites within a plant functional type, was also relatively small (standard deviation was generally less than 25% of the mean). Previous studies have demonstrated that canopy characteristics (Sánchez et al., 2015), water availability, and nutrients (Christina et al., 2015) as well as radiation conditions (Gitelson et al., 2015; Wang et al., 2018) could contribute to variations in ε_{max}. The possible interannual variation of ε_{max} induced by such biophysical and environmental factors was explicitly presented in our method, shown by Eq. 5-6. A further analysis between the biophysical underlying water use efficiency ($uWUE_a$=GPP·VPD$^{0.5}$/ET, Zhou et al. (2014)) and annual ε_{max} (Figure S5-4) showed that photosynthetic capacity co-varied with the vegetation water use and the atmospheric water demand.

5.4.3 Possible implications and limitations

The WUE-based ε_{max} estimates can be directly incorporated with LUE models at local to regional scales according to species and biome types for GPP estimation. With a narrow range of ε_{max} (0.83-1.62 g C MJ^{-1} PAR for C3 dominated ecosystems, Figure 5-2), uncertainty of the GPP estimate is likely to be reduced using our ε_{max} values across different ecosystems (compared with other parameterisation schemes, Figure S5-3). Moreover, this WUE-based method uses T/PET as a top-down limiting factor instead of the ambiguous f in the LUE model. This treatment not only simplifies the parameterisation of ε_{max}, but also avoids the possible uncertainties brought about by multiplying various limiting factors (e.g., LAI, VPD, soil water, etc.) to quantify f. Additionally, because all variables required by this WUE-based method are readily available at flux sites, local ε_{max} estimates can be easily obtained with high credibility. Measurements from these flux sites are considered highly reliable and accurate as eddy covariance represents the state of the art technique. As such, ε_{max} estimates using the WUE-based method are likely to be more robust than estimates from traditional methods, and the use of this method can help to assess model uncertainty in GPP estimation. This is especially true when model structure and data reliability require further evaluation, while the ε_{max} value is theoretically and biophysically consistent.

A limitation of the WUE-based method for estimating ε_{max} is the assumption that transpiration (T) can be approximated by total evapotranspiration (ET) under high vegetation coverage. While this assumption is valid under complete or high vegetation coverage across the landscape, T can be considerably less than ET in non-forest ecosystems (WET, GRA, and WSA). More accurate ε_{max} estimates would be possible from transpiration measured with sap flow gauges

and/or isotopic techniques (Roupsard et al., 2006; Wang et al., 2014; Wei et al., 2017). For simplicity, this study also assumed that the fraction of absorbed PAR is the same as that of absorbed R_n. This assumption needs to be explored further for different canopy characteristics (e.g., leaf inclination angle, nutrient status, phenology) and climate and radiation conditions (e.g., direct and diffuse radiation, atmospheric CO_2 concentration) (Dai et al., 2004; Turner et al., 2003; Wang et al., 2018).

5.5 Conclusion

This study proposed a new method to estimate ε_{max} based on the water and carbon coupling principle. The method was examined at 52 global flux sites across different vegetation species and biome types. Results showed that the method was capable of distinguishing vegetation types with different photosynthetic pathways. The estimated ε_{max} for seven main biomes, globally distributed, agreed well with experimental and modelling methods. The WUE-based method is simple and the ε_{max} estimates could be incorporated into LUE models for better GPP simulation. The method could also be used to better understand the behaviour and variation of this parameter across species and biomes considering interrelated water and carbon processes.

Acknowledgments

The authors acknowledge the FLUXNET community for sharing the free use eddy covariance data. MODIS product (MOD15A2) was provided by the Land Processes Distributed Active Archive Centre (LPDAAC). The first author was supported by the joint scholarship of University of Technology Sydney and China Scholarship Council, and the CSIRO postgraduate top-up scholarship. This study was also supported by the CAS Pioneer Hundred Talents Program. The authors declare no conflict of interest.

Supporting information

Text S1. Deduction of potential transpiration based on the Priestley & Taylor equation.

According to Priestley & Taylor (1972), potential evapotranspiration (PET) can be calculated as

$$PET = \alpha_{PT} \frac{\Delta}{\Delta + \gamma} R_n \qquad Eq.5-s1$$

where R_n is total net radiation, Δ is the slope of saturation vapour pressure versus temperature, γ is the psychrometric constant. α_{PT} is the Priestley Taylor coefficient.

Similarly, potential transpiration (PT) can be calculated for a vegetated surface as

$$PT = \alpha_{PT} \frac{\Delta}{\Delta + \gamma} R_{n\_c} \qquad Eq.5-s2$$

where R_{n_c} is the net radiation of a canopy. R_{n_c} can be estimated using the fraction of R_n (f_{R_n}) absorbed by vegetation as

$$R_{n_c} = R_n f_{R_n} \qquad Eq.5-s3$$

By combining Eq. 5-s1, 5-s2, and 5-s3, one can get

$$PT = \alpha_{PT} \frac{\Delta}{\Delta + \gamma} R_n f_{R_n} \qquad Eq.5-s4$$

Further substituting $\alpha_{PT} \frac{\Delta}{\Delta+\gamma} R_n$ by Eq. 5-s1, we have

$$PT = PET f_{R_n} \qquad Eq.5-s5$$

Eq. s5 is used as Eq. 5-4 in the main manuscript. Previous studies that also used the fraction analogy to estimate PT from PET are found in Brisson et al. (1993), Guan & Wilson (2009), Impens & Lemeur (1969), and Childs et al., (1977).

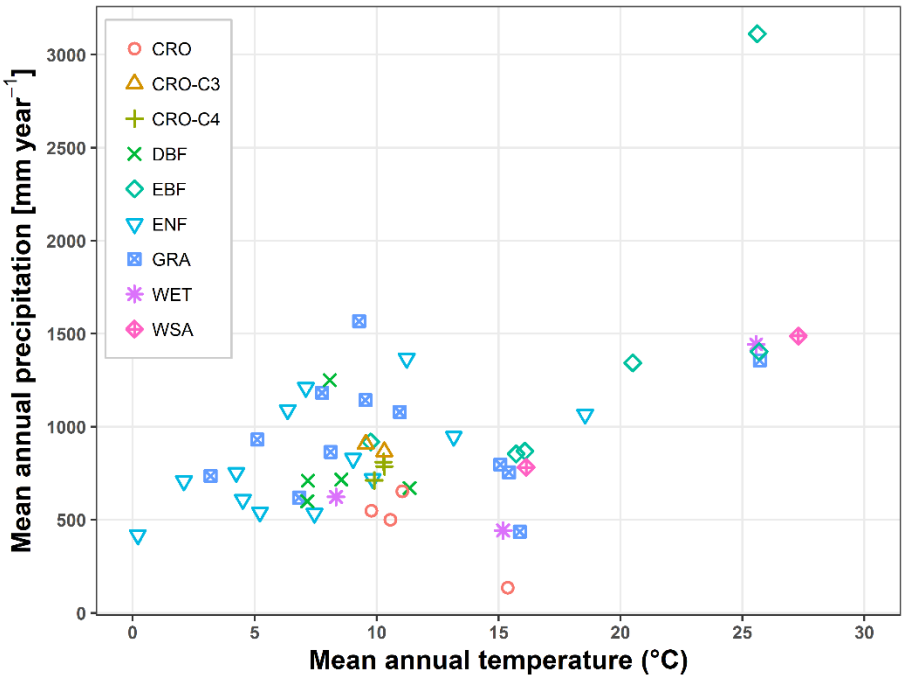

Figure S5-1. Mean annual precipitation (vertical axis) and temperature (horizontal axis), respectively at the flux sites used in this study. Plant functional type abbreviations used to represent biome groups were cropland (CRO), deciduous broadleaf forest (DBF), evergreen broadleaf forest (EBF), evergreen needle leaf forest (ENF), grassland (GRA), wetland (WET), and woody savanna (WSA).

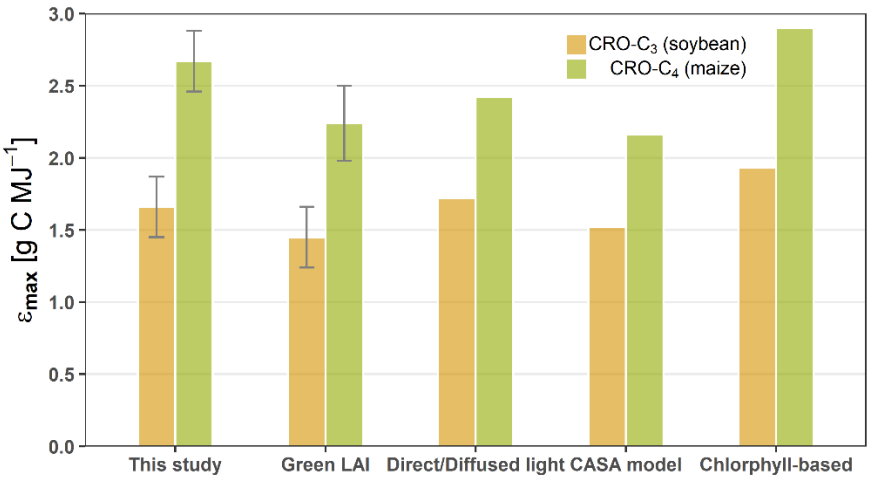

Figure S5-2. Comparison of mean ε_{max} for C_3 (soybean) and C_4 (maize) crops from observational and modelling approaches at flux sites US-Ne1, US-Ne2, and US-Ne3. Error bars represent one standard deviation about the mean where data were available. Horizontal axis labels indicate the following: 'Green LAI' is from Gitelson et al. (2018), based on measurements of green LAI and intercepted PAR; 'Direct/Diffused light' is from Nguy-Robertson et al. (2015), where direct and diffused light is considered using an LUE-based model; 'CASA model' is from Chen et al. (2011), where the Carnegie-Ames-Stanford-Approach (CASA) is optimised with MODIS data; 'Chlorophyll-based' is from Zhang et al. (2016, 2017), where PAR absorbed by canopy chlorophyll is used to optimise a satellite-based Vegetation Photosynthesis Model (VPM). All units of ε_{max} were converted to g C MJ^{-1} PAR.

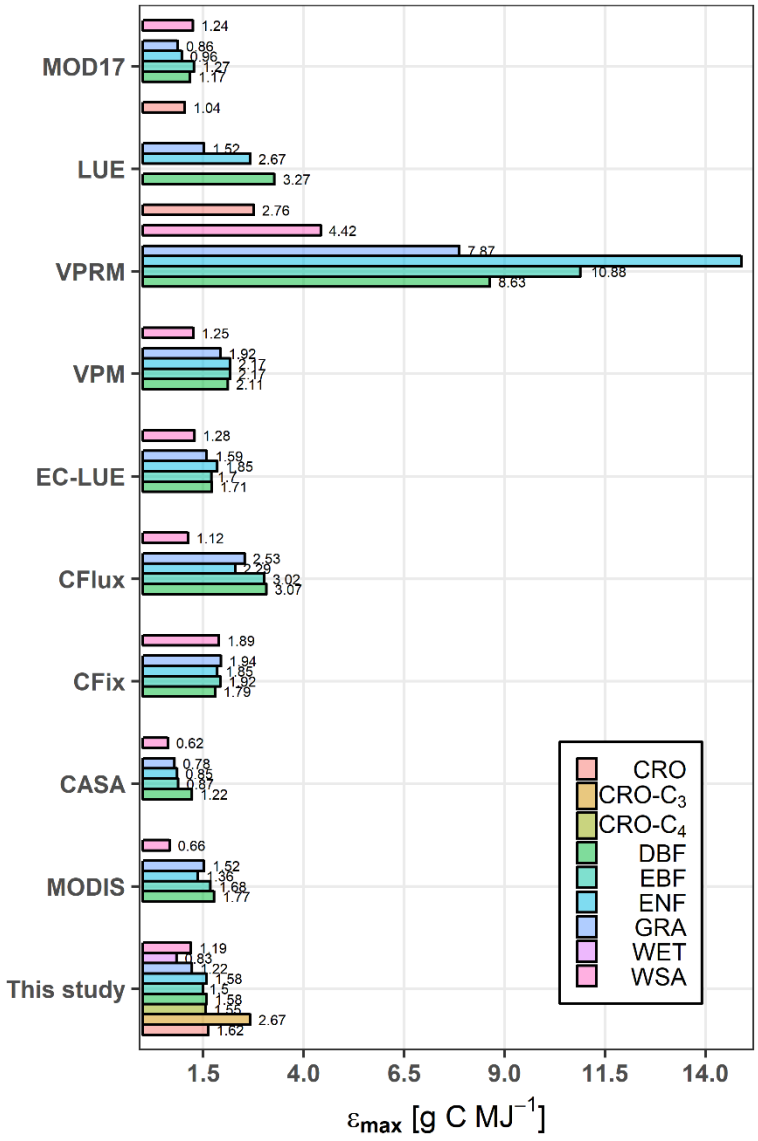

Figure S5-3. WUE-based ε_{max} estimates from this study compared with different LUE-based modelling approaches across ecosystems. MOD17: look-up-table based on PFT from Running and Zhao 2015. LUE: a LUE model optimized at China flux sites from Wang et al. (2010). Other models optimized at 156 global flux sites from Yuan et al. (2014): CASA: Carnegie–Ames–Stanford Approach; CFix: Carbon Fix; CFlux: Carbon Flux; EC-LUE: Eddy Covariance-Light Use Efficiency; MODIS-GPP: Moderate Resolution Imaging Spectroradiometer GPP algorithm; VPM: Vegetation Production Model; VPRM: Vegetation Production and Respiration Model. Biome types grouped and colored by PFT following the same as Figure S5-1.

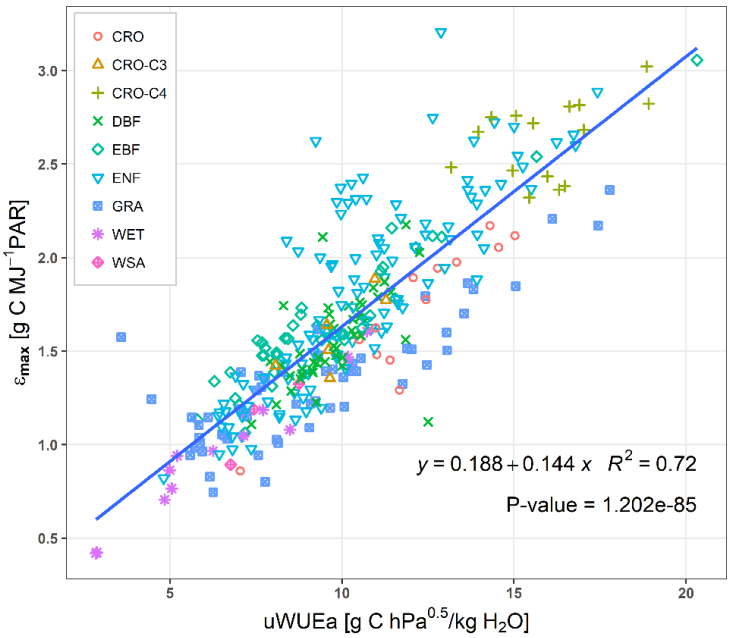

Figure S5-4. Relationship between the estimated ε_{max} and the underlying water use efficiency ($_{u}WUE_a$ = GPP·VPD$^{0.5}$/ET) across biome types. Biome types grouped and colored by plant functional type as in Figure S5-1.

Table S5-1. Summary of the 52 eddy covariance flux sites used in this study. Site descriptions include site identifier (ID), site name, latitude, longitude, plant functional type (PFT), period of record (Years), mean annual precipitation (Prcp mm/y) and mean annual temperature (MAT ^{o}C). PFT abbreviation were cropland (CRO), deciduous broadleaf forest (DBF), evergreen broadleaf forest (EBF), evergreen needle leaf forest (ENF), grassland (GRA), wetland (WET) and woody savanna (WSA). C_3 refers to soybean and C_4 refer to maize at site US-Ne1, US-Ne2, US-Ne3. Estimated ε_{max} and ${}_{u}WUE_{a}$ are also shown for each site, as well as R^2 from the WUE-based method between GPP·PET and ET·PAR for ε_{max} estimation.

Site ID	Site name	PFT	Latitude	Longitude	Years	Prcp (mm/y)	MAT (°C)	ε_{max}	R^2	${}_{u}WUE_{a}$
AT-Neu	Neustift	GRA	47.12	11.32	2002-2012	620	6.82	1.86	0.90	14.56
AU-DaP	Daly River Savanna	GRA	-14.06	131.32	2008-2013	1357	25.72	1.02	0.93	8.43
AU-Fog	Fogg Dam	WET	-12.55	131.31	2006-2008	1443	25.56	0.51	0.86	3.39
AU-How	Howard Springs	WSA	-12.49	131.15	2002-2014	1489	27.30	1.06	0.94	7.14
AU-Rig	Riggs Creek	GRA	-36.65	145.58	2012-2014	436	15.87	1.40	0.93	9.52
AU-Tum	Tumbarumba	EBF	-35.66	148.15	2002-2014	919	9.75	1.73	0.78	10.33
BR-Sa3	Santarem-Km83-Logged Forest	EBF	-3.02	-54.97	2002-2004	1405	25.69	1.15	0.82	7.00
CA-Man	Manitoba - Northern Old Black Spruce	ENF	55.88	-98.48	2007-2008	324	-0.97	1.20	0.81	6.96
CA-NS2	UCI-1930 burn site	ENF	55.91	-98.52	2002-2004	201	-1.45	1.35	0.90	8.44
CA-SF1	Saskatchewan - Western Boreal, forest burned in 1977	ENF	54.49	-105.82	2003-2006	418	0.20	1.27	0.91	8.38
CA-SF2	Saskatchewan - Western Boreal, forest burned in 1989	ENF	54.25	-105.88	2002-2005	265	-0.20	1.60	0.92	10.34
CH-Cha	Chamau	GRA	47.21	8.41	2005-2014	1144	9.54	1.41	0.88	10.05
CH-Fru	Früebüel	GRA	47.12	8.54	2005-2014	1183	7.76	1.35	0.91	7.34
CH-Oe1	Oensingen grassland	GRA	47.29	7.73	2006-2006	1567	9.28	0.75	0.94	6.26
CN-Cha	Changbaishan	MF	42.40	128.10	2003-2005	468	4.36	1.86	0.90	11.45

CN-Din	Dinghushan	EBF	23.17	112.54	2003-2005	1344	20.51	1.34	0.87	7.43
CN-Ha2	Haibei Shrubland	WET	37.61	101.33	2004-2005	515	-1.63	0.89	0.93	5.08
CN-Qia	Qianyanzhou	ENF	26.74	115.06	2003-2004	1067	18.55	1.29	0.87	8.02
CZ-wet	Trebon (CZECHWET)	WET	49.02	14.77	2006-2014	624	8.33	1.22	0.92	8.33
DE-Geb	Gebesee	CRO	51.10	10.91	2003-2014	549	9.79	1.76	0.91	12.27
DE-Hai	Hainich	DBF	51.08	10.45	2002-2009	717	8.55	1.64	0.91	10.39
DE-Lkb	Lackenberg	ENF	49.10	13.30	2013-2013	754	4.24	0.82	0.92	4.82
DE-Obe	Oberbärenburg	ENF	50.79	13.72	2009-2014	1090	6.35	2.35	0.88	12.96
DE-RuR	Rollesbroich	GRA	50.62	6.30	2011-2014	865	8.10	1.17	0.91	8.90
DE-Seh	Selhausen	CRO	50.87	6.45	2009-2009	500	10.56	1.48	0.97	11.01
DE-Tha	Tharandt	ENF	50.96	13.57	2002-2014	829	9.03	2.42	0.87	14.76
FI-Hyy	Hyytiala	ENF	61.85	24.29	2002-2014	609	4.51	1.71	0.92	10.28
FR-Fon	Fontainebleau-Barbeau	DBF	48.48	2.78	2005-2014	671	11.35	1.61	0.88	9.69
FR-Gri	Grignon	CRO	48.84	1.95	2004-2007	654	11.05	1.94	0.96	12.30
FR-LBr	Le Bray	ENF	44.72	-0.77	2002-2008	947	13.16	1.59	0.87	9.89
GF-Guy	Guyaflux (French Guiana)	EBF	5.28	-52.92	2004-2014	3113	25.61	1.54	0.88	7.85
IT-Cp2	Castelporziano2	EBF	41.70	12.36	2012-2014	868	16.08	1.36	0.75	8.36
IT-Cpz	Castelporziano	EBF	41.71	12.38	2002-2008	855	15.72	1.88	0.85	11.46
IT-Lav	Lavarone	ENF	45.96	11.28	2003-2014	1211	7.10	2.36	0.84	10.44
IT-MBo	Monte Bondone	GRA	46.01	11.05	2003-2013	932	5.10	1.22	0.92	6.70
IT-Tor	Torgnon	GRA	45.84	7.58	2008-2013	735	3.18	0.97	0.97	5.71
NL-Hor	Horstermeer	GRA	52.24	5.07	2004-2011	1079	10.94	0.99	0.71	6.18

NL-Loo	Loobos	ENF	52.17	5.74	2002-2013	722	9.83	2.09	0.88	10.16
RU-Fyo	Fyodorovskoye	ENF	56.46	32.92	2002-2014	541	5.21	1.48	0.80	8.26
US-ARb	ARM Southern Great Plains burn site- Lamont	GRA	35.55	-98.04	2005-2005	756	15.43	1.33	0.98	11.76
US-ARc	ARM Southern Great Plains control site- Lamont	GRA	35.55	-98.04	2005-2005	797	15.07	1.20	0.98	10.07
US-Blo	Blodgett Forest	ENF	38.90	-120.63	2002-2007	1367	11.23	1.06	0.95	7.56
US-Ha1	Harvard Forest EMS Tower (HFR1)	DBF	42.54	-72.17	2002-2012	1251	8.08	1.85	0.84	11.12
US-Me2	Metolius mature ponderosa pine	ENF	44.45	-121.56	2002-2014	1144	21.78	1.21	0.94	7.15
US-Myb	Mayberry Wetland	WET	38.05	-121.77	2012-2012	534	7.44	1.53	0.85	10.65
US-NR1	Niwot Ridge Forest (LTER NWT1)	ENF	40.03	-105.55	2002-2014	443	15.19	0.71	0.92	4.85
US-Ne1	Mead - irrigated continuous maize site	CRO-C4	41.17	-96.48	2002-2012	788	10.32	2.62	0.96	15.25
US-Ne2	Mead - irrigated maize-soybean rotation site	CRO-C4	41.16	-96.47	2003, 2005, 2007 2009-2012	843	10.29	2.50	0.96	15.87
		CRO-C3	41.16	-96.47	2002, 2004, 2006, 2008	860	10.33	1.47	0.96	9.03
US-Ne3	Mead - rainfed maize-soybean rotation site	CRO-C4	41.18	-96.44	2003, 2005, 2007, 2009, 2011	712	9.94	2.87	0.96	18.90
		CRO-C3	41.18	-96.44	2002, 2004, 2006, 2008, 2010, 2012	912	9.53	1.84	0.98	11.08
US-Ton	Tonzi Ranch	WSA	38.43	-120.97	2005-2005	782	16.13	1.32	0.88	8.75
US-Tw3	Twitchell Alfalfa	CRO	38.12	-121.65	2013-2013	135	15.38	1.29	0.95	11.67

US-UMB	Univ. of Mich. Biological Station	DBF	45.56	-84.71	2002-2014	600	7.15	1.42	0.90	9.25
US-UMd	UMBS Disturbance	DBF	45.56	-84.70	2007-2014	710	7.17	1.38	0.87	9.23

Reference

Albrizio, R., & Steduto, P. (2005). Resource use efficiency of field-grown sunflower, sorghum, wheat and chickpea: I. Radiation use efficiency. *Agricultural and Forest Meteorology*, *130*(3–4), 254–268. https://doi.org/10.1016/j.agrformet.2005.03.009

Beer, C., Ciais, P., Reichstein, M., Baldocchi, D., Law, B. E., Papale, D., et al. (2009). Temporal and among-site variability of inherent water use efficiency at the ecosystem level. *Global Biogeochemical Cycles*, *23*(2), 1–13. https://doi.org/10.1029/2008GB003233

Bolton, J. R., & Hall, D. O. (1991). the Maximum Efficiency of Photosynthesis. *Photochemistry and Photobiology*, *53*(4), 545–548. https://doi.org/10.1111/j.1751-1097.1991.tb03668.x

Brisson, N., Olioso, A., & Clastre, P. (1993). Daily transpiration of field soybeans as related to hydraulic conductance, root distribution, soil potential and midday leaf potential. *Plant and Soil*, *154*(2), 227–237. https://doi.org/10.1007/BF00012528

Britton, C. M., & Dodd, J. D. (1976). Relationships of photosynthetically active radiation and shortwave irradiance. *Agricultural Meteorology*, *17*(1), 1–7. https://doi.org/10.1016/0002-1571(76)90080-7

Cannell, M. G. R., Sheppard, L. J., & Milne, R. (1988). Light use efficiency and woody biomass production of poplar and willow. *Forestry*, *61*(2), 125–136. https://doi.org/10.1093/forestry/61.2.125

Chen, B., Chen, J. M., Mo, G., Black, T. A., & Worthy, D. E. J. (2008). Comparison of regional carbon flux estimates from CO2 concentration measurements and remote sensing based footprint integration. *Global Biogeochemical Cycles*, *22*(2). https://doi.org/10.1029/2007GB003024

Chen, B., Coops, N. C., Fu, D., Margolis, H. A., Amiro, B. D., Black, T. A., et al. (2012). Characterizing spatial representativeness of flux tower eddy-covariance measurements across the Canadian Carbon Program Network using remote sensing and footprint analysis. *Remote Sensing of Environment*, *124*, 742–755. https://doi.org/10.1016/J.RSE.2012.06.007

Chen, T., Van Der Werf, G. R., Dolman, A. J., & Groenendijk, M. (2011). Evaluation of cropland maximum light use efficiency using eddy flux measurements in North America and Europe. *Geophysical Research Letters*, *38*(14), 1–5. https://doi.org/10.1029/2011GL047533

Childs S. W., Gilley J. R., & Splinter W. E. (1977). A Simplified Model of Corn Growth under Moisture Stress. *Transactions of the ASAE*, *20*(5), 0858–0865. https://doi.org/10.13031/2013.35664

Choudhury, B. J. (2000). A sensitivity analysis of the radiation use efficiency for gross photosynthesis and net carbon accumulation by wheat. *Agricultural and Forest Meteorology*, *101*(2–3), 217–234. https://doi.org/10.1016/S0168-1923(99)00156-2

Christina, M., Le Maire, G., Battie-Laclau, P., Nouvellon, Y., Bouillet, J. P., Jourdan, C., et al. (2015). Measured and modeled interactive effects of potassium deficiency and water deficit on gross primary productivity and light-use efficiency in Eucalyptus grandis plantations. *Global Change Biology*, *21*(5), 2022–2039.

https://doi.org/10.1111/gcb.12817

Cramer, W., Kicklighter, D. W., Bondeau, A., Moore, B., Churkina, G., Nemry, B., et al. (1999). Comparing global models of terrestrial net primary productivity (NPP): overview and key results. *Global Change Biology*, *5*(1), 1–15. https://doi.org/10.1046/j.1365-2486.1999.00001.x

Dai, Y., Dickinson, R. E., & Wang, Y. (2004). A Two-Big-Leaf Model for Canopy Temperature, Photosynthesis, and Stomatal Conductance. *Journal of Climate*, *17*(12), 2281–2299. https://doi.org/10.1175/1520-0442(2004)017<2281:ATMFCT>2.0.CO;2

Dewar, R. C., Medlyn, B. E., & McMurtrie, R. E. (1998). A mechanistic analysis of light and carbon use efficiencies. *Plant, Cell & Environment*, *21*(6), 573–588. https://doi.org/10.1046/j.1365-3040.1998.00311.x

Field, C. B. (1991). Ecological Scaling of Carbon Gain to Stress and Resource Availability. *Response of Plants to Multiple Stresses*, 35–65. https://doi.org/10.1016/B978-0-08-092483-0.50007-4

Fu, D., Chen, B., Zhang, H., Wang, J., Black, T. A., Amiro, B. D., et al. (2014). Estimating landscape net ecosystem exchange at high spatial–temporal resolution based on Landsat data, an improved upscaling model framework, and eddy covariance flux measurements. *Remote Sensing of Environment*, *141*, 90–104. https://doi.org/10.1016/J.RSE.2013.10.029

Gallagher, J. N., & Biscoe, P. V. (1978). Radiation absorption, growth and yield of cereals. *The Journal of Agricultural Science*, *91*(1), 47–60. https://doi.org/10.1017/S0021859600056616

Gan, R., Zhang, Y., Shi, H., Yang, Y., Eamus, D., Cheng, L., et al. (2018). Use of satellite leaf area index estimating evapotranspiration and gross assimilation for Australian ecosystems. *Ecohydrology*, (January), e1974. https://doi.org/10.1002/eco.1974

Gitelson, A. A., & Gamon, J. A. (2015). The need for a common basis for defining light-use efficiency: Implications for productivity estimation. *Remote Sensing of Environment*, *156*, 196–201. https://doi.org/10.1016/j.rse.2014.09.017

Gitelson, A. A., Peng, Y., Arkebauer, T. J., & Suyker, A. E. (2015). Productivity, absorbed photosynthetically active radiation, and light use efficiency in crops: Implications for remote sensing of crop primary production. *Journal of Plant Physiology*, *177*, 100–109. https://doi.org/10.1016/j.jplph.2014.12.015

Gitelson, A. A., Arkebauer, T. J., & Suyker, A. E. (2018). Convergence of daily light use efficiency in irrigated and rainfed C3 and C4 crops. *Remote Sensing of Environment*, *217*, 30–37. https://doi.org/10.1016/J.RSE.2018.08.007

Guan, H., & Wilson, J. L. (2009). A hybrid dual-source model for potential evaporation and transpiration partitioning. *Journal of Hydrology*, *377*(3–4), 405–416. https://doi.org/10.1016/J.JHYDROL.2009.08.037

Hanks, R. J. (1974). Model for Predicting Plant Yield as Influenced by Water Use, (1804).

Hanks, R. J. (1983). Yield and water-use relationships: An overview. *Limitations to Efficient Water Use in Crop Production*, 393–411.

He, H., Liu, M., Xiao, X., Ren, X., Zhang, L., Sun, X., et al. (2014). Large-scale estimation and uncertainty analysis of gross primary production in Tibetan alpine grasslands. *Journal of Geophysical Research: Biogeosciences*, *119*(3), 466–486.

https://doi.org/10.1002/2013JG002449

Hu, Z., Shi, H., Cheng, K., Wang, Y. P., Piao, S., Li, Y., et al. (2018). Joint structural and physiological control on the interannual variation in productivity in a temperate grassland: A data-model comparison. *Global Change Biology*, (August 2017), 2965–2979. https://doi.org/10.1111/gcb.14274

Impens, I., & Lemeur, R. (1969). Extinction of net radiation in different crop canopies. *Archiv Für Meteorologie, Geophysik Und Bioklimatologie Serie B*, *17*(4), 403–412. https://doi.org/10.1007/BF02243377

Katul, G., Manzoni, S., Palmroth, S., & Oren, R. (2010). A stomatal optimization theory to describe the effects of atmospheric CO2 on leaf photosynthesis and transpiration. *Annals of Botany*, *105*(3), 431–442. https://doi.org/10.1093/aob/mcp292

Kergoat, L., Lafont, S., Arneth, A., Le Dantec, V., & Saugier, B. (2008). Nitrogen controls plant canopy light-use efficiency in temperate and boreal ecosystems. *Journal of Geophysical Research: Biogeosciences*, *113*(4). https://doi.org/10.1029/2007JG000676

Knauer, J., Zaehle, S., Medlyn, B. E., Reichstein, M., Williams, C. A., Migliavacca, M., et al. (2018). Towards physiologically meaningful water-use efficiency estimates from eddy covariance data. *Global Change Biology*, *24*(2), 694–710. https://doi.org/10.1111/gcb.13893

Landsberg, J. J., & Waring, R. H. (1997). A generalised model of forest productivity using simplified concepts of radiation-use efficiency, carbon balance and partitioning. *Forest Ecology and Management*, *95*(3), 209–228. https://doi.org/https://doi.org/10.1016/S0378-1127(97)00026-1

Leuning, R., Zhang, Y. Q., Rajaud, A., Cleugh, H., & Tu, K. (2008). A simple surface conductance model to estimate regional evaporation using MODIS leaf area index and the Penman-Monteith equation. *Water Resources Research*, *44*(10), W10419. https://doi.org/10.1029/2007WR006562

Li, A., Bian, J., Lei, G., & Huang, C. (2012). Estimating the maximal light use efficiency for different vegetation through the CASA model combined with time-series remote sensing data and ground measurements. *Remote Sensing*, *4*(12), 3857–3876. https://doi.org/10.3390/rs4123857

Maes, W. H., Gentine, P., Verhoest, N. E. C., & Miralles, D. G. (2018). Potential evaporation at eddy-covariance sites across the globe. *Hydrology and Earth System Sciences Discussions*, (February), 1–38. https://doi.org/10.5194/hess-2018-470

Medlyn, B. E. (1998). Physiological basis of the light use efficiency model. *Tree Physiology*. Retrieved from http://treephys.oxfordjournals.org/content/18/3/167.short

Medlyn, B. E., Duursma, R. A., Eamus, D., Ellsworth, D. S., Prentice, I. C., Barton, C. V. M., et al. (2011). Reconciling the optimal and empirical approaches to modelling stomatal conductance. *Global Change Biology*, *17*(6), 2134–2144. https://doi.org/10.1111/j.1365-2486.2010.02375.x

Medlyn, B. E., De Kauwe, M. G., Lin, Y. S., Knauer, J., Duursma, R. A., Williams, C. A., et al. (2017). How do leaf and ecosystem measures of water-use efficiency compare? *New Phytologist*. https://doi.org/10.1111/nph.14626

Milly, P. C. D., & Dunne, K. A. (2016). Potential evapotranspiration and continental drying. *Nature Climate Change*, *6*(10), 946–949. https://doi.org/10.1038/nclimate3046

Monteith, J. L. (1972). Solar Radiation and Productivity in Tropical Ecosystems. *Journal of Applied Ecology*, *9*(3), 747–766. https://doi.org/10.2307/2401901

Monteith, J. L. (1977). Climate and the Efficiency of Crop Production in Britain [and Discussion]. *Philosophical Transactions of the Royal Society B: Biological Sciences*, *281*(980), 277–294. https://doi.org/10.1098/rstb.1977.0140

Monteith, J. L. (1986). How do crops manipulate water supply and demand? *Philosophical Transactions of the Royal Society of London. Series A, Mathematical and Physical Sciences*, *316*(1537), 245 LP – 259. Retrieved from http://rsta.royalsocietypublishing.org/content/316/1537/245.abstract

Monteith, J. L. (1988). Does transpiration limit the growth of vegetation or vice versa? *Journal of Hydrology*, *100*(1–3), 57–68. https://doi.org/10.1016/0022-1694(88)90181-3

Nguy-Robertson, A., Suyker, A., & Xiao, X. (2015). Modeling gross primary production of maize and soybean croplands using light quality, temperature, water stress, and phenology. *Agricultural and Forest Meteorology*, *213*, 160–172. https://doi.org/10.1016/j.agrformet.2015.04.008

Norby, R. J., Sholtis, J. D., Gunderson, C. A., & Jawdy, S. S. (2003). Leaf dynamics of a deciduous forest canopy: no response to elevated CO2. *Oecologia*, *136*(4), 574–584. https://doi.org/10.1007/s00442-003-1296-2

Pagán, B., Maes, W., Gentine, P., Martens, B., & Miralles, D. (2019). Exploring the Potential of Satellite Solar-Induced Fluorescence to Constrain Global Transpiration Estimates. *Remote Sensing*, *11*(4), 413. https://doi.org/10.3390/rs11040413

Passioura, J. B. (1982). Water in the Soil-Plant-Atmosphere Continuum BT - Physiological Plant Ecology II: Water Relations and Carbon Assimilation. In O. L. Lange, P. S. Nobel, C. B. Osmond, & H. Ziegler (Eds.) (pp. 5–33). Berlin, Heidelberg: Springer Berlin Heidelberg. https://doi.org/10.1007/978-3-642-68150-9_2

Potter, C. S., Randerson, J. T., Field, C. B., Matson, P. A., Vitousek, P. M., Mooney, H. A., & Klooster, S. A. (1993). Terrestrial ecosystem production: A process model based on global satellite and surface data. *Global Biogeochemical Cycles*, *7*(4), 811–841. https://doi.org/10.1029/93GB02725

Priestley, C. H. B., & Taylor, R. J. (1972). On the Assessment of Surface Heat Flux and Evaporation Using Large-Scale Parameters. In *Monthly Weather Review* (Vol. 100, pp. 81–92). https://doi.org/10.1175/1520-0493(1972)100<0081:OTAOSH>2.3.CO;2

Prince, S. D. (1991). A model of regional primary production for use with coarse resolution satellite data. *International Journal of Remote Sensing*, *12*(6), 1313–1330. https://doi.org/10.1080/01431169108929728

Raymond Hunt, E., J. (1994). Relationship between woody biomass and PAR conversion efficiency for estimating net primary production from NDVI. *International Journal of Remote Sensing*, *15*(8), 1725–1730. https://doi.org/10.1080/01431169408954203

Reichstein, M., Falge, E., Baldocchi, D., Papale, D., Aubinet, M., Berbigier, P., et al. (2005). On the separation of net ecosystem exchange into assimilation and ecosystem respiration: Review and improved algorithm. *Global Change Biology*, *11*(9), 1424–1439. https://doi.org/10.1111/j.1365-2486.2005.001002.x

Ritchie, J. T. (1983). Efficient water use in crop production: discussion on the generality of relations between biomass production and evapotranspiration. *Limitations to Efficient*

Water Use in Crop Production, 29–44. https://doi.org/10.2134/1983.limitationstoefficientwateruse.c2

Roupsard, O., Bonnefond, J. M., Irvine, M., Berbigier, P., Nouvellon, Y., Dauzat, J., et al. (2006). Partitioning energy and evapo-transpiration above and below a tropical palm canopy. *Agricultural and Forest Meteorology*, *139*(3–4), 252–268. https://doi.org/10.1016/j.agrformet.2006.07.006

Ruimy, A., Saugier, B., & Dedieu, G. (1994). Methodology for the estimation of terrestrial net primary production from remotely sensed data. *Journal of Geophysical Research: Atmospheres*, *99*(D3), 5263–5283. https://doi.org/10.1029/93JD03221

Ruimy, A., Jarvis, P. G., Baldocchi, D. D., & Saugier, B. (1995). CO2 Fluxes over Plant Canopies and Solar Radiation: A Review. *Advances in Ecological Research*, *26*, 1–68. https://doi.org/10.1016/S0065-2504(08)60063-X

Ruimy, A., Kergoat, L., Bondeau, A., & Intercomparison, T. P. O. F. T. P. N. M. (1999). Comparing global models of terrestrial net primary productivity (NPP): analysis of differences in light absorption and light-use efficiency. *Global Change Biology*, *5*(S1), 56–64. https://doi.org/10.1046/j.1365-2486.1999.00007.x

Running, S. W., & Zhao, M. (2015). Daily GPP and Annual NPP (MOD17A2/A3) products NASA Earth Observing System MODIS Land Algorithm - User's guide V3, 28. https://doi.org/http://doi.org/10.5067/MODIS/MOD17A3H.006

Running, S. W., Nemani, R. R., Heinsch, F. A., Zhao, M., Reeves, M., & Hashimoto, H. (2004). A Continuous Satellite-Derived Measure of Global Terrestrial Primary Production. *BioScience*, *54*(6), 547–560. Retrieved from http://dx.doi.org/10.1641/0006-3568(2004)054[0547:ACSMOG]2.0.CO

Sánchez, M. L., Pardo, N., Pérez, I. A., & García, M. A. (2015). GPP and maximum light use efficiency estimates using different approaches over a rotating biodiesel crop. *Agricultural and Forest Meteorology*, *214–215*, 444–455. https://doi.org/10.1016/J.AGRFORMET.2015.09.012

Shi, H., Li, L., Eamus, D., Cleverly, J., Huete, A., Beringer, J., et al. (2014). Intrinsic climate dependency of ecosystem light and water-use-efficiencies across Australian biomes. *Environmental Research Letters*, *9*(10), 104002. https://doi.org/10.1088/1748-9326/9/10/104002

Sinclair, T. R., & Horie, T. (1989). Leaf Nitrogen, Photosynthesis, and Crop Radiation Use Efficiency: A Review. *Crop Science*, *29*(1), 90. https://doi.org/10.2135/cropsci1989.0011183X002900010023x

Sinclair, T. R., & Muchow, R. C. (1999). Radiation Use Efficiency. In D. L. B. T.-A. in A. Sparks (Ed.) (Vol. 65, pp. 215–265). Academic Press. https://doi.org/https://doi.org/10.1016/S0065-2113(08)60914-1

Stewart, J., Hagan, R., Pruitt, W., Danielson, R., Franklin, W., Hanks, R., et al. (1977). Optimizing crop production through control of water and salinity levels in the soil. *Reports*, (January). https://doi.org/Reports. Paper 67

Turner, D. P., Ritts, W. D., Cohen, W. B., Gower, S. T., Zhao, M., Running, S. W., et al. (2003). Scaling Gross Primary Production (GPP) over boreal and deciduous forest landscapes in support of MODIS GPP product validation. *Remote Sensing of Environment*, *88*(3), 256–270. https://doi.org/10.1016/j.rse.2003.06.005

Veroustraete, F., Sabbe, H., & Eerens, H. (2002). Estimation of carbon mass fluxes over Europe using the C-Fix model and Euroflux data. *Remote Sensing of Environment*, *83*(3), 376–399. https://doi.org/https://doi.org/10.1016/S0034-4257(02)00043-3

Wagle, P., Gowda, P. H., Xiao, X., & Anup, K. C. (2016). Parameterizing ecosystem light use efficiency and water use efficiency to estimate maize gross primary production and evapotranspiration using MODIS EVI. *Agricultural and Forest Meteorology*, *222*, 87–97. https://doi.org/10.1016/j.agrformet.2016.03.009

Wang, H., Jia, G., Fu, C., Feng, J., Zhao, T., & Ma, Z. (2010). Deriving maximal light use efficiency from coordinated flux measurements and satellite data for regional gross primary production modeling. *Remote Sensing of Environment*, *114*(10), 2248–2258. https://doi.org/10.1016/j.rse.2010.05.001

Wang, L., Stephen, P. G., & Kelly, K. C. (2014). Global synthesis of vegetation control on evapotranspiration partitioning. *Geophysical Research Letters*, *41*(19), 6753–6757. https://doi.org/10.1002/2014GL061439

Wang, S., Ibrom, A., Bauer-Gottwein, P., & Garcia, M. (2018). Incorporating diffuse radiation into a light use efficiency and evapotranspiration model: An 11-year study in a high latitude deciduous forest. *Agricultural and Forest Meteorology*, *248*, 479–493. https://doi.org/10.1016/J.AGRFORMET.2017.10.023

Wei, S., Yi, C., Fang, W., & Hendrey, G. (2017). A global study of GPP focusing on light-use efficiency in a random forest regression model. *Ecosphere*, *8*(5). https://doi.org/10.1002/ecs2.1724

Wei, Z., Yoshimura, K., Wang, L., Miralles, D. G., Jasechko, S., & Lee, X. (2017). Revisiting the contribution of transpiration to global terrestrial evapotranspiration. *Geophysical Research Letters*, *44*(6), 2792–2801. https://doi.org/10.1002/2016GL072235

de Wit, C. T. (1958). Transpiration and crop yields. *Versl. Landbouwk. Onderz. 64. 6.*, (64), 88. https://doi.org/.

Wohlfahrt, G., & Gu, L. (2015). The many meanings of gross photosynthesis and their implication for photosynthesis research from leaf to globe. *Plant, Cell and Environment*, *38*(12), 2500–2507. https://doi.org/10.1111/pce.12569

Woodgate, W., Disney, M., Armston, J. D., Jones, S. D., Suarez, L., Hill, M. J., et al. (2015). An improved theoretical model of canopy gap probability for Leaf Area Index estimation in woody ecosystems. *Forest Ecology and Management*, *358*, 303–320. https://doi.org/10.1016/J.FORECO.2015.09.030

Xiao, X., Zhang, Q., Braswell, B., Urbanski, S., Boles, S., Wofsy, S., et al. (2004). Modeling gross primary production of temperate deciduous broadleaf forest using satellite images and climate data. *Remote Sensing of Environment*, *91*(2), 256–270. https://doi.org/https://doi.org/10.1016/j.rse.2004.03.010

Yuan, W., Liu, S., Zhou, G., Zhou, G., Tieszen, L. L., Baldocchi, D., et al. (2007). Deriving a light use efficiency model from eddy covariance flux data for predicting daily gross primary production across biomes. *Agricultural and Forest Meteorology*, *143*(3–4), 189–207. https://doi.org/10.1016/J.AGRFORMET.2006.12.001

Yuan, W., Cai, W., Xia, J., Chen, J., Liu, S., Dong, W., et al. (2014). Global comparison of light use efficiency models for simulating terrestrial vegetation gross primary production based on the LaThuile database. *Agricultural and Forest Meteorology*, *192–193*, 108–

120. https://doi.org/10.1016/J.AGRFORMET.2014.03.007

Zhang, L., Hu, Z., Fan, J., Zhou, D., & Tang, F. (2014). A meta-analysis of the canopy light extinction coefficient in terrestrial ecosystems. *Frontiers of Earth Science*, *8*(4), 599–609. https://doi.org/10.1007/s11707-014-0446-7

Zhang, Yao, Xiao, X., Jin, C., Dong, J., Zhou, S., Wagle, P., et al. (2016). Consistency between sun-induced chlorophyll fluorescence and gross primary production of vegetation in North America. *Remote Sensing of Environment*, *183*, 154–169. https://doi.org/10.1016/j.rse.2016.05.015

Zhang, Yao, Xiao, X., Wu, X., Zhou, S., Zhang, G., Qin, Y., & Dong, J. (2017). A global moderate resolution dataset of gross primary production of vegetation for 2000–2016. *Scientific Data*, *4*, 170165. https://doi.org/10.1038/sdata.2017.165

Zhang, Yao, Xiao, X., Wolf, S., Wu, J., Wu, X., Gioli, B., et al. (2018). Spatio-Temporal Convergence of Maximum Daily Light-Use Efficiency Based on Radiation Absorption by Canopy Chlorophyll. *Geophysical Research Letters*, *45*(8), 3508–3519. https://doi.org/10.1029/2017GL076354

Zhang, Yongqiang, Kong, D., Gan, R., Chiew, F. H. S., McVicar, T. R., Zhang, Q., & Yang, Y. (2019). Coupled estimation of 500 m and 8-day resolution global evapotranspiration and gross primary production in 2002–2017. *Remote Sensing of Environment*, *222*, 165–182. https://doi.org/https://doi.org/10.1016/j.rse.2018.12.031

Zheng, Y., Zhang, L., Xiao, J., Yuan, W., Yan, M., Li, T., & Zhang, Z. (2018). Sources of uncertainty in gross primary productivity simulated by light use efficiency models: Model structure, parameters, input data, and spatial resolution. *Agricultural and Forest Meteorology*, *263*, 242–257. https://doi.org/10.1016/J.AGRFORMET.2018.08.003

Zhou, S., Yu, B., Huang, Y., & Wang, G. (2014). The effect of vapor pressure deficit on water use efficiency at the subdaily time scale. *Geophysical Research Letters*, *41*, 5005–5013. https://doi.org/10.1002/2014GL060741.Received

Zhou, S., Yu, B., Zhang, Y., Huang, Y., & Wang, G. (2016). Partitioning evapotranspiration based on the concept of underlying water use efficiency. *Water Resources Research*, *52*(2), 1160–1175. https://doi.org/10.1002/2015WR017766

Zhou, S., Yu, B., Zhang, Y., Huang, Y., & Wang, G. (2018). Water use efficiency and evapotranspiration partitioning for three typical ecosystems in the Heihe River Basin, northwestern China. *Agricultural and Forest Meteorology*, *253–254*, 261–273. https://doi.org/10.1016/J.AGRFORMET.2018.02.002

Chapter 6. Final conclusions and future research

6.1 Final conclusions

Water and carbon exchanges over terrestrial ecosystems are of vital importance in determining ecohydrological processes, and there processes have significant implications for natural resources management that affect ecological, hydrological, and agricultural interests. This study systematically investigated the key water and carbon variables by developing and analysing ecohydrological models that are practical yet effective across a wide variety of ecosystems within the Australian continent and across the globe over multiple spatiotemporal scales. The simple ecohydrological models developed and analytical results presented in this study provide insights into the underlying relationship between water and carbon processes, and can be used to interpret quantity, variability and uncertainty of water and carbon estimates.

To include carbon constraints on water estimates without compromising model simplicity and effectiveness, a simple canopy conductance model was developed and incorporated with the Penman-Monteith equation to simultaneously simulate water loss (i.e., ET) and carbon gain (i.e., GPP) over terrestrial ecosystems (Chapter 2). The model had seven parameters and used remotely-sensed LAI and routinely available meteorological inputs. Examination of the model across nine eddy covariance flux sites covering five Australian ecosystem types showed that the model generally performed well for both ET and GPP (NSE>0.65 and simulated values explained >75% of the variation of observed values). Sensitivity analysis indicated that the model could be further simplified by reducing the insensitive parameters (from 7 to 4). Comparison of ET and GPP estimates with the MODIS product further demonstrated the reliability of the model. Thus it is concluded that the model is robust and advantageous and has the potential to be used for longer temporal and larger spatial scales.

To systematically evaluate the interrelated key ecohydrological processes under climate change, a simple ecohydrological model was developed to simultaneously estimate Q, ET, and GPP (Chapter 3). The model used a typical lumped hydrological model as the base model that was then further developed to incorporate the process-based canopy conductance model developed in the previous section of this thesis. Model performance was evaluated by comparing Q, ET, and GPP simulations to observations at catchment and eddy covariance flux site scales. Results demonstrated the overall satisfactory capability of the model, where NSE was about 0.64 for Q across 63 catchments and simulations of ET were comparable to observations at across 13

adjacent flux sites. Under the increased CO_2 scenario (45% increase in CO_2 concentration), the modeling experiment indicated an increase in Q (12%) and GPP (23%), but a decrease in ET (-4%) in response to biophysical regulation. A more significant change in ET found for non-forest catchments (-5%) than for forest catchments (-2%). These results highlight the importance of vegetation control over key ecohydrological processes. The model is more advanced in representing physiological mechanisms while inheriting the simplicity and accuracy of traditional conceptual hydrological models (with only 12 free parameters and simple model structure). We consider the model to be more practical than most sophisticated modelling schemes. Therefore, the model developed here can serve as an intermediate solution to effectively quantify and evaluate variations in key ecohydrological variables including Q, ET, and GPP.

To investigate ET partitioning based on carbon constraint, the coupled water and carbon canopy conductance model developed earlier in this thesis was used to partition ET into T and E at a wide variety of grassland sites across the globe (Chapter 4). The model was optimised to obtain the best ET and GPP estimates at individual sites (NSE and $R^2 > 0.7$), then the T estimates were used to evaluate the variation, uncertainty, and controlling factors of T/ET across spatiotemporal scales. Results showed that with ET partitioning constrained by GPP, the T/ET estimates exhibited strong seasonality, with high T/ET (close to 1) during the growing season and low T/ET (close to 0) during the non-growing seasons. The average T/ET varied greatly across sites (0.10-0.87, averaging about 0.5). Seasonal variation of T/ET was well explained by LAI at seven out of 15, while the spatial variation was more likely to be explained by precipitation. Comparison of T/ET estimates with an empirical ET partitioning method which was also based on GPP demonstrated that the uncertainty of T/ET was more significant at high and low vegetated sites. Even though ET has been studied extensively as a single variable, this study emphasised the importance and challenge of evaluating ET components, including temporal and spatial variation of T and E and the factors controlling T/ET in order to enhance quantification and interpretation of ecohydrological process.

In addition to investigating water processes based on carbon constraint as discussed in the above sections, this thesis also attempted to evaluate carbon processes from a water-based perspective as an integrated system (Chapter 5). The mechanistic coupling relationship between carbon uptake and vegetative water loss was employed to develop a new method for estimating the key parameter used for carbon quantification, namely the maximum light use efficiency (ε_{max}). The method used was a simple analytical approach which required only four

variables readily available at eddy covariance flux sites. The method provided reliable estimates of ecosystem ε_{max} for different species and biome groups widely distributed across the world. The estimated ε_{max} values (1.48±0.33 $g\,C\,MJ^{-1}$ PAR for C_3 and 2.63±0.21 $g\,C\,MJ^{-1}$ PAR for C_4 vegetation dominated ecosystems) based on vegetation water use can be used as an independent parameter set to better simulate GPP and investigate carbon and water interactions.

6.2 Limitations and future research

In spite of the overall contributions of this thesis presented above, there are a number of limitations which require further investigation in the future.

(1) Model development. This is regarding the work summarized in Chapter 2. Although the PML_V2 model developed in this thesis produced reasonably accurate ET and GPP estimates, the model is only a diagnostic water and carbon model, but not a fully coupled one. This is because (a) the canopy conductance is only a function of energy availability and CO_2 concentration. This means the model simulates only one-direction (response) rather than two-directions (response-feedback) stomata behavior. In fact, stomatal conductance varies along with carbon uptake and water loss interactively, thus requiring two-direction representation in the model. Further model development should consider interactive simulation of canopy conductance in relation to GPP and T; and (b) the model used LAI as an input to derive GPP, which is a diagnostic approach, but not actually the correct sequence. This is because vegetation uses photosynthetic production to generate leaves (resulting in LAI). Hence, LAI is a product of photosynthesis that in principle should be calculated from GPP. Incorporation of this sequence is important for evaluating eCO_2 impact on ecohydrological processes, especially the variation of water and carbon estimates. To be specific, with increased CO_2 in the atmosphere, GPP should increase due to the 'fertilization' effect, thereby leading to increased LAI. As a result, T will increase due to increased LAI (structural feedback), which in turn compensates for the T reduction that is a consequence of stomatal closure (biophysical response). Therefore, it is expected that significant uncertainty can exist in estimates and variations in water flows (ET, Q) and carbon budget in terms of both magnitude and direction. Hence, it appears that future model development will be required to incorporate interactive processes that support better and more robust quantification and interpretation of ecohydrological processes especially under a changing environment.

(2) Model validation. This is related to work summarized in Chapter 3 and Chapter 4. Although the model simulations have been validated against available datasets in this thesis, it is not yet clear whether (a) the components of ET are estimated appropriately, including the temporal and spatial characteristics. It was shown that even when ET was partitioned with carbon constraint considering the coupled relationship between T and GPP, there was still noticeable uncertainty in T/ET estimates (as seen with model comparison and observational values reported in the literature). Considering the critical role that T plays in regulating energy, water, and carbon budgets, it is suggested that further study should be undertaken to validate model simulations of not only the total value of ET, but also the components of ET based on available and reliable data. Such investigations will be especially important for eCO_2 impact analysis and interpretation; (b) whether the catchment scale ET and GPP estimates are accurate/reliable. Due to data limitations, the ET and GPP estimates at catchment scale were only compared to the measurements made at adjacent flux sites in this thesis (Chapter 3). In principle there exits great spatial footprint discrepancy between the two measurement scales. Therefore observational ET and GPP values at catchment scale should be used to evaluate the model performance and robustness. However, such regional data are not available and almost impossible to obtain. Future study could either incorporate regional data products or conduct multi-model comparisons to investigate the reliability of the model simulations.

(3) The ε_{max} estimates provided in Chapter 5 can be directly employed to develop a simple GPP model based on the LUE framework, similar to those GPP models based on remote sensing data. Moreover, with ε_{max} estimates constrained by vegetation water use (higher reliability), the parameterization of LUE models can be better evaluated and uncertainty accounted for by investigating other limiting factors that could be incorporated into the model rather than forcing ε_{max} to unrealistic values. Additionally, the ε_{max} method developed in this thesis was based on the assumption that WUE is relatively conservative after considering atmospheric water demand. In reality, WUE can vary under different conditions (e.g., temperature and nutrient stress). Thus further research is required to test the possible uncertainty due to such environmental limitations.